






Universitat Autònoma de Barcelona

ADVERTIMENT. L'accés als continguts d'aquesta tesi queda condicionat a l'acceptació de les condicions d'ús establertes per la següent llicència Creative Commons:  http://cat.creativecommons.org/?page_id=184

ADVERTENCIA. El acceso a los contenidos de esta tesis queda condicionado a la aceptación de las condiciones de uso establecidas por la siguiente licencia Creative Commons:  <http://es.creativecommons.org/blog/licencias/>

WARNING. The access to the contents of this doctoral thesis it is limited to the acceptance of the use conditions set by the following Creative Commons license:  <https://creativecommons.org/licenses/?lang=en>

Study of the cytotoxic activity and immunogenicity of the
differentiated morphotypes of the genus *Mycobacterium*,
in relation with their cell wall composition.

by

Marta Llorens Fons

Directed by Dr. Marina Luquín Fernández

Department of Genetics and Microbiology

Universitat Autònoma de Barcelona



Universitat Autònoma de Barcelona

February, 2018

Study of the cytotoxic activity and immunogenicity of the
differentiated morphotypes of the genus *Mycobacterium*,
in relation with their cell wall composition.

by

Marta Llorens Fons

Thesis submitted to obtain the degree of Doctor of Philosophy in Microbiology, from
the Department of Genetics and Microbiology by Universitat Autònoma de Barcelona.



Universitat Autònoma de Barcelona

With the approval of the director and supervisor

Dr. Marina Luquín Fernández

Bellaterra, February, 2018

A tots aquells que conscientment o inconscient heu aportat el vostre granet de sorra. Però, sobretot, a l'Oriol i al Jaume, els homes més bons del món.

Gràcies!



Hold your breath, Paulina Siniatkina. Painting exhibited at the headquarters of the World Health Organization (WHO) in Geneva, March 2017.

Paulina Siniatkina is a Russian artist who suffered of tuberculosis in 2015 and she created this collection of painting to fight the stigma attached to this disease.

"People who are not infected react aggressively: they blame and avoid communication with those ill with tuberculosis. As a result, tuberculosis patients are afraid to speak out and they hide or lie about what is actually happening to them. As long as people are afraid to talk about it, this disease will continue to spread."

Index of Content

Abstract.....	XI
Resum.....	XIII
Abbreviations.....	XV
1. Introduction.....	1
1.1. Mycobacteria and their diseases.....	3
1.2. Pulmonary tuberculosis	15
1.3. Mycobacterial cell wall.....	21
1.4. <i>Mycobacterium vaccae</i> and the vaccine against tuberculosis	33
2. Objectives.....	37
3. Material and methods	41
3.1. Initial preparations.....	43
3.2. Cell-based in vitro models	45
3.3. Biochemist analysis.....	50
3.4. Electronic microscopy.....	53
3.5. Microbiologic methods	55
4. Results.....	59
4.1. Effect of <i>M. abscessus</i> in pulmonary epithelial cells.....	61
4.2. The most superficial lipids in <i>M. abscessus</i> cell wall.....	65
4.3. Study of the toxicity and function of TPP.....	74
4.4. Superficial extraction in other Mycobacteria.....	81
4.5. Cellular response to the different morphotypes of <i>M. vaccae</i>	91

5. Discussion	97
6. Conclusions.....	107
7. Bibliography	111
8. Manuscripts of this thesis	131

Abstract

Mycobacterium is a genus of microorganisms that comprise important human pathogens, such as the etiological agent of tuberculosis, *Mycobacterium tuberculosis*. Many mycobacterial species present two differentiated morphotypes, the rough (R) one characterized by bacillar organization in structures that reassemble cords; and the smooth (S) one without any bacillar aggregation. In pathogenic mycobacteria, R morphotypes are shown to produce more severe illnesses in infected patients than S morphotypes. In fact, this relationship between virulence and cord formation is known since 1947. Studying how bacteria aggregate will help to understand the different virulence associated to the two morphotypes of mycobacteria.

The thesis here presented consists on the study of the cytotoxicity and immunogenicity of these two differentiated morphotypes, the R with a cording phenotype and the S with a non-cording phenotype, in *Mycobacterium abscessus* and *Mycobacterium vaccae*. And, in the case of *M. abscessus*, how these effects in virulence and the cord formation can be related to its cell wall composition.

The two morphotypes of *M. abscessus* were used to infect human alveolar epithelial cells, and the ones from *M. vaccae*, in murine macrophages. The results, in both cases, showed that R morphotypes have major effect in suppressing cellular growth and a higher capacity to trigger cytokine production than S morphotypes.

Superficial lipidic extractions were performed in *M. abscessus*, as the virulence and the cord formation might be related with the expression of determinate external cell wall components. Trehalose polyphleates (TPP) were identified in the superficial extracts from R morphotypes of *M. abscessus*, but TPP were absent in S morphotype extracts. Although this compound was not cytotoxic for human and murine cells, TPP presented aggregative potential.

When analyzing the superficial expression of TPP in other mycobacterial species, another superficial compound, mycolate ester wax, was detected in *Mycobacterium smegmatis*, with a similar migration pattern to TPP. In this work, this compound was clearly characterized as pentatriacontatrienyl mycolate, as some uncertainties regarding its structure were previously reported.

In conclusion, R morphotypes from *M. abscessus* and *M. vaccae* produced a major cytotoxic effect and major immunogenicity that S morphotypes in cell-based *in vitro* models. In the case of *M. abscessus*, this major virulence was accompanied with the superficial expression of TPP, a compound with aggregative properties. These last results point TPP as candidate molecules responsible for the cord formation in R morphotypes of *M. abscessus*.

Resum

Mycobacterium és un gènere de microorganismes que compren importants patògens de la humanitat, com l'agent etiològic de la tuberculosi, *Mycobacterium tuberculosis*. Moltes espècies de micobacteris presenten dos morfotips diferenciats, el rugós (R, de l'anglès "rough") caracteritzat per la capacitat dels bacteris d'organitzar-se formant estructures que recorden cordes; i el llis (S, de l'anglès "smooth") sense organització dels bacils. En micobacteris patògens s'ha descrit que els morfotips R produeixen malalties més severes en pacients infectats que els morfotips S. De fet, la relació entre virulència i formació de cordes es coneix des de 1947. De manera que estudiar com els bacteris s'agreguen ajudarà a entendre aquesta diferència entre la virulència associada als dos morfotips de micobacteris.

La tesi presentada a continuació consisteix en un estudi de la citotoxicitat i la immunogenicitat d'aquests dos morfotips diferenciats, el R amb fenotip formador de cordes i el S amb fenotip no formador de cordes, en *Mycobacterium abscessus* i *Mycobacterium vaccae*. I, en el cas de *M. abscessus*, com aquests efectes en la virulència i la formació de cordes pot estar relacionat amb la composició de la seva paret cel·lular.

Els dos morfotips de *M. abscessus* van ser usats per a infectar cèl·lules epitelials alveolars humanes, i els morfotips de *M. vaccae* per infectar macròfags murins. En els dos casos els resultats van mostrar un major efecte supressor del creixement cel·lular i una capacitat superior d'activar la producció de citocines per part dels morfotips R.

Com s'ha comentat, la virulència dels micobacteris i la seva capacitat per formar cordes pot estar relacionada amb l'expressió de determinats components cel·lulars exteriors. Per aquest motiu es van fer extraccions superficials lipídiques en *M. abscessus*. En aquests extractes superficials es van poder identificar els poliflets de trehalosa (TPP, de l'anglès "trehalose polyphleates"), però només en els extractes dels morfotips R. Els TPP no estaven presents en els extractes de morfotips S. Aquest compost no va presentar citotoxicitat en front a cèl·lules humanes i murines. Tot i així, es va detectar potencial agregatiu.

Analitzant l'expressió superficial de TPP en altres espècies de micobacteris es va detectar un altre compost superficial en *Mycobacterium smegmatis*, amb un patró de migració molt semblant al de TPP. En aquesta tesi, aquest compost va ser correctament

caracteritzat com a pentatriacontatrienil micolat, ja que en treballs previs s'havien detectat incerteses en referència a la seva estructura.

En conclusió, els morfotips R de *M. abscessus* i *M. vaccae* produeixen major efecte citotòxic i immunogènic que els morfotips S en models cel·lulars *in vitro*. En el cas de *M. abscessus*, aquesta major virulència està acompanyada d'una expressió superficial de TPP, un compost amb propietats agregatives. Aquest últim resultat senyala TPP com una molècula candidata a ser responsable de la formació de cordes en els morfotips R de *M. abscessus*.

Abbreviations

AG: Arabinogalactan	MTT: 3-(4,5-dimethylthiazol-2-yl)-2,5-diphenyltetrazolium bromide
ATCC: American type culture collection	NMR: Nuclear magnetic resonance
BCG: Bacillus Calmette-Guérin	NTM: Nontuberculous mycobacteria
BSA: Bovine serum albumin	OL: Outer layer
CFU: Colony forming unit	OsO ₄ : Osmium tetroxide
CLSM: Confocal laser scanning microscope	PAT: Polyacetyltrehalose
CM: Complete medium	PBS: Phosphate-buffered saline
DAT: Diacyltrehalose	PDIM/DIM: Phthiocerol dimycocerosate
DMEM: Dulbecco's Modified Eagle's Medium	PE: Petroleum ether
DMSO: Dimethyl sulfoxide	PG: Peptidoglycan
DPPC: Dipalmitoyl phosphatidylcholine	PGL: Phenol glycolipids
DSMZ: Deutsche Sammlung von Mikroorganismen und Zellkulturen	PIM: Phosphatidyl- <i>myo</i> -inositol mannosides
EDL: Electrodense layer	PM: Plasma membrane
ETL: Electro-transparent layer	PMA: Phorbol myristate acetate
GPL: Glycopeptidolipids	PTTM: Pentatriacontatrienyl mycolate
h.p.i.: Hours post-infection	R: Rough
LAM: Lipoarabinomannan	RPMI: Roswell Park Memorial Institute medium
LM: Lipomannan	S: Smooth
LOS: Lipooligosaccharides	SEM: Scanning electron microscopy
IL-6: interleukin 6	SL: Sulfolipids
IL-8: interleukin 8	TAG: Triacylglycerides
INF- γ : Interferon gamma	TDM: Trehalose dimycolate
MS: Mass spectrometry	TEM: Transmission electron microscopy
MALDI: Matrix-assisted laser desorption/ionization	TLC: Thin layer chromatography
MMDAG: Monomeromycetyl diacylglycerol	TLR: Toll like receptor
MOI: multiplicity of infection	TMC: Trudeau Mycobacterial Culture

TMM: Trehalose monomycolate

TNF- α : Tumor necrosis factor α

TPP: Trehalose polyphleates

WHO: World health organization

ZN: Ziehl-Neelsen

1

Introduction

1.1. Mycobacteria and their diseases

Inside the Actinobacteria phylum there is the *Mycobacteriaceae* family, that contains only one genus, *Mycobacterium*. This genus is formed by aerobic and microaerobic bacteria, slightly curved or straight nonmotile rods. The size of the bacilli is between 0.2-0.6 μm of width and between 1.0-10 μm of length (Wayne and Kubica, 1986; Hartmans et al., 2006) (Figure 1.1.1).

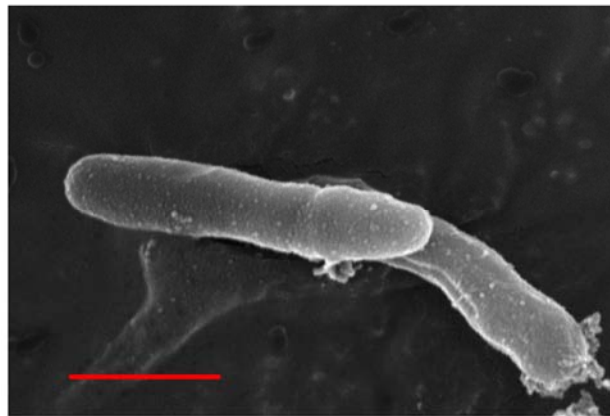


Figure 1.1.1 Image of two isolated *Mycobacterium kansasii* bacilli obtained by scanning electron microscopy. Bar size 1 μm .

The principal features that characterize the genus *Mycobacterium* are:

- Acid-fastness: Mycobacteria have a specific cell wall composition, rich in lipids, that confer them resistance to decolorization with acids. This means that mycobacteria can be identified by a staining technique that comprises an acid decolorization step, as Ziehl-Neelsen or Auramine-Rhodamine staining (Abe, 2003).
- Mycolic acids: Long fatty acids found in the cell wall. There are 7 types of mycolic acids, and the different pattern of expression of these in the cell wall facilitates the classification of mycobacteria species (Rogall et al., 1990; Laval et al., 2001).
- High G-C content: In their DNA mycobacteria have a content of cytosine and guanine between 61-71% (Lévy-Frébault and Portaels, 1992).

The genus *Mycobacterium* contains important human pathogens, such as *Mycobacterium tuberculosis*, *Mycobacterium leprae* and *Mycobacterium ulcerans*. *M.*

tuberculosis is the etiological agent of tuberculosis but there are other mycobacteria genetically related that can cause this disease, as *Mycobacterium africanum*, *Mycobacterium bovis* and *Mycobacterium canetti*. These bacteria represent what it is called *Mycobacterium tuberculosis* complex.

M. tuberculosis infects one-third of the world population and the World Health Organization (WHO) reported 1.7 million of deaths in 2016 due to tuberculosis (WHO, 2017). This disease is widely spread, but as many infectious diseases, it affects mostly undeveloped countries (Figure 1.1.2).

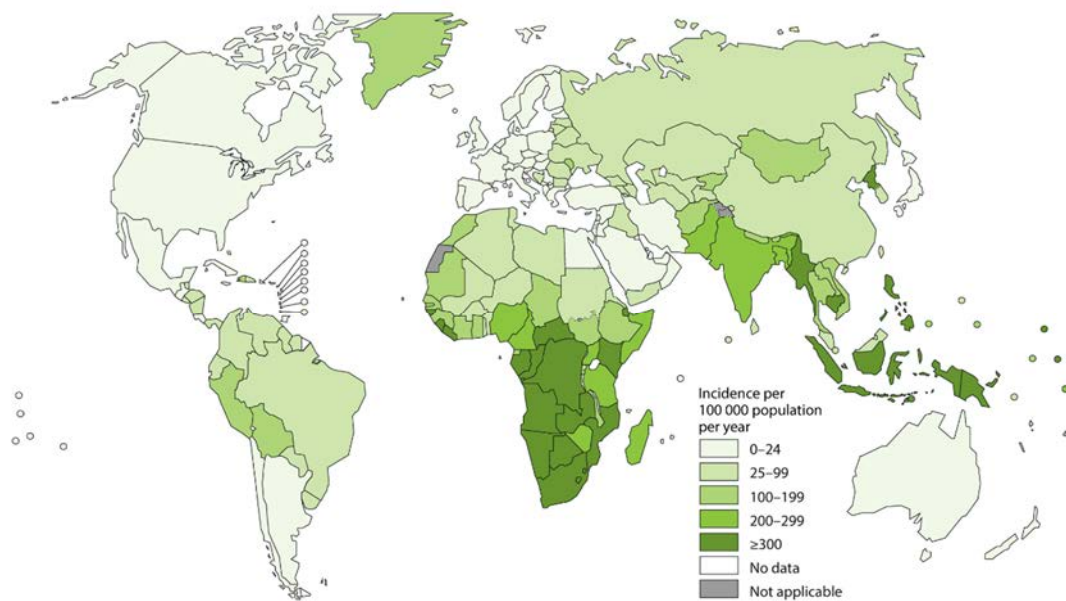


Figure 1.1.2 Estimated tuberculosis incidence rate in 2016. Obtained from the WHO Global Tuberculosis Report 2017.

Tuberculosis is mainly a respiratory disease and the principal symptoms are cough with sputum (and in the worst cases containing blood), chest pain, fever, night sweats and weight loss. *M. tuberculosis* start an infection in the lungs. When the pulmonary cells identify the bacteria, they induce the production of a granuloma, an aggregation of cells from the immune system, to surround and erase *M. tuberculosis*. However, these bacilli can avoid destruction by host's immune system and can use granuloma to produce latent infection (Philips and Ernst, 2012). Inside the granuloma, cells are induced to die and this necrotic material can fill pulmonary cavities (Figure 1.1.3). Granuloma formation and infection *per se* induce pulmonary tissue destruction that later is replaced with fibrotic material, and this repaired tissue has no capacity of

air exchange. All of this leads to a high damage of the lungs that affect host respiratory system (Draper and Daffé, 2005). Pulmonary tuberculosis is explained in more details in point 1.2.

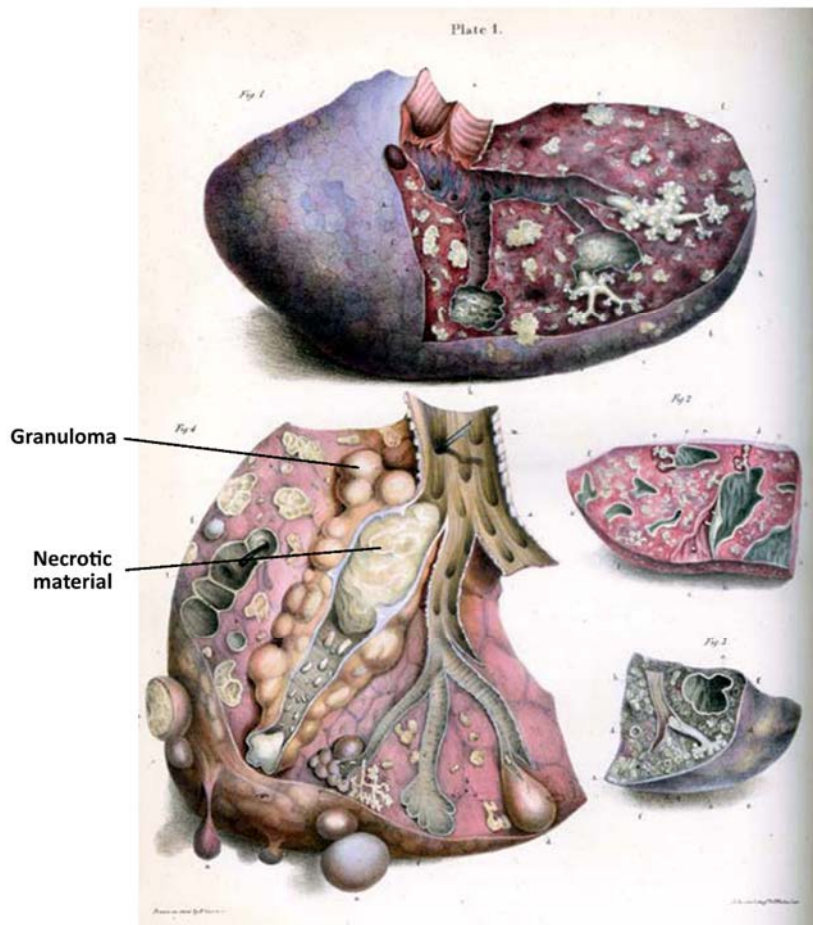


Figure 1.1.3 Robert Carswell's illustration of a tuberculous lung, obtained from Good and Cooper, 1835.

M. tuberculosis can also cause extrapulmonary tuberculosis, that can have the following manifestations:

- Tuberculous lymphadenitis: Is the most frequent derived disease. Consist of an inflammation or enlargement of lymph nodes, being cervical adenopathy the most common.
- Skeletal tuberculosis: When involving the spine, an infection is produced in the vertebral body that brings to a destruction of the intervertebral disc and adjacent vertebrae. When the affectation is articular, it produces an arthritis of the hip or knee with slow progression.

- Pleural tuberculosis: Characterized by cough, pleuritic chest pain, fever or dyspnea. It can be resolved without therapy, but tuberculosis may recur.

- Central nervous system tuberculosis: When it happens, the most common manifestation is tuberculous meningitis. A tubercle is formed in the lateral ventricles of the brain. If it breaks, it produces an intense inflammation of the meninges that can lead to stupor or coma.

- Miliary tuberculosis: Progressive and disseminated form of tuberculosis, characterized by tiny lesions. Chest radiographies show a pattern of tiny spots (1-5 mm) distributed through all the lung.

The cases of extrapulmonary tuberculosis have raised since the epidemic by human immunodeficiency virus. An affected immune system can fail in containing *M. tuberculosis* in the lungs, letting it spread to all body (Golden and Vikram, 2005).

In addition to the species that are part of the *Mycobacterium tuberculosis* complex, the genus *Mycobacterium* contains more than 170 species that inhabit the environment (Figure 1.1.4). Some of them are important re-emerging opportunistic pathogens causing lung diseases and extrapulmonary infections (Primm et al., 2004; Falkinham III, 2009, 2013; van der Werf et al., 2014). The overall prevalence of lung disease related to nontuberculous mycobacteria (NTM) is increasing worldwide and is caused by *Mycobacterium avium* complex, *Mycobacterium kansasii*, and increasingly, *Mycobacterium abscessus*, which is the NTM species most commonly implicated in human pulmonary disease (McShane and Glassroth, 2015; Brown-Elliott, 2016; Koh et al., 2017). Similarly to *M. tuberculosis*, *M. abscessus* induces the production of granulomas and persists inside these, developing caseous lesions in pulmonary tissue (Medjahed et al., 2010). The term “caseous” goes for the aspect of the granuloma, as the necrosed center looks like white cheese. *M. abscessus* pulmonary infections are of special importance in patients with underlying respiratory diseases such as bronchiectasis and cystic fibrosis (McShane and Glassroth, 2015; Brown-Elliott, 2016; Koh et al., 2017). In some of these patients, the therapeutic treatment is ineffective, and they experience chronic infections for long periods of time, frequently with a fatal outcome.

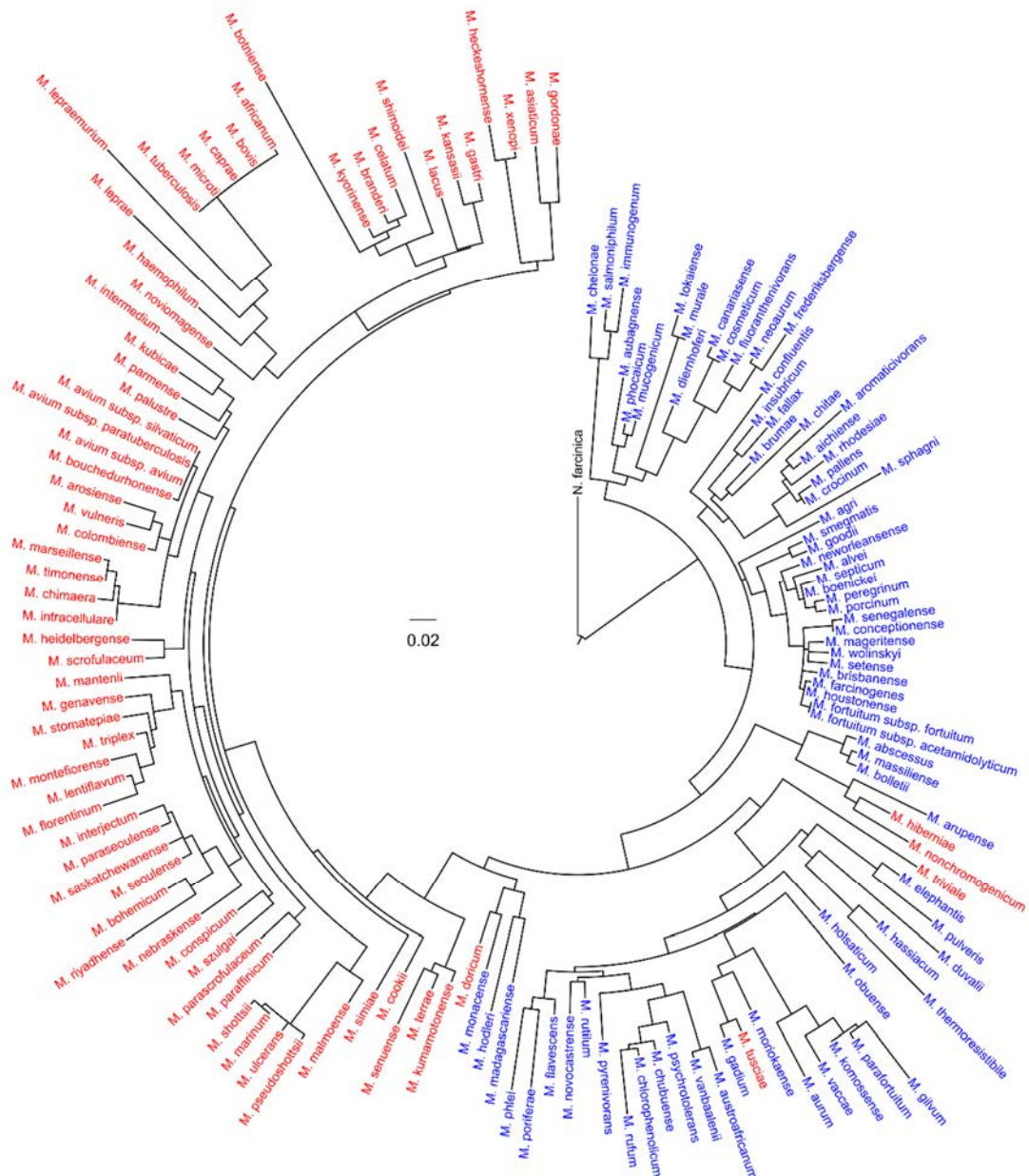


Figure 1.1.4 Phylogenetic tree of *Mycobacterium* genus rooted with *Nocardia farcinica*. Obtained from Dai et al., 2011. In blue are represented rapidly growing mycobacteria and in red, slowly growing mycobacteria. The scale bar is equivalent to 0.02 substitution/site.

As it is seen in figure 1.1.4, mycobacteria can be classified depending on the speed of growth. When colonies appear between 3 days and 1 week, bacteria are considered fast growing, as it is the case of *M. abscessus*, *Mycobacterium smegmatis* or *Mycobacterium vaccae*. However, when colonies are not seen until 3 weeks of growth, bacteria are classified as slow growing, like *M. tuberculosis*, *M. bovis* or *M. kansasii*.

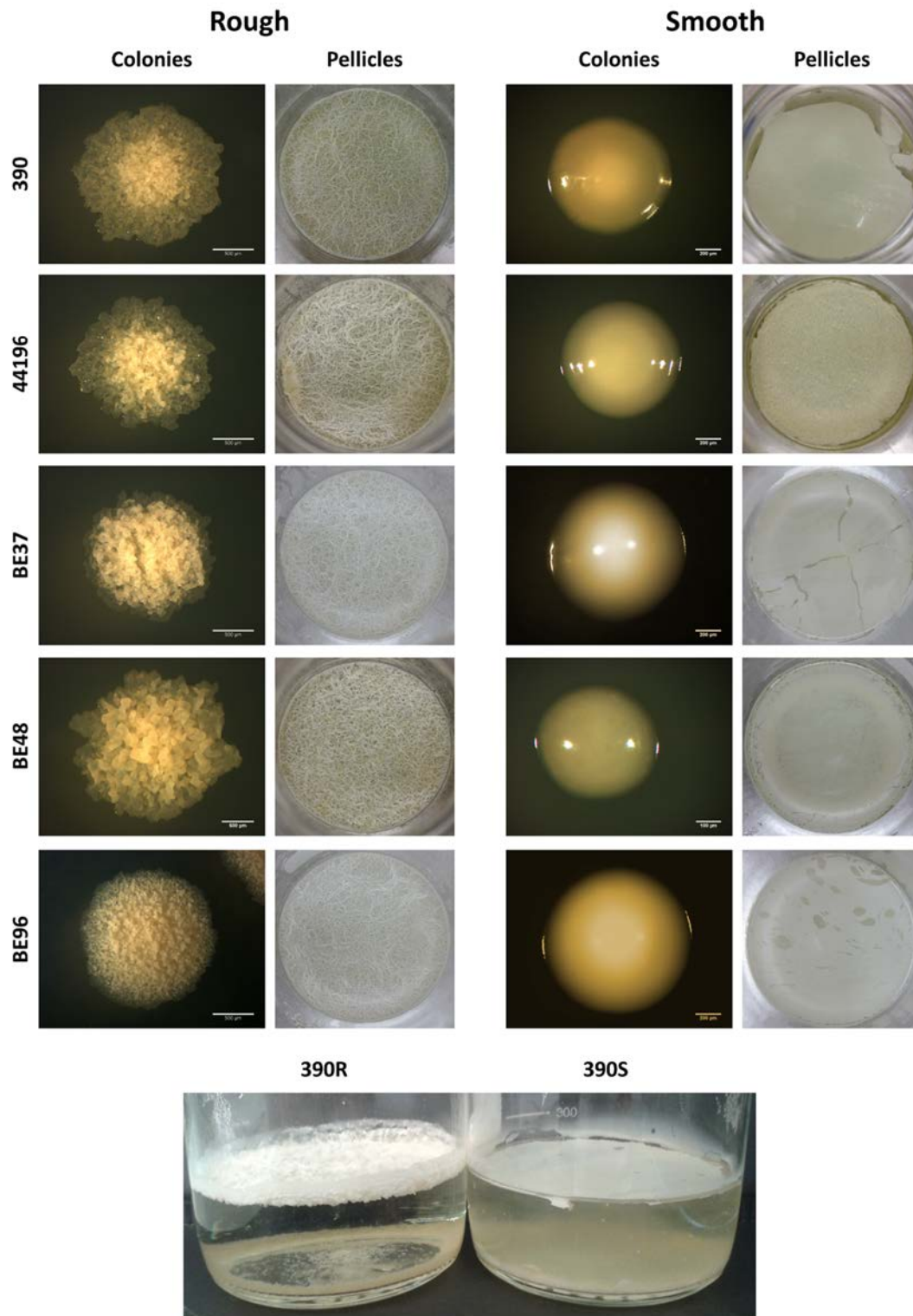


Figure 1.1.5 Colony morphology and pellicle aspect of different strains of *M. abscessus* with their two morphotypes separated. For colonies images bar size 500 μm in all R morphotypes and 200 μm in S morphotypes, except for BE48S with a bar size of 100 μm . At the bottom of the figure there is an example of the planktonic growth in S morphotypes, totally absent in R morphotypes.

Mycobacterial strains display different colony morphologies when grown in solid media. Rough colonies (R) are characterized by an irregular dry surface with many wrinkles and crests, whereas smooth colonies (S) show an even, bright and moist texture (Belisle and Brennan, 1989; Muñoz et al., 1998; Rüger et al., 2014) (Figure 1.1.5, Table 1.1.1). *M. tuberculosis* has a highly conserved R morphotype, whereas non-tuberculous mycobacterial species show both morphotypes, and spontaneous S to R and R to S morphology shifts have also been described (Byrd and Lyons, 1999; Howard et al., 2006; Agustí et al., 2008; Park et al., 2015).

Bacilli of some mycobacterial species, when grow in liquid culture display a strong propensity to attach to each other forming pellicles at the air-liquid interface with a variety of microscopic as well as macroscopic multicellular structures (Julián et al., 2010). Pellicles formed by R morphotypes are thick and wrinkled, while S morphotypes produce thin pellicles with a flat surface (Figure 1.1.5, Table 1.1.1). It is of importance distinguish between *Biofilm* and *Pellicle*. A biofilm is considered a bacterial growth attached to a solid surface, while a pellicle is a bacterial growth floating on the surface of a liquid culture media (Zambrano and Kolter, 2005).

Another phenotypic difference between R and S morphotypes is that R morphotypes show increased cellular aggregation. The bacilli of R morphotypes remain attached during replication, forming compact colonies containing structures that resemble cords (Howard et al., 2006; Agustí et al., 2008). These structures were described for the first time by Robert Koch in *M. tuberculosis* (Koch, 1882). In liquid media, R morphotypes aggregate to form clumps, and large clumps acquire cord morphologies (Julián et al., 2010; Sánchez-Chardi et al., 2011; Brambilla et al., 2012) (Figure 1.1.6, Table 1.1.1). In contrast, no bacillar organization is detected in S morphotypes (Figure 1.1.7, Table 1.1.1). Cords are snake-like structures that are formed through end-to-end and side-to-side aggregation of bacilli, in which the orientation of the long axis of each cell is parallel to the long axis of the cord (Julián et al., 2010). In *M. abscessus*, cording was described for the first time in the 390R strain as well as the lack of cording of the related 390S morphotype (Howard et al., 2006).

Clumps and cords are not laboratory artefacts, as the presence of the clumps and cords of *M. abscessus* and *Mycobacterium marinum* have been reported in zebrafish (Clay et al., 2008; Bernut et al., 2014). Furthermore, the presence of *M. bovis* BCG cords

in the cytoplasm of macrophages and the dendritic cells of mouse splenic granulomas (Ufimtseva, 2015) and clumps of *M. abscessus* in the sputum of patients with cystic fibrosis have been reported (Qvist et al., 2013).

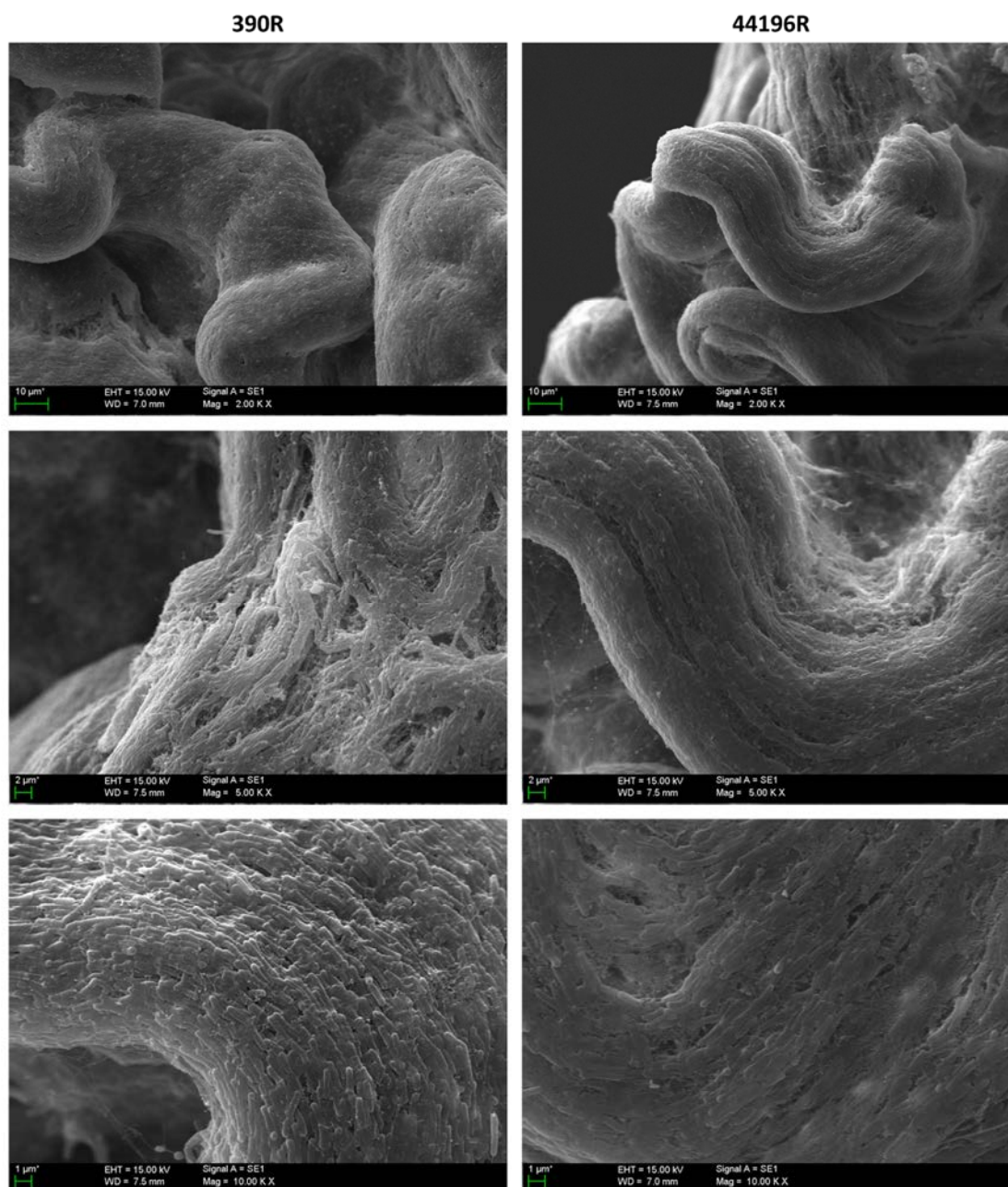


Figure 1.1.6 SEM microographies of 390R and 44196R *M. abscessus* strains, where it is possible to observe cord formation. Bar size 10 µm (first row), 2 µm (second row), 1 µm (third row).

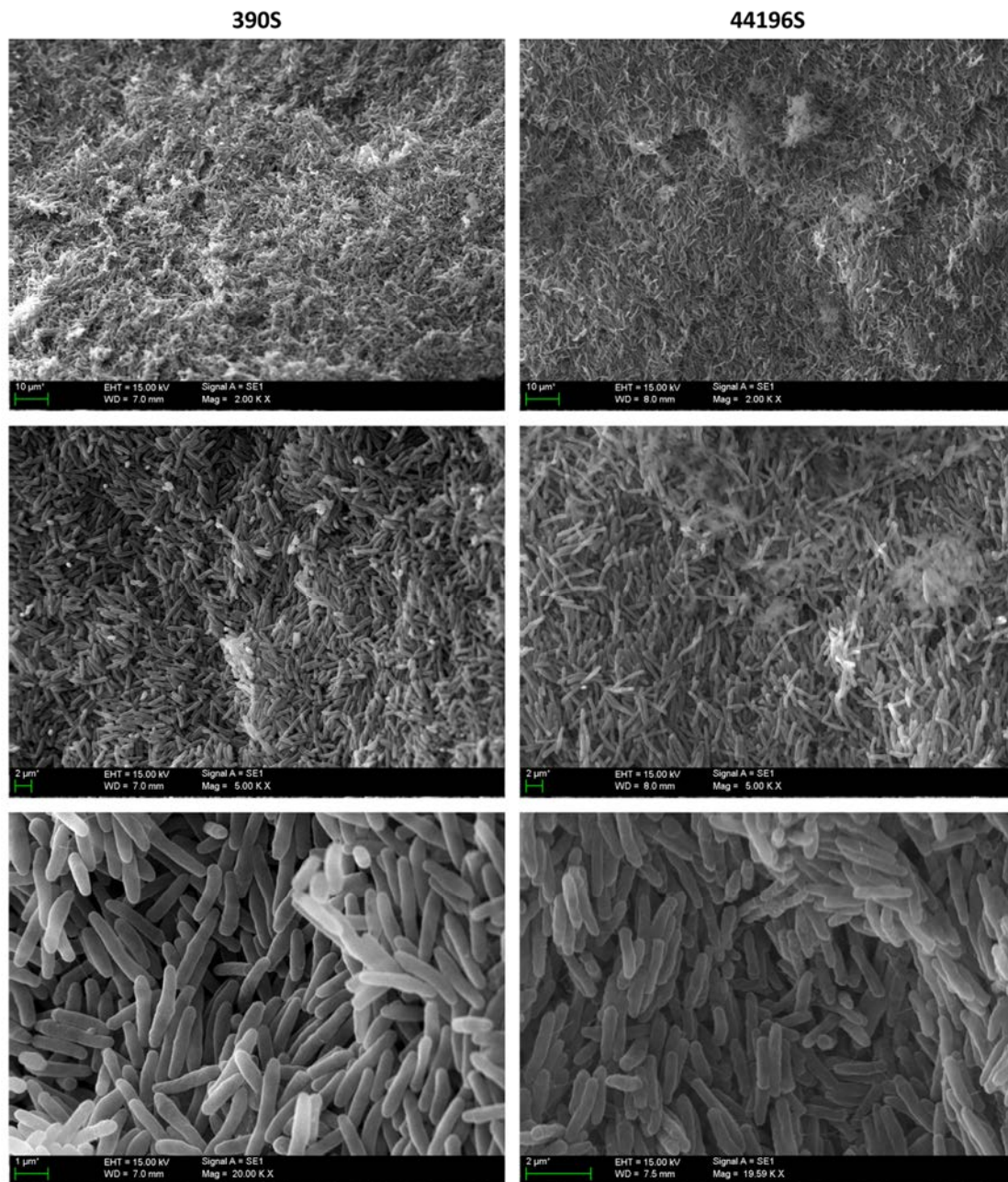


Figure 1.1.7 SEM micrographies of 390S and 44196S *M. abscessus* strains. In this case no organization of the bacilli is observed. Bar size 10 μm (first row), 2 μm (second row), 1 μm (third row).

Table 1.1.1 Phenotypic feature of the different morphotypes found in mycobacteria

	Colony	Pellicle	Cord formation
R morphotype	Rough	Thick	+
S morphotype	Smooth	Thin	-

Various studies have reported that R morphotypes produce the most severe illness in humans. As said before, *M. tuberculosis* has a highly conserved R morphotype. However, there is a species called *Mycobacterium canettii*, also referred to as “smooth tubercle bacilli”, that is closely related to *M. tuberculosis* and exhibits an S morphotype. In contrast to *M. tuberculosis*, isolates of *M. canettii* are rare and restricted to some regions of Africa. A recent study reported the increased virulence of a spontaneous R morphotype of *M. canettii* versus the wild S morphotype (Boritsch et al., 2016).

For the NTM there are different studies where the R morphotypes of *M. avium*, *M. kansasii* and *M. abscessus* are shown to be more virulent than the S morphotypes (Belisle and Brennan, 1989; Kansal et al., 1998; Catherinot et al., 2007). In a study from 2015, Park et al. analyzed 50 serial isolates from nine patients with persistent *M. abscessus* infections for 8 years, on the basis of colony morphology (Park et al., 2015). The authors found that R isolates predominated at later times during the disease. In 6 out of the 9 patients, the colony morphology of the serial isolates was initially S before becoming predominantly R. Serial isolates from the other 3 patients showed R colony morphology throughout the course of the disease.

The increasing clinical importance of *M. abscessus* has piqued the interest of several groups of researchers who have developed different animal models with which to study the pathogenesis of this species (for a recent review, see Bernut et al., 2017). In these studies, R morphotypes have been found to be hyperlethal for mice and zebra fish embryos, whereas S morphotypes are unable to produce infection (Byrd and Lyons, 1999; Howard et al., 2006; Bernut et al., 2014; Roux et al., 2016).

The observations from human and animals indicate that the ability to switch between S and R morphotypes allows *M. abscessus* to transition between a colonizing phenotype and a more virulent, invasive form.

Also related with these two morphotypes, the formation of very wrinkled pellicles at the air-liquid surface has been related with a major hydrophobicity and virulence in *M. tuberculosis* strains. This bacterium seems to be able to modulate the proportion of less polar lipids in the outer part of the cell wall. When this proportion increase *M. tuberculosis* became more hydrophobic rising the chances of being transmitted by aerosol (Jankute et al., 2017).

And the last phenotypic feature, cord formation, has also been described as a virulence factor. Middlebrook in 1947 defined the relationship between virulence and cord formation in *M. tuberculosis*. He described that cord formation is a factor that condition the capacity of bacteria to spread on the surface of liquid and solid media. He also described that the avirulent bacilli were devoid of oriented growth (Middlebrook et al., 1947). Later, various studies performed with natural and constructed mutants of *M. tuberculosis* have confirmed this correlation (for a review, see Glickman 2008).

Recently, Brambilla et al. related clumps of cording morphology to virulence in *M. abscessus* (Brambilla et al., 2016). In that study was shown that both morphotypes of *M. abscessus* were able to grow inside macrophages but exhibited distinct behaviors. Phagosomes of macrophages infected with R morphotypes contained more than one bacillus at 3 hours post-infection (h.p.i), and of those, up to 30% of phagosomes contained clumps of more than 5 bacilli. In contrast, phagosomes of macrophages infected with S morphotypes contained mainly isolated bacilli (Brambilla et al., 2016). Other studies support these results (Byrd and Lyons, 1999; Roux et al., 2016). At 48-72 h.p.i, macrophages infected by Brambilla and collaborators with R morphotypes were destroyed, thus releasing large clumps of bacilli outside the cells; however, macrophages infected with S morphotypes were unaffected (Figure 1.1.8).

Bernut et al. used zebra fish embryos to visualize extracellular clumps, which grow extensively forming cords that were unphagocytatable for macrophages and neutrophils promoting rapid larval death (Bernut et al., 2016b). In this model, the S morphotype was unable to produce infection. In addition, the same group produced an R mutant defective in cording that exhibited impaired replication in zebra fish (Halloum et al., 2016).

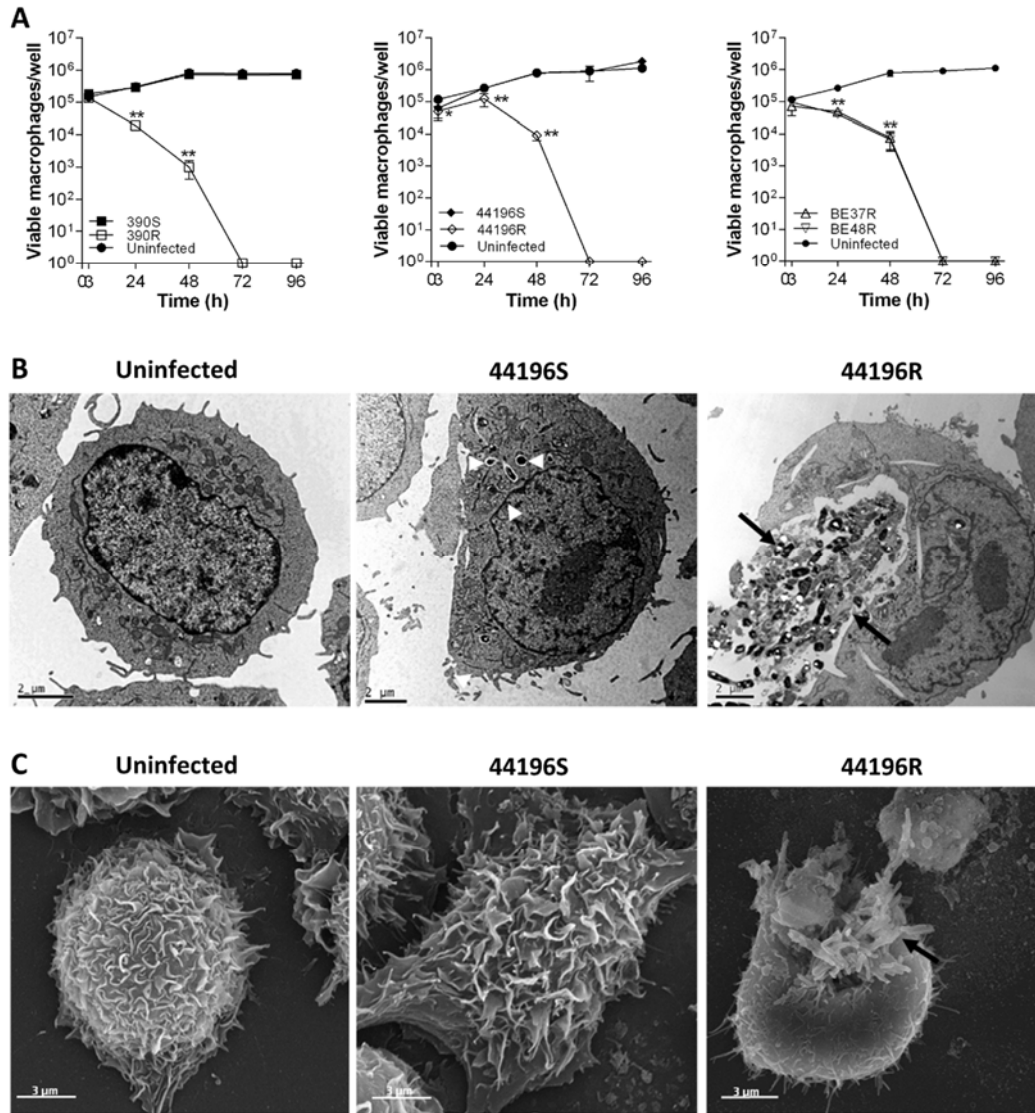


Figure 1.1.8 Adapted from Brambilla et al., 2016. **A** Viability of macrophages infected with *M. abscessus* strains. **B** Transmission electron microscopy images of macrophages uninfected and infected with the different morphotypes of *M. abscessus* DSMZ 44196. Bar size 2 μ m. **C** Scanning electron microscopy images of the same conditions. Bar size 3 μ m. White arrows indicate isolated bacilli, black arrows indicate bacterial clumps.

So, most features and virulence are related with clump formation. Bacteria aggregate and produce clumps that become cords. This organization is observed macroscopically as rough colonies or wrinkled pellicles. And these phenotypes are related with a higher virulence. This means that understanding how bacteria aggregate will help in tuberculosis treatment.

1.2. Pulmonary tuberculosis

Lungs are the principal organ affected by mycobacteria. When breathing, air achieves the lower respiratory track passing through the trachea, and branches into the bronchi and bronchioles. From there, air is conducted to the respiratory zone, composed by alveolar ducts that end by microscopic alveoli (Figure 1.2.1). The gas exchange necessary for the respiration will take place in these terminal alveoli (Drake et al., 2009).

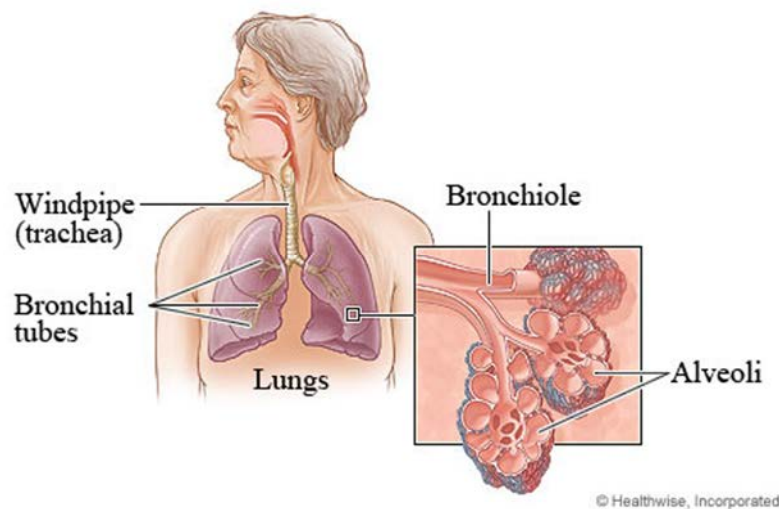


Figure 1.2.1 Picture obtained from the website of Alberta Health Service, Canada

Alveolar epithelial cells and alveolar macrophages are the first cells to encounter causative agents of pulmonary diseases, as they are *M. tuberculosis* and *M. abscessus*. The human lung is comprised of approximately 40 cell types, but the alveolar epithelium is composed mostly by type I and type II pneumocytes, which are disposed forming a cell layer that acts as a barrier (Castranova et al., 1988) (Figure 1.2.2). Initially it was considered that, once inhaled, *M. tuberculosis* was transported to the bloodstream by alveolar macrophages and blood monocytes. But later it was described that *M. tuberculosis* was capable of invade and survive inside human type II alveolar epithelial cells (Lin et al., 1998; Bermudez et al., 2002). Inside alveolar epithelial cells mycobacteria would divide faster than inside macrophages and this overgrowth would result in cell death and bacterial dissemination (Dobos et al., 2000). *M. tuberculosis* invade alveolar epithelial cells by macropinocytosis. However, it has also been

described that these pulmonary cells can internalize non-pathogenic mycobacteria by the same mechanism (García-Pérez et al., 2008).

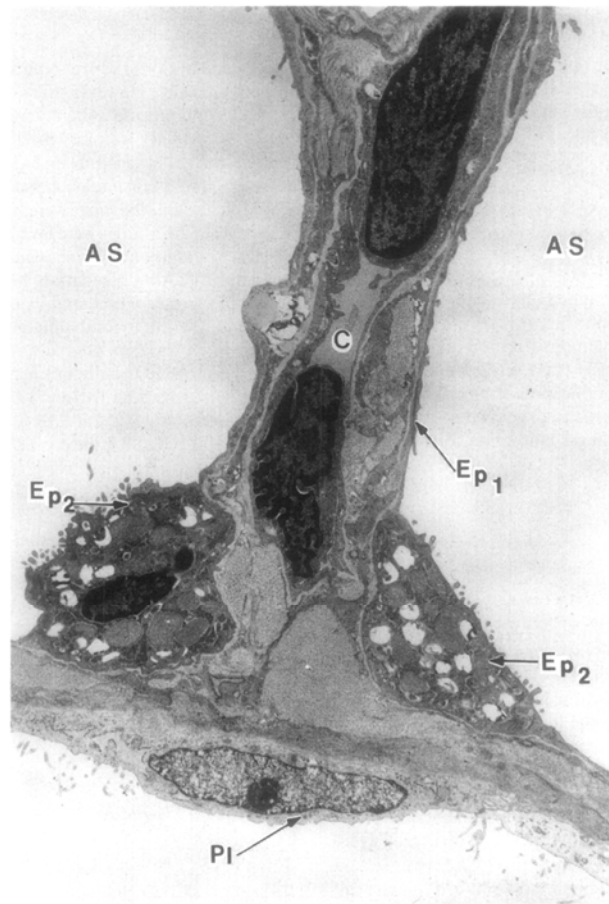


Figure 1.2.2 Micrograph of the alveolar septal region of a rat lung (x3200). Obtained from Castranova et al., 1988. AS (alveolar air space), C (pulmonary capillary), Ep1 (type I epithelial cell), Ep2 (type 2 epithelial cell), PI (visceral pleura).

Mycobacteria are intracellular pathogens, but they have two mechanisms to enter different cell type:

- **Phagocytosis:** Characteristic of cells from the immune system, specially macrophages. Phagocytic cells recognize mycobacteria by pathogen-associated molecular patterns. Receptors in charge of this recognition active intracellular signaling pathways that induce actin polymerization and formation of the phagocytic cup. Phagosome is formed when the phagocytic cup encloses and then it starts its maturation (Figure 1.2.3). During this process, the protein and lipid composition of the phagosome is constantly changing. The first stage after the closure of the phagocytic cup is *early phagosome* (around 10 min after uptake). This vesicle lacks the proton pumping vesicular ATPase, so it is

characterized by a slightly acidic pH between 6-6.5. The maturation of the phagosome leads to the formation of *late phagosomes* (10-30 min). This process involves the acquisition of lysosome-associated membrane proteins and newly synthesized lysosomal enzymes. These molecules have anti-bacterial activity. Vesicular ATPase is collected to function in the late phagosomal membrane, acidifying the lumen pH around 5. The last step of the phagocytosis is the formation of the *phagolysosome* (later than 30 min) by phagosome and lysosome fusion, a vesicle with pH of 4-4.5 (Weiss and Schaible, 2015). Mycobacteria can interfere with phagosomal maturation and leave the vesicle in early phagosome properties, with an almost neutral pH (Rohde et al., 2007).

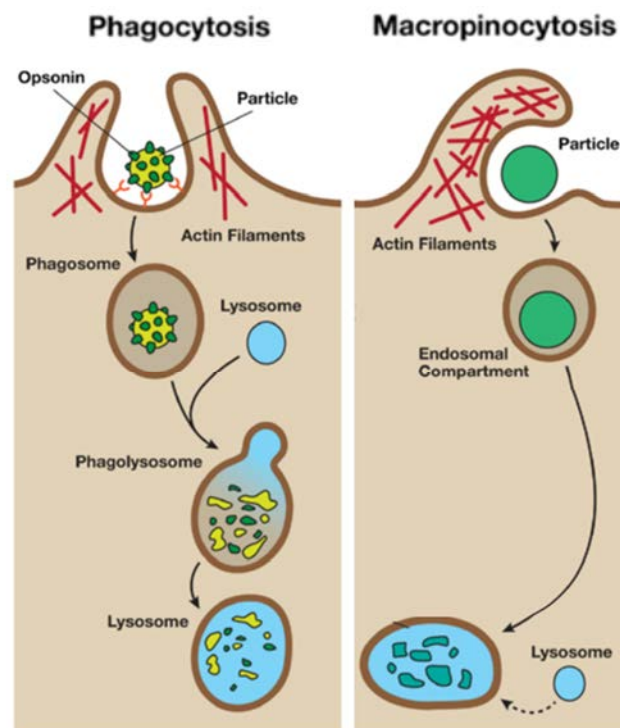


Figure 1.2.3 Schematic representation of phagocytosis and macropinocytosis. Adapted from Stern et al., 2012.

- **Macropinocytosis:** This process is also signal-dependent and involves actin-mediated membrane ruffling. The difference with phagocytosis is that it consists of a fluid phase uptake mechanism (Figure 1.2.3). Phagocytic and non-phagocytic cells use macropinocytosis to internalize particles and fluid, and the process is activated by growth factors or phorbol esters. The content of the macropinosome can merge with the lysosomal compartment, but is not the usual fate of these vesicles (Lim and Gleeson, 2011; Stern et al., 2012). However,

M. tuberculosis and *M. smegmatis* can activate macropinocytosis, stimulate fluid phase uptake, to be internalized into alveolar epithelial cells (García-Pérez et al., 2008).

Once in the alveolar cavity mycobacteria find approximately 30 type II alveolar epithelial cells for each alveolar macrophage (Bermudez et al., 2002). This proportion permits to assume that alveolar epithelial cells will have an interaction with the mycobacteria. By producing chemokines, these epithelial cells are related with the initiation of the acute inflammatory response to microbial pathogens (Lin et al., 1998).

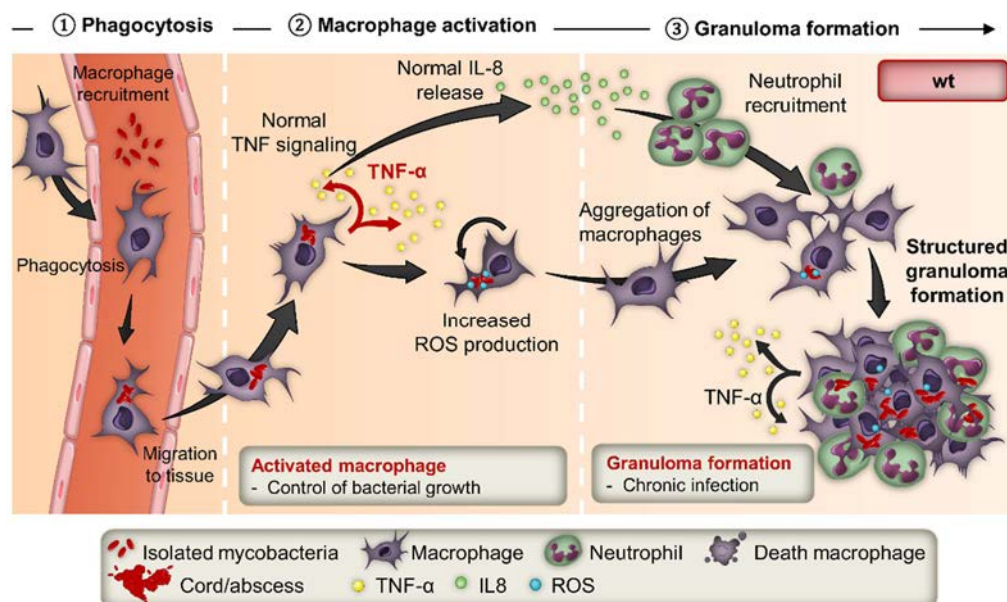


Figure 1.2.4 Schema of granuloma formation obtained from Bernut et al., 2016a.

Pulmonary tuberculosis, and the extrapulmonary form of the disease, evolve in granuloma formation. This process starts with mycobacterial phagocytosis. Macrophages with bacteria inside travel to the bloodstream and migrate to the tissue, where they start their activation. Invaded macrophages produce tumor necrosis factor α (TNF- α) as a signal to activate more macrophages, recruit other immune system cells and prevent bacillar activation (Bernut et al., 2016a) (Figure 1.2.4). Granuloma is composed by monocyte derived cells and antigen-specific T lymphocytes that are recruited to the area of infection. The recruitment of these cells is related to the immune response in which chemokine production by alveolar epithelial cells also plays

an important role (Wickremasinghe et al., 1999). This means that interaction between alveolar epithelial cells and pathogenic mycobacteria may have an important contribution to the pulmonary disease.

It has been found that respiratory epithelial cells secrete chemokine interleukine-8 (IL-8) after the infection of pathogenic respiratory bacteria (DiMango et al., 1995; Méndez-Samperio et al., 2006). There are four subgroups of chemokines based on structural criteria, and the major subgroup are the CXC chemokines (Zlotnik and Yoshie, 2000). IL-8 is a CXC chemokine, produced by alveolar epithelial cells that induce the attraction of neutrophils to the inflammatory infiltrate contributing to the neutrophilic inflammatory response (Hoheisel et al., 1994; Lin et al., 1998; Kim et al., 2011). This chemokine also attracts T lymphocytes and monocytes (Wickremasinghe et al., 1999; Méndez-Samperio et al., 2006). IL-8 has been found in bronchoalveolar lavage fluid of patients with pulmonary tuberculosis, where there is also a high presence of neutrophils, in proportion with the amount of this chemokine (Zhang et al., 1995).

However, alveolar epithelial cells infected with *M. tuberculosis* do not produce TNF- α , IL-10 nor IL-12 p40 (Lin et al., 1998). Also, the production of IL-8 in response to the infection by *M. tuberculosis* do not depend on the production of TNF- α , IL-1 β or IL-6, indicating that IL-8 production is part of the initial inflammatory response. Still, Wickremasinghe et al. described the role of IL-1 as a mediator in immune response to pulmonary tuberculosis showing the release of IL-8 by epithelial cells induced by IL-1. Also in Wickremasinghe et al., they demonstrated that alveolar epithelial cells produce higher concentrations of IL-8 induced by monocytes that have phagocytosed *M. tuberculosis* than the concentrations induced by the presence of *M. tuberculosis* (Wickremasinghe et al., 1999). This reaffirms the participation of alveolar epithelium cells in host immune response. In the earliest stages of the infection, this low quantity of IL-8 produced by alveolar epithelium cells will recruit the neutrophils and T lymphocytes to start the response to the infection.

The release of IL-8 has also been described as an effect of the activation of toll-like receptors (TLR). For that reason, the presence of this cytokine in a cell culture supernatant can be a signal of TLR stimulation by the pathogen present in the culture (Davidson et al., 2011). TLR are a family of pattern recognition receptors present on

macrophages, dendritic cells and respiratory epithelial cells that mediate the host innate immune response by recognizing pathogen-associated molecular patterns (Underhill et al., 1999).

Alveolar epithelial cells can express up to 11 TLR on the cell surface (Garcia-Perez et al., 2012). Means et al. demonstrated in 1999 that two distinct members of the TLR family mediated cell activation and cytokine production when macrophages were infected with *M. tuberculosis* (Means et al., 1999a). TLR2 and TLR4 seem to be key receptors for the recognition of mycobacterial antigens and activation of macrophages and other cells of innate immunity (Heldwein and Fenton, 2002; Stenger and Modlin, 2002).

Type II epithelial cells are responsible also to secrete surfactant proteins A and D (Ferguson et al., 2006; Sequeira et al., 2014). Pulmonary surfactant is a multimolecular complex responsible to reduce the surface tension of the alveoli. This allows the expansion of the lung during inspiration and maintain alveolar stability (Li et al., 2012). However, it has been described the implication of pulmonary surfactant in host defense functions against *M. tuberculosis* infection (Gaynor et al., 1995; Ferguson et al., 2006). One of these previous studies has reported that pulmonary surfactant proteins A and D induce the agglutination of *M. tuberculosis* bacilli (Ferguson et al., 2006). Despite proteins, in the pulmonary surfactant there are also phospholipids, and the most abundant is dipalmitoyl phosphatidylcholine (DPPC). This surfactant phospholipid is also secreted by type II epithelial cells (Chimote and Banerjee, 2005).

1.3. Mycobacterial cell wall

Mycobacteria are considered gram-positive bacteria; however, their cell wall is characteristic of their genus and different of what is considered “gram-positive”. The principal difference is the lipid content, in mycobacteria may represents up to 40% of the cell free mass, but in other gram-positive bacteria represents less than 5%.

The interest in knowing the structure of this atypical cell wall has raised because it has been recognized that mycobacterial cell wall components play an essential role in disease pathogenesis. Some drugs used for tuberculosis chemotherapy target the synthesis of various cell wall components (Jankute et al., 2015).

Based on the schema proposed by Zuber et al. (Zuber et al., 2008), mycobacterial cell wall has four differentiated layers (Figure 1.3.1), the common plasma membrane (PM); an electrodense layer (EDL) and an electro-transparent layer (ETL) that compose the cell wall core; and the outer layer (OL). The density of EDL can be related with the possible presence of peptidoglycan in this layer. In contrast, the fact that ETL is removed when bacteria are treated with alkaline hydrolysis indicate that this layer contains lipids (Draper, 1971).

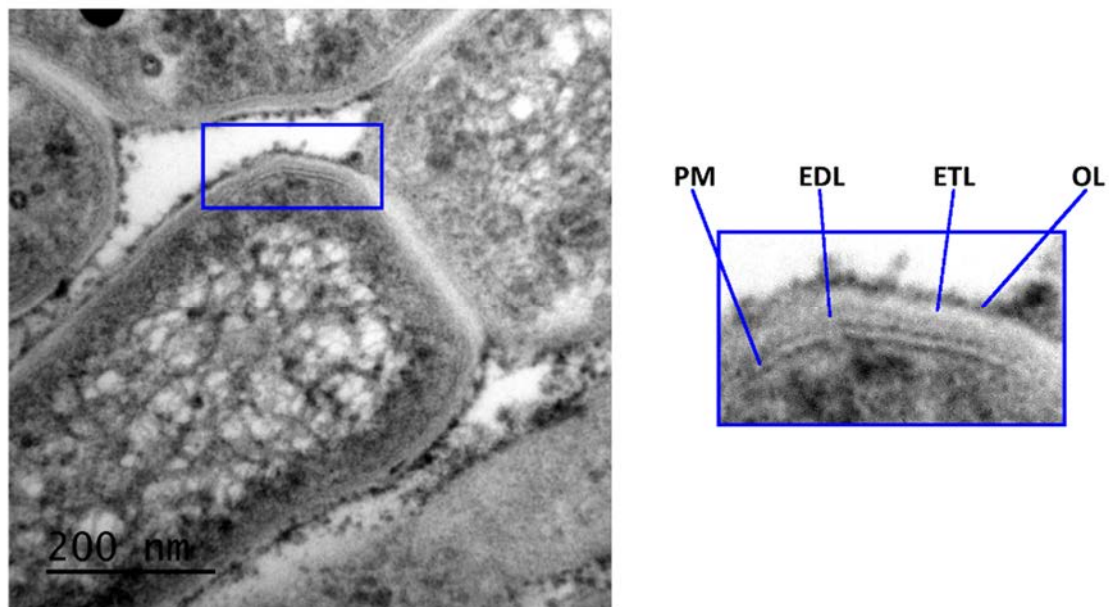


Figure 1.3.1 Image of *M. abscessus* obtained by transmission electron microscopy. A detail of the cell wall is magnified. PM (plasma membrane), EDL (electrodense layer), ETL (electro-transparent layer), OL (outer layer).

It is not 100% known how the different components of the cell wall organize. However, there are many schematic representations of mycobacteria cell envelope that are supposed to be close to the true cell wall organization. One schematic representation of *M. tuberculosis* cell envelope developed by Daffé et al. (Daffé et al., 2014) is shown in Figure 1.3.2.

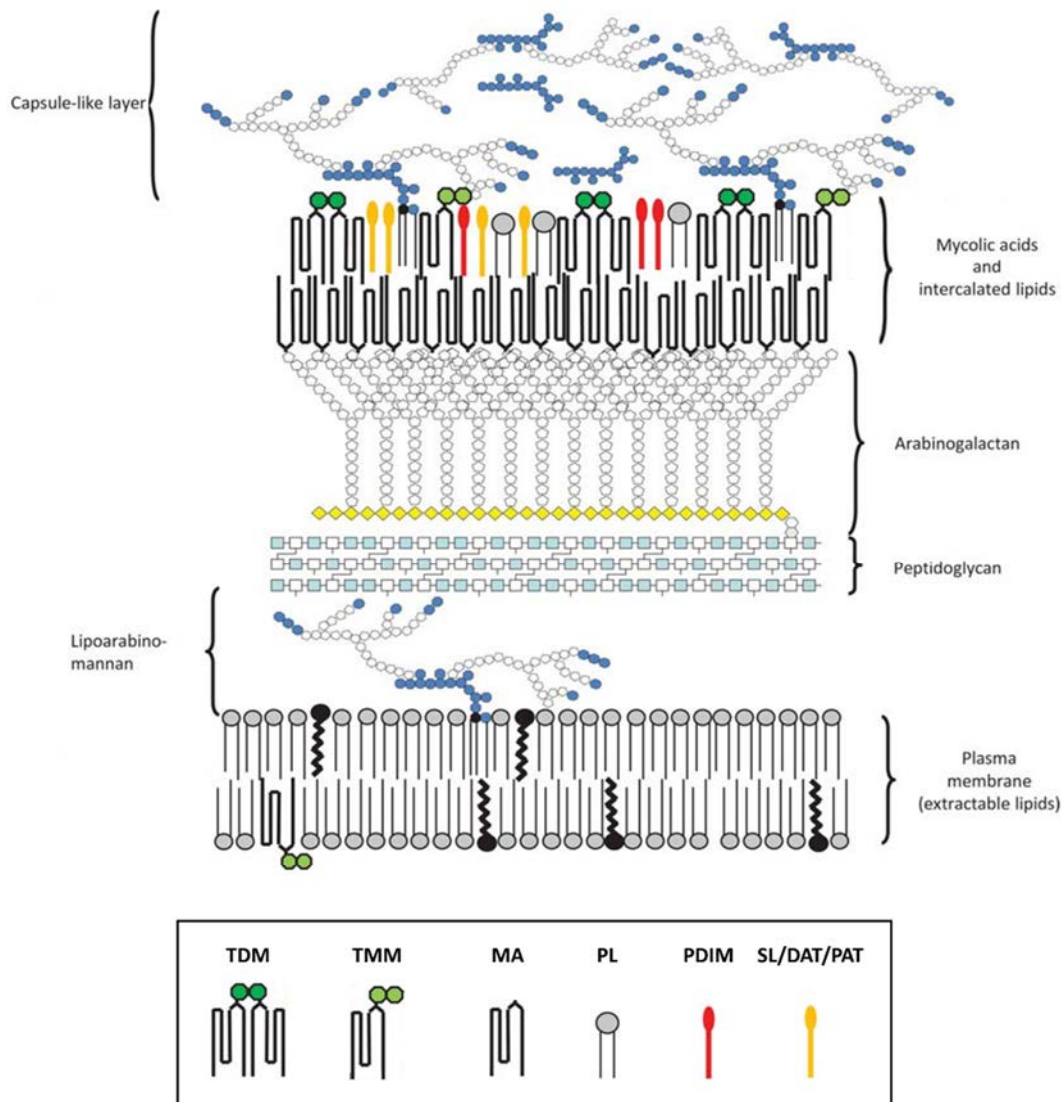


Figure 1.3.2 Schematic representation of *M. tuberculosis* cell envelope. Adapted from Daffé et al., 2014. As the author comment, lipids and glycolipids are represented in probable locations; but proteins and peptides are not shown in this schema. TDM (trehalose dimycolate), TMM (trehalose monomycolate), MA (mycolic acid), PL (phospholipid), PDIM (phthiocerol dimycocerosate), SL (sulfolipid), DAT (diacyltrehalose), PAT (polyacyltrehalose).

Below are detailed the most important compounds found in mycobacteria cell wall. Their description is organized using the differentiated layers shown by Zuber et al. (Zuber et al., 2008) and the schematic organization represented by Daffé et al. (Daffé et al., 2014). However, how the different compounds organize between these compartments seems to be species-dependent (Ortalo-Magné et al., 1996).

Plasma membrane (PM) and periplasm

The main structural lipids of mycobacterial PM are phospholipids (Crellin et al., 2013), amphipathic polar lipids frequently found in PM of all bacteria. Apolar lipids are also found in this compartment, in a small proportion, but their nature remains unknown (Bansal-Mutalik and Nikaido, 2014).

In some mycobacteria has been described a periplasmatic space between PM and EDL (Zuber et al., 2008). Phospholipids can also be detected in the periplasm and in the cell wall core (Figure 1.3.2).

The most important phospholipids from this compartment and found in all Mycobacteria are:

- Phosphatidyl-*myo*-inositol mannosides (PIM): The base of these compounds is a molecule of phosphatidylinositol. In the case of PIM, this molecule carries 1 to 6 mannose residues, generating 6 different types of phospholipid (Figure 1.3.3) (Crellin et al., 2013). PIM are recognized by TLR of innate immune cells. They serve as a pathogen associated molecular pattern activating the production of TNF- α (Jones et al., 2001; Krutzik and Modlin, 2004).
- Lipomannan and Lipoarabinomannan (LM and LAM): In this case, the phosphatidylinositol carries longer mannose polymers, with arabinan modifications, in the case of LAM (Figure 1.3.3). The length of the mannan chain and the degree of branching is species-specific. LM and LAM seem to be anchored to both plasma membrane and cell wall core, and PIM serve as membrane anchors for these phospholipids (Pitarque et al., 2008). LAM has been described also as capable of activating TLR from the immune system (Means et al., 1999b). It has different roles in modulating the immune response.

Inhibits interferon(INF)- γ -mediated activation of macrophages (Sibley et al., 1988); neutralize cytotoxic potential of oxygen free radicals, a known cytotoxic mechanism of active macrophages (Chan et al., 1991); and in some cases can interfere in the production of TNF- α (Roach et al., 1993).

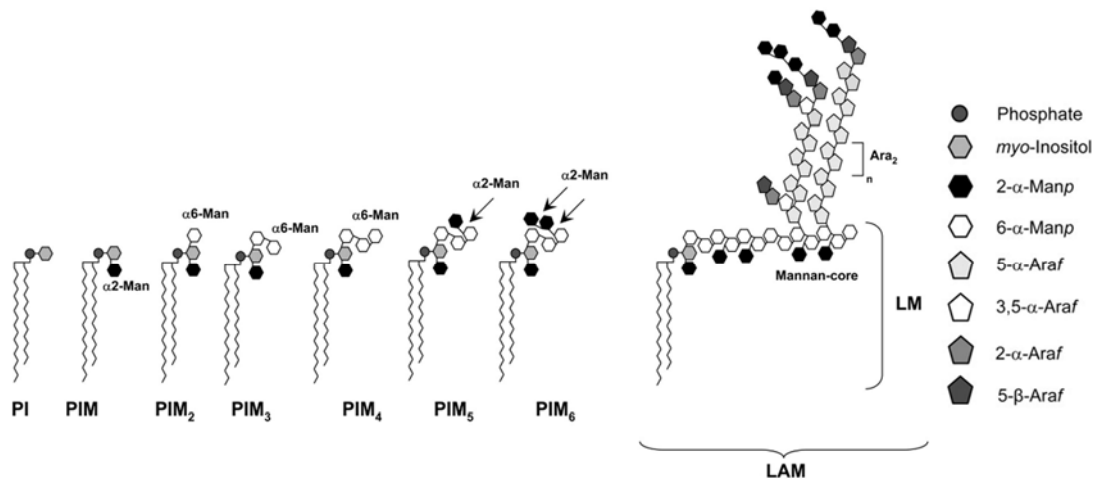


Figure 1.3.3 Structure of *M. tuberculosis* phosphatidyl-myo-inositol mannosides (PIM), lipomannan (LM) and lipoarabinomannan (LAM). Adapted from Torrelles et al., 2006.

Peptidoglycan-arabinogalactan complex zone (EDL)

The inner part of the cell wall core consists of peptidoglycan covalently attached to the heteropolysaccharide arabinogalactan. This second compound is esterified to mycolic acids from the outer part of the cell wall core (Figure 1.3.4).

- **Peptidoglycan (PG):** Consist of a glycan structure with short peptide side chains. This molecule is produced by almost all bacteria, and provides shape, rigidity and osmotic stability. However, mycobacterial PG has a characteristic modification, an oxidation in the glycan structure that is believed to increase PG strength (Jankute et al., 2015).

- **Arabinogalactan (AG):** Macromolecule that contains mostly galactose and arabinose in ring form (furanose), that define the two parts of the molecule, the galactan component and the arabinan component (Figure 1.3.4). AG is highly branched and is covalently attached to PG residues on the galactant

component, and attached to mycolic acids on the arabinan component (Jankute et al., 2015).

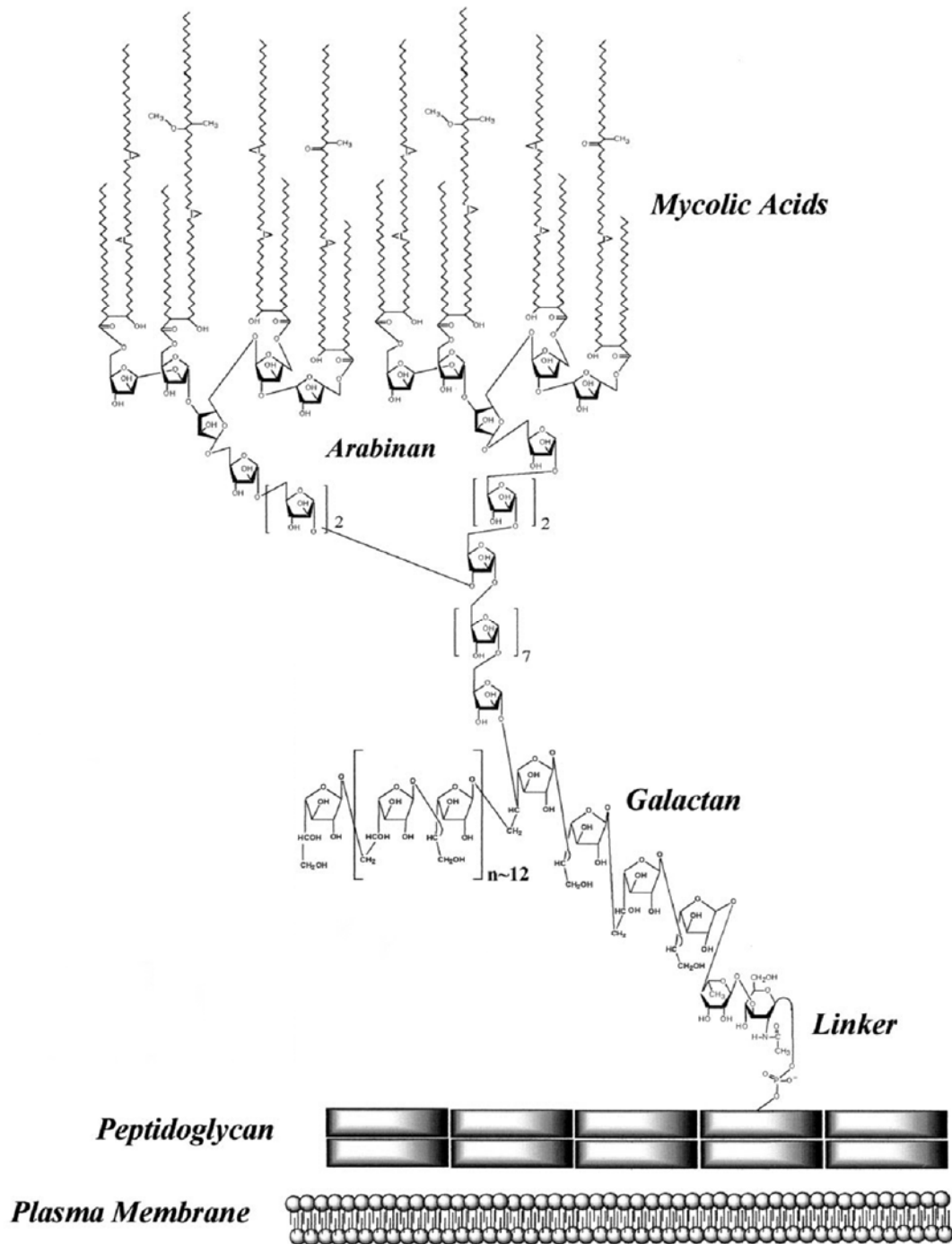


Figure 1.3.4 Structure of arabinogalactan from *M. tuberculosis*. Adapted from Scherman et al., 2003.

Mycolic acids and intercalated lipids zone (ETL)

This part of the cellular envelope is full of mycolic acids and trehalose esters, compounds with rising interest due to their role in host-pathogen interaction (Daffé and Draper, 1998). The outer part of the cell wall core consists on:

- **Mycolic acids:** Fatty acids formed by a long chain, named meromycolic chain (of up to 90 carbons), with α -alkyl residues β -hydroxylated. As explained before, mycolic acids are characteristic molecules of *Mycobacterium* genus, representing major cell envelope components. The chemical groups attached to the meromycolic chain can be diverse, creating different mycolate types (Laval et al., 2001) (Figure 1.3.5). Most mycobacteria produce a combination of different types of mycolic acids, and this feature is used for taxonomic classification (Minnikin et al., 1984). These compounds are found covalently attached to AG or esterifying trehalose and glycerol, where they contribute to the fluidity and permeability of the cell wall. Mycolic acids linked to AG organize with intercalated lipids to form a permeability barrier. This confers to mycobacterial cell wall an extremely low fluidity and permeability, that could be related with the important antibiotic resistance characteristic of mycobacteria (Jarlier and Nikaido, 1990; Liu et al., 1996). Isoniazid is the most efficient antituberculous drug. Its target is mycolic acid biosynthesis pathway, opening the door to other antibiotics (Laval et al., 2001). This low permeability also affects nutrient uptake, and that would be the reason of a slowing growth in mycobacteria. Variations in the mycolate composition can have an effect in the physiology and virulence of the mycobacteria. As an example, Dubnau et al. constructed an *M. tuberculosis* mutant deficient in the production of oxygenated mycolic acids (keto- and methoxymycolate). This mutant had important affectations in its cell wall permeability and showed an attenuated pattern when infecting mice (Dubnau et al., 2000). Another example is the one presented by Halloum et al., where they generated an *M. abscessus* mutant with an altered production of α -mycolate that showed a decrease in cord formation (Halloum et al., 2016).

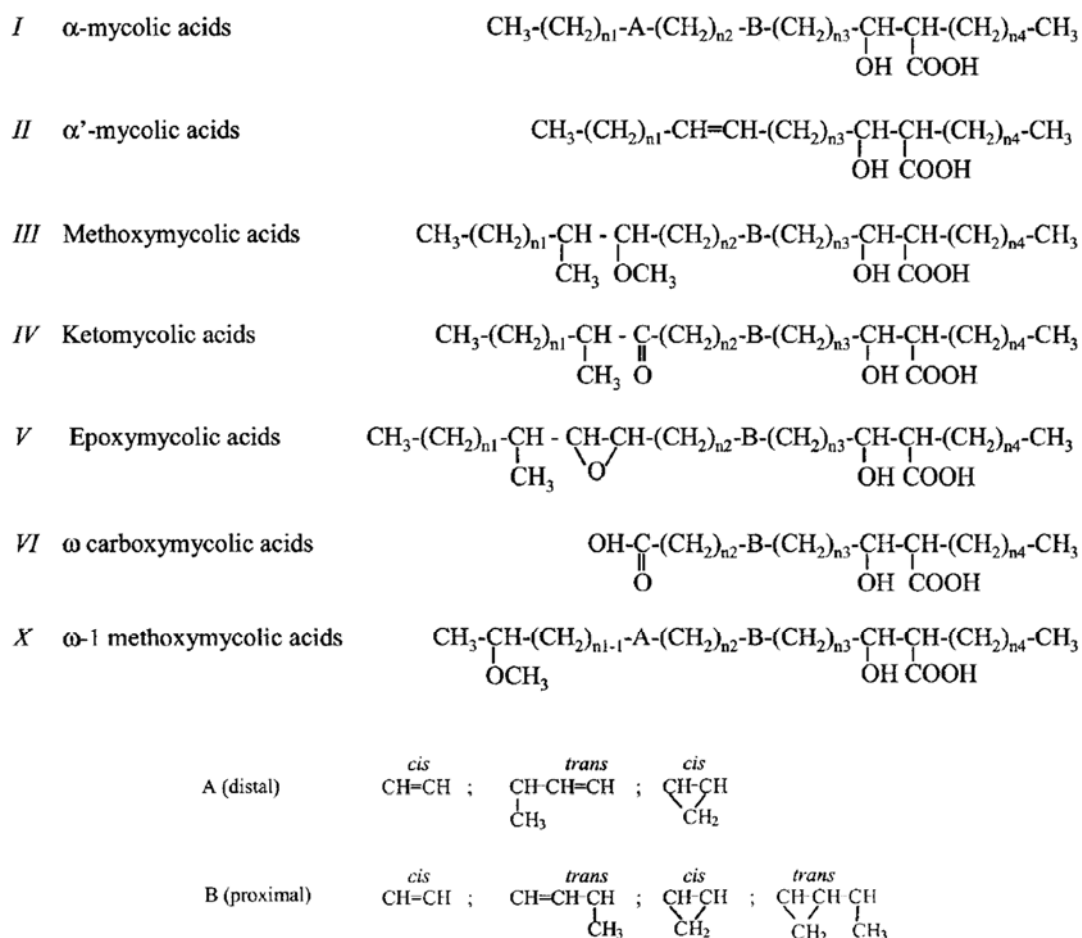


Figure 1.3.5 Structure of the major mycolic acids described in mycobacteria. The main values of n_1 and n_3 are 15, 17, and 19; those of n_2 depend on the nature of A and B. When no methyl branch is present in A and B, or when a methyl branch occurs in both A and B, n_2 is 12, 14, and 16. In contrast, when a methyl branch is present in A or B, n_2 is 13, 15, or 17. n_4 is always 19, 21, or 23. Obtained from Laval et al., 2001.

- **Triacylglycerides (TAG):** Consist in a molecule of glycerol esterified with three fatty acids. TAG are considered the main apolar lipid in mycobacteria when glycerol is the major carbon source in the culture media and they have been isolated from all mycobacteria examined (Daffé et al., 2014). These molecules are found in the cell wall core, but it has been described that Mycobacteria accumulates TAG in the form of intracellular droplets (Ortalo-Magné et al., 1996). This accumulation may serve as an energy reserve (Daniel et al., 2004). Reed et al. observed that the different strains of hypervirulent *M. tuberculosis* W-Beijing lineage accumulate large quantities of TAG when grown *in vitro* and with aerobic conditions. The reason is an upregulation of a gene that

codifies for a TAG synthetase. Superexpression of this molecule is a consequence of the activation of the “dormancy regulon”, a collection of genes that gives the bacilli the capacity to survive inside the host, in conditions of microaerophilia or anaerophilia. All in all, the superexpression of TAG is not a virulence factor *per se*, but it is an indicator of the presence of the “dormancy regulon”, which it is related to virulence. Also, this constitutive superexpression confers the mycobacteria the ability to survive under starvation conditions, using this stored lipids (Reed et al., 2007).

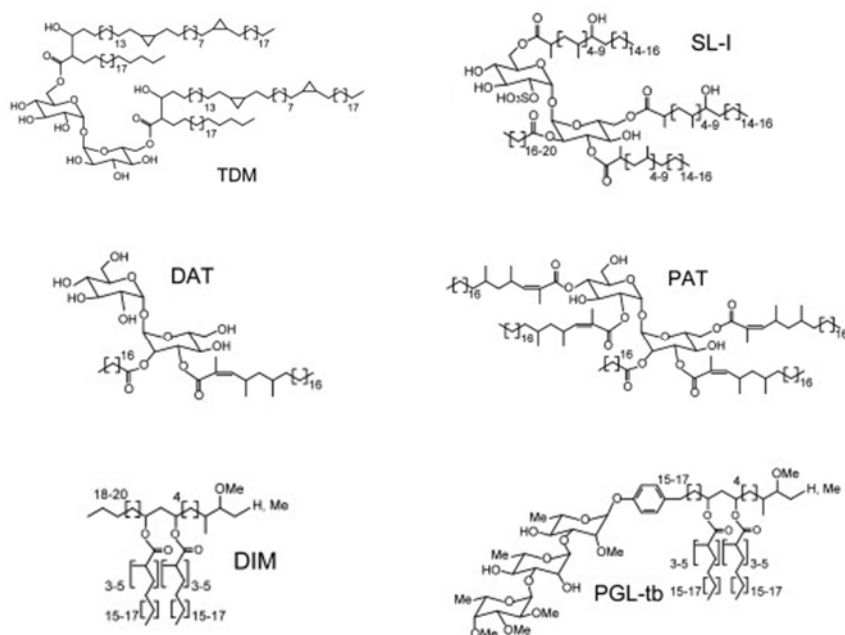


Figure 1.3.6 *M. tuberculosis* lipids, adapted from Neyrolles and Guilhot, 2011. TDM (trehalose dimycolate), SL (sulfolipid), DAT (diacyltrehalose), PAT (polyacyltrehalose), DIM (phthiocerol dimycocerosate), PGL-tb (phenol glycolipids).

- Trehalose mono/dimycolate (TMM and TDM): Trehalose esterified with mycolic acids at the position 6 for TMM and positions 6 and 6' for TDM (Figure 1.3.6). These compounds are found all over *Mycobacterium* genus, and TDM is described as the major responsible of the characteristic inflammation from mycobacterial infections (Linares et al., 2012). In 1950 Bloch disrupted *M. tuberculosis* cords by adding the organic solvent petroleum ether (PE) on top of a pellicle formed by this *Mycobacterium*. He considered that recovering the PE

he was extracting the compound responsible of cord formation. Bloch also described that the product of this extraction had a lethal effect when injected in mice (Bloch, 1950). Later, Noll analyzed the extraction product and described TDM as the responsible of the extract toxicity. However, TDM was only around 1% of the total extract (Noll and Bloch, 1955). TDM was defined by Bloch as “cord factor” just because it was obtained from cord-forming bacteria. Nevertheless, TDM was wrongly related with cord formation until it was described the presence of TDM in non-cording bacteria (Glickman, 2008).

- Sulfolipids (SL): Trehalose esters acylated with 3-4 acyl groups, exclusively found in *M. tuberculosis*, where the most abundant SL is SL-1 (Daffé et al., 2014) (Figure 1.3.6). Middlebrook described the presence of SL in H37Rv *M. tuberculosis* and the absence of this compound in the attenuated corresponding strain H37Ra (Middlebrook et al., 1947). This was the first signal of virulence relationship. Goren et al. postulated that SL inhibited phagosome-lysosome fusion (Goren et al., 1976), but later Pabst et al. described the action of SL as an inhibition of phagosome activation (Pabst et al., 1988).

- Di/polyacyltrehalose (DAT and PAT): Species-specific trehalose esters, only obtained from *M. tuberculosis*-complex species. In the case of DAT, trehalose is acylated twice, while PAT have five acyl groups (Daffé et al., 2014) (Figure 1.3.6). These trehalose esters have a biological activity involved in modulating host immune response (Lee et al., 2007). Passemar et al. suggest that *M. tuberculosis* DAT and PAT will block phagosome acidification, encouraging intracellular growth (Passemar et al., 2014).

- Lipooligosaccharides (LOS): Species-specific trehalose esters poly-O-acylated and glycosylated by an oligosaccharidyl unit, produced by a number of *Mycobacterium* species, as *M. marinum*, *M. kansasii*, *M. smegmatis*, and some strains of *M. tuberculosis* (Daffé et al., 2014). LOS are highly antigenic molecules and in some mycobacterial species can have immunomodulatory activities. In *M. marinum* LOS inhibit TNF- α secretion by infected macrophages (Rombouts et al., 2009). Belisle and Brennan, in 1989, determined in *M. kansasii* a relationship between the presence of LOS and the smooth morphology, based on the results that rough colonies did not show LOS on their wall (Belisle and

Brennan, 1989). They related their results with the ones from Collins and Cunningham, who observed that some strains of *M. kansasii* made a chronic infection and some others were cleaned from the infected mice (Collins and Cunningham, 1981). Belisle and Brennan described a link between the absence of LOS and the persistence of these mycobacteria inside laboratory animals. They suggest that the lack of LOS leaves phenol glycolipids and AG exposed on the cell wall.

- Phthiocerol dimycocerosate (PDIM/DIM): Long-chain β -diol (phthiocerol) esterified by two polymethyl-branched fatty acids (mycocerosic acids) (Figure 1.3.6). PDIM are found in abundance in the cell wall core contributing to the impermeability of the mycobacterial envelope (Camacho et al., 2001). However, these compounds are present in a limited number of mycobacterial species, in concrete they have been found in *M. tuberculosis*, *M. bovis*, *M. leprae*, *M. kansasii*, *Mycobacterium microti*, *Mycobacterium gastri*, and *Mycobacterium haemophilum* (Daffé et al., 2014). The relation between the production of PDIM and *M. tuberculosis* virulence has been described previously (Camacho et al., 1999; Cox et al., 1999; Domenech et al., 2005). Domenech and Reed demonstrated in 2009 that subculturing H37Rv *M. tuberculosis* several times, this bacterium loses the ability to produce PDIM. And when it fails in this production it also shows an attenuated phenotype in infections *in vivo* (Domenech and Reed, 2009). Camacho et al. generated a mutant deficient in PDIM production, that showed a high cell wall permeability that was traduced in a major sensitivity to detergents (Camacho et al., 2001).

- Phenol glycolipids (PGL): Glycosylated phenolic derivates of PDIM, and the glycosyl moiety is formed by one to four residues depending on the species (Figure 1.3.6). These compounds are found in the same species as PDIM, although they are not expressed by all strains (Daffé et al., 2014). PGLs from *M. tuberculosis* and *M. kansasii* tested in human neutrophils were shown to stimulate the production of oxygen metabolites (Fäldt et al., 1999), and for the tubercle bacillus was possible to establish a relationship between the presence of PGL-tb in the cell wall and a phenotype of hypervirulence (Onwueme et al., 2005). Most of the clinical isolate of *M. tuberculosis* and most of the laboratory

strains do not produce PGLs, but these components are detected in some strains of the hypervirulent *M. tuberculosis* W-Beijing lineage as an important virulence factor (Tsenova et al., 2005; Sinsimer et al., 2008). Furthermore, Tabouret et al. described that PGL-1, from *M. leprae*, induces a preferential phagocytosis by complement receptor 3, that evolve in a lower inflammatory response (Tabouret et al., 2010).

- Glycopeptidolipids (GPL): Species-specific molecules produced by many NTM, including *M. abscessus*, *M. smegmatis*, *M. avium* and *Mycobacterium xenopi*. These molecules have a lipopeptidyl core amidated by a tripeptide and bonded to an aminoalcohol. This structure constitutes the apolar GPLs or non-serovar specific GPLs. However, it exists polar GPLs or serovar specific GPLs, that contain a glycosylation in their tripeptide tail, and that have a high immunogenicity (Daffé et al., 2014). GPLs are amphipathic molecules, because they are composed of hydrophobic fatty acyl chains with hydrophilic carbohydrate groups (Pang et al., 2013). There are different studies that relate the S colony morphology of NTM and the presence of GPL in their cell wall (Barrow and Brennan, 1982; Eckstein et al., 2000). Howard et al described this relationship between the expression of GPL in the cell wall and the colonial morphology in *M. abscessus* (Howard et al., 2006). The absence of GPL has also been linked to a major hydrophobicity and aggregation of the bacteria (Etienne et al., 2002), and the presence of GPL has been related with motility and biofilm formation (Howard et al., 2006).

Capsule or outer layer (OL)

The capsule is composed by a variety of lipids, glycolipids, polysaccharides, lipoglycans and proteins, that are noncovalently attached to the cell wall core. The most abundant components are polysaccharides and proteins. However, some specie-specific glycolipids can be found in large amounts, like GPL (Draper, 1974). One of the three capsular polysaccharides identified in many mycobacteria is arabinomannan with an identical structure to LAM. The main difference is the lack of phosphatidyl-*myo*-inositol anchor (Figure 1.3.3), suggesting that arabinomannan might derivate from LAM (Daffé et al., 2014).

Mostly all proteins and lipids found in mycobacterial outer layer are also present in the cell wall core and periplasm (Daffé et al., 2014). Specie-specific trehalose esters are found in a big proportion in the capsule, while TMM and TDM are not in the outer layer of all mycobacteria. PDIM and PGL are also found in the capsule of *M. tuberculosis* and other pathogenic mycobacteria (Ortalo-Magné et al., 1996).

So, as a conclusion, there are many studies describing that the S to R variation is accompanied by the loss of surface glycolipids, such as LOS in some bacteria from *M. tuberculosis* complex or GPL in some NTM (Belisle and Brennan, 1989; Muñoz et al., 1998; Pang et al., 2013). This loss unmask cell wall components related with innate immune response, like PIM (Krutzik and Modlin, 2004), facilitating bacterial lung colonization (Catherinot et al., 2007; Rhoades et al., 2009). These cell wall components that are masked by surface glycolipids are also involved in bacterial aggregation, even though the nature of the compound responsible for cord formation is unknown to date.

1.4. *Mycobacterium vaccae* and the vaccine against tuberculosis

As explained, tuberculosis is a major public health threat and only a quarter of patients have access to adequate therapy (WHO, 2017). Also, mycobacterial infections are not easy to treat with antibiotics and the appearance of resistance to standard therapy is an increasing problem. For those reasons immunotherapy is an important research line to fight tuberculosis.

Robert Koch, considered the father of clinical microbiology, developed the first immunotherapy used in patients with tuberculosis. He achieved to modify beneficially the immune response in front of tuberculosis in guinea pigs by injecting them an extract of tubercle bacilli (Koch, 1890). However, this method fell into disrepute after some unsuccessful attempts in human patients with fatal result.

The immunotherapeutic strategy that was following Koch consisted on increasing necrosis of the tuberculous lesions. Superficial lesions would be removed and deep lesions would be converted in caseous granulomas. These abscesses would be contained with fibrous walls and the patient would acquire immune tolerance to the bacillary antigens. Inside these caseous granulomas bacilli would be in state of dormancy. (Stanford et al., 2004).

Many years later Spahlinger developed two new immunotherapies against tuberculosis. The first one was based on injecting bacilli in stationary phase, although he thought that the bacilli were dead. And the second one consisted on treating patients with horse sera immunised with those “dead bacilli” (Spahlinger et al., 1934). These treatments followed the second immunotherapeutic strategy, suppress necrosis and increase active destruction of tubercle bacilli by cellular immune response (Stanford et al., 2004).

At that moment, it was believed that the induction of a limited tuberculous process was necessary for a successful immunization. However, Friedmann suggested that it might be less dangerous to treat tuberculosis patients with less pathogenic mycobacteria. So he started a new immunotherapy with *Mycobacterium chelonae*, described by himself and obtained from a diseased turtle (Fowler, 1930).

And finally Calmette and Guérin, in 1921 and after 13 years of sub-culturing *M. bovis*, obtained an attenuated strain that they called *M. bovis* BCG (Bacillus Calmette-Guérin). Also in 1921, they started to vaccinate newborns with this strain and 7 years later a decrease in the mortality due tuberculosis disease was detected (Nègre et al., 1926).

Nowadays, the only vaccine available to protect against tuberculosis disease is the one containing *M. bovis* BCG (Barker et al., 2009). This attenuated vaccine provides high defence against the development of extrapulmonary tuberculosis. However, the protection against pulmonary disease in children is around 50% (Colditz et al., 1994). So, as this vaccine only protects partially, is important to find new strategies to vaccine against tuberculosis disease.

This current vaccine protects by inducing neutralizing antibodies. Nevertheless, it has been suggested that the best protection against *M. tuberculosis* infection and disease is a robust cellular immune response (Kaufmann et al., 2010). That is why the new vaccine candidates are based on inducing the classical Th1 cytokines (INF- γ and TNF- α) from immunity cells.

Considering the progress of the tuberculosis disease, different type of vaccines are need: to protect infants, young adults, people with latent tuberculosis, and patients co-infected with *M. tuberculosis* and HIV (Evans et al., 2016).

The WHO describes in their Global Tuberculosis Report 2017 that there are 12 new vaccines in different phase of trial (Figure 1.4.1). There is only one candidate in phase III, Vaccae™.

M. vaccae is an environmental rapid-growing bacterium that has been used as therapeutic vaccine. Killed bacteria is injected in patients with active tuberculosis together with or following chemotherapy, to cure the disease or to prevent recurrence. Many studies demonstrate that immunotherapy with *M. vaccae* as an adjunct to anti-tuberculosis treatment is safe and well tolerated (Yang et al., 2010). This therapy is of especial interest in patients co-infected with HIV or with drug-resistant *M. tuberculosis* (Andersen and Kaufmann, 2014).

It has been demonstrate that infection with one mycobacterial species give cross-protection against other species (Edwards et al., 1982; Fine, 1995). The reason of this

cross-protection is unknown. However, evidences suggest that immune system might recognize antigens commons to all mycobacteria (de Bruyn and Garner, 2010).

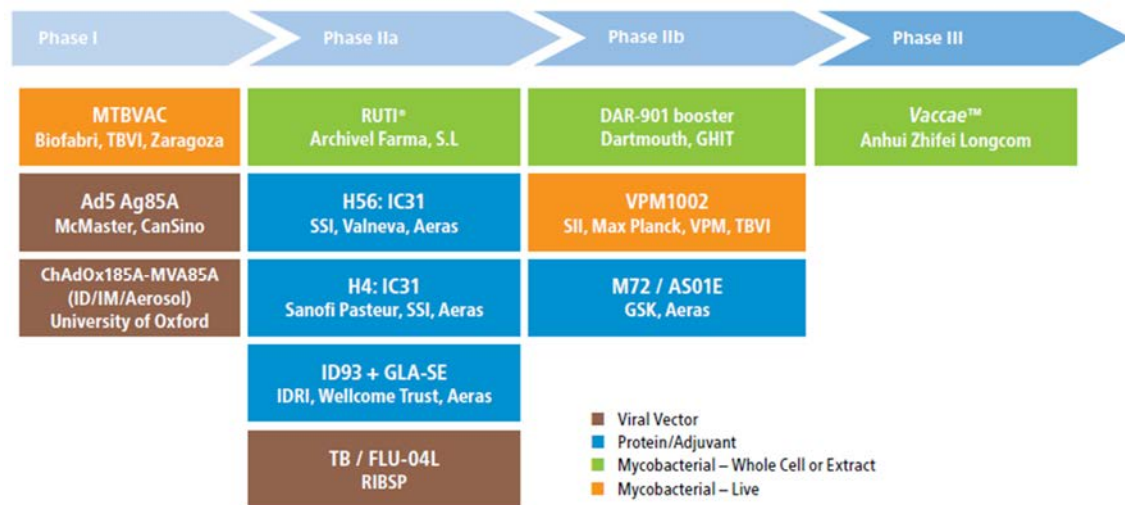


Figure 1.4.1 The global development pipeline for new tuberculosis vaccines, August 2017. This information was given by vaccine sponsors. Figure obtained from de Global Tuberculosis Report 2017, WHO.

There are two available preparations of *M. vaccae* to be used as immunotherapy:

- The original one, developed by Stanford et al. in 1990. The strain used was isolated from Uganda and was initially smooth. After a few passages they obtained an stable rough variant, that was called R877R, and these bacteria are injected after irradiation (Stanford et al., 1990).
- Vaccae™ vaccine. It is a bacterial lysate from heat-killed *M. vaccae* type strain (smooth). It has been developed in China and the Food and Drug Administration of this country have recognized Vaccae™ as an immunotherapeutic agent that facilitate tuberculosis treatment in people infected with drug-susceptible *M. tuberculosis* (Evans et al., 2016).

So, *M. vaccae* immunotherapy is performed apparently with both S and R morphotypes. There are only few studies testing differential antigenic effect between the two morphotypes (Rodríguez-Güell et al., 2006). However, it will be of interest to perform a study in macrophages to see if the two morphotypes induce a differential activation of these immune cells.

2

Objectives

The objectives for this thesis were the following

1. Study if the two morphotypes of *M. abscessus* have a different cytotoxic effect when infecting alveolar epithelial cell line A549.
2. Observe if there is a diverse activation of the TLR in A549 infected with the different morphotypes of *M. abscessus*.
3. Detect if surfactant phospholipid DPPC has any effect on the clumping capacity of R morphotype of *M. abscessus*.
4. Study the most superficial lipids in *M. abscessus* by using a variant of Bloch's technique for superficial extraction.
5. Test if these superficial compounds have any antigenic activity and find if there is any relationship between these compounds and cord formation.
6. Try if these compounds are also superficially exposed in other mycobacteria and analyze if there are other interesting superficial lipids.
7. Study if there is any difference macrophages activation when infecting J774 murine macrophages with the two morphotypes of *M. vaccae*.

3

Material and methods

3.1. Initial preparations

Mycobacterial strains and growth conditions

For *M. abscessus* the bacterial strains used in this work were *M. abscessus* 390; *M. abscessus* type strain ATCC 19977^T/DSMZ 44196^T; and BE37, BE48 and BE96, three clinical isolates from pulmonary disease patients hospitalized at Bellvitge University Hospital in Barcelona, Spain. These clinical isolates were identified using polymerase chain reaction and reverse hybridization (GenoType Mycobacterium CM®, Hain Lifescience, Germany) and the partial sequencing of 16S rRNA.

R and S morphotypes of *M. abscessus* 390 and DSMZ 44196^T were obtained in previous studies (Byrd and Lyons, 1999; Brambilla et al., 2016). For the clinical isolates *M. abscessus* BE37 and BE48, the strains were initially R, but the S morphotype was obtained after several passages on agar medium. For *M. abscessus* BE96 it occurred the other way around. The clinical isolate was initially S, but after several passages the R morphotype was obtained.

The other mycobacteria used in this work were R and S morphotype from *M. vaccae* ATCC 15483^T/DSMZ 43292^T (Agustí et al., 2008); R morphotype from *M. kansasii* ATCC 12478^T/DSMZ 44162^T/TMC 1204 (Belisle and Brennan, 1989); *Mycobacterium brumae* ATCC 51384^T/DSMZ 44177^T (Noguera-Ortega et al., 2016); and *M. smegmatis* ATCC 35797/TMC 1515 (Secanella-Fandos et al., 2011).

All mycobacteria were grown in Middlebrook 7H9 (Difco, USA), broth and agar, supplemented with 10% Albumin-Dextrose-Catalase (ADC), and Middlebrook 7H10 agar (Difco, USA) supplemented with 10% Oleic-Albumin-Dextrose-Catalase (OADC), at 37°C for 1 week, except *M. kansasii* that needed 3 weeks to grow.

Preparation of bacterial suspension

Colonies of *M. abscessus* and *M. vaccae*, cultivated for 1 week at 37°C, were scraped from 7H9 agar plates and vigorously shaken in a tub with glass beads (Schlesinger et al., 1990; Julián et al., 2010). The bacteria were subsequently resuspended in phosphate-buffered saline (PBS), and large aggregates were allowed to sit for 15 minutes. The supernatant was recovered and adjusted to the McFarland standard 1,

followed by centrifugation at 1500 g for 10 minutes at 4°C. The supernatant was removed, and the pellet was resuspended in the necessary volume for each experiment. To break up the aggregates, the suspension was sonicated in an ultrasonic cell water bath three times for 30 seconds each (Stokes et al., 2004; Julián et al., 2010).

Coating of beads

Amine-modified yellow-green latex beads (Sigma, USA) with an average diameter of 1 µm were used, and coated following variations of the protocols described by Kang and Schlesinger (Kang and Schlesinger, 1998) and by Vergne et al. (Vergne et al., 2004). Briefly, 5 µl of bead suspension at an initial concentration of 4.6×10^{10} beads/ml were transferred to a tube, washed twice with 0.05 M carbonate-bicarbonate buffer (pH 9.6) and coated with purified trehalose polyphosphates (TPP), obtained from the R morphotype of the *M. abscessus* 390 strain, and maintained in dimethyl sulfoxide (DMSO) (Merck, Germany). Beads were incubated in 8% DMSO in PBS with 0.8 mg/ml of TPP for 2 h at 37°C with agitation. Control uncoated beads were treated with 8% DMSO in PBS without TPP. After the 2 h incubation, the beads were washed twice with PBS and blocked with 5% bovine serum albumin (BSA) (Roche, Germany) in PBS for 1 h at 37°C with agitation, to prevent nonspecific binding. After that, beads were washed once with 0.5% BSA in PBS.

The successful coating with TPP was demonstrated by staining the beads with Nile Red (Sigma-Aldrich, USA). Briefly, 1 µl of 0.5 mg/ml Nile Red in ethanol was added to 50 µl of beads, which were incubated for 10 min at 37°C. Then, the beads were washed three times with PBS (Christensen et al., 1999), and 10 µl of the bead suspension was spread on a slide by using a coverslip. Nile Red-stained TPP-coated beads were observed with a confocal laser scanning microscope (CLSM) using a TCS-SP5 CLSM (Leica, Germany) with a PlanApo 63 (numerical aperture [NA] 1.4) oil objective.

3.2. Cell-based *in vitro* models

Cell lines and culture media

To perform part of the work presented in this thesis three cell lines were used. To study the effect of *M. abscessus* in the pulmonary epithelia it was used the human alveolar epithelial cell line A549 (ATCC CCL-185). And to test the toxicity of TPP, besides A549, two macrophages cell lines were used, the murine macrophage cell line J774A.1 (ATCC TIB-67) and the human monocyte cell line THP-1 (ATCC TIB-202).

Cells were maintained at 37°C in a humidified atmosphere of 5% CO₂. A549 and J774 cells were cultured in Dulbecco's modified Eagle's medium with L- glutamine and high glucose (DMEM) (Gibco, Austria); and THP-1 in Roswell Park Memorial Institute medium (RPMI) (Lonza, Belgium). Both media were supplemented with 10% heat-inactivated fetal bovine serum (FBS) (HyClone, UK), 100 U/ml penicillin G (LERN, Spain), and 100 µg/ml streptomycin (Reig Jofre, Spain). At this point media were considered to be complete medium (CM).

Study of cell viability by MTT assay

A549 and J774 cells were seeded into 96-well tissue culture plates (Thermo Fisher Scientific, Denmark) at a density of 1.5×10^4 cells per well in CM and incubated for 24 h. THP-1 cells were also seeded into 96-well plates but at a density of 5×10^4 cells per well and induced to differentiate in macrophages by the addition of phorbol myristate acetate (PMA) (Abcam, United Kingdom) at a final concentration of 100 nM. The medium of THP-1 cells was replaced 72 h later, and the cells were incubated for 24 h in CM without PMA.

A549 cells were infected with 5 strains of *M. abscessus* (390, 44196, BE37, BE48 and BE96) and with both morphotypes of each, at a multiplicity of infection (MOI) of 10:1. Uncoated beads and TPP A-coated beads were added to the culture of A549, J774 and THP-1 at an optimized ratio of 30 beads per cell (Brambilla, 2015). J774 and THP-1 macrophages were also infected with *M. abscessus* 390R at a MOI 10:1 as a virulence control. CM without antibiotic in the case of bacterial infection, and with antibiotic for the treatment with beads.

The medium was removed 3 h later, and the cultures were washed three times with PBS and then incubated with CM. When fresh medium was added, the cultures were maintained at 37° C in a humidified atmosphere of 5% CO₂ and the washing protocol was repeated every 24h (Byrd and Lyons, 1999).

At different time points (24, 48 and 72 h) the MTT (3-(4,5-dimethylthiazol-2-yl)-2,5-diphenyltetrazolium bromide) assay (Sigma-Aldrich, USA) was performed, except for the THP-1 cell line. Once differentiated, THP-1 macrophages do not have metabolic activity, for that reason MTT assay was only measured after 3 hours post-infection (h.p.i.).

The MTT assay was performed as described previously (Noguera-Ortega et al., 2016). Briefly, the culture supernatant was removed and it was added to each well 100 µl of a solution of 10% MTT (5mg/ml in PBS) in CM. The plates were incubated 3h at the same conditions of growth, 37°C in a humidified atmosphere of 5% CO₂. Afterward, 100 µl of acid-isopropanol were added and mixed to dissolve the blue formazan crystals produced by MTT. Then the plates were read at the wavelength of 550nm with a microplate reader Infinite® F200 (Tecan, Switzerland).

For all the results obtained, viability was calculated using the control wells that contained uninfected or untreated cells as a reference representing 100% growth.

Study of cell viability by trypan blue exclusion assay

In this case, J774 macrophages were seeded into 48-well tissue culture plates (Thermo Fisher Scientific, Denmark) at a density of 3x10⁴ cells per well, and were infected as previously described by a bacterial suspension of *M. vaccae* R (MOI 10:1) and *M. vaccae* S (MOI 100:1). At different time points after infection (24, 48, 72 and 96 hours), the supernatant was removed, and the macrophages were gently washed with PBS, trypsinized (trypsin-EDTA, PAA, Austria) for 10 minutes and subsequently stained with trypan blue (Gibco, USA). Viable macrophages were counted using a Neubauer chamber, and viability was calculated using the control wells that contained uninfected cells as a reference representing 100% growth.

Study of cell viability by CLSM counting

For the CLSM assay, 2.5×10^5 J774 macrophages per well were plated in culture dishes (MatTek, USA) and infected with *M. vaccae* as described above. At different time points after infection (24, 48, 72 and 96 h), the macrophages were labelled with 0,5 $\mu\text{l/ml}$ of green fluorescent 4 mM Calcein acetoxymethyl and 0,2 $\mu\text{l/ml}$ of red fluorescent 2 mM Ethidium homodimer-1, LIVE/DEAD® Viability/Cytotoxicity Kit (Molecular Probes, USA) for 10 minutes at room temperature, and then washed with CM before being observed. Labelled macrophages were examined under a CLSM (FV1000-Olympus) using a Plan Apo 20x (numerical aperture [NA], 1.5). For the processing of the images ImageJ software (National Institutes of Health, USA) was used. Ten random fields were taken for each treatment and the mean value of live cells per field was calculated. Viability was calculated using the control wells that contained uninfected cells as a reference representing 100% growth.

Study of cytokine production

A549 and J774 cells were seeded into 48-well culture plates at a density of 3×10^4 cells per well. Cells were infected or treated with beads as described before. However, for this study the wells were not washed every 24 h. Cell supernatants were recovered at different time points and centrifuged to eliminate cells that had detached from the well.

For A549 cells the concentrations of IL-8 (BD Biosciences, USA) was determined, following the manufacturer instructions. On the other hand, in the supernatant of J774 cells were measured the concentration of TNF- α (R&D Systems, USA) and IL-6 (BD Biosciences, USA), also following the manufacturer instructions.

Study of the phagocytosis and phagolysosome fusion

J774 macrophages were seeded onto CLSM culture dishes (MatTek, USA) at a concentration of 2.5×10^5 cells per dish. For the phagocytosis analysis, cells were infected with *M. vaccae* or treated with beads as described before. CM was removed, and the macrophages were washed three times with fresh CM to remove extracellular bacteria, followed by fixation with 4% paraformaldehyde (Sigma-Aldrich, USA) in PBS

for 10 minutes. Subsequently, the macrophages were washed with PBS and air dried for 30 minutes.

For CLSM observation, the mycobacteria were stained with Auramine-Rhodamine (BD Biosciences, USA) according to the manufacturer's instructions. Briefly, samples were covered with Auramine-Rhodamine for 25 minutes and washed with abundant water. Then samples were treated with the destaining solution provided by the kit for 2 minutes, washed again with water, counterstained with potassium permanganate for 4 minutes and washed with water for the last time.

The macrophages were labelled with 1 μ l red fluorescent CellMask (Molecular Probes, USA)/ml of PBS for 10 minutes at room temperature and subsequently washed with PBS. The images were obtained using a TCS-SP5 CLSM (Leica, Germany) equipped with a Plan Apo 63x (numerical aperture [NA], 3.0) oil objective in horizontal (x-z) optical sections. Ten fields per sample (approximately two hundred macrophages) were considered.

For the study of the phagolysosome fusion J774 macrophages in the CLSM culture dishes were cultured in DMEM with LysoTracker Red DND-99 (Life Technologies, USA) at a concentration of 1:10000. 24 h after the seeding, cells were placed in contact with beads in order to compare the phagolysosome fusion between macrophages with uncoated beads *versus* macrophages with TPP-coated beads. After 24 h, dishes were observed using a TCS-SP5 CLSM (Leica, Germany) with a PlanApo 63 (numerical aperture [NA], 1.4) oil objective, operating at a zoom of 2.5. One hundred macrophages were counted for each sample, and colocalization between LysoTracker and the green fluorescence produced by the beads was calculated using Pearson's correlation coefficient.

Granuloma-like structure analysis

J774 macrophages infected with the two morphotypes of *M. vaccae* were seeded onto 8-well sterile glass chamber slides (Thermo Fisher Scientific, Denmark) and infected as described above. At 72 h.p.i. the supernatants were removed, and the samples were heat-fixed and stained using the Ziehl-Neelsen method. Briefly, the slides were covered with basic fencated fuchsin, heated with the flame and seated for 7

minutes. The heating was repeated twice and the slides were washed with tap water. Then the samples were covered with destaining solution (97:3 ethanol 96-hydrochloric acid) for 2 minutes and washed with abundant water. Finally, the samples were counterstained with methylene blue for 1 minute, and washed with abundant water.

Observations and images were obtained using an optical microscope (Leica, Germany) equipped with a DM500 digital camera system.

3.3. Biochemist analysis

Superficial lipid extraction

A superficial lipid extract of the pellicles formed by *M. abscessus* (390R and S, 44196R and S, BE48R and S), *M. vaccae* R, *M. kansasii* R, *M. brumae* and *M. smegmatis* was performed by using a modification of Bloch's protocol (Bloch, 1950). Briefly, pellicles of the different mycobacteria were filtered. Then, avoiding the complete drying of the pellicles, 1.5g of each sample were placed in a beaker with 40 ml of PE (40-60°C b.p.) and agitated for 5 min. After that, the PE extracts were filtered and evaporated.

Analysis of the lipidic components of the PE extract

A series of thin layer chromatographies (TLC) were performed to study the lipidic profile of the PE extracts from *M. abscessus*, using 10 µl of all samples for each TLC. For unidimensional TLCs, the mobile phases that were used were PE 60-80°C/diethyl ether (90:10, v/v), chloroform/methanol (85:15, v/v), chloroform/methanol/water (60:35:8, v/v/v; and 90:10:1, v/v/v), and PE 60-80°C/diethyl ether (90:10, v/v). For bidimensional TLCs, the mobile phases used were first direction PE 60-80°C/ethyl acetate (98:2, v/v, thrice), second direction PE 60-80°C/acetone (98:2, v/v, once); first direction PE 60-80°C/acetone (98:2, v/v, thrice), second direction toluene/acetone (95:5, v/v, once); first direction chloroform/methanol (96:4, v/v, once), second direction toluene/acetone (80:20, v/v, once); and first direction chloroform/methanol/water (100:14:0.8, v/v/v, once), second direction chloroform/acetone/methanol/water (50:60:2.5:3, v/v/v/v, once). Compounds in the TLC plates were revealed by using anthrone (Merck, Germany; 1% in sulfuric acid) or phosphomolybdic acid (VWR, USA; 10% in ethanol) and then heating the plate at 120°C, or by using molybdenum blue (Sigma, USA) without heat.

For the other mycobacteria, it was only performed the unidimensional TLC PE 60-80°C/diethyl ether (90:10, v/v), because it was a screening of the compounds observed by this elution system.

Purification of compounds X, Y, Z and TAG of *M. abscessus* and Spot A from *M. smegmatis*

Compounds X, Y, Z and TAG from *M. abscessus* and Spot A from *M. smegmatis* were purified by column chromatography. Approximately 50 mg of PE extract obtained as described above was added to a Silica Gel 60 (Merck, Germany) column. A series of solvent mixtures of PE 60-80°C with increasing concentrations of diethyl ether was used for the elution of the PE-extracted components.

The dried fractions containing compounds X, Y, Z and TAG from *M. abscessus* and Spot A from *M. smegmatis* were used for mass spectrometry (MS) and nuclear magnetic resonance (NMR).

MS analysis of compounds X, Y and Z

For MS analysis, purified compounds X, Y and Z were dissolved in 50 µl of chloroform/methanol (2:1, v/v). This suspension was mixed with a matrix made of 10 mg/ml 1,8,9-anthracenetriol (ditranol) at a 1:1 ratio, and 1 µl of the mix was deposited on a ground steel plate. The sample was analyzed using a negative polarity reflectron and an acceleration voltage of 25kV in a MALDI-TOF UltrafleXtreme (Bruker Daltonics, USA). The calibration was performed using external calibrators (Bruker Daltonics, USA).

MS analysis of Spot A

This analysis was performed using ESI/MS, MALDI/MS and MALDI-LIFT/MS. For ESI+ purified Spot A was dissolved in 500 µl of chloroform/isopropanol (3:1, v/v) and manually injected to a micrOTOF-Q II (Bruker Daltonics, USA). For MALDI Spot A followed the same treatment as described before for compounds X, Y and Z from *M. abscessus*. To obtain the fragmentation spectrum of some specific signals a LIFT method was used.

NMR analysis of compounds X, Y, Z and TAG of *M. abscessus* and Spot A of *M. smegmatis*

Purified compounds were dissolved in 600 μL of CDCl_3 (99.80% D, Cortecnet, France) and transferred to 5-mm-diameter NMR tubes. NMR experiments were recorded on a Bruker Avance II 600 (Bruker Biospin, USA) equipped with a 5 mm TBI probe with Z-gradients that operated at ^1H and ^{13}C NMR frequencies of 600.13 and 150.90 MHz, respectively, and at 298.0 K. 1D ^1H NMR spectra were acquired using a standard 90° pulse sequence with an acquisition time of 1.71 s and a relaxation delay of 3 s. Data sets were collected as 32k data points with a spectral width of 9590 Hz and as the sum of 128 transients. The resulting free induction decays were Fourier transformed, manually phased, and baseline corrected. All spectra were calibrated using the residual solvent signal (chloroform) at a chemical shift (δ) of 7.27 ppm. The relative molar ratios of characteristic molecular moieties were determined by the integration of representative resonances.

2D ^1H , ^1H -COSY (Correlation Spectroscopy); ^1H , ^1H -TOCSY (Total Spectroscopy); ^1H , ^{13}C -HSQC (Heteronuclear Single Quantum Coherence); ^1H , ^{13}C -HMBC (Heteronuclear Multiple Bond Correlation) and ^1H -DOSY (Diffusion Ordered Spectroscopy) experiments were performed using standard Bruker pulse sequences and acquired under routine conditions. Chemical shifts were referenced to the residual solvent signals (δ_{H} , 7.26 and δ_{C} , 77.0 ppm), the data are expressed in ppm and coupling constant (J) values in Hz. Proton signal multiplicity is indicated in the text by d (doublet), t (triplet), dd (double doublet) and m (multiplet). In the case of compounds Y and Z, standard 1D ^{31}P spectra were also recorded.

3.4. Electronic microscopy

Samples preparation for transmission electron microscopy observation

M. abscessus (390R and S, 44196R and S, BE48R and S) and *M. smegmatis* pellicles were collected in sterilized filters, passed to a tube and processed for transmission electron microscopy (TEM) observation. Then the bacteria were fixed in 4% formaldehyde and 5% glutaraldehyde in 0.1 M HEPES (4-(2-hydroxyethyl)piperazine-1-ethanesulfonic acid) buffer (pH 7.4).

J774 macrophages infected with *M. vaccae* were fixed with a solution containing 2% (wt/vol) paraformaldehyde (Merck, Ireland) and 2.5% (vol/vol) glutaraldehyde (Merck, Ireland) in 0.1 M phosphate buffer (Sigma-Aldrich, USA) at pH 7.4 for 1 hour. After that, the infected macrophages were recovered using a cell scraper.

After the fixation, all samples were processed by conventional preparation (Bleck et al., 2010; Lee et al., 2011). Briefly, post-fixation was performed with 2% osmium tetroxide (OsO₄) in PBS for 1 h at room temperature. Then, the samples were dehydrated in an ascending ethanol series and post-stained with saturated uranyl acetate at the 90% ethanol step for 30 min at 37°C. Bacteria were finally embedded in epoxy resin, and ultrathin sections were made (Bleck et al., 2010).

M. abscessus and *M. smegmatis* samples were also stained with the OTO method, as described by Seligman et al. (Seligman et al., 1966). Briefly, ultrathin sections that were previously fixed with OsO₄ but were not post-stained with uranyl acetate were exposed to a 1% hot aqueous solution of TCH (thiocarbohydrazide) for 1 h at 50°C, and this was followed by four to eight washes with hot water. Then, the sections were again exposed to OsO₄ (Seligman et al., 1966; Hall et al., 2012). This method results in further deposition of osmium on the samples and increases contrast (Belazi et al., 2009).

All samples were observed using a JEOL 1400 (Japan) TEM equipped with a Gatan ES1000W Erlangshen CCD (USA) camera.

Samples preparation for scanning electron microscopy observation

Pellicles of *M. abscessus* and *M. smegmatis* were processed for scanning electron microscopy (SEM) as previously described (Julián et al., 2010). Briefly, the bacteria

were recovered and fixed in 2.5% (vol/vol) glutaraldehyde in 0.1 M phosphate buffer (pH 7.4) for 2 h at 4°C. Subsequently, the samples were washed 4 times for 10 minutes each in 0.1 M phosphate buffer, post-fixed in 1% (wt/vol) OsO₄ and 0.7% ferrocyanide in phosphate buffer, followed by washing with water, dehydration in an ascending ethanol series (50, 70, 80, 90, and 95% for 10 min each and twice with 100% ethanol), and critical-point drying with CO₂. The samples were coated with gold and observed using an SEM EVO (Zeiss, Germany) at 15 kV.

3.5. Microbiologic methods

Observation of cords after application of PE to *M. abscessus* pellicles

After the superficial extraction with PE, one part of the cellular residue formed by the treated bacteria was recovered in a tube with glass beads, which was shaken for 10 min. Then, 2 ml of PBS were added, the tube was shaken for 10 s, and 3 drops of the suspension were placed in a slide and left to dry. As a control, bacteria were treated with the same protocol but without the PE extraction step. All the samples were stained using Ziehl-Neelsen stain as described before.

Another part of the cellular residue was plated in agar plates to test the viability of the treated bacteria by colony forming unit (CFU) count and to observe the colonial morphology. After growing, these treated bacteria were inoculated in Middlebrook 7H9 broth and the biopellicles formed were extracted with PE as described above. To prove if PE-treatment had any effect in the virulence of the bacteria, J774 macrophages were also infected with *M. abscessus* 390R PE-treated.

Study of bead organization after coating

To determine the organization of TPP-coated and uncoated beads, images of the bead suspension were obtained using a CLSM and analyzed with ImageJ software (National Institutes of Health, USA). The analysis described 3 types of aggregates, depending on their area: fewer than 3 μm^2 , between 3 μm^2 and 6 μm^2 , and more than 6 μm^2 (Brambilla et al., 2016). The area covered by each type of aggregate was added, and the statistical analysis was performed to determine the percentages of area that was covered by each type of aggregate.

Assay of bacterial suspension exposed to dipalmitoyl phosphatidylcholine

A variation of the method of Schwab et al. (Schwab et al., 2009) was used. Briefly, in a 24-well culture plate 100 μl of 13.5 mg/ml DPPC (Sigma-Aldrich, USA) in PBS was added to each well, and 100 μl of PBS per well was added to the control wells. The plate was incubated at 37°C for 30 minutes, and subsequently 200 μl of a bacterial suspension of *M. abscessus* 390R, prepared as previously described, was added to each

well. After incubating the plate for 30 minutes at 37°C, the content of each well was mixed once with a micropipette and counted using CLSM. Bacteria were labelled with Phenolic Auramine (Mycobacteria Fluorescent Stain – Fluka, USA), according to the manufacturer's instructions, and the images were generated using a TCS-SP5 CLSM (Leica, Germany) with a Plan Apo 63x (numerical aperture [NA], 1.4) oil objective, operating at a zoom of 1.8. To analyse the clump sizes, horizontal (x-z) optical sections of twenty fields for each sample were captured, and the fluorescence intensity and area were measured. To quantify the size ranges based on the number of bacilli in each clump, the area sizes were classified as described: areas $\leq 3 \mu\text{m}^2$ were considered as 1-2 bacilli, areas between 3 and $6 \mu\text{m}^2$ were considered as 3-4 bacilli, and areas $> 6 \mu\text{m}^2$ were considered as 5 or more bacilli. The images were processed using ImageJ software (National Institutes of Health, USA).

Statistical analysis

Analysis were made using multiple *t*-tests. Statistical significance was determined using the Holm-Sidak method, an extension of the Holm-Bonferroni method, in Prism 6 (Version 6.01, GraphPad Software, USA). Differences were considered to be significant at $p < 0.05$.

4

Results

4.1. Effect of *M. abscessus* in pulmonary epithelial cells

***M. abscessus* R morphotypes had a suppressive effect in A549 growth**

It was possible to see an important decline of growth in A549 cells infected with R morphotypes of the strains 390, 44196, BE37, BE48 and BE96 (Figure 4.1.1). These bacteria had an important suppressive effect, being 390R the most virulent with a $27.03\% \pm 4.36$ of growth of A549 cells at 72 h.p.i., and BE96R the gentler with a $39.68\% \pm 3.96$ of growth also at 72 h.p.i. Some suppressive effect was observed in cells infected with S morphotypes. However, the growth never declined the 70%. At 72 h.p.i growth of A549 cells infected with S morphotypes went from $70.48\% \pm 4.12$ in the case of 390S to $93.25\% \pm 2.38$ for BE96S (Figure 4.1.1). So, R morphotypes had a major impact in the growth of A549 than S morphotypes. This difference could be observed in general and comparing between the two morphotypes of each strain (Figure 4.1.1).

R morphotypes induced more production of IL-8 in A549 than S morphotypes

In the case of IL-8 production all R morphotypes induced the secretion of this interleukin in an important quantity in comparison with the normal production of uninfected control cells (Figure 4.1.2). Some production of IL-8 was detected in cells infected with S morphotypes, but just in a few cases this production was significantly different than the production of the uninfected control cells (Figure 4.1.2).

The production induced by R morphotypes was higher than the production induced by the S morphotypes, being at 72 h.p.i. more than ten times higher in the case of the BE48 strain. BE48R induced the production of $10285.30 \text{ pg/ml} \pm 478.3$ of IL-8, while the cells infected with BE48S produced $788.38 \text{ pg/ml} \pm 49.75$ at 72 h.p.i (Figure 4.1.2). In all cases the production of IL-8 induced by bacteria was always superior when A549 were infected with an R morphotype.

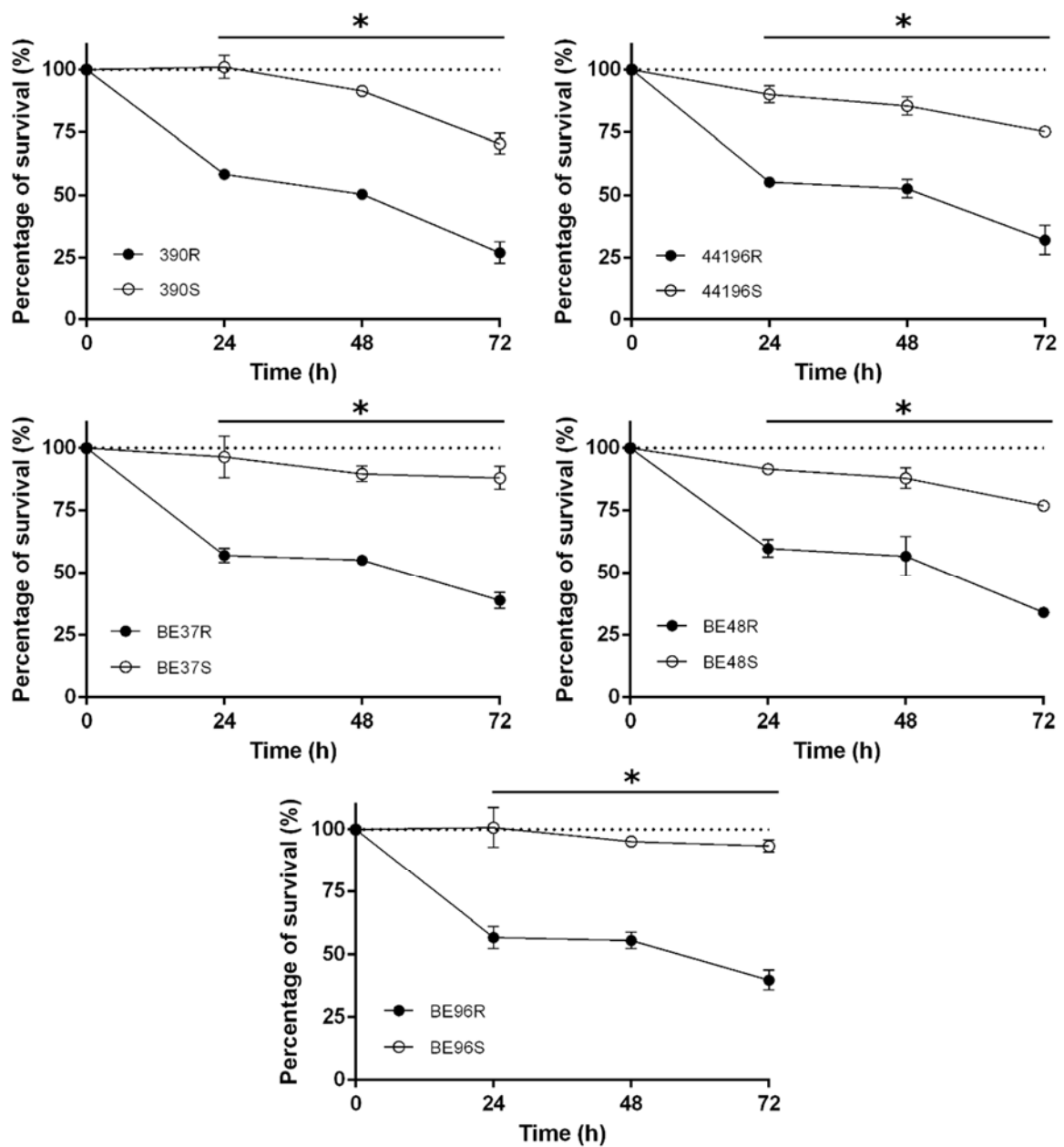


Figure 4.1.1 Viability of A549 cells when infected with the two morphotypes of each strain of *M. abscessus* studied. Significant differences were detected between cells infected with R morphotype and S morphotype of each strain ($*p < 0.05$). The results represent the mean \pm SD of triplicate infections.

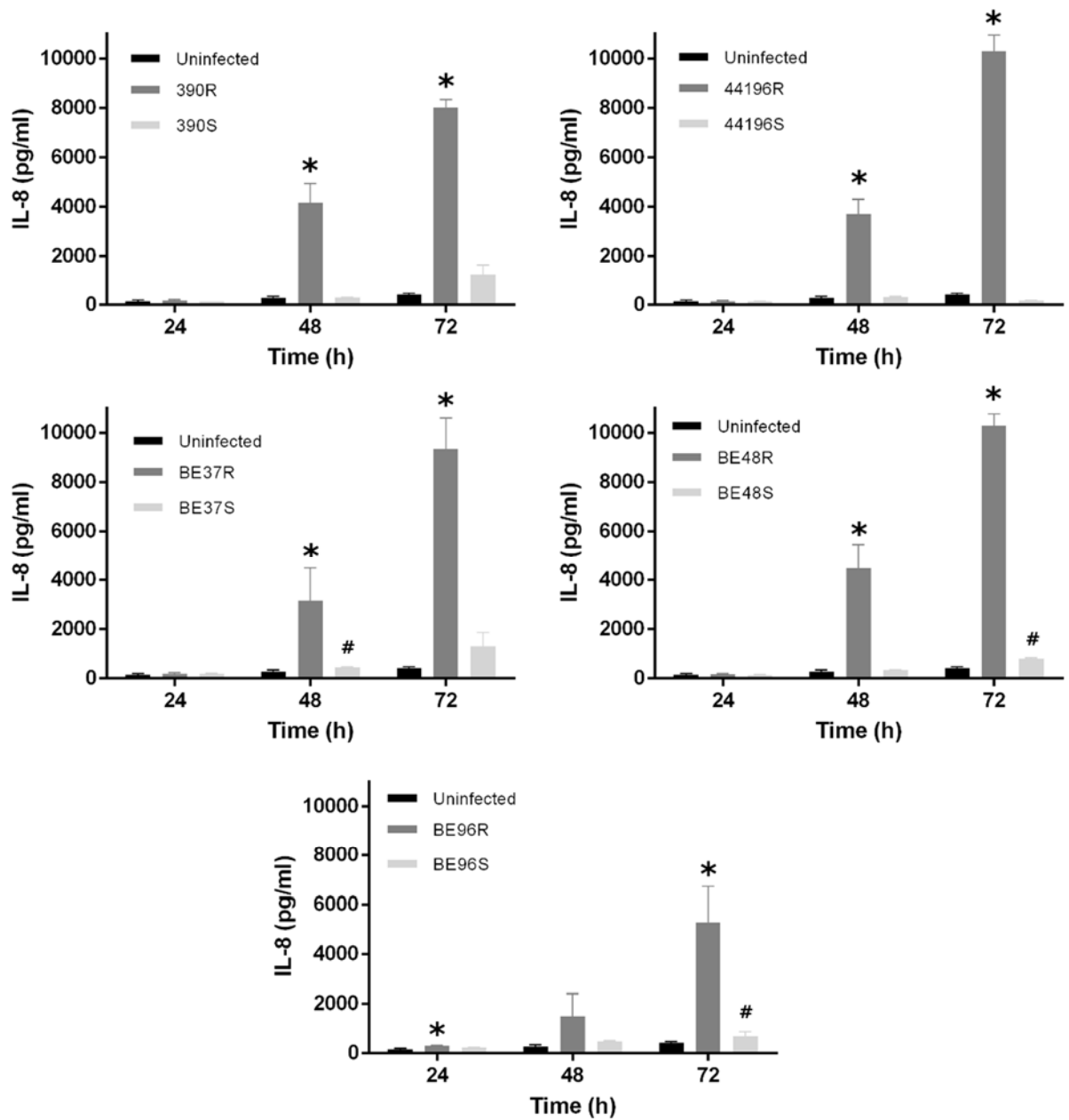


Figure 4.1.2 IL-8 production of A549 cells when infected with the two morphotypes of each strain of *M. abscessus* studied. * indicates significant difference between R and S morphotypes; # indicates significant differences between Uninfected and S morphotypes. The results represent the mean \pm SD of triplicate infections.

The contact with the major component of pulmonary surfactant did not affect the bacterial clump size

To determine whether DPPC, one of the most abundant lipids of pulmonary surfactant, could disaggregate mycobacterial clumps, a suspension of *M. abscessus* 390R was incubated with DPPC, and the formation of aggregates was comparatively quantified from the 390R suspension in PBS. No significant differences were observed between the two samples. The percentage of isolated bacilli was $67.1\% \pm 11.5$ (mean \pm SD) for the suspension treated with DPPC and $73.6\% \pm 9.6$ for the control with PBS. Clumps with 3-4 bacilli constituted $14.3\% \pm 1.5$ of the DPPC suspension and $11\% \pm 1.8$ of the PBS suspension, and large aggregates constituted $18.5\% \pm 10$ and $15.4\% \pm 7.8$, respectively, of the clumps observed (Figure 4.1.3).

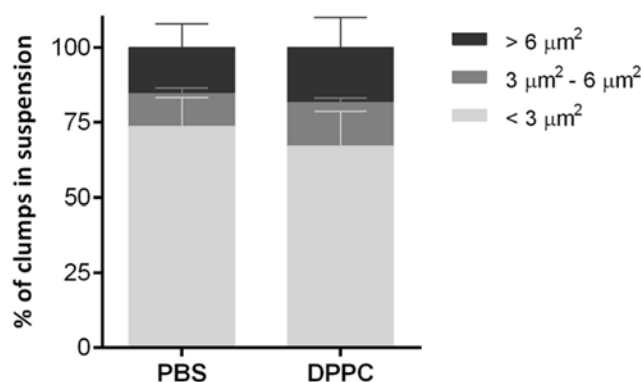


Figure 4.1.3 Results of the analysis of the percentages of clumps of different sizes present in bacteria suspensions treated with dipalmitoyl phosphatidylcholine (DPPC) and the negative control with phosphate saline buffer (PBS). The results represent the mean \pm SD of triplicate preparations.

4.2. The most superficial lipids in *M. abscessus* cell wall

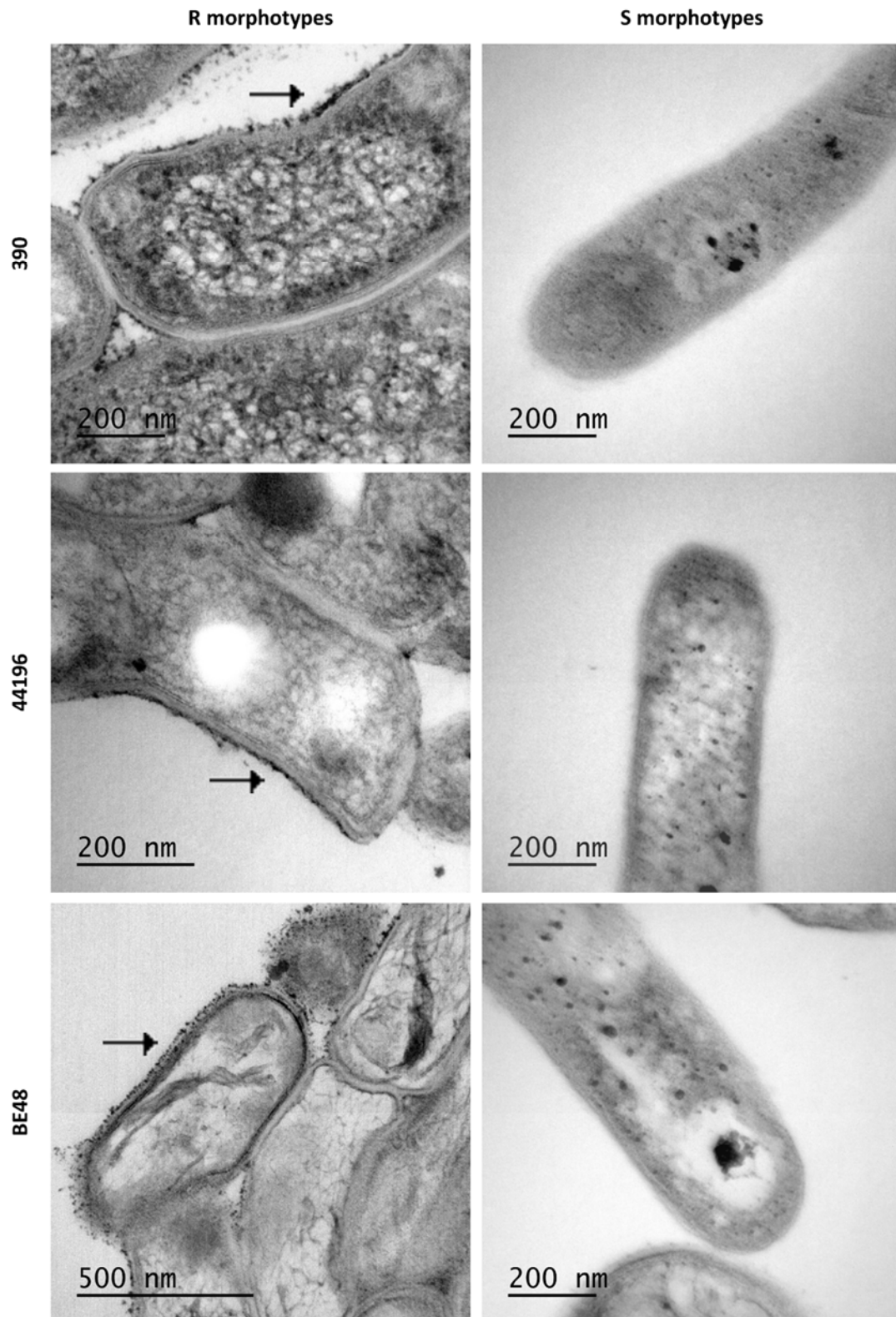


Figure 4.2.1 An electron-dense material is observed on the cell wall of R morphotypes. Images obtained by TEM of *M. abscessus* bacilli. Arrows indicate the accumulation of electron-dense material on the wall of the R morphotype.

R morphotypes had an electrodense material in the outer layer of the cell wall

When bacilli of the R and S morphotypes of *M. abscessus* were visualized by TEM, some electrodense layers and some electrotransparent layers were detected on their cell wall. It was of special interest that electrodense material irregularly accumulated in the outer layer of the bacilli from the R morphotype (Figure 4.2.1), whereas this material did not accumulate in the S morphotype cell wall (Figure 4.2.1). When a minor magnification of the TEM images was analyzed, the cord organization in the R morphotype and the accumulation of this electrodense material outside the cord were observed (Figure 4.2.2A).

The OTO stain provides a major contrast of the lipidic components because it augments the OsO₄ deposit on these lipids. An important accumulation of OsO₄ was observed outside the bacilli in R morphotypes from the samples treated with this stain, and no accumulation was observed in S morphotypes (Figure 4.2.2B).

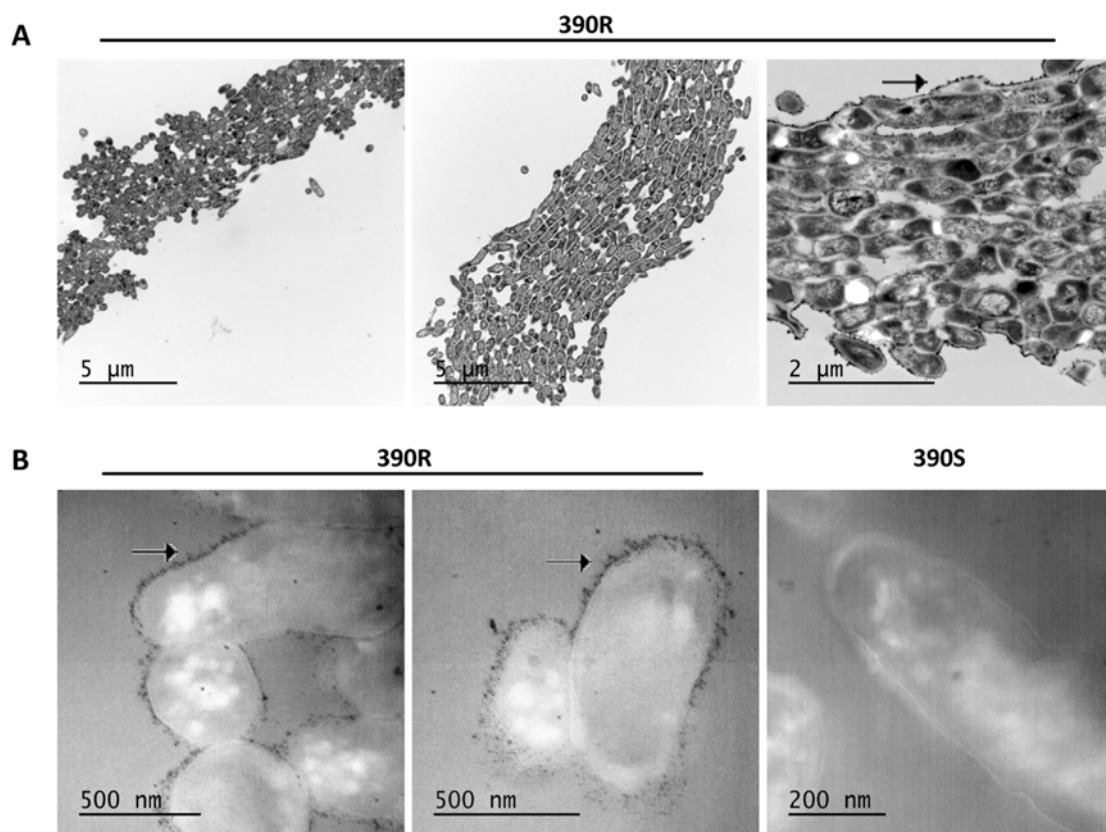


Figure 4.2.2 **A** Example of cord formation in *M. abscessus* 390R. Arrows indicate the accumulation of electrodense material outside the cord. **B** Images of OTO staining, showing an important deposit of OsO₄ in the R morphotype and no deposits in the S morphotype. Images from *M. abscessus* 390R. Similar images were obtained from the other strains.

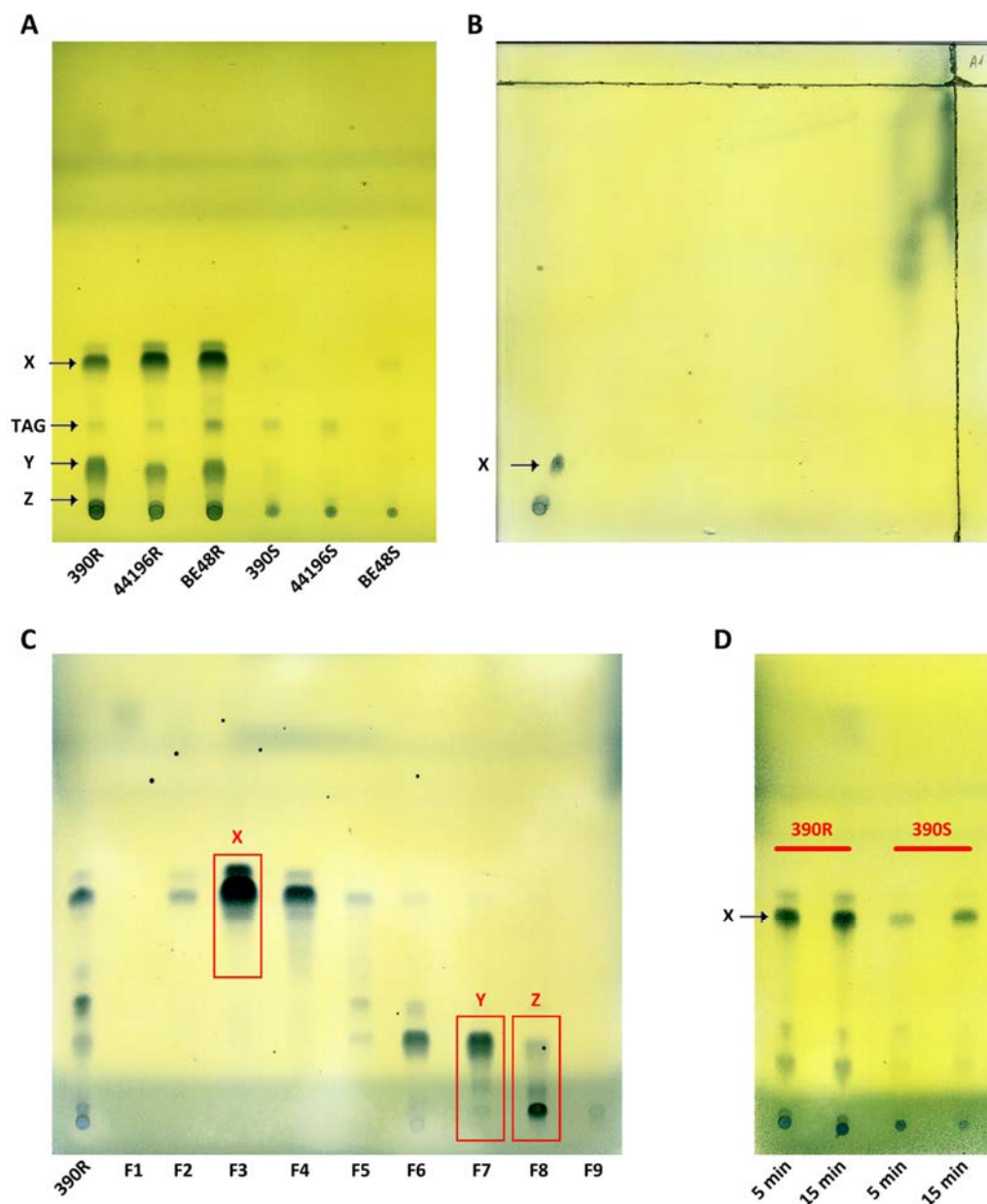


Figure 4.2.3 **A** TLC of all PE extracts. The solvent system used was PE 60-80°C/diethyl ether (90:10, v/v). **B** Bidimensional TLC of the PE extract from 390R M. abscessus eluted with PE 60-80°C/ethyl acetate (98:2, v/v, thrice, first direction) and PE 60-80°C/acetone (98:2, v/v, once, second direction). **C** TLC of all the fractions (F1-F9) obtained when performing a column chromatography to the PE extract from 390R M. abscessus. The solvent system used was PE 60-80°C/diethyl ether (90:10, v/v). Fractions 3, 7 and 8, corresponding to compound X, compound Y and compound Z, were analyzed by NMR and MS. **D** TLC of the PE extracts obtained from 390R and 390S after 5 minutes and after 15 minutes of extraction. The solvent system used was PE 60-80°C/diethyl ether (90:10, v/v). All these TLC were revealed with 10% phosphomolybdic acid. X (Compound X), TAG (Triacylglycerides), Y (Compound Y), Z (Compound Z).

TPP were detected in the superficial PE extract from the R morphotypes

Organic material was detected only when PE extracts from R morphotypes were developed in unidimensional TLC eluted with PE 60-80°C/diethyl ether (90:10, v/v) (Figure 4.2.3A) and bidimensional TLC eluted with PE 60-80°C/ethyl acetate (98:2, v/v, thrice, first direction) and PE 60-80°C/acetone (98:2, v/v, once, second direction) (Figure 4.2.3B). When PE extracts were monitored with other TLC developing systems, no organic material was observed. In samples from R morphotypes, two relevant compounds (X and Y) were observed when unidimensional TLC plates were revealed with phosphomolybdic acid (Figure 4.2.3A). After PE extracts were fractionated on a silica gel column, a third compound that was retained at the point of sample application in TLC was purified (compound Z) (Figure 4.2.3C). Only trace amounts of compound X were detected in samples from 390S and BE48S strains (Figure 4.2.3A), and none of the compounds were detected in the 44196S extract. When extraction with PE was extended from 5 to 15 min, compound X spots showed more intensity in S morphotype samples, thus suggesting that S morphotypes can synthesize this compound but that it is not exposed on the surface (Figure 4.2.3D).

Trace amounts of TAG were detected in all the morphotypes. No other lipidic compounds were detected in these PE extracts. Also, no differences in the lipidic profile were observed in the PE extracts from bacteria cultured after being extracted.

Purified compound X was identified by NMR spectroscopy and mass spectrometry as TPP type A (Figure 4.2.4). The identification was made on the basis of comparison with previous data (Burbaud et al., 2016). Figure 4.2.4B shows the ^1H NMR spectrum of TPP A. The characteristic ^1H and ^{13}C resonances of TPP A glucosyl units were clearly observed. A doublet at 5.28 ppm corresponding to anomeric proton H1, the characteristic triplet at 5.50 ppm corresponding to H3 and peaks at 5.07 (t), 5.03 (dd), 4.20 (m), 3.98 (m) and 3.97 (m) ppm corresponding to H4, H2, H6, H6' and H5, respectively, were identified. ^1H , ^1H -COSY correlations, as well as carbon resonances of glucosyl units, obtained from ^1H , ^{13}C -HSQC and ^1H , ^{13}C -HMBC spectra, were in accordance with the TPP A structure and with previously described values. The intense signals corresponding to the polyunsaturated fatty acyl substituents are indicated in the figure. The MALDI-TOF/MS analysis further confirmed the identity of the molecule (Figure 4.2.4C) (Burbaud et al., 2016). Residual TAG was detected by both NMR and MS

(indicated with asterisks in the ^1H spectrum on Figure 4.2.4B). TAG of the 390R strain were purified and identified by NMR (Figure 4.2.5).

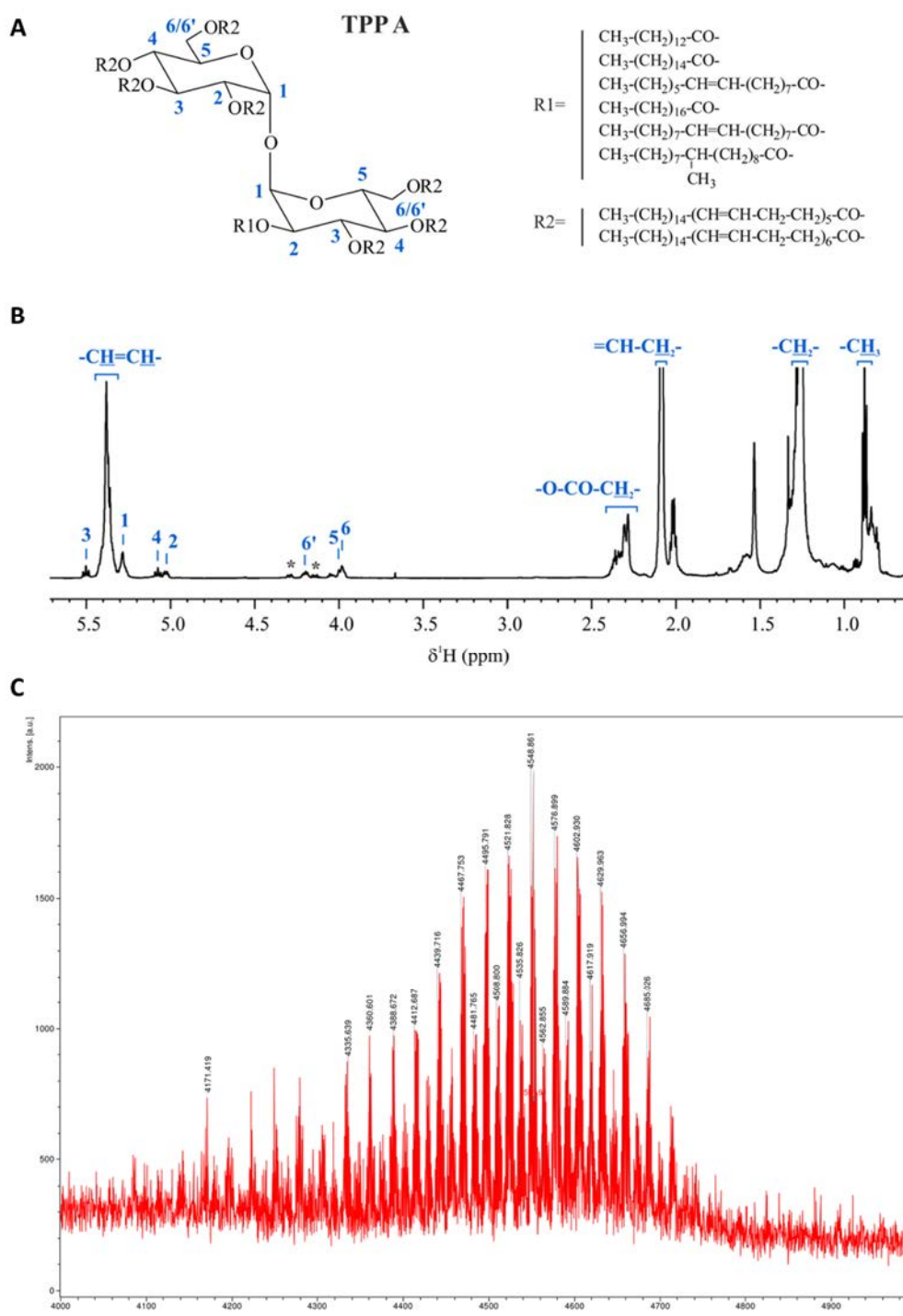


Figure 4.2.4 **A** Chemical structure of Compound X purified from *M. abscessus* 390R. Length and structure of R1 and R2 were obtained from Burbaud et al., 2016. **B** ^1H NMR spectra of compound X in CDCl_3 with peaks corresponding to the TPP A assignment (asterisks denote signals of TAG impurities). **C** MALDI-TOF mass spectrum of compound X (region between m/z 4000 and 5000 is magnified).

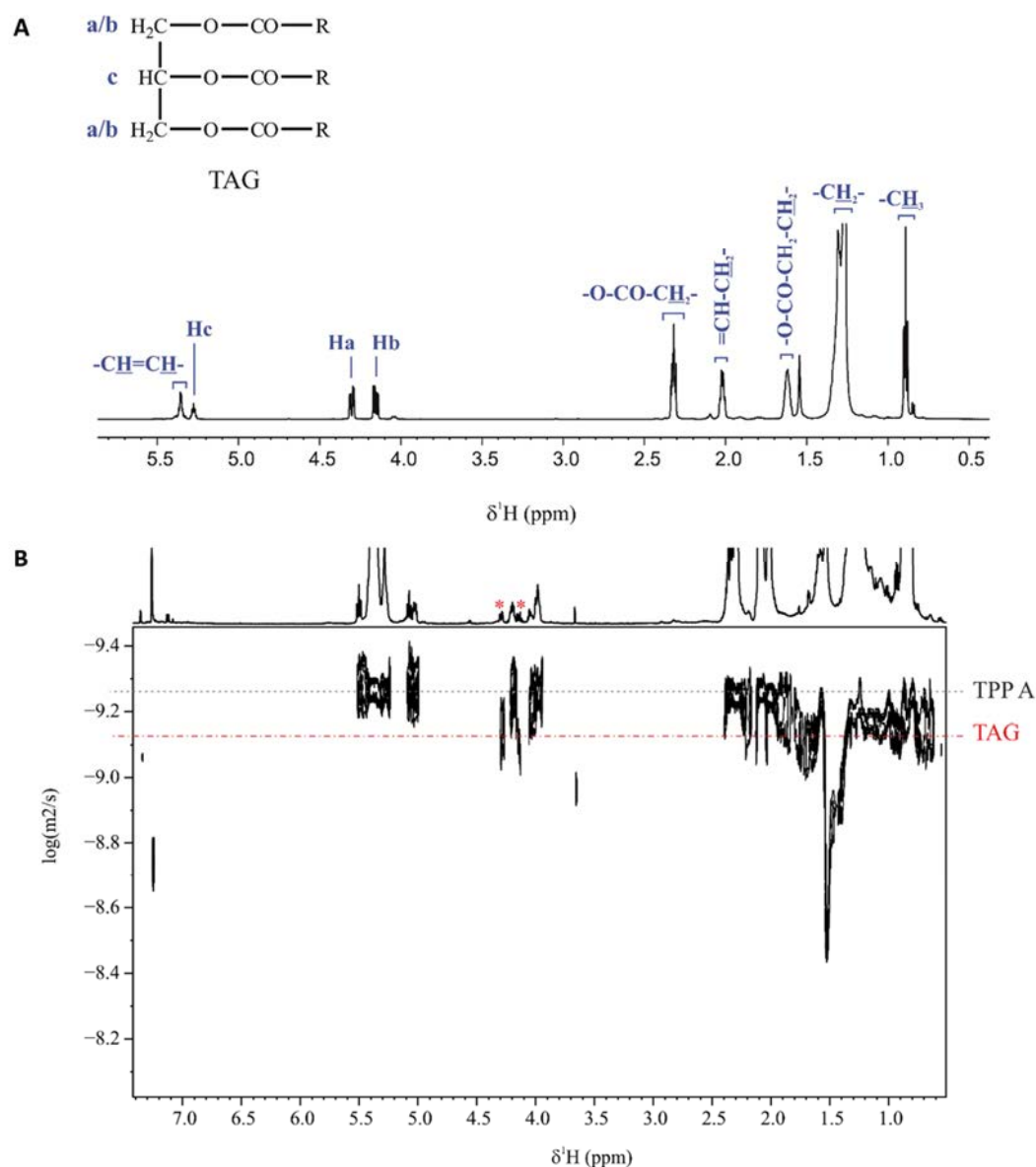


Figure 4.2.5 **A** ^1H NMR spectrum of TAG from PE extract of 390R M. abscessus strain in CDCl_3 , at a magnetic field of 600.13 MHz and 298.0 K of temperature. **B** 2D DOSY spectrum of TPP-A from PE extract of 390R M. abscessus strain in CDCl_3 at a magnetic field of 600.13 MHz and 298.0 K of temperature; asterisks denote signals of TAG.

Compounds Y and Z were isolated and analyzed separately by NMR spectroscopy and MS. The concerted analysis of the NMR spectra allowed for their ^1H and ^{13}C NMR characterization (Figures 4.2.6 and 4.2.7). Both compounds were identified as TPP molecules. The ^1H spectra and 2D correlations showed the same signals as TPP A plus some new peaks. In both cases, the presence of a characteristic multiunsaturated

system (broad peak at δ_H 5.4 ppm correlated via HSQC to a peak at δ_C 127-130 ppm), as well as methylene (δ_H 1.2-1.3 ppm) and methyl groups (δ_H 0.9 ppm) characteristic of alkyl chains were observed.

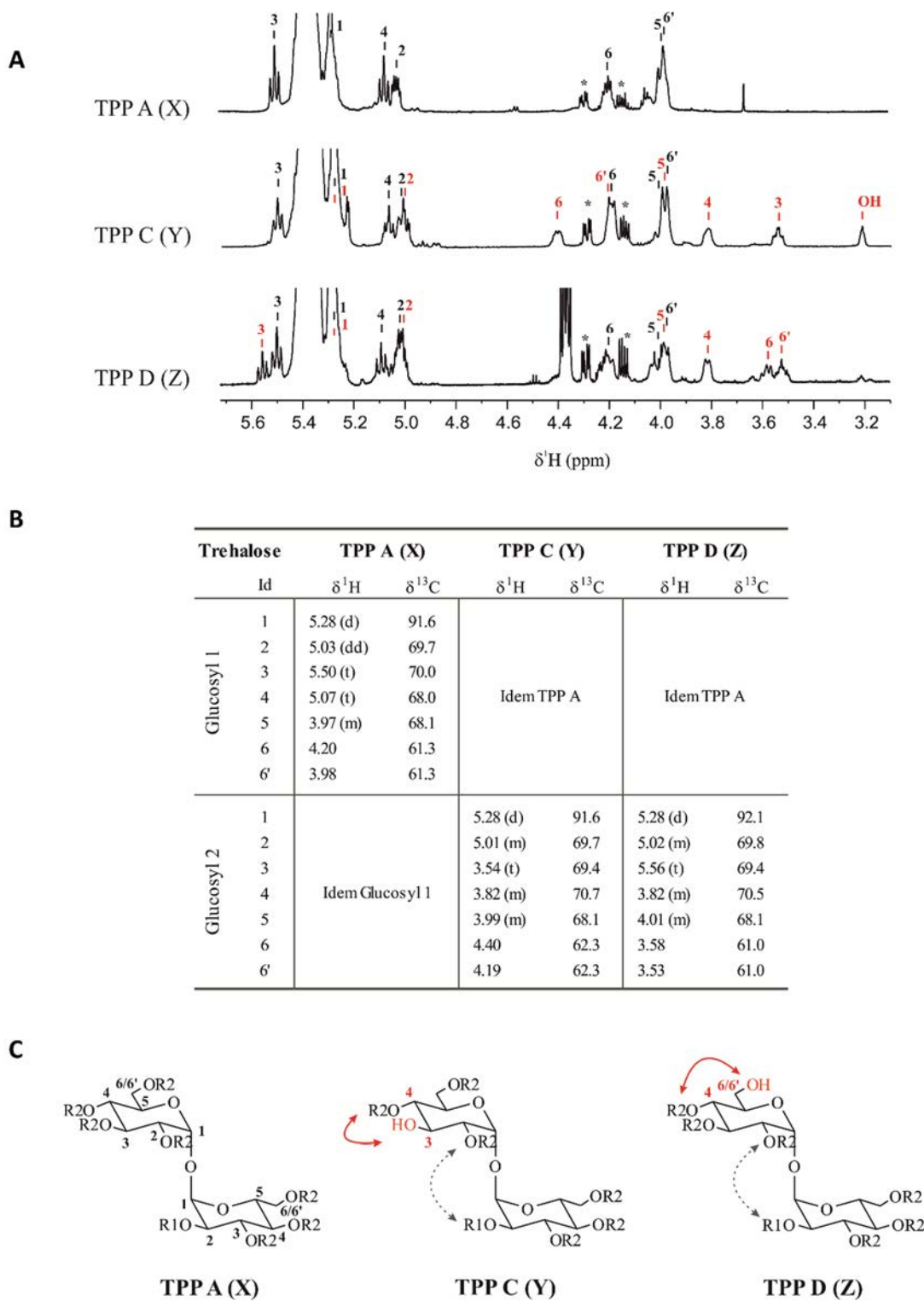


Figure 4.2.6 **A** 1H NMR spectra in $CDCl_3$ (enlargement of the region between 5.7 and 3.4 ppm); asterisks denote signals of TAG; **B** 1H and ^{13}C NMR characterization of the trehalose units and **C** suggested structures for TPP A (compound X), TPP C (compound Y) and TPP D (compound Z).

The same ^1H and ^{13}C NMR signals corresponding to the TPP A trehalose unit were exhibited in spectra of Y and Z, thus suggesting that they have a common glucosyl residue. In the case of compound Y, H3 (3.54 ppm) and H4 (3.82 ppm) of the second glucosyl residue were strongly shielded compared with those of TPP A (5.50 and 5.07 ppm, respectively), which suggests that position 3 and/or 4 are not acylated. Similarly, H4 (3.82 ppm), H6 (3.58 ppm) and H6' (3.53 ppm) of the second glucosyl residue of Z were strongly shielded compared with analogous protons of TPP A (5.07, 4.20 and 3.98 ppm, respectively), which suggests that position 4 and/or 6 are not acylated. These results were supported by MS analyses (Figure 4.2.8). Compounds Y and Z yielded analogous MALDI-TOF MS spectra, which indicates that they are structural isomers. Their mass also suggested the lack of one R2 substituent compared with TPP A (an envelope of peaks between m/z 4093 and 3849 for Y and Z, in contrast with m/z 4596 and 4297 for TPP A).

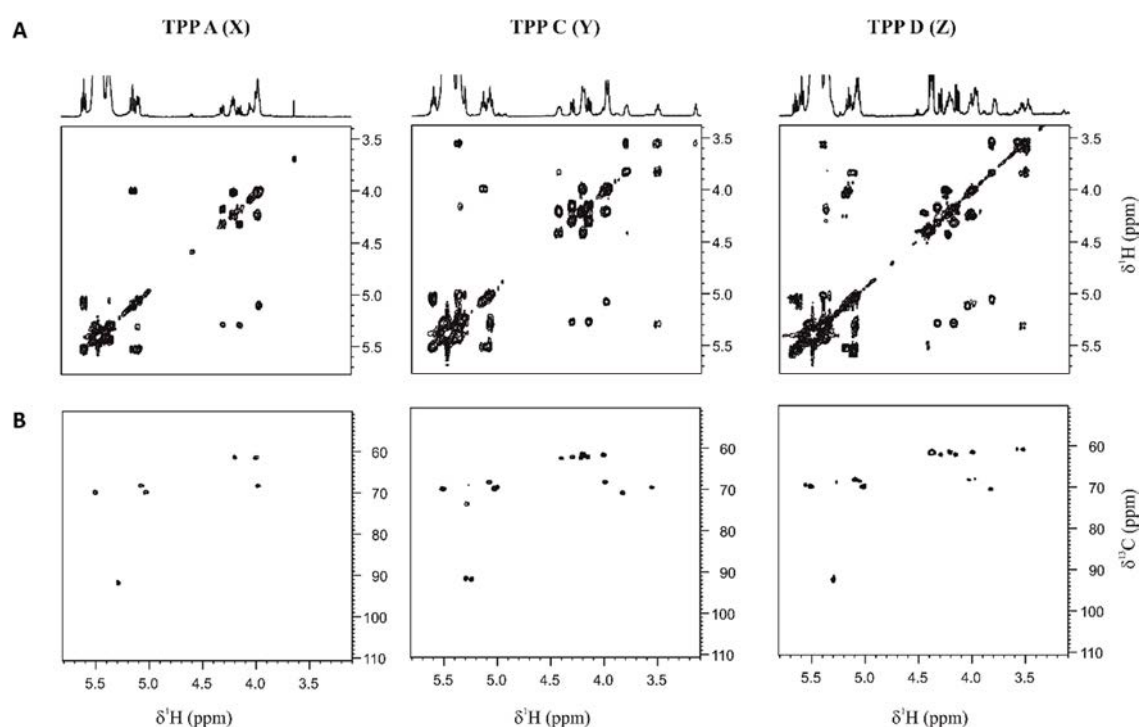


Figure 4.2.7 **A** 2D ^1H , ^1H -COSY and **B** ^1H , ^{13}C -HSQC of TPP A (compound X), TPP C (compound Y) and TPP D (compound Z) in CDCl_3 .

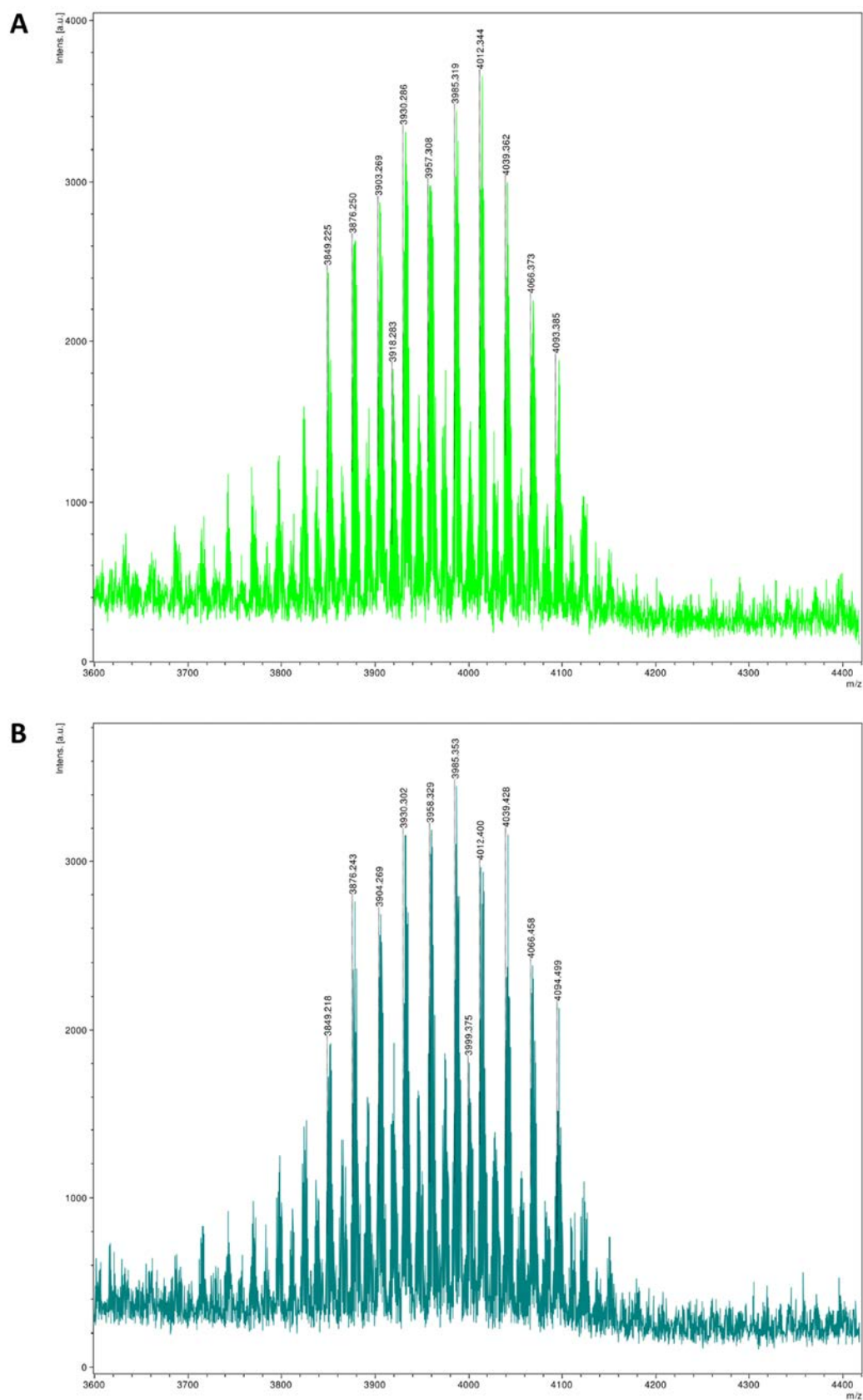


Figure 4.2.8 MALDI-TOF MS spectra of **A** TPP C (compound Y) and **B** TPP D (compound Z) (region between m/z 3600 and 4400 was magnified).

4.3. Study of the toxicity and function of TPP

TPP-coated beads had no effect on the viability of J774 macrophages

As observed with CLSM, macrophages did not distinguish between uncoated and TPP A-coated beads in phagocytosis (Figure 4.3.1A). Both types of beads were found inside the cells and in a similar ratio. J774 macrophages with phagocytized uncoated beads represented a percentage of $32.39\% \pm 5.08$ from the total of counted macrophages, and macrophages with phagocytized TPP A-coated beads represented the $37.69\% \pm 9.73$. Related with the possible toxicity of TPP A, no differences were observed when analyzing the colocalization of the beads inside the macrophages with acidic vesicles. Pearson's correlation coefficient was of 0.40 ± 0.16 for uncoated beads and of 0.54 ± 0.15 for TPP A-coated beads (the results represent the mean \pm SD of triplicate preparations) (Figure 4.3.1B).

Moreover, macrophage viability was not altered after the interaction with TPP A-coated beads. No significant differences were observed in the viability of macrophages in contact with uncoated beads or TPP A-coated beads (Figure 4.3.1C). When cytokine production was analyzed, no production of TNF- α and IL-6 was detected in macrophages treated either with uncoated or TPP A-coated beads (data not shown). Similar results were obtained when macrophages were in contact with beads coated with the mix of TPP molecules (TPP A, Y and Z compounds), that is no effect on the viability of the macrophages was observed (Figure 4.3.1C) and no production of TNF- α and IL-6 was detected (data not shown). Bacteria from R morphotype had the expected action in front of macrophages, as it has been already published (Brambilla et al., 2016). 390R strain killed all macrophages within 72h. No difference between these results and the results obtained from bacteria PE-treated were observed (Figure 4.3.1C).

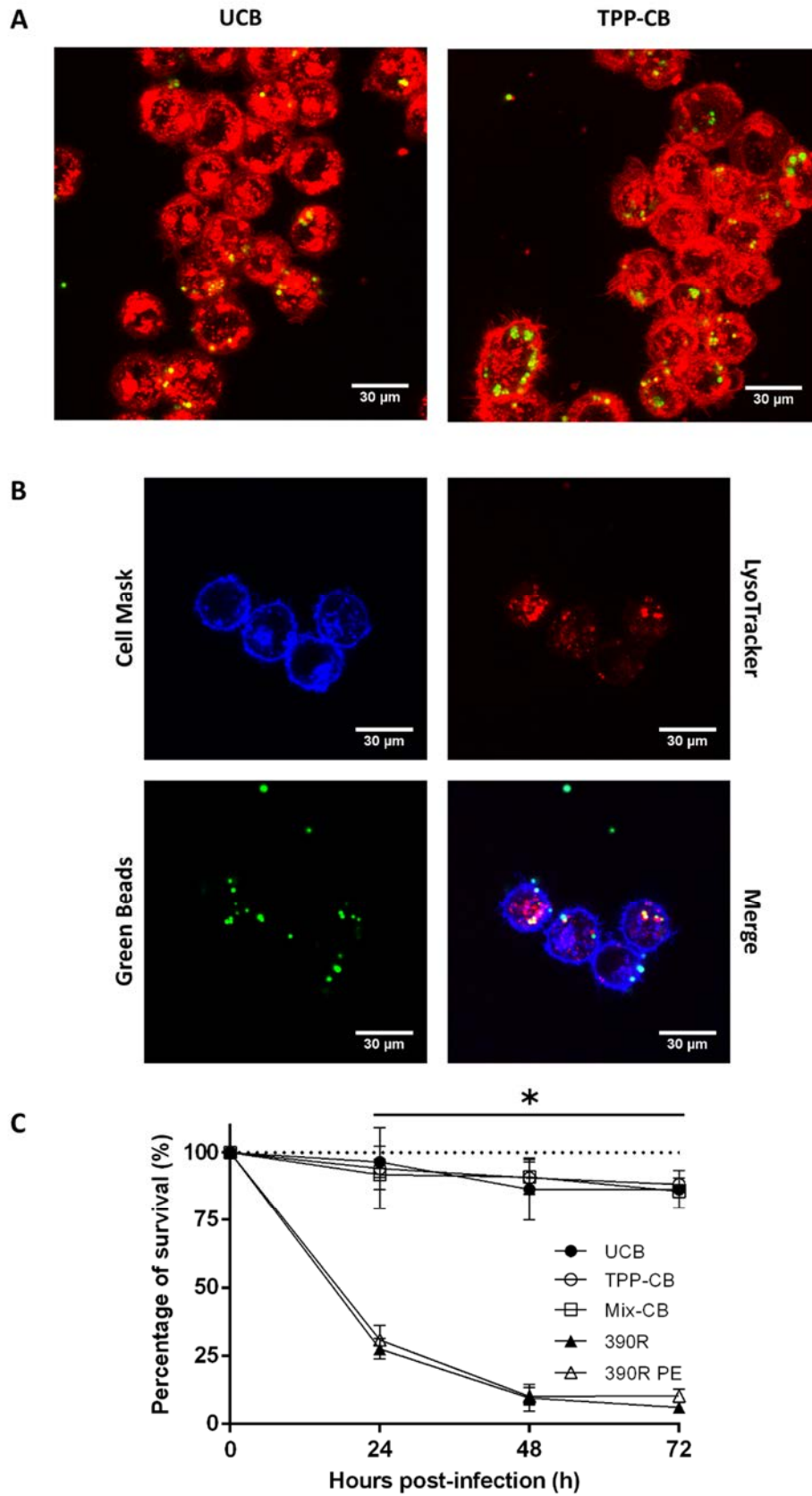


Figure 4.3.1 A Example of the images obtained by CLSM that were used to study the phagocytosis of the beads; macrophages phagocytose both types of beads. Bar size 30μm.

B Images of colocalization of beads and acidic vesicles. Macrophages in blue stained with Cell Mask Deep Red, beads in green and acidic vesicles in red with LysoTracker Red. Bar size 30µm.

C Viability of macrophages treated with uncoated beads (UCB); TPP A-coated beads (TPP-CB); beads coated with TPP A, compound Y and Z (Mix-CB); 390R M. abscessus strain (390R) and 390R M. abscessus PE treated (390R PE). Significant differences were detected only between macrophages treated with beads and macrophages infected with bacteria (* $P < 0.05$). The data are representative of one out of three independent experiments.

TPP-coated beads had no effect in A549 growth

No effect in the growth of A549 was observed when these cells were treated with uncoated beads and with TPP A-coated beads. The growth was never reduced or inhibited when the cells were putted in contact with uncoated beads, but no effect of the TPP was detected neither in relation with the growth of the A549 cells (Figure 4.3.2A).

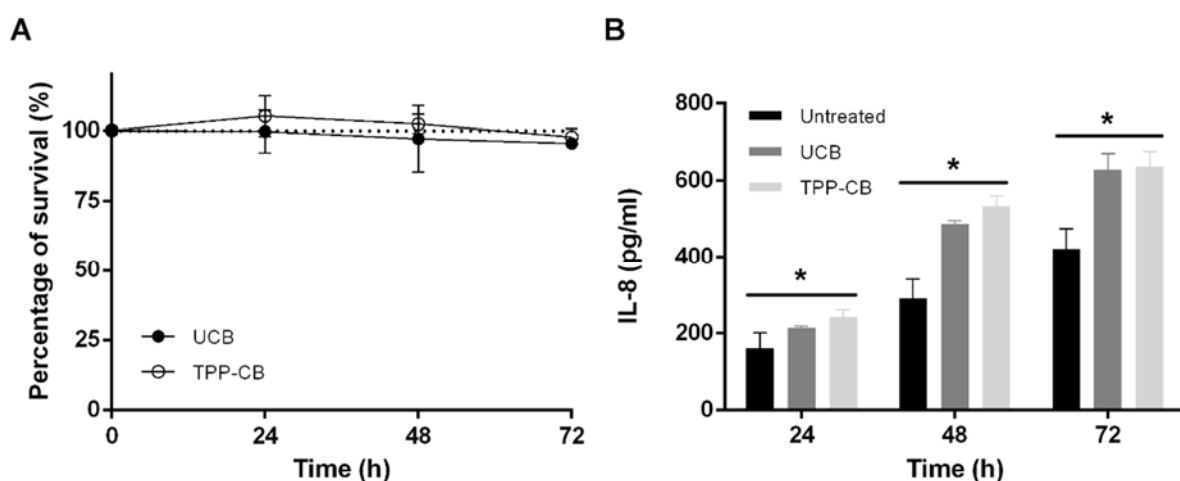


Figure 4.3.2 A Viability of A549 cells that were treated with TPP-coated and uncoated beads.

No significant differences were observed. The data are mean \pm SD of three independent experiments. **B** IL-8 production of A549 cells treated with TPP-coated and uncoated beads. No significant differences were observed between the production of IL-8 induced by the uncoated beads and the production induced by the TPP-coated beads. However, the treatment with beads induced the production of a significant small amount of IL-8. The data are mean \pm SD of three independent experiments. UCB (Uncoated beads), TPP-CB (TPP-coated beads), * ($p < 0.05$).

TPP A-coated beads induced the production of small amount of IL-8 by A549, a little quantity that was significantly different from the amount produced by the untreated cells. However, this quantity was practically insignificant when compared to the quantity of IL-8 produced due the presence of an R morphotype of *M. abscessus*. This small amount of IL-8 was also induced by the uncoated beads. No significant differences were detected between the quantity of IL-8 induced by uncoated beads and the quantity induced by TPP A-coated beads (Figure 4.3.2B).

TPP-coated beads had no effect in THP-1 viability

After 3 hours of interaction with uncoated beads and TPP-coated beads no difference in the viability of the human macrophages THP-1 was detected. Also, the viability of these cells was near 100%. In contrast, THP-1 cells infected with 390R strain showed a decrease in the viability of 12%, that was significant in comparison with the viability of the THP-1 cells infected with the S morphotype of this strain. 390S did not affect the cells, the percentage of viability was also near to 100% (Figure 4.3.3).

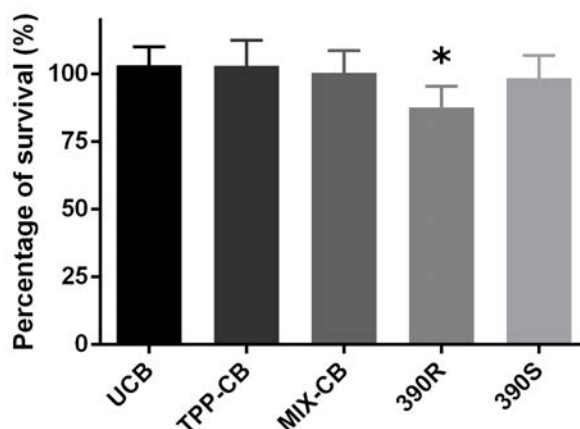


Figure 4.3.3 Percentage of survival of THP-1 human macrophages after 3 hours in contact with uncoated and TPP-coated beads, and after 3 hours of infection with 390R and 390S *M. abscessus*. The reduction of the viability in the case of 390R was significant, (* $p < 0.05$), in comparison with the effect of 390S or of the beads. The data are mean \pm SD of three independent experiments. UCB (Uncoated beads), TPP-CB (TPP A-coated beads), Mix-CB (beads coated with TPP A, compound Y and Z).

Cord disorganization was observed after treatment of pellicles of R morphotypes with PE

Pellicles of R morphotypes that were untreated or treated with PE were observed by using optical microscopy after they were stained with the Ziehl-Neelsen method. Bacteria in the untreated samples were aggregated, forming clumps and cords, and only a few bacteria were solitary (Figure 4.3.4). However, disintegration of clumps and cords was observed in samples treated with PE. In these samples, higher amounts of free bacteria in all the fields monitored from each preparation were clearly observed. Although in some points there were still some aggregates, the disorganization of the clumps and cords was evident (Figure 4.3.4).

Regarding viability, no effect of the PE treatment was observed in the CFU count. The viability of the bacteria was not affected for the extraction, and the same occurred with the colonial morphology.

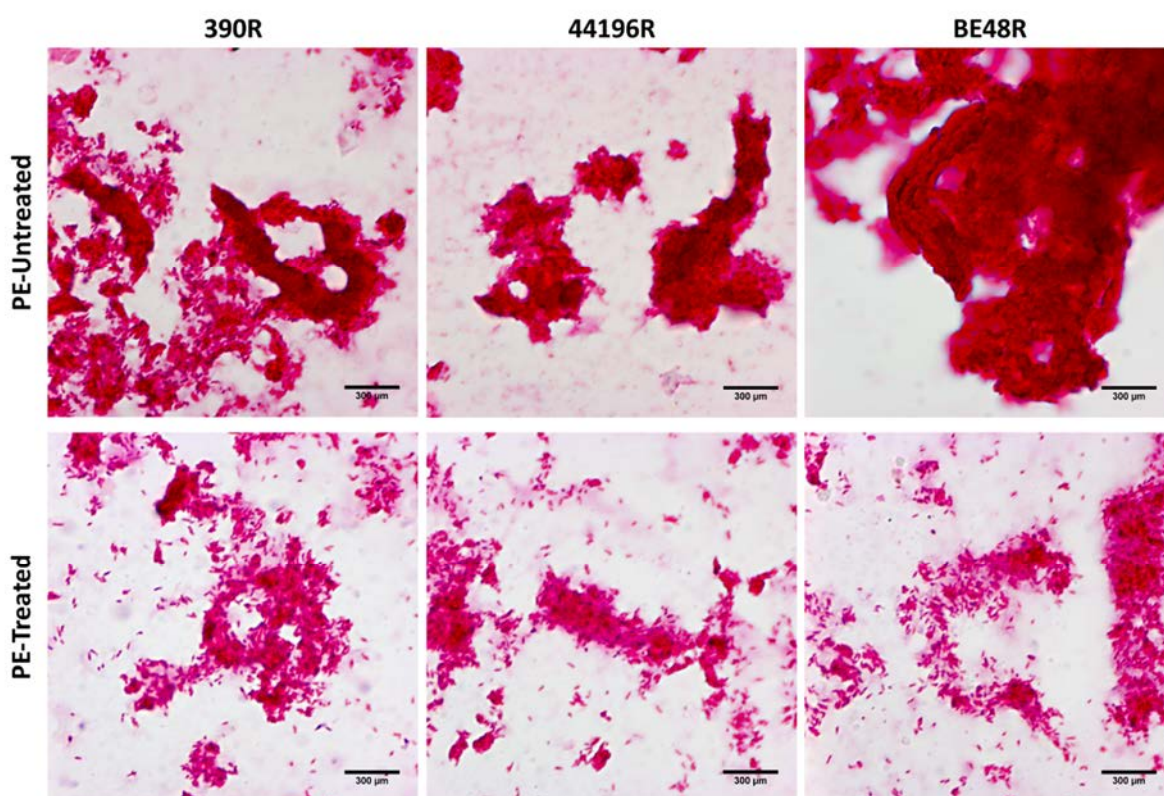


Figure 4.3.4 Observation by optical microscopy of untreated and treated with PE for 5 minutes' samples, both stained using the Ziehl-Neelsen method. Cord disorganization in PE-treated bacteria is observed. Bar size 300μm.

TPP-coated beads formed aggregates

The coating of beads by TPP A was confirmed by CLSM, because Nile Red stained the lipids coating the beads (Figure 4.3.5A and B), and these beads appeared to be surrounded by red fluorescence. When observed by CLSM, the TPP A-coated beads presented more aggregation than uncoated beads. Statistical analysis showed significant differences between the areas of the aggregates of the two samples, thus indicating that TPP A-coated beads produced larger aggregates than uncoated beads (Figure 4.3.5C). The percentage of aggregates that were larger than $6\ \mu\text{m}^2$ was $20.4\% \pm 5.7$ (mean \pm SD) for the uncoated beads and $38.9\% \pm 6.2$ ($p < 0.05$) for the TPP A-coated beads. The difference in area between aggregates of uncoated beads that were smaller than $3\ \mu\text{m}^2$ ($57.0\% \pm 2.3$ of the area covered) and aggregates of TPP A-coated beads of the same size ($38.8\% \pm 7.5$ of the area covered) was also significant (Figure 4.3.5C). These results are obtained from beads coated with TPP A. However, as mentioned, beads were coated also with a mix of the three compounds described by NMR (TPP A, Y and Z), all TPP molecules, and no differences were observed between the results obtained with the beads coated with TPP A and those obtained with the beads coated with the mix of TPP molecules (TPP A, Y and Z compounds).

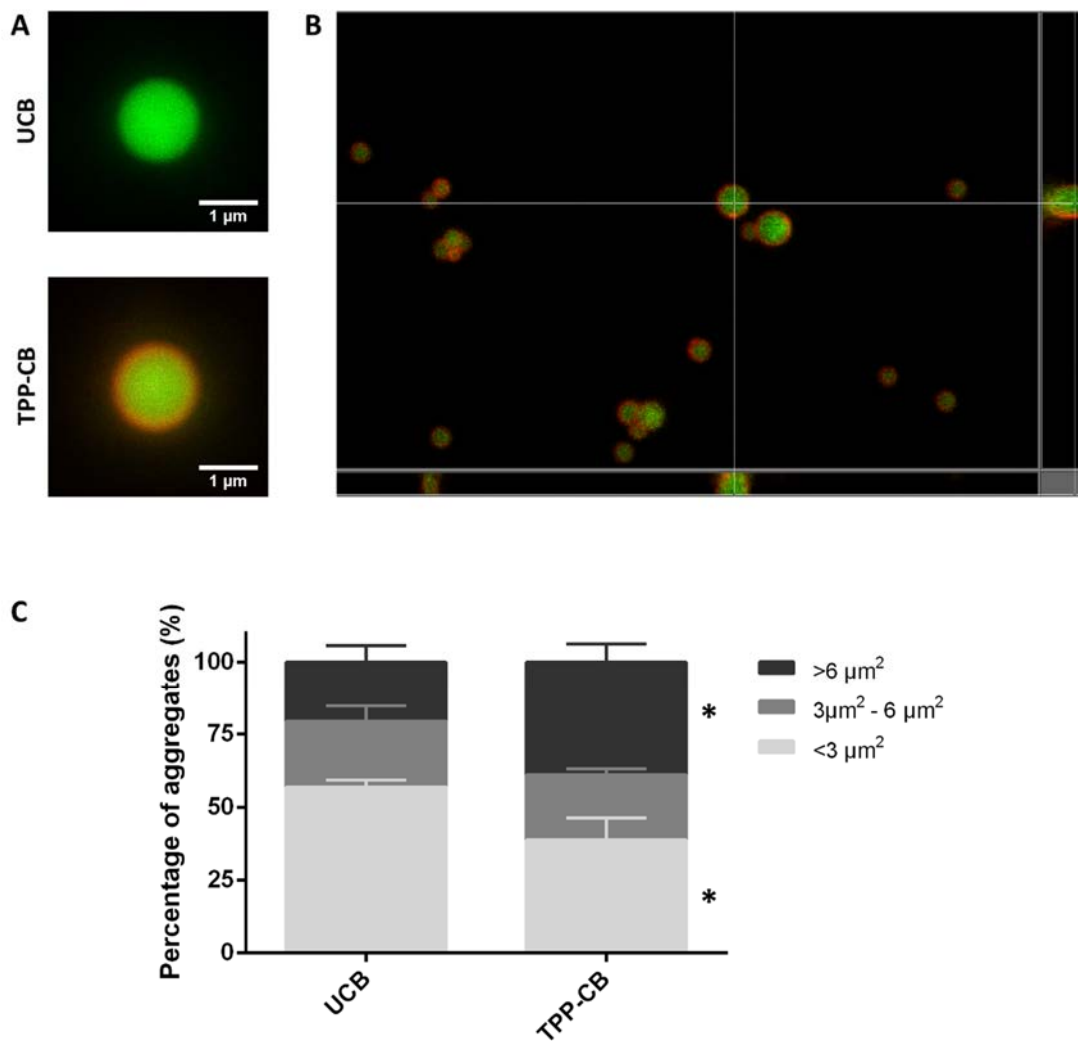


Figure 4.3.5 Beads are covered by TPP and aggregate. **A-B** Beads are in green and TPP-coating is observed as the red covering, owing to staining with Nile Red. Bar size in **A** 1 μm . **C** Results of the study of bead aggregation. * $p < 0.05$ in multiple t -test. The results represent the mean \pm SD of triplicate preparations.

4.4. Superficial extraction in other Mycobacteria

No TPP were detected in the PE extracts performed in different Mycobacteria

As the TLC shows in figure 4.4.1A, there was no significant amount of TPP in the superficial extraction performed in the R morphotypes of *M. vaccae* and *M. kansasii*, and in *M. brumae* and *M. smegmatis*. However, in this last *Mycobacterium* a compound was detected near the TPP spot (Figure 4.4.1B).

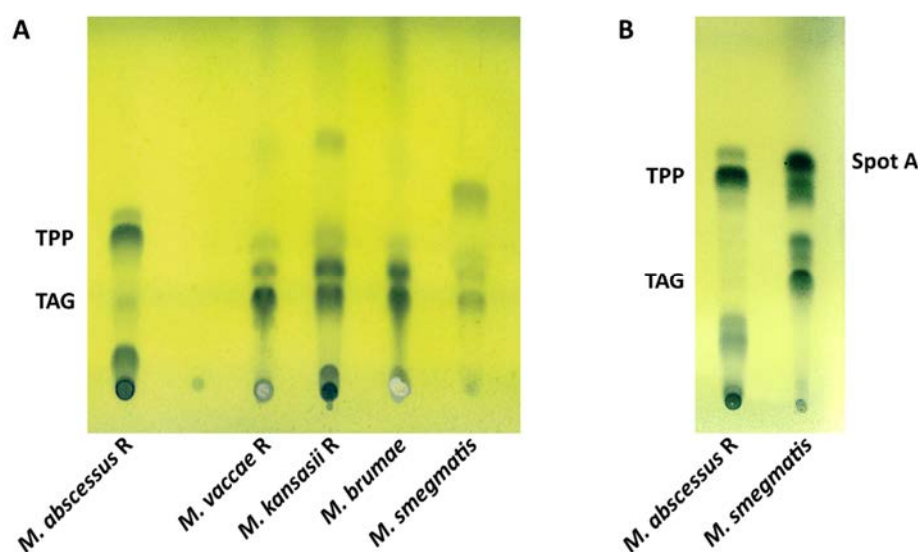


Figure 4.4.1 **A** TLC of the PE extracts from the R morphotypes of *M. abscessus* 390, *M. vaccae* and *M. kansasii*, and from *M. brumae* and *M. smegmatis*. **B** Direct comparison of the PE extract from *M. abscessus* 390R and *M. smegmatis*. In both cases the solvent system used was PE 60-80°C/diethyl ether (90:10, v/v), and the TLC was revealed with 10% phosphomolybdic acid. TPP (Trehalose polyphleates), TAG (Triacylglycerides).

Detection of Spot A in *M. smegmatis* and confirmation of the structure by MS

Spot A was visualized by using TLC in the PE extract from *M. smegmatis*. This compound was less polar than triacylglycerides, which were observed below (Figure 4.4.2). After column chromatography, purified Spot A was recovered in the fraction eluted with 94:6 PE 60-80°C (b.p.)/diethyl ether (v/v). A small amount of the dried solid of the purified Spot A was analyzed by ESI-MS and MALDI-TOF to confirm that the extracted compound corresponded to the same molecule analyzed and described in previous works (Chen et al., 2006; Pacheco et al., 2013).

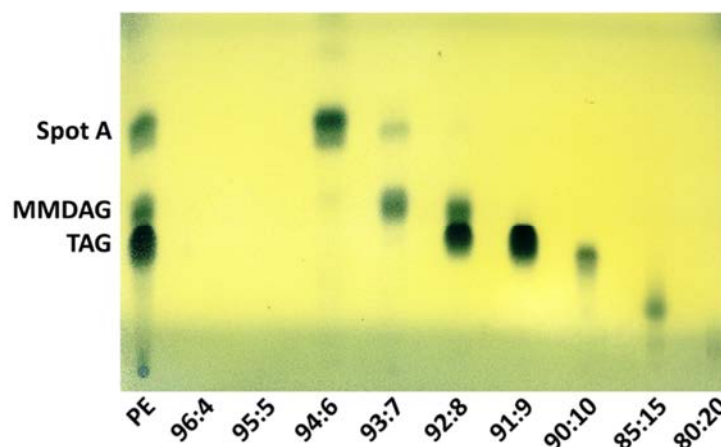


Figure 4.4.2 TLC of the different fractions obtained by column chromatography from PE extract of *M. smegmatis*. Spot A indicate the spot of mycolate ester wax, MMDAG indicate the monomeromycolyl diacylglycerols and TAG the triacylglycerols. The first line of the TLC represents PE extract before fractionated using the chromatography column, and the other lines represent the eluted fractions obtained from the column chromatography eluted with the indicated proportions of PE 60-80°C (b.p.)/diethyl ether (v/v).

The ESI-MS spectrum was similar to the one presented by Pacheco et al. (Pacheco et al., 2013) with coincident peaks as at m/z 1589 and m/z 1631 (Figure 4.4.3A). The positive MALDI spectrum was consistent with the results of the ESI-MS and reproduced the results obtained by Chen et al. (Chen et al., 2006). The three peaks separated by an increment of m/z of 14 corresponding to m/z 1616, m/z 1630 and m/z 1644 were observed also in the spectrum presented by Chen et al. (Figure 4.4.3B)

Finally, a positive MALDI-LIFT spectrum of the parent $[M+H]^+$ at m/z 1630, confirmed the presence of a fragment of m/z 1145 corresponding to mycolic acids type I of *M. smegmatis* (Laval et al., 2001) (Figure 4.4.3C).

Molecular structure characterization of Spot A by NMR spectroscopy

The rest of the dried solid was dissolved in $CDCl_3$ and analyzed by NMR spectroscopy. The NMR analysis, together with the MS information, confirmed the structure of the molecule as pentatriacontatrienyl mycolate (PTTM) (35:3) **1**, shown in Figure 4.4.4; where the PTTM **1** is formed by three methyl substituted olefinic units (A,

B and C) in the carbon chain and the mycoloyl part contains *trans* double bonds (*trans*-db) and *cis* cyclopropane (*cis*-cp) in its structure.

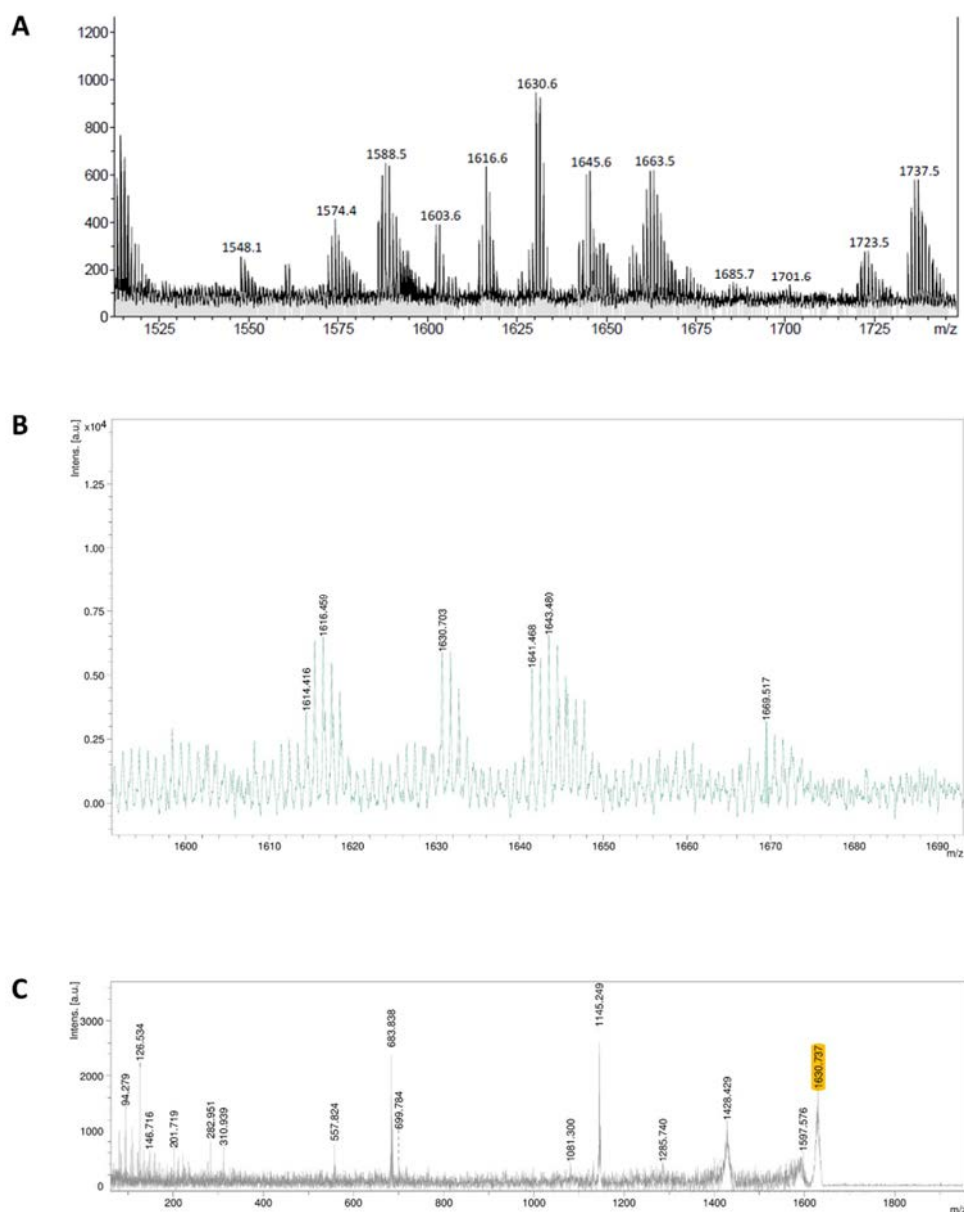


Figure 4.4.3 **A** ESI+ MS, amplifying the region between 1500 m/z and 1750 m/z. **B** positive MALDI mass spectrum, amplifying the region between 1600 m/z and 1700 m/z and **C** positive MALDI-LIFT spectrum of the parent $[M+H]^+$ at 1630 m/z of the extract corresponding to Spot A.

The complete ^1H and ^{13}C NMR characterization of the molecule was achieved by the performance of a battery of 1D and 2D NMR experiments (1D ^1H , 1D ^1H selective TOCSY, ^1H - ^1H COSY, ^1H - ^1H TOCSY and ^1H - ^1H NOESY, ^1H - ^{13}C HSQC and ^1H - ^{13}C HMBC)

and the coordinated analysis of the resulting spectra. The detailed NMR study was performed with a Bruker Avance 600 spectrometer working at 298.0 K.

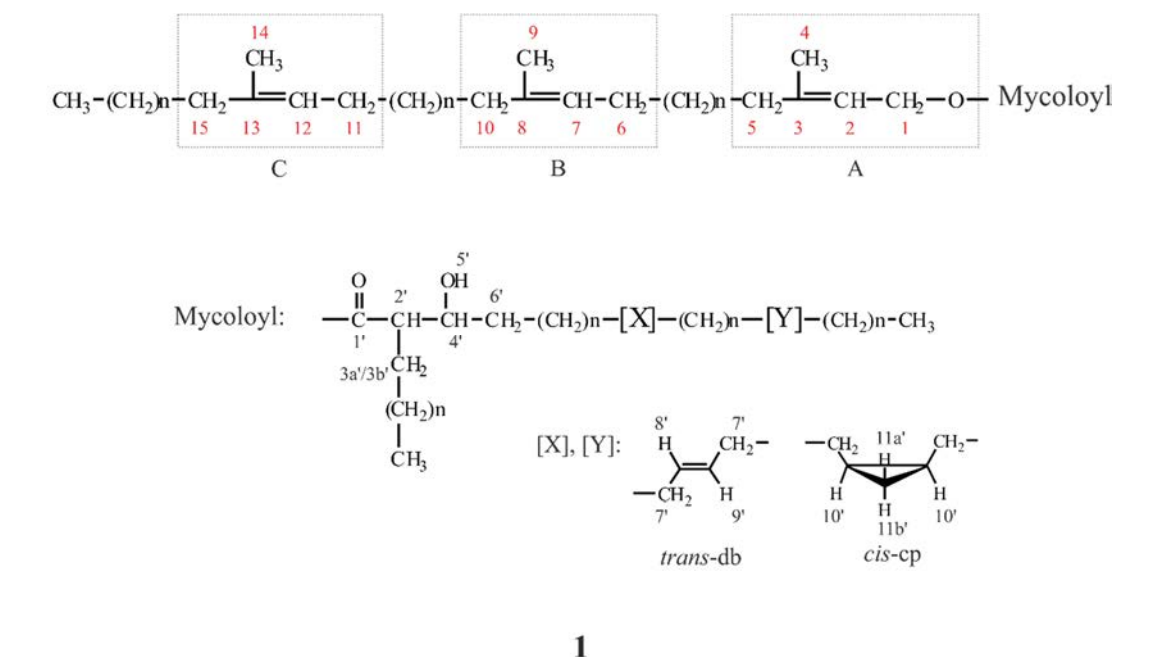


Figure 4.4.4 Structure of the pentatriacontatrienyl mycolate (35:3) **1**.

The ^1H NMR spectrum of the sample is represented in Figure 4.4.5, with the resonances of the PTTM, compound **1**, assigned. Peaks corresponding to protons of the pentatriacontatrienyl structure and the mycoloyl unit are indicated in red and black numbers, respectively.

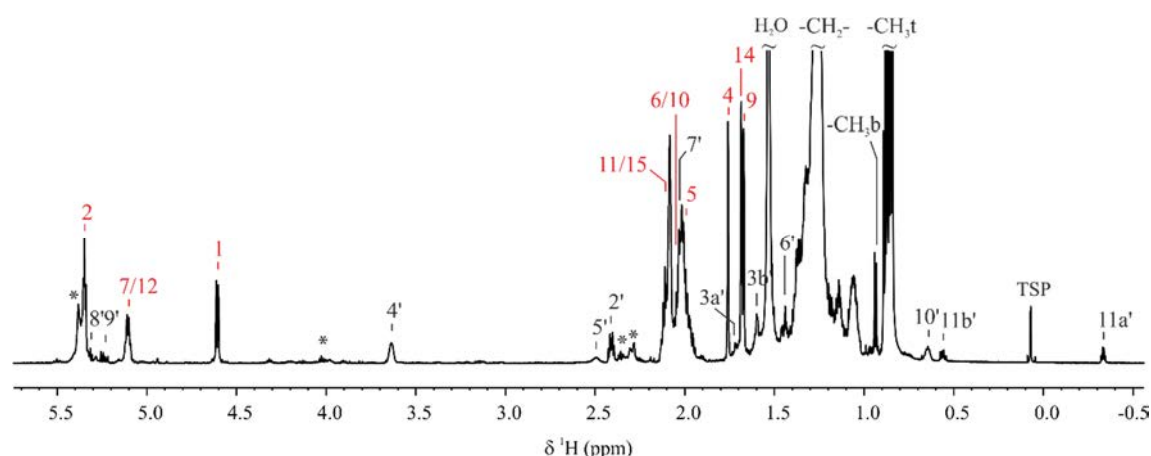


Figure 4.4.5 ^1H -NMR spectrum of purified Spot A, with signals of PTTM **1** assigned. Asterisks indicate residual amount of TTP type A. Spectrum acquired at 298.0 K and at a magnetic field of 600 MHz.

Regarding the pentatriacontatrienyl structure, in red in Figure 4.4.5, there was a characteristic sharp doublet at 4.61 ppm with a coupling constant, J , of 7.2 Hz corresponding to H1, which correlated to C1 peak at 60.8 ppm via HSQC. As well, the same H1 signal correlated to olefinic H2 (triplet at 5.35 ppm) via COSY, with methyl protons H4 (sharp intense singlet at 1.76 ppm) via TOCSY and with olefinic quaternary carbon C3 (142.5 ppm) via HMBC. H2 and H4 signals correlated to the peak of methylene protons adjacent to the double bond, H5 (2.01 ppm), via TOCSY. Signals of carbons directly bonded to spin system A protons (Figure 4.4.4) were assigned via HSQC. By an analogous reasoning, proton and carbon chemical shifts of spin systems B and C of the pentatriacontatrienyl moiety were identified. Olefinic protons H7 signal resonated at 5.14 ppm as a triplet (with a J of 5.9 Hz), being partially overlapped with analogous H12 (5.13 ppm) triplet of spin system C. H7 correlated via COSY to H6 (2.04 ppm) and via TOCSY to methyl protons H9 (an intense singlet at 1.69 ppm) and to methylene protons H10 (2.03 ppm). Similarly to spin systems A and B, spin system C was assigned presenting as characteristic resonances H12 (triplet at 5.13 partially overlapped with H7 triplet) and methyl protons H14 (intense singlet at 1.67 ppm). C6 to C15 resonances were identified via HSQC and HMBC. To elucidate the position of spin systems B and C in the molecular structure, NOE signals between proton resonances of different spin systems were searched in the 2D NOESY correlation without success. The order suggested in Table 4.4.1 was based on the slight difference between chemical shifts of protons H7 and H12, but it would be possible that the assignment of spin system B corresponded to C and *viceversa*. This fact, however, does not affect the molecular structure, just the assignment of the peaks.

Signals corresponding to the mycoloyl unit were indicated in black in Figure 4.4.5. At 2.41 ppm α -carboxylic proton H2' (directly bonded to C2' at 50.9 ppm via HSQC) correlated via COSY to β -carboxylic protons H3a' and H3b' (1.71 and 1.59 ppm) (bonded to C3' at 29.7 ppm) and to β -carboxylic proton H4' at 3.64 ppm (bonded to C4' at 72.2 ppm). The broad signal at 2.49 ppm corresponded to the hydroxylic proton, H5'. The spectrum showed typical signals corresponding to olefinic protons of *trans* double bonds, multiplets at 5.34 and 5.24 ppm (H8' and H9', respectively). Also, the protons adjacent to the double bond, H7', were identified at 2.02 ppm via COSY and TOCSY correlations. Typical signals corresponding to *cis*-cyclopropane rings were observed at 0.65 (H10', broad), 0.56 (H11b' ddd, 8.2, 8.2, 4.2 Hz) and -0.34 ppm (H11a', ddd, 4.2,

5.3, 5.3 Hz). Regarding the whole molecule, methylene chains resonated about 1.28-1.23 ppm (broad intense signal), branched methyl groups, CH₃b, at 0.94 ppm (d, 6.7 Hz) and terminal methyl groups, CH₃t, resonated between 0.89 and 0.84 ppm (t, 6.8 Hz) (Yuan and Barry, 1996; Watanabe et al., 1999).

Finally, HMBC correlations between H1 and H2' with same carboxylic carbon C1' at 175.5 ppm, confirmed that both structures, pentatriacontatrienyl and mycoloyl, belonged to the same molecule. In addition to, peak integrations were in accordance with the described structure. The full ¹H and ¹³C characterization of compound **1** was collected in Table 4.4.1 and 2D correlations were gathered in Figure 4.4.6.

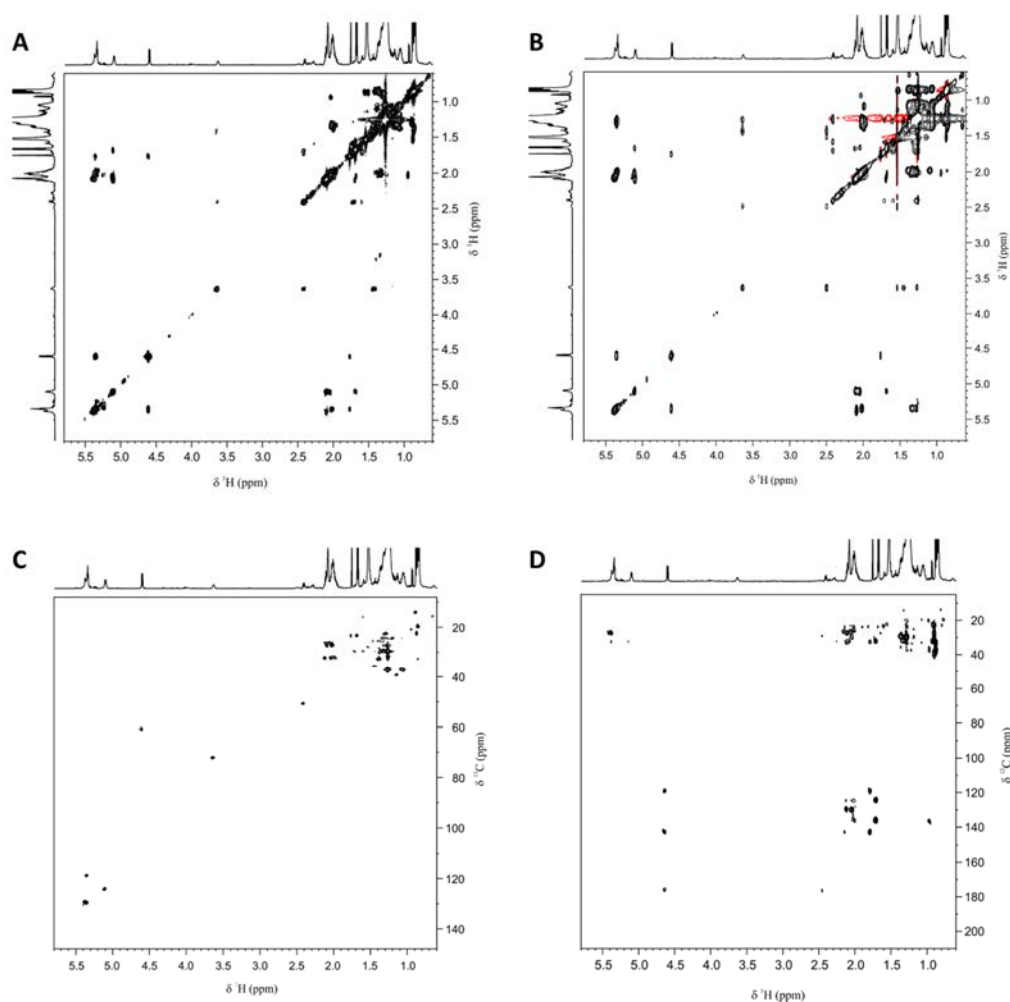


Figure 4.4.6 *A* ¹H-¹H COSY, *B* ¹H-¹H TOCSY, *C* ¹H-¹³C HSQC and *D* ¹H-¹³C HMBC of sample corresponding to TLC Spot A (pentatriacontatrienyl mycolate **1**). All the spectra were recorded at a magnetic field of 600.13 MHz and at 298.0 K of temperature.

A residual amount of TPP A in Spot A was observed by both NMR spectra (indicated with asterisks in Figure 4.4.5) and in the MS spectra (data not shown). (Burbaud et al., 2016; Seeliger and Moody, 2016; Llorens-Fons et al., 2017).

Rapid detection, identification and differentiation from other mycolate derivatives of PTTM 1 by 1D ^1H NMR

The unambiguous identification of mycolate ester wax found in *M. smegmatis* as pentatriacontatrienyl mycolate (PTTM) **1** (Figure 4.4.4) and its complete ^1H and ^{13}C NMR structural elucidation (Table 4.4.1), allows from now on the quick direct detection and identification of this mycolate derivative and its differentiation from others by the performance of a simple 1D ^1H NMR experiment. The characteristic doublet at 4.61 ppm (corresponding to H1 of the trienyl chain), the three intense singlets at 1.76, 1.69 and 1.67 ppm (corresponding to the alkene methyl substituents of the trienyl chain) and the intense peaks related to the unsaturation of the trienyl chain, makes simple the identification and differentiation of **1** from other mycolate derivatives, such as methyl mycolates. This is exemplified in Figure 4.4.7. Finally, ^1H qNMR (quantitative NMR) spectroscopy could be applied, as well, for the rapid quantification of PTTM **1** (Pauli et al., 2012).

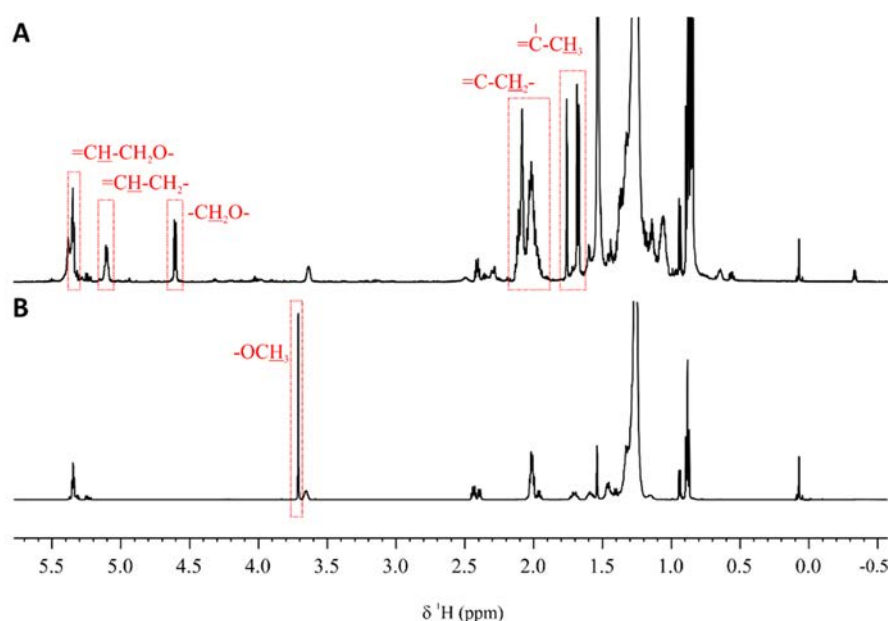


Figure 4.4.7 ^1H -NMR spectrum of **A** a pentatriacontatrienyl mycolate from *M. smegmatis* and **B** a methyl mycolate from *M. abscessus*. Spectra acquired in CDCl_3 , at 298.0 K and at a magnetic field of 600 MHz.

***M. smegmatis* showed rough colonies but no cord formation**

In fact, the colonies from *M. smegmatis* presented an intermediate morphotype, because they were wrinkled as rough colonies but they looked wet as smooth colonies (Figure 4.4.8A). This last feature it is likely to be related with the presence of PTTM 1 in the most external part of the cell wall. The pellicles produced by *M. smegmatis* were not totally flat but they weren't thick and consistent (Figure 4.4.8B).

In the TEM images a small accumulation of electrodense material was observed around the bacilli. However, this accumulation was less important than the TPP accumulation outside *M. abscessus*. With OTO stain it was possible to see that there was a mild accumulation of OsO_4 in the outer layer, almost no detectable (Figure 4.4.8C).

TEM showed a lack of organization of the bacilli that was confirmed by SEM. As it is possible to see in figure 4.4.9, *M. smegmatis* did not produced cords. So, it cannot be always associated wrinkled colonies with cord formation.

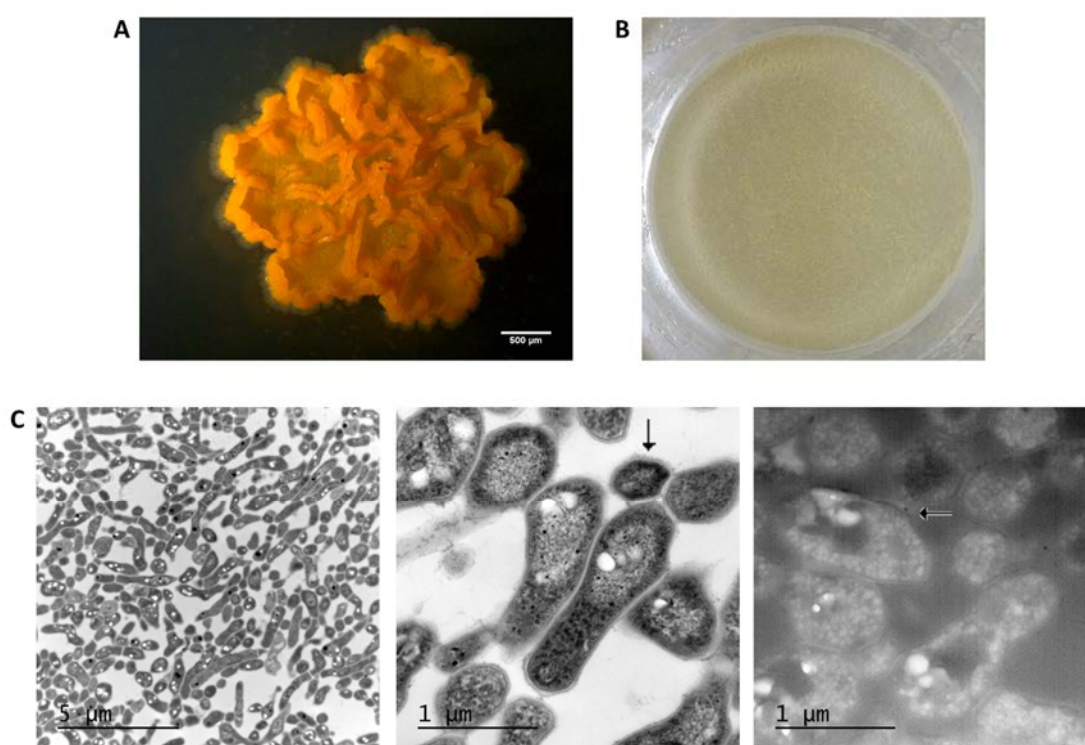


Figure 4.4.8 Images of **A** a colony and **B** a pellicle from *M. smegmatis*. Bar size in **A** 500 μm. **C** Images obtained by TEM of *M. smegmatis* bacilli. The one in the right is obtained from the OTO stain. Arrows indicate the almost not significant accumulation of electrodense material on the cell wall.

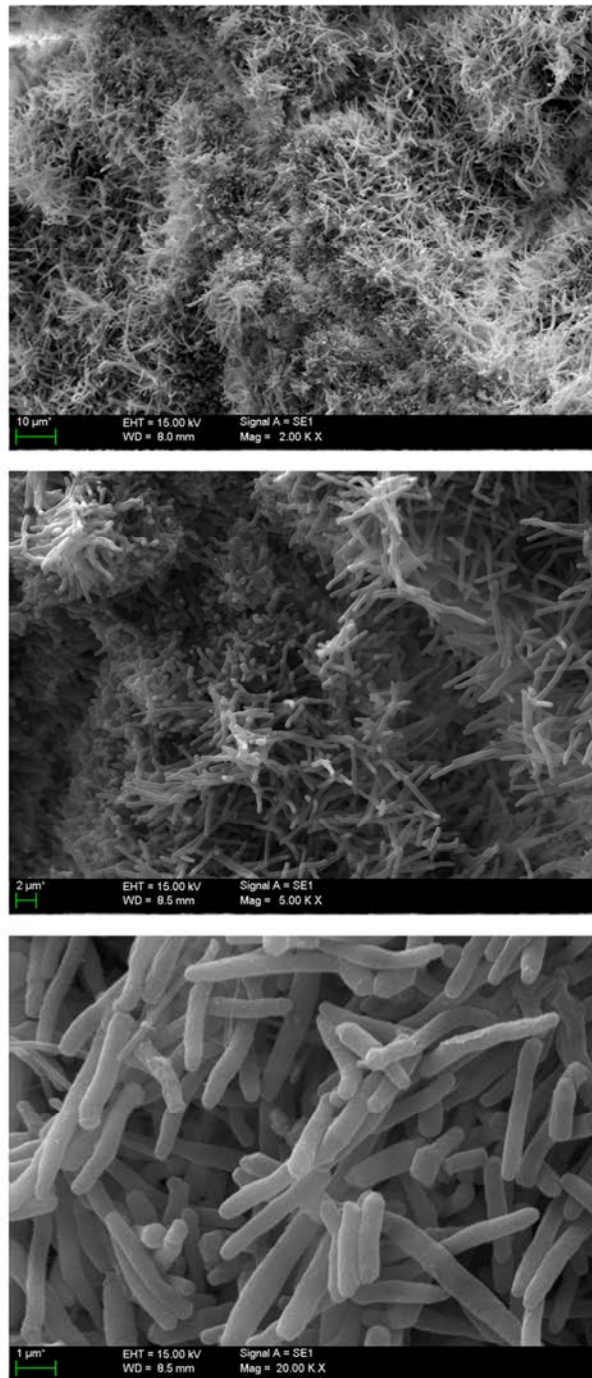


Figure 4.4.9 SEM micrographies of *M. smegmatis*. No organization of the bacilli is observed.
 Bar size 10 µm (first row), 2 µm (second row), 1 µm (third row).

Table 4.4.1 ^1H and ^{13}C NMR chemical shifts and H-H J couplings of PTTM 1.

Id	^1H		^{13}C	
	δ (^1H) [ppm]	(mult.,* $J_{\text{H,H}}$) [Hz]	δ (^{13}C) [ppm]	
1	4.606	(d, $J_{1,2}=7.2$)	60.82	A
2	5.353	(t, $J_{2,1}=7.2$)	118.95	
3	-		142.54	
4	1.759	(s)	23.29	
5	2.011	(m, ov)	32.02	
6	2.043	(m, ov)	32.20	B
7	5.138	(t, $J_{7,6}=5.9$)	124.37	
8	-		135.83	
9	1.686	(s)	23.32	
10	2.034	(m, ov)	32.20	
11	2.089	(m, ov)	32.34	C
12	5.128	(t, $J_{12,11}=5.9$)	124.21	
13	-		135.83	
14	1.671	(s)	23.32	
15	2.101	(m, ov)	32.34	
1'	-		175.49	Mycoloyl
2'	2.410	(m)	50.89	
3a'	1.711	(m, ov)	29.68	
3b'	1.593	(m, ov)	29.68	
4'	3.636	(m, br)	72.21	
5'	2.495	(m, br)	-	
6'	1.441	(m)	35.88	
7'	2.016	(m, ov)	n.d. **	
8'	5.339	(dd, ov.)	n.d.	
9'	5.236	(dd, $J_{9',8'}=15.3$ $J_{9',7'}=7.6$)	n.d.	
10'	0.644	(m, br)	n.d.	
11a'	-0.334	(ddd, $J_{11a',10'}=5.3$ $J_{11a',10'}=5.3$ $J_{11a',11b'}=4.2$)	n.d.	
11b'	0.559	(ddd, $J_{11b',10'}=8.2$ $J_{11b',10'}=8.2$ $J_{11b',11a'}=4.2$)	n.d.	
-CH2-	[1.285-1.232]		[30.65-28.91]	
-CH3b	0.94	(d, $J=6.7$)	20.76	
-CH3t	[0.894-0.841]		[14.17 - 22.51]	

* s (Singlet), d (doublet), t(triplet), ddd (doublet of doublets of doublets), m (multiplet), br (broad), ov (overlapped). ** n.d. (not detected, not enough signal).

4.5. Cellular response to the different morphotypes of *M. vaccae*

R morphotype of *M. vaccae* affected J774 macrophages growth

Using two different techniques, trypan blue exclusion assay and macrophages counting by CLSM, it was observed that J774 cells infected with the R morphotype of *M. vaccae* had a reduced growth in comparison with the uninfected cells or the cells infected with the S morphotype of *M. vaccae*. In fact, there was a significant difference between the growth of the cells infected with the R morphotype of *M. vaccae* and the cells infected with the S morphotype. After 96 h.p.i. R morphotype of *M. vaccae* was not able to kill all the macrophages, but it induced an inhibition of the cell growth of 35-40% in comparison with the uninfected culture. Macrophages infected with S morphotype showed approximately 100% of viability (Figure 4.5.1).

Both morphotypes were found inside J774 macrophages

J774 murine macrophages phagocyted both morphotypes of *M. vaccae* (Figure 4.5.2). After 3 h.p.i. $55.4\% \pm 6.9$ of the macrophages studied had bacteria of R morphotype inside. For S morphotype the percentage was lower, even if macrophages were infected with a superior MOI for this morphotype. Macrophages that had phagocyted S morphotype after 3 h.p.i. represented a $33.9\% \pm 8.7$ (Figure 4.5.2A).

This phagocytosis was also analyzed by TEM, where no differences in the aspect of the phagosomes were observed (Figure 4.5.2B).

R morphotype induced a weak TNF- α production by J774 macrophages

The amount of TNF- α produced by macrophages infected with S morphotype was so close to the limit of detection of the ELISA that was considered to be no significant. On the other hand, J774 macrophages infected with R morphotype produced a higher TNF- α quantity that was significantly different to the amount produced by S morphotype (Figure 4.5.3A). However, this amount of TNF- α induced by R morphotype of *M. vaccae* was 10 times less than the amount induced by R morphotype of *M. abscessus* (Brambilla et al., 2016).

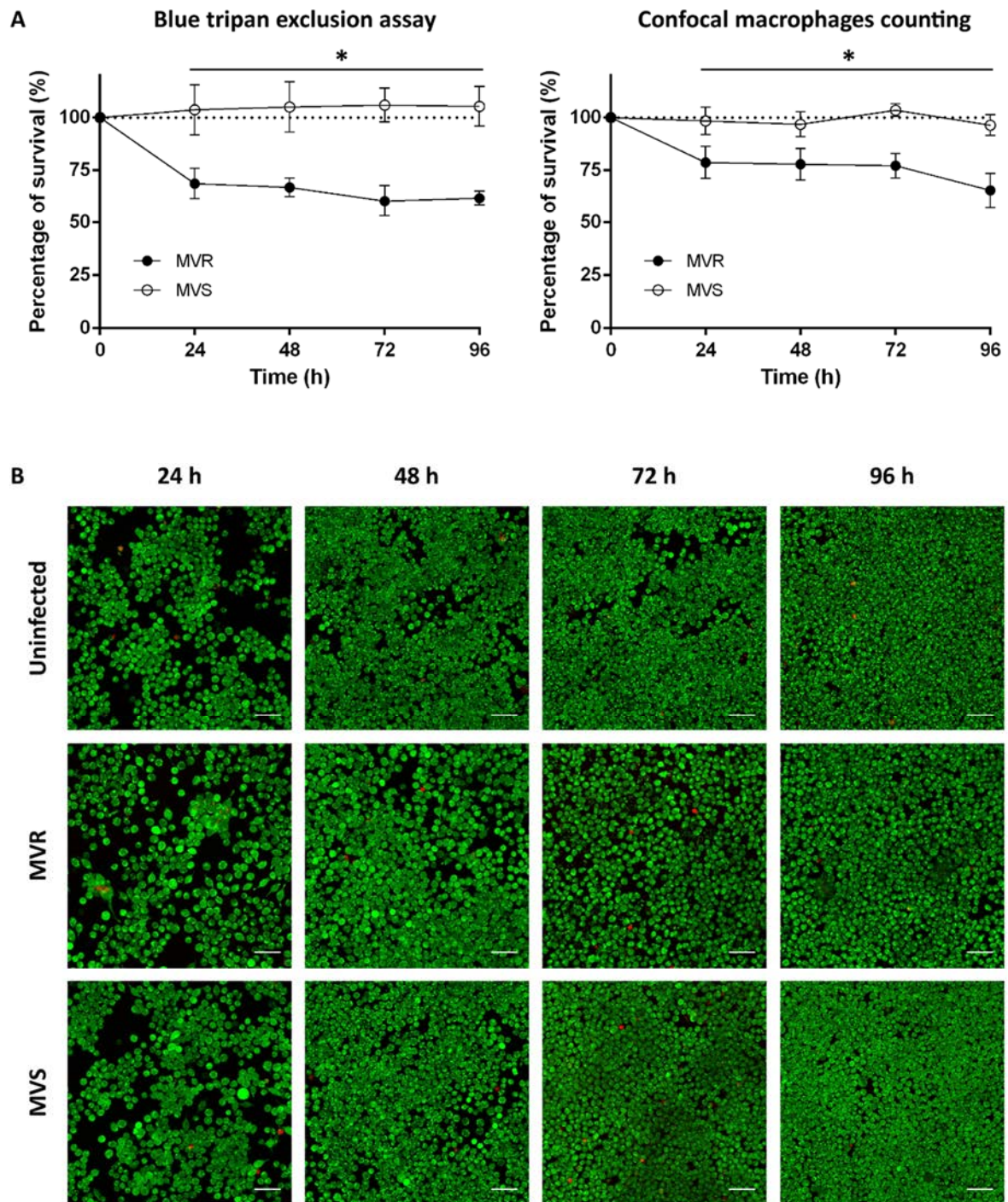


Figure 4.5.1 **A** Results of J774 macrophages viability tested by trypan blue exclusion assay and macrophage counting by CLSM. * $p < 0.05$ in multiple t -test. The data are representative of one out of three independent experiments. **B** Example of the reduced growth of the macrophages when infected with *R* morphotype, and how macrophages infected with *S* morphotype grow as the uninfected. Images obtained by CLSM. Bar size 50 μm .

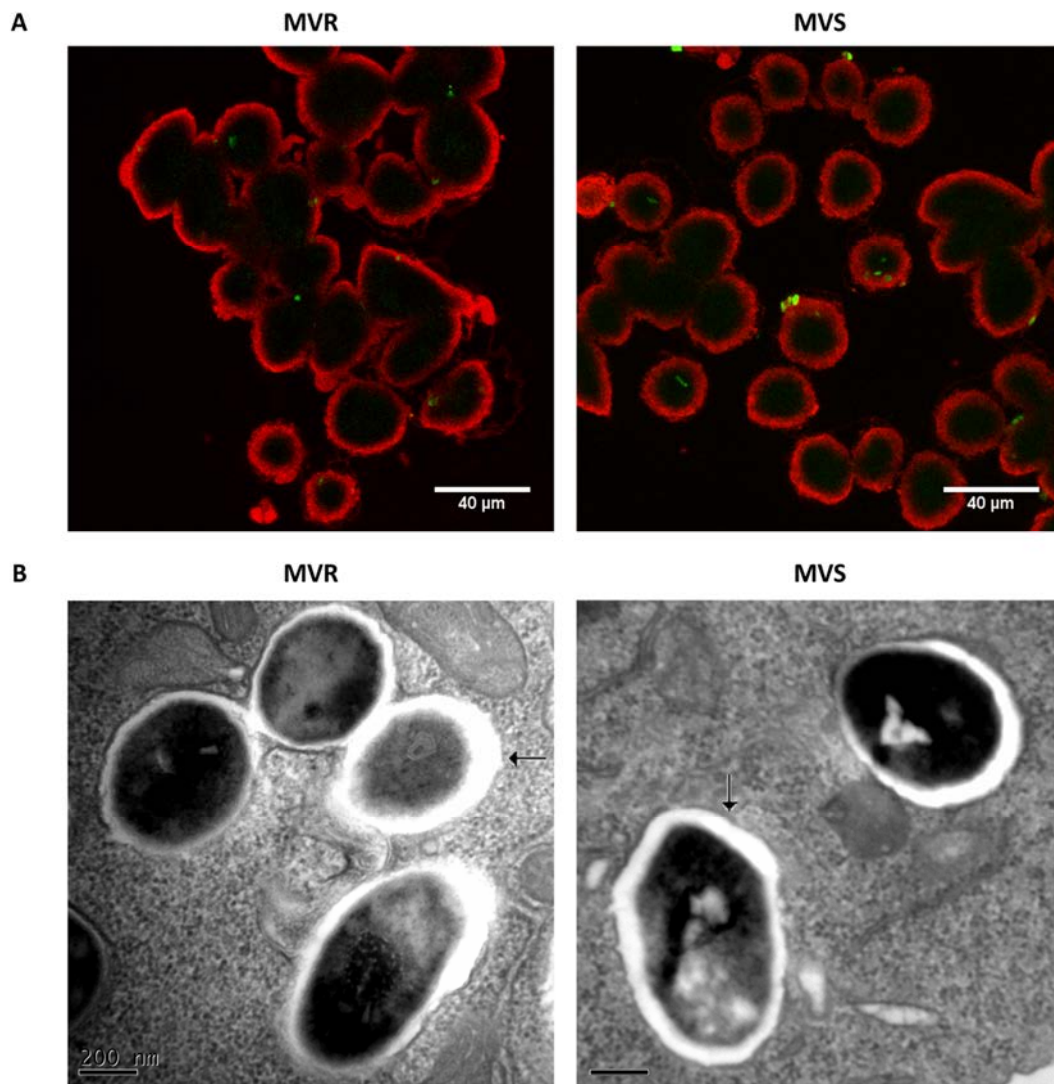


Figure 4.5.2 **A** Macrophages infected with *M. vaccae*. Both morphotypes are found inside J774 cells. Images obtained by CLSM. Macrophages in red stained with CellMask and bacteria in green stained with Auramine-Rhodamine. **B** TEM images of bacteria phagocytosed by J774 macrophages. Bar size 200 nm.

This weak production of TNF- α induced by R morphotype of *M. vaccae* was related with a feeble recruitment of macrophages around the bacteria producing granuloma-like structures (Figure 4.5.3B). In the cultures of J774 cells infected with S morphotype some bacterial growth was observed around the macrophages but no granuloma-like formation was detected (Figure 4.5.3B).

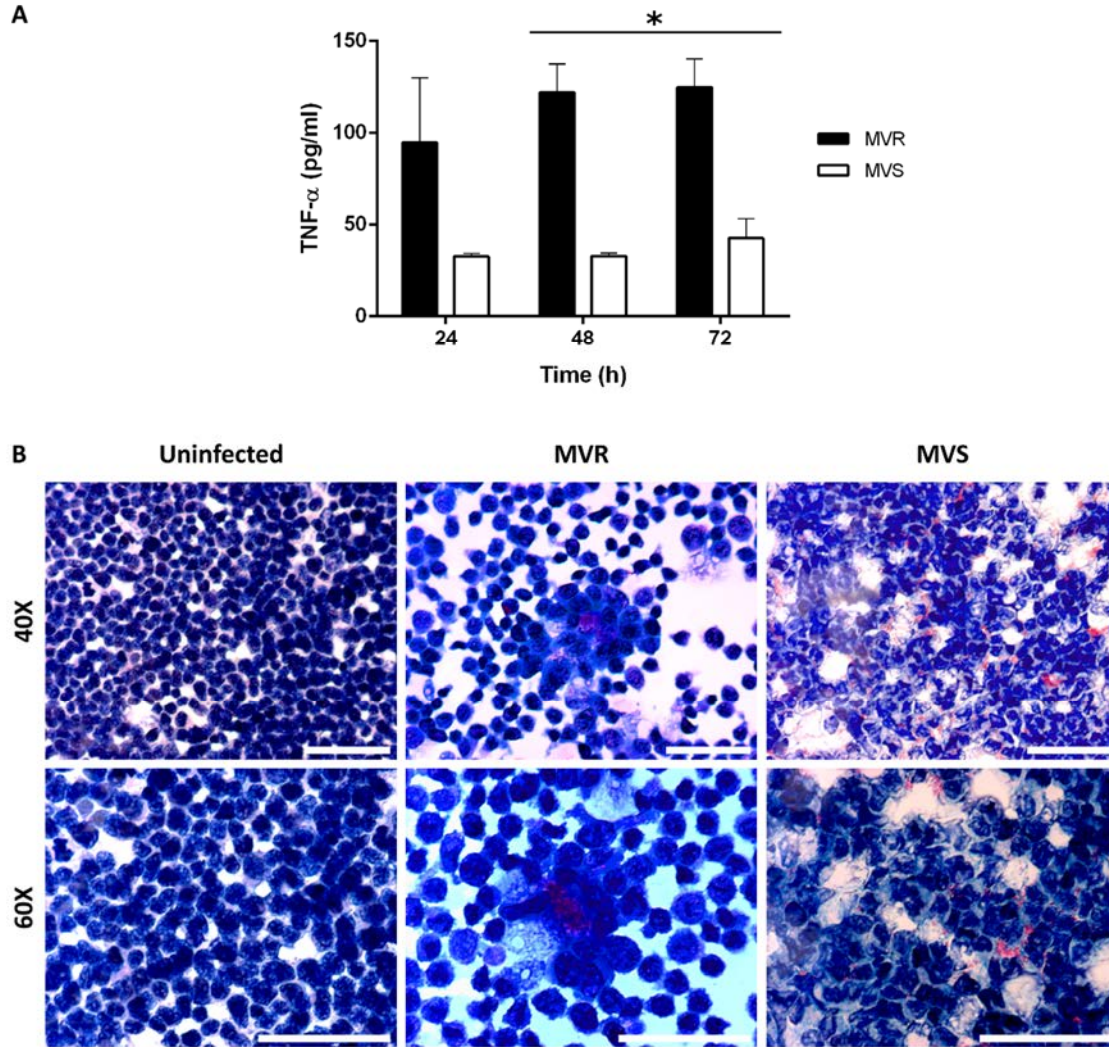


Figure 4.5.3 **A** TNF- α production of macrophages infected with the two morphotypes of *M. vaccae* at different time points. * $p < 0.05$ in multiple *t*-test. The results represent the mean \pm SD of triplicate infections. **B** Example of weak granuloma-like formation in J774 cultures infected with *R* morphotype of *M. vaccae*. No granuloma-like formation was observed in the cells infected with *S* morphotype. Images were obtained by optical microscope and the samples were stained by Ziehl-Neelsen method. Bar size 50 μ m.

5

Discussion

Tuberculosis disease, as explained before, implies a destruction of pulmonary tissue, by a cytotoxic effect in alveolar epithelial cells and by a huge immune response that evolve in a granuloma formation. In this work was tested if *M. abscessus* produced these two types of affectation in respiratory epithelium.

A549 is an immortal cell line isolated from a human lung adenocarcinoma. This cell line is functionally similar to the human alveolar epithelial cells, it forms confluent monolayers with the characteristic morphology of Type II cells from alveolar epithelium (Foster et al., 1998; Roy et al., 2004). A549 has been used to study the response of epithelial cells to different intracellular pathogens like *Mycoplasma pneumoniae* and *Chlamydia pneumoniae* (Yang et al., 2002, 2003). These cells have also been used to study the interaction of mycobacteria with respiratory epithelium (Bermudez et al., 2002; García-Pérez et al., 2008).

In this sense, it was tested if *M. abscessus* had a cytotoxic effect when infecting alveolar epithelial cell line A549 and if this effect was differential between the two morphotypes. The results were that *M. abscessus* suppressed A549 growth and R morphotypes of the 5 different strain used where more cytotoxic than the S morphotype. So, in the pathology produced by *M. abscessus*, there is some induction of cellular death in infected alveolar epithelia, higher in the case of R morphotypes.

Related with the activation of the immune system characteristic of tuberculosis disease, Lin et al. infected A549 cells with 4 strains of *M. tuberculosis* (H37Rv, H37Ra and two clinical isolates) and they found that all 4 induced the production of IL-8, including the H37Ra strain, which it is attenuated. In contrast, *M. avium* couldn't induce the production of IL-8 in A549. The authors related the production of IL-8 by A549 cells with the capacity of the different bacteria to grow inside these epithelial cells, as *M. tuberculosis* can invade and grow in human alveolar epithelial cells and was detected inside A549, while *M. avium* did not shown significant growth when cultured with A549 (Lin et al., 1998). In relation with *M. abscessus*, Ribeiro et al. described that *M. abscessus* could invade A549 cells and proliferate in it (Ribeiro et al., 2017).

However, Davidson et al. got into more detail and linked the production of IL-8 in A549 cells to the activation of their TLR. In this case, the production of this cytokine would not be related to the capacity of the bacteria to enter A549 but to their cell wall composition. The authors described that *M. abscessus* 390S, expressing GPL, was not

able to activate TLR of A549 and no production of IL-8 was detected. But *M. abscessus* 390R, that had no GPL on the cell wall, induced a significant production of IL-8. When they made a 390S mutant defective in GPL expression, they detected significant amounts of IL-8 (Davidson et al., 2011).

The results exposed in this work agree with the ones from Davidson and collaborators. R morphotypes of all *M. abscessus* strains studied induced a significant production of IL-8, while the induction by S morphotypes was only statistically significant in few cases and with an important difference with the IL-8 induced by their corresponding R morphotype.

All R morphotypes studied are devoid of GPL expression in their cell wall. In relation with this, it has been proposed that the loss of GPL that occurs in the transition between S morphotype to R morphotype in *M. abscessus* unmask cell wall lipids related with virulence (Howard et al., 2006; Rhoades et al., 2009). These unmasked components of the cell envelope surface would be recognized by TLR and would induce IL-8 production.

Kim et al. demonstrated in 2011 the adaptation capacity of the mycobacteria to survive in the host by changing the induction of some genes. To test this, the authors infected A549 epithelial cells with *M. smegmatis* and they analyzed the expression of determinate genes of the mycobacteria. The most highly induced gene encoded a lipoprotein involved in the synthesis of the mycobacterial cell envelop (Kim et al., 2011), demonstrating the importance of the exposed cell wall components for the development of the disease.

This links to the second part of this thesis, where the most superficial lipids in *M. abscessus* were studied. In TEM images obtained from R morphotypes it was possible to see an accumulation of electron dense material in the outermost layer that was absent in S morphotypes. This layer may correspond to the capsule described by Daffé et al., composed mostly by polysaccharides and proteins (Daffé et al., 2014). *M. abscessus* samples were treated with OsO₄, a commonly used stain for lipids in electron microscopy, that makes the lipids appear as an electron dense zone (Daffé et al., 1989; Bleck et al., 2010). Other technique used in this purpose was OTO staining, which enhances OsO₄ accumulation, (Seligman et al., 1966; Daffé et al., 1989). These data

corroborate that the electrodense material detected in the outer layer had a high lipidic content. As mentioned before, Draper affirmed that large amounts of specie-specific glycolipids could also be detected in the capsule (Draper, 1971). This is not the case of GPL, as R morphotypes are devoid of this glycolipid, but it will be the case of some other cell wall component first unmasked by GPLs in the S morphotypes and then overexpressed in the adapted R morphotypes.

To analyze the lipids responsible of this electrodense outer layer, a superficial extraction was performed in *M. abscessus* pellicles, and only one major compound was extracted. This superficial compound was highly present in R morphotypes extractions, but represented only a shadow in S morphotype extractions. Using NMR and MS this compound was identified as TPP A, denominated A because the structural characterization showed that was similar to the recently described TPP A from *M. smegmatis* (Burbaud et al., 2016). The other two spots detected in R morphotype extractions were also characterized as minor TPP species.

TPPs were first characterized in *Mycobacterium phlei*. Their structure consists of a trehalose acylated with long polyunsaturated fatty acids (called phleic acids because they were also first described in *M. phlei*) (Asselineau et al., 1969, 1972; Asselineau and Montrozier, 1976).

Burbaud et al. extracted TPP from both morphotypes of *M. abscessus*. However they used an extraction protocol that obtains deeper compounds (Burbaud et al., 2016). The extraction protocol used in the present work was developed to obtain the most superficial lipidic compounds. This mild extraction is not enough to extract GPLs from S morphotype, what suggests that TPP in these morphotypes would be unexposed, covered by GPL.

The next step was to find a reason why the switch between S to R morphotype let TPP exposed. As said before, the loss of GPLs might expose some cell wall components recognized by TLR. PIMs are the major *M. abscessus* TLR2 ligands, however, they are not considered the only one (Rhoades et al., 2009). For that reason, the cytotoxicity of TPP and their capacity of cell activation were tested infecting epithelial cells and macrophages with TPP A-coated beads. Another possible effect of an unmasked component is to interfere in phagosome-lysosome fusion, as it is the case of another trehalose ester, SL (Goren et al., 1976).

No effect on cell growth was detected in any case, which means that these exposed TPP produce no cytotoxicity themselves. J774 macrophages phagocytized uncoated and TPP A-coated beads with similar ratios, and no effect in preventing phagosome-lysosome fusion was detected. Immunogenic cell activation was measured with the production of IL-8 in epithelial cells and the production of TNF- α and IL-6 in macrophages. Again, no cytokine production was detected in any case. Taken together, these results indicate that TPP are not a virulence factor *per se*. Then, why are exposed in a big amount in R morphotypes?

The superficial extraction protocol used in this thesis was inspired by the work made by Bloch in 1950. In that pioneering study, Bloch managed to disrupt *M. tuberculosis* cords in only few minutes by using organic solvents but not with aqueous solutions (Bloch, 1950). For that reason, he considered that he was extracting the compound responsible for cord formation and its nature was lipidic. Cords are the first virulence factor described in *M. tuberculosis* (Middlebrook et al., 1947). Genetic validation of the link between cording and virulence in *M. tuberculosis* and *M. abscessus* has been obtained through natural and constructed mutants, most of which exhibit alterations in the synthesis or structure of the lipids of the cell wall; thus, they are consistent with Bloch studies attributing the formation of cords to a lipidic substance (Glickman, 2008). However, to date, there are only candidate molecules to be responsible of cording. The cording factor remains unknown.

When PE, one of the organic solvents used by Bloch, was applied to *M. abscessus* R morphotypes pellicles of the present work, some cord disruption was observed. This means that PE was extracting a superficial compound related with cording. Besides, as explained before, this superficial extraction of R morphotypes contained mostly TPP.

To prove if TPP were related with clumps and cord formation, the aggregation of TPP A-coated beads, with bacterial size, was analyzed. And the results were positive, TPP A-coated beads had more tendency to form clumps than uncoated beads. These results bring to the conclusion that TPP have aggregative capacities and will be an interesting candidate molecule to be the cording factor in *M. abscessus*.

TPP are one of the largest known lipids in mycobacteria (Seeliger and Moody, 2016), and their role in the mycobacterial envelope is unknown, but the results obtained in the present work suggest that TPP may be necessary for the formation of

clumps and cords. The very hydrophobic nature of clumps and cords is in accord with the surface exposure of these giant lipids.

As said before, TPP are not a virulence factor *per se*. However, they may contribute to the formation of clumps. In Brambilla et al., clump formation in *M. abscessus* was directly related with virulence (Brambilla et al., 2016). Although TPP are not TLR ligand, as demonstrated previously, the loss of GPL might let exposed other compounds that have been associated with hyper-proinflammatory responses, as PIM, LM, LAM or lipoproteins (Gilleron et al., 2008; Rhoades et al., 2009; Roux et al., 2011). When macrophages will meet and phagocytize a bacterial clump they will have to face a large amount of immunostimulatory cell wall components, and this will activate a major immune response than the one produced by a single mycobacterium.

Besides, when mycobacteria get to the alveoli, pulmonary surfactant has no effect in decreasing the bacterial clump size. The results shown in this work demonstrate that the contact with the most abundant phospholipid in the pulmonary surfactant is not enough to disaggregate mycobacterial clumps.

papA3, pks, fadD23, and mmpL10 are genes involved in the biosynthesis and transport of TPP (Burbaud et al., 2016). By creating mutants deficient for these genes it will be possible to confirm the role of TPP in *M. abscessus* cording. No TPP has been detected in *M. tuberculosis*, but studying the biosynthesis of these giant molecules, Burbaud et al. suggest that TPP are the functional homologs of SL, DAT and PAT of *M. tuberculosis* (Burbaud et al., 2016). Consequently, it will be of great interest to study the relationship of these acylated trehaloses and cording in the tubercle bacilli.

TPP might be the cording factor in *M. abscessus*. However, no TPP were detected in the superficial extracts from the other NTM analyzed, *M. vaccae* R, *M. kansasii* R, *M. brumae* and *M. smegmatis*. Burbaud et al. extracted and analyzed TPP from *M. smegmatis*, but as explained before, they performed a different type of extraction (Burbaud et al., 2016). However, in the superficial extraction of *M. smegmatis* it was found a new compound with a similar migration in TLC to TPP.

This new compound, firstly called Spot A, was analyzed by MS and NMR, and when comparing the results obtained with the related studies, some uncertainties regarding

the structure of the Spot A were detected. Initially, this lipid was characterized by Chen et al. (Chen et al., 2006) as mycoloyl diacylglycerol, based on MS analyses. Later, Pacheco et al. (Pacheco et al., 2013) described the same molecule as a PTTM, also based on MS. Both studies were performed using the same analytical technique and agreed that the structure of Spot A was based in a mycolate derivative. The confusion was with the carbon chain.

An in-depth structural study allowed to clearly characterize Spot A as PTTM 1. The characterization was based on the concerted analyses of 1D and 2D NMR experiments and the compound mass was confirmed by MS. The presented results allow the future quick direct detection and identification of the lipid by a simple 1D ¹H NMR experiment

When analyzing PTTM from *M. smegmatis*, a small amount of TPP was detected. This means that like the S morphotype of *M. abscessus*, *M. smegmatis* can produce TPP, but this compound is not superficially exposed. Maybe PTTM are masking TPP, as happens in *M. abscessus* with GPLs.

This hypothesis is reinforced with the fact that the studied strain of *M. smegmatis* is not able to produce cords. Its colonies looked wrinkled, but no bacillar organization was detected in microscopic preparations. Subsequently, it will be of interest to construct a mutant deficient in PTTM production and observe if it is able to organize.

When passing from S to R morphotype, *M. abscessus* loss GPLs, as explained before. However, other NTM that do not produce these glycolipids, loss other cell wall components in the switch between S to R morphotype. For instance, *M. kansasii* and *Mycobacterium mucogenicum* loss LOS in this transition (Belisle and Brennan, 1989; Muñoz et al., 1998). *M. smegmatis* might loss PTTM when passing to a cording morphotype exposing TPP, as an hypothesis. And *M. vaccae* loss a long-chain saturated polyester when passing from S to R morphotype (Rodríguez-Güell et al., 2006). So, it is known that the most external cell wall components from *M. vaccae* varies between morphotypes.

As explained in the introduction, *M. vaccae* is an important mycobacterium used as immunotherapeutic agent. There are two available preparations of *M. vaccae*, but

each one contains a different morphotype. In the present work a comparison of the cytotoxic and the immunostimulatory effect of the R and the S morphotypes of *M. vaccae* was performed in J774 murine macrophages.

The first difference between morphotypes was that R morphotype suppressed macrophages growth, while cells infected with S morphotype had the same growth as the control. Macrophages phagocytosed half of the R morphotype bacteria, and a little less percentage of S morphotype. However, near 34% of the S morphotype bacteria were phagocytosed and the cellular growth was not affected.

The second difference was the weak but significant immunostimulatory effect of the R morphotype. A small amount of TNF- α was induced indicating macrophages activation. This effect is the one looked in the new tuberculosis vaccines, to induce Th1 cytokines from immunity cells.

These results indicate that, like in most NTM, there is a difference between both morphotypes and the rough one is the most immunostimulatory. Stanford's *M. vaccae* vaccine is prepared with an R morphotype. But, Vaccae™, the Chinese one, is based on the Type strain, that initially was described as S. It is unknown if Anhui Zhifei Longcom, the company responsible for the production of Vaccae™, has obtained the R morphotype. Otherwise, the S morphotype, as shown in this work, has no immunostimulatory effect, it would be a non-suitable candidate as a vaccine.

6

Conclusions

The conclusions for this thesis are the following

1. *M. abscessus* produces a cytotoxic effect in human alveolar epithelial cell line A549. R morphotype of *M. abscessus* have a more virulent effect than the S morphotype, with a major suppression of growth and inducing a major production of IL-8.

2. The contact with the major component of pulmonary surfactant does not affect the bacterial clump size in *M. abscessus*.

3. There is an important accumulation of lipids seen as electrodense material in the outer layer of the cell wall in the R morphotypes of *M. abscessus*, that it is absent in the S morphotypes.

4. TPP are the major compounds obtained from superficial lipid extraction in *M. abscessus* pellicles, but are only found in the R morphotype.

5. No toxic effect is seen when J774 macrophages, A549 epithelial cells and THP-1 monocytes are treated with TPP-coated beads.

6. The treatment of *M. abscessus* R morphotype pellicles with petroleum ether produces a disorganization of their cords.

7. The coating of beads with TPP enhances their aggregation.

8. *M. vaccae* R, *M. kansasii* R, *M. brumae* and *M. smegmatis* do not express TPP in their most superficial part of the cell wall.

9. Instead, *M. smegmatis* express a compound called mycolic ester wax. This compound has clearly characterized as PTTM 1.

10. From now on, the detection, identification and quantification of PTTM 1 can be easily carried out by the performance of a simple 1D ¹H spectrum.

11. Even if the colonies and the pellicles of *M. smegmatis* are wrinkled no cord formation is observed when the ultrastructure of these are studied.

12. Both morphotypes of *M. vaccae* are found inside J774 murine macrophages. However, only the R morphotype has a negative effect in cell growth. This morphotype is more antigenic as induces cytokine production.

7

Bibliography

- Abe, C. (2003). Standardization of laboratory tests for tuberculosis and their proficiency testing. *Kekkaku* 78, 541–551.
- Agustí, G., Astola, O., Rodríguez-Güell, E., Julián, E., and Luquin, M. (2008). Surface spreading motility shown by a group of phylogenetically related, rapidly growing pigmented mycobacteria suggests that motility is a common property of mycobacterial species but is restricted to smooth colonies. *J. Bacteriol.* 190, 6894–6902.
- Andersen, P., and Kaufmann, S. H. E. (2014). Novel vaccination strategies against tuberculosis. *Cold Spring Harb. Perspect. Med.* 4.
- Asselineau, C. P., Mohtrozier, H., and Promé, J. (1969). Présence d'acides polyinsaturés dans une bactérie. *Eur. J. Biochem.* 10, 580–584.
- Asselineau, C. P., and Montrozier, H. L. (1976). Étude du processus de biosynthèse des acides phléiques, acides polyinsaturés synthétisés par *Mycobacterium phlei*. *Eur. J. Biochem.* 63, 509–518.
- Asselineau, C. P., Montrozier, H. L., Promé, J., Savagnac, A. M., and Welby, M. (1972). Étude d'un glycolipide polyinsaturé synthétisé par *Mycobacterium phlei*. *Eur. J. Biochem.* 28, 102–109.
- Bansal-Mutalik, R., and Nikaido, H. (2014). Mycobacterial outer membrane is a lipid bilayer and the inner membrane is unusually rich in diacyl phosphatidylinositol dimannosides. *Proc. Natl. Acad. Sci. U. S. A.* 111, 4958–4963.
- Barker, L. F., Brennan, M. J., Rosenstein, P. K., and Sadoff, J. C. (2009). Tuberculosis vaccine research: the impact of immunology. *Curr. Opin. Immunol.* 21, 331–338.
- Barrow, C., and Brennan, P. J. (1982). Isolation in high frequency of rough variants of *Mycobacterium intracellulare* lacking C-mycoside glycopeptidolipid antigens. *J. Bacteriol.* 150, 381–384.
- Belazi, D., Solé-Domènech, S., Johansson, B., Schalling, M., and Sjövall, P. (2009). Chemical analysis of osmium tetroxide staining in adipose tissue using imaging ToF-SIMS. *Histochem. Cell Biol.* 132, 105–115.
- Belisle, J. T., and Brennan, P. J. (1989). Chemical basis of rough and smooth variation in mycobacteria. *J. Bacteriol.* 171, 3465–3470.

- Bermudez, L. E., Sangari, F. J., Kolonoski, P., Petrofsky, M., and Goodman, J. (2002). The efficiency of the translocation of *Mycobacterium tuberculosis* across a bilayer of epithelial and endothelial cells as a model of the alveolar wall is a consequence of transport within mononuclear phagocytes and invasion of alveolar epithelial c. *Infect. Immun.* 70, 140–146.
- Bernut, A., Herrmann, J.-L., Kissa, K., Dubremetz, J.-F., Gaillard, J.-L., Lutfalla, G., et al. (2014). *Mycobacterium abscessus* cording prevents phagocytosis and promotes abscess formation. *Proc. Natl. Acad. Sci. U. S. A.* 111, E943--52.
- Bernut, A., Herrmann, J.-L., Ordway, D., and Kremer, L. (2017). The Diverse Cellular and Animal Models to Decipher the Physiopathological Traits of *Mycobacterium abscessus* Infection. *Front. Cell. Infect. Microbiol.* 7, 100.
- Bernut, A., Nguyen-Chi, M., Halloum, I., Herrmann, J. L., Lutfalla, G., and Kremer, L. (2016a). *Mycobacterium abscessus*-Induced Granuloma Formation Is Strictly Dependent on TNF Signaling and Neutrophil Trafficking. *PLoS Pathog.* 12, e1005986.
- Bernut, A., Viljoen, A., Dupont, C., Sapriel, G., Blaise, M., Bouchier, C., et al. (2016b). Insights into the smooth-to-rough transitioning in *Mycobacterium bolletii* unravels a functional Tyr residue conserved in all mycobacterial MmpL family members. *Mol. Microbiol.* 99, 866–883.
- Bleck, C. K. E., Merz, A., Gutierrez, M. G., Walther, P., Dubochet, J., Zuber, B., et al. (2010). Comparison of different methods for thin section em analysis of *Mycobacterium smegmatis*. *J. Microsc.* 237, 23–38.
- Bloch, H. (1950). Studies on the virulence of tubercle bacilli; isolation and biological properties of a constituent of virulent organisms. *J. Exp. Med.* 91, 197–218, pl.
- Boritsch, E. C., Frigui, W., Cascioferro, A., Malaga, W., Etienne, G., Laval, F., et al. (2016). pks5-recombination-mediated surface remodelling in *Mycobacterium tuberculosis* emergence. *Nat. Microbiol.* 1, 15019.
- Brambilla, C. (2015). Estudio de la formación de cuerdas microscópicas en el género *Mycobacterium* y su implicación en la virulencia de *Mycobacterium abscessus*.
- Brambilla, C., Llorens-Fons, M., Julián, E., Noguera-Ortega, E., Tomàs-Martínez, C.,

- Pérez-Trujillo, M., et al. (2016). Mycobacteria clumping increase their capacity to damage macrophages. *Front. Microbiol.* 7, 1562.
- Brambilla, C., Sánchez-Chardi, A., Pérez-Trujillo, M., Julián, E., and Luquín, M. (2012). Cyclopropanation of α -mycolic acids is not required for cording in *Mycobacterium brumae* and *Mycobacterium fallax*. *Microbiology* 158, 1615–1621.
- Brown-Elliott, B. A. (2016). Rapidly Growing Mycobacteria. *Microbiol. Spectr.* 5.
- Burbaud, S., Laval, F., Lemassu, A., Daffé, M., Guilhot, C., and Chalut, C. (2016). Trehalose Polyphleates Are Produced by a Glycolipid Biosynthetic Pathway Conserved across Phylogenetically Distant Mycobacteria. *Cell Chem. Biol.* 23, 278–289.
- Byrd, T. F., and Lyons, C. R. (1999). Preliminary characterization of a *Mycobacterium abscessus* mutant in human and murine models of infection. *Infect. Immun.* 67, 4700–4707.
- Camacho, L. R., Constant, P., Raynaud, C., Laneelle, M. A., Triccas, J. A., Gicquel, B., et al. (2001). Analysis of the phthiocerol dimycocerosate locus of *Mycobacterium tuberculosis*. Evidence that this lipid is involved in the cell wall permeability barrier. *J. Biol. Chem.* 276, 19845–54.
- Camacho, L. R., Ensergueix, D., Perez, E., Gicquel, B., and Guilhot, C. (1999). Identification of a virulence gene cluster of *Mycobacterium tuberculosis* by signature-tagged transposon mutagenesis. *Mol. Microbiol.* 34, 257–267.
- Castranova, V., Rabovsky, J., Tucker, J. H., and Miles, P. R. (1988). The alveolar type II epithelial cell: A multifunctional pneumocyte. *Toxicol. Appl. Pharmacol.* 93, 472–483.
- Catherinot, E., Clarissou, J., Etienne, G., Ripoll, F., Emile, J. F., Daffé, M., et al. (2007). Hypervirulence of a rough variant of the *Mycobacterium abscessus* type strain. *Infect. Immun.* 75, 1055–1058.
- Chan, J., Fan, X. D., Hunter, S. W., Brennan, P. J., and Bloom, B. R. (1991). Lipoarabinomannan, a possible virulence factor involved in persistence of *Mycobacterium tuberculosis* within macrophages. *Infect. Immun.* 59, 1755–1761.
- Chen, J. M., German, G. J., Alexander, D. C., Ren, H., Tan, T., and Liu, J. (2006). Roles of Lsr2 in colony morphology and biofilm formation of *Mycobacterium smegmatis*. *J.*

Bacteriol. 188, 633–641.

- Chimote, G., and Banerjee, R. (2005). Lung surfactant dysfunction in tuberculosis : Effect of mycobacterial tubercular lipids on dipalmitoylphosphatidylcholine surface activity. *Colloids and Surfaces* 45, 215–223.
- Christensen, H., Garton, N. J., Horobin, R. W., Minnikin, D. E., and Barer, M. R. (1999). Lipid domains of mycobacteria studied with fluorescent molecular probes. *Mol. Microbiol.* 31, 1561–1572.
- Clay, H., Volkman, H. E., and Ramakrishnan, L. (2008). Tumor necrosis factor signaling mediates resistance to mycobacteria by inhibiting bacterial growth and macrophage death. *Immunity* 29, 283–94.
- Colditz, G. A., Brewer, T. F., Berkey, C. S., Wilson, M. E., Burdick, E., Fineberg, H. V., et al. (1994). Efficacy of BCG Vaccine in the Prevention of Tuberculosis. *JAMA* 271, 698.
- Collins, F. M., and Cunningham, D. S. (1981). Systemic *Mycobacterium kansasii* infection and regulation of the alloantigenic response. *Infect. Immun.* 32, 614–624.
- Cox, J. S., Chess, B., McNeil, M., and Jacobs, W. R. (1999). Complex lipid determines tissue-specific replication of *Mycobacterium tuberculosis* in mice. *Nature* 402, 79–83.
- Crellin, P. K., Luo, C.-Y., and Morita, Y. S. (2013). Metabolism of Plasma Membrane Lipids in Mycobacteria and Corynebacteria. *Lipid Metab.*, 460.
- Daffé, M., Crick, D. C., and Jackson, M. (2014). Genetics of Capsular Polysaccharides and Cell Envelope (Glyco)lipids. *Microbiol Spectr.* 2, 1–46.
- Daffé, M., and Draper, P. (1998). The envelope layers of mycobacteria with reference to their pathogenicity. *Adv. Microb. Physiol.* 39, 131–203.
- Daffé, M., Dupon, M., and Gas, N. (1989). The cell envelope of *Mycobacterium smegmatis*: cytochemistry and architectural implications. *FEMS Microbiol. Lett.* 52, 89–93.
- Dai, J., Chen, Y., and Lauzardo, M. (2011). Web-accessible database of hsp65 sequences from *Mycobacterium* reference strains. *J. Clin. Microbiol.* 49, 2296–2303.
- Daniel, J., Deb, C., Dubey, V. S., Sirakova, T. D., Abomoelak, B., Morbidoni, H. R., et al. (2004). Induction of a novel class of diacylglycerol acyltransferases and triacylglycerol accumulation in *Mycobacterium tuberculosis* as it goes into a

- dormancy-like state in culture. *J. Bacteriol.* 186, 5017–5030.
- Davidson, L. B., Nessar, R., Kempaiah, P., Perkins, D. J., and Byrd, T. F. (2011). *Mycobacterium abscessus* glycopeptidolipid prevents respiratory epithelial TLR2 signaling as measured by H β D2 gene expression and IL-8 release. *PLoS One* 6.
- de Bruyn, G., and Garner, P. (2010). “*Mycobacterium vaccae* immunotherapy for treating tuberculosis,” in *Cochrane Database of Systematic Reviews*, ed. G. de Bruyn (Chichester, UK: John Wiley & Sons, Ltd), CD001166.
- DiMango, E., Zar, H. J., Bryan, R., and Prince, A. (1995). Diverse *Pseudomonas aeruginosa* gene products stimulate respiratory epithelial cells to produce interleukin-8. *J. Clin. Invest.* 96, 2204–2210.
- Dobos, K. M., Spotts, E. A., Quinn, F. D., and King, C. H. (2000). Necrosis of lung epithelial cells during infection with *Mycobacterium tuberculosis* is preceded by cell permeation. *Infect. Immun.* 68, 6300–6310.
- Domenech, P., and Reed, M. B. (2009). Rapid and spontaneous loss of phthiocerol dimycocerosate (PDIM) from *Mycobacterium tuberculosis* grown in vitro: Implications for virulence studies. *Microbiology* 155, 3532–3543.
- Domenech, P., Reed, M. B., and Barry, C. E. (2005). Contribution of the *Mycobacterium tuberculosis* MmpL protein family to virulence and drug resistance. *Infect. Immun.* 73, 3492–3501.
- Drake, R., Vogl, A. W., and Mitchell, A. W. M. (2009). *Gray’s Anatomy for Students*.
- Draper, P. (1971). The walls of *Mycobacterium lepraemurium*: chemistry and ultrastructure. *J. Gen. Microbiol.* 69, 313–324.
- Draper, P. (1974). The mycoside capsule of *Mycobacterium avium*. *J. Gen. Microbiol.* 83, 431–433.
- Draper, P., and Daffé, M. (2005). *Tuberculosis and the Tubercle Bacillus*. , eds. D. N. McMurray, W. R. Jacobs, Jr., S. T. Cole, and K. D. Eisenach American Society of Microbiology.
- Dubnau, E., Chan, J., Raynaud, C., Mohan, V. P., Lan  elle, M. A., Yu, K., et al. (2000). Oxygenated mycolic acids are necessary for virulence of *Mycobacterium tuberculosis* in mice. *Mol. Microbiol.* 36, 630–637.

- Eckstein, T. M., Inamine, J. M., Lambert, M. L., and Belisle, J. T. (2000). A genetic mechanism for deletion of the *ser2* gene cluster and formation of rough morphological variants of *Mycobacterium avium*. *J. Bacteriol.* 182, 6177–6182.
- Edwards, M. L., Goodrich, J. M., Muller, D., Pollack, A., Ziegler, J. E., and Smith, D. W. (1982). Infection with *Mycobacterium avium-intracellulare* and the protective effects of bacille calmette-guerin. *J. Infect. Dis.* 145, 733–741.
- Etienne, G., Villeneuve, C., Billman-Jacobe, H., Astarie-Dequeker, C., Dupont, M.-A., and Daffé, M. (2002). The impact of the absence of glycopeptidolipids on the ultrastructure, cell surface and cell wall properties, and phagocytosis of *Mycobacterium smegmatis*. *Microbiology* 148, 3089–3100.
- Evans, T. G., Schrager, L., and Thole, J. (2016). Status of vaccine research and development of vaccines for tuberculosis. *Vaccine* 34, 2911–2914.
- Fäldt, J., Dahlgren, C., Karlsson, A., Ahmed, A. M. S., Minnikin, D. E., and Ridell, M. (1999). Activation of human neutrophils by mycobacterial phenolic glycolipids. *Clin. Exp. Immunol.* 118, 253–260.
- Falkinham III, J. O. (2009). Surrounded by mycobacteria: Nontuberculous mycobacteria in the human environment. *J. Appl. Microbiol.* 107, 356–367.
- Falkinham III, J. O. (2013). Ecology of Nontuberculous Mycobacteria—Where Do Human Infections Come from? *Semin Respir Crit Care Med* 34, 95–102.
- Ferguson, J. S., Martin, J. L., Azad, A. K., McCarthy, T. R., Kang, P. B., Voelker, D. R., et al. (2006). Surfactant protein D increases fusion of *Mycobacterium tuberculosis*-containing phagosomes with lysosomes in human macrophages. *Infect. Immun.* 74, 7005–7009.
- Fine, P. E. M. (1995). Variation in protection by BCG: implications of and for heterologous immunity. *Lancet* 346, 1339–1345.
- Foster, K. A., Oster, C. G., Mayer, M. M., Avery, M. L., and Audus, K. L. (1998). Characterization of the A549 Cell Line as a Type II Pulmonary Epithelial Cell Model for Drug Metabolism. *Exp. Cell Res.* 243, 359–366.
- Fowler, W. C. (1930). A preliminary report on the treatment of tuberculosis with turtle vaccine. *Tubercle* 12, 12–17.

- Garcia-Perez, B. E., Castrejon-Jimenez, N. S., and Luna-Herrera, J. (2012). "The role of non-phagocytic cells in Mycobacterial infections," in *Understanding Tuberculosis - Analyzing the Origin of Mycobacterium tuberculosis Pathogenicity*, ed. P.-J. Cardona (InTech).
- García-Pérez, B. E., Hernández-González, J. C., García-Nieto, S., and Luna-Herrera, J. (2008). Internalization of a non-pathogenic mycobacteria by macropinocytosis in human alveolar epithelial A549 cells. *Microb. Pathog.* 45, 1–6.
- Gaynor, C. D., McCormack, F. X., Voelker, D. R., McGowan, S. E., and Schlesinger, L. S. (1995). Pulmonary surfactant protein A mediates enhanced phagocytosis of *Mycobacterium tuberculosis* by a direct interaction with human macrophages. *J Immunol* 155, 5343–5351.
- Gilleron, M., Jackson, M., Nigou, J., and Puzo, G. (2008). *The Mycobacterial Cell Envelope*, eds. G. Avenir, M. Daffé, and J.-M. Reyrat American Society of Microbiology.
- Glickman, M. S. (2008). "Cording, Cord Factors, and Trehalose Dimycolate," in *Mycobact. cell Envel.*, eds. M. Daffé and J.-M. Reyrat (Washington, DC: ASM Press), 63–73.
- Golden, M. P., and Vikram, H. R. (2005). Extrapulmonary tuberculosis: An overview. *Am. Fam. Physician* 72, 1761–1768.
- Good, J. M., and Cooper, S. (1835). *The Study of Medicine - Volum 2*.
- Goren, M. B., D'Arcy Hart, P., Young, M. R., and Armstrong, J. A. (1976). Prevention of phagosome-lysosome fusion in cultured macrophages by sulfatides of *Mycobacterium tuberculosis*. *Proc. Natl. Acad. Sci.* 73, 2510–2514.
- Hall, D. H., Hartwieg, E., and Nguyen, K. C. Q. (2012). Modern Electron Microscopy Methods for *C. elegans*. *Methods Cell Biol.* 107, 93–149.
- Halloum, I., Carrère-Kremer, S., Blaise, M., Viljoen, A., Bernut, A., Le Moigne, V., et al. (2016). Deletion of a dehydratase important for intracellular growth and cording renders rough *Mycobacterium abscessus* avirulent. *Proc. Natl. Acad. Sci.* 113, E4228–E4237.
- Hartmans, S., de Bont, J. A. M., and Stackebrandt, E. (2006). "The genus *Mycobacterium* - Nonmedical," in *The Prokaryotes*, eds. M. Dworkin, S. Falkow, E. Rosenberg, K.-H.

- Schleifer, and E. Stackebrandt (New York, NY: Springer New York), 889–918.
- Heldwein, K. A., and Fenton, M. J. (2002). The role of Toll-like receptors in immunity against mycobacterial infection. *Microbes Infect.* 4, 937–944.
- Hoheisel, G. B., Tabak, L., Teschler, H., Erkan, F., Kroegel, C., and Costabel, U. (1994). Bronchoalveolar lavage cytology and immunocytology in pulmonary tuberculosis. *Am. J. Respir. Crit. Care Med.* 149, 460–463.
- Howard, S. T., Rhoades, E., Recht, J., Pang, X., Alsup, A., Kolter, R., et al. (2006). Spontaneous reversion of *Mycobacterium abscessus* from a smooth to a rough morphotype is associated with reduced expression of glycopeptidolipid and reacquisition of an invasive phenotype. *Microbiology* 152, 1581–1590.
- Jankute, M., Cox, J. A. G. G., Harrison, J., and Besra, G. S. (2015). Assembly of the Mycobacterial Cell Wall. *Annu. Rev. Microbiol.* 69, 405–423.
- Jankute, M., Nataraj, V., Lee, O. Y.-C., Wu, H. H. T., Ridell, M., Garton, N. J., et al. (2017). The role of hydrophobicity in tuberculosis evolution and pathogenicity. *Sci. Rep.* 5, 1–10.
- Jarlier, V., and Nikaido, H. (1990). Permeability barrier to hydrophilic solutes in *Mycobacterium chelonae*. *J. Bacteriol.* 172, 1418–1423.
- Jones, B. W., Means, T. K., Heldwein, K. A., Keen, M. A., Hill, P. J., Belisle, J. T., et al. (2001). Different Toll-like receptor agonists induce distinct macrophage responses. *J. Leukoc. Biol.* 69, 1036–1044.
- Julián, E., Roldán, M., Sánchez-Chardi, A., Astola, O., Agustí, G., and Luquin, M. (2010). Microscopic cords, a virulence-related characteristic of *Mycobacterium tuberculosis*, are also present in nonpathogenic mycobacteria. *J. Bacteriol.* 192, 1751–60.
- Kang, B. K., and Schlesinger, L. S. (1998). Characterization of mannose receptor-dependent phagocytosis mediated by *Mycobacterium tuberculosis* lipoarabinomannan. *Infect. Immun.* 66, 2769–2777.
- Kansal, R. G., Gomez-Flores, R., and Mehta, R. T. (1998). Change in colony morphology influences the virulence as well as the biochemical properties of the *Mycobacterium avium* complex. *Microb. Pathog.* 25, 203–214.

- Kaufmann, S. H., Hussey, G., and Lambert, P. H. (2010). New vaccines for tuberculosis. *Lancet* 375, 2110–2119.
- Kim, S. Y., Sohn, H., Choi, G. E., Cho, S. N., Oh, T., Kim, H. J., et al. (2011). Conversion of *Mycobacterium smegmatis* to a pathogenic phenotype via passage of epithelial cells during macrophage infection. *Med. Microbiol. Immunol.* 200, 177–191.
- Koch, R. (1882). Classics in infectious diseases. The etiology of tuberculosis: Robert Koch. Berlin, Germany 1882. *Rev. Infect. Dis.* 4, 1270–1274.
- Koch, R. (1890). An address on bacteriological research. *Br. Med. J.*, 380–383.
- Koh, W.-J., Jeong, B.-H., Kim, S.-Y., Jeon, K., Park, K. U., Jhun, B. W., et al. (2017). Mycobacterial Characteristics and Treatment Outcomes in *Mycobacterium abscessus* Lung Disease. *Clin. Infect. Dis.* 64, 309–316.
- Krutzik, S. R., and Modlin, R. L. (2004). The role of Toll-like receptors in combating mycobacteria. *Semin. Immunol.* 16, 35–41.
- Laval, F., Lanéelle, M. A., Déon, C., Monsarrat, B., and Daffé, M. (2001). Accurate Molecular Mass Determination of Mycolic Acids by MALDI - TOF Mass Spectrometry. *Anal. Chem.* 73, 4537–4544.
- Lee, J., Repasy, T., Papavinasasundaram, K., Sasseti, C., and Kornfeld, H. (2011). *Mycobacterium tuberculosis* induces an atypical cell death mode to escape from infected macrophages. *PLoS One* 6, e18367.
- Lee, K.-S., Dubey, V. S., Kolattukudy, P. E., Song, C.-H., Shin, A.-R., Jung, S.-B., et al. (2007). Diacyltrehalose of *Mycobacterium tuberculosis* inhibits lipopolysaccharide- and mycobacteria-induced proinflammatory cytokine production in human monocytic cells. *FEMS Microbiol. Lett.* 267, 121–128.
- Lévy-Frébault, V. V, and Portaels, F. (1992). Proposed minimal standards for the genus *Mycobacterium* and for description of new slowly growing *Mycobacterium* species. *Int. J. Syst. Bacteriol.* 42, 315–323.
- Li, Y., Wang, Y., and Liu, X. (2012). The role of airway epithelial cells in response to mycobacteria infection. *Clin. Dev. Immunol.* 2012.
- Lim, J. P., and Gleeson, P. A. (2011). Macropinocytosis: An endocytic pathway for internalising large gulps. *Immunol. Cell Biol.* 89, 836–843.

- Lin, Y., Zhang, M., and Barnes, P. F. (1998). Chemokine production by a human alveolar epithelial cell line in response to *Mycobacterium tuberculosis*. *Infect. Immun.* 66, 1121–6.
- Linares, C., Bernabéu, A., Luquin, M., and Valero-Guillén, P. L. (2012). Cord factors from atypical mycobacteria (*Mycobacterium alvei*, *Mycobacterium brumae*) stimulate the secretion of some pro-inflammatory cytokines of relevance in tuberculosis. *Microbiology* 158, 2878–2885.
- Liu, J., Barry, C. E., Besra, G. S., and Nikaido, H. (1996). Mycolic acid structure determines the fluidity of the mycobacterial cell wall. *J. Biol. Chem.* 271, 29545–29551.
- Llorens-Fons, M., Pérez-Trujillo, M., Julián, E., Brambilla, C., Alcaide, F., Byrd, T. F., et al. (2017). Trehalose Polyphosphates, External Cell Wall Lipids in *Mycobacterium abscessus*, Are Associated with the Formation of Clumps with Cording Morphology, Which Have Been Associated with Virulence. *Front. Microbiol.* 8, 1–15.
- McShane, P. J., and Glassroth, J. (2015). Pulmonary disease due to nontuberculous mycobacteria current state and new insights. *Chest* 148, 1517–1527.
- Means, T. K., Lien, E., Yoshimura, A., Wang, S., Golenbock, D. T., and Fenton, M. J. (1999a). The CD14 ligands lipoarabinomannan and lipopolysaccharide differ in their requirement for Toll-like receptors. *J. Immunol.* 163, 6748–55.
- Means, T. K., Wang, S., Lien, E., Yoshimura, A., Golenbock, D. T., and Fenton, M. J. (1999b). Human toll-like receptors mediate cellular activation by *Mycobacterium tuberculosis*. *J. Immunol.* 163, 3920–3927.
- Medjahed, H., Gaillard, J. L., and Reyrat, J. M. (2010). *Mycobacterium abscessus*: a new player in the mycobacterial field. *Trends Microbiol.* 18, 117–123.
- Méndez-Samperio, P., Miranda, E., and Vázquez, A. (2006). Expression and secretion of CXCL-8 and CXCL-10 from *Mycobacterium bovis* BCG-infected human epithelial cells: Role of IL-4. *Mediators Inflamm.* 2006, 1–6.
- Middlebrook, G., Dubos, R. J., and Pierce, C. (1947). Virulence and morphological characteristics of mammalian tubercle bacilli. *J. Exp. Med.* 86, 175–184.
- Minnikin, D. E., Minnikin, S. M., Parlett, J. H., Goodfellow, M., and Magnusson, M. (1984). Mycolic acid patterns of some species of *Mycobacterium*. *Arch. Microbiol.* 139, 225–

- Muñoz, M., Raynaud, C., Lanéeelle, M., Julián, E., López Marín, L. M., Silve, G., et al. (1998). Specific lipooligosaccharides of *Mycobacterium mucogenicum* sp. nov.(formerly *Mycobacterium chelonae*-like organisms): identification and chemical characterization. *Microbiology* 144, 137–148.
- Nègre, L., Calmette, A., Guérin, C., and Boquet, A. (1926). Prémunition des nouveau-nés contre la tuberculose par le vaccin B.C.G. (1921 à 1926). *Ann. Inst. Pasteur*.
- Neyrolles, O., and Guilhot, C. (2011). Recent advances in deciphering the contribution of *Mycobacterium tuberculosis* lipids to pathogenesis. *Tuberculosis* 91, 187–195.
- Noguera-Ortega, E., Secanella-Fandos, S., Eraña, H., Gasión, J., Rabanal, R. M., Luquin, M., et al. (2016). Nonpathogenic *Mycobacterium brumae* Inhibits Bladder Cancer Growth In Vitro, Ex Vivo, and In Vivo. *Eur. Urol. Focus* 2, 67–76.
- Noll, H., and Bloch, H. (1955). Studies on the chemistry of the cord factor of *Mycobacterium tuberculosis*. *J. Biol. Chem.* 214, 251–265.
- Onwueme, K. C., Vos, C. J., Zurita, J., Soll, C. E., and Quadri, L. E. N. (2005). Identification of phthiodiolone ketoreductase, an enzyme required for production of mycobacterial diacyl phthiocerol virulence factors. *J. Bacteriol.* 187, 4760–4766.
- Ortalo-Magné, A., Lemassu, A., Lanéeelle, M. A., Bardou, F., Silve, G., Gounon, P., et al. (1996). Identification of the surface-exposed lipids on the cell envelopes of *Mycobacterium tuberculosis* and other mycobacterial species. *J. Bacteriol.* 178, 456–461.
- Pabst, M. J., Gross, J. M., Brozna, J. P., and Goren, M. B. (1988). Inhibition of macrophage priming by sulfatide from *Mycobacterium tuberculosis*. *J. Immunol.* 140, 634–40.
- Pacheco, S. A., Hsu, F. F., Powers, K. M., and Purdy, G. E. (2013). MmpL11 protein transports mycolic acid-containing lipids to the mycobacterial cell wall and contributes to biofilm formation in *Mycobacterium smegmatis*. *J. Biol. Chem.* 288, 24213–24222.
- Pang, L., Tian, X., Pan, W., and Xie, J. (2013). Structure and function of *Mycobacterium* glycopeptidolipids from comparative genomics perspective. *J. Cell. Biochem.* 114, 1705–1713.

- Park, I. K., Hsu, A. P., Tettelin, H. H., Shallom, S. J., Drake, S. K., Ding, L., et al. (2015). Clonal diversification, changes in lipid traits and colony morphology in *Mycobacterium abscessus* clinical isolates. *J. Clin. Microbiol.* 53, 3438–3447.
- Passemar, C., Arbués, A., Malaga, W., Mercier, I., Moreau, F., Lepourry, L., et al. (2014). Multiple deletions in the polyketide synthase gene repertoire of *Mycobacterium tuberculosis* reveal functional overlap of cell envelope lipids in host-pathogen interactions. *Cell. Microbiol.* 16, 195–213.
- Pauli, G., Jaki, B., Gödecke, T., and Lankin, D. (2012). Quantitative ¹H NMR: development and potential of a method for natural products analysis - An Update. *J. Nat. Prod.* 75, 834–851.
- Philips, J. A., and Ernst, J. D. (2012). Tuberculosis Pathogenesis and Immunity. *Annual Reviews* .
- Pitarque, S., Larrouy-Maumus, G., Payré, B., Jackson, M., Puzo, G., and Nigou, J. (2008). The immunomodulatory lipoglycans, lipoarabinomannan and lipomannan, are exposed at the mycobacterial cell surface. *Tuberculosis* 88, 560–565.
- Primm, T. P., Lucero, C. A., and Falkinham, J. O. (2004). Health impacts of environmental mycobacteria. *Clin. Microbiol. Rev.* 17, 98–106.
- Qvist, T., Eickhardt-Sørensen, S. R., Katzenstein, T. L., Pressler, T., Iversen, M., Andersen, C. B., et al. (2013). First evidence of *Mycobacterium abscessus* biofilm in the lungs of chronically infected CF patients. *J. Cyst. Fibros.* 12, S2.
- Reed, M. B., Gagneux, S., DeRiemer, K., Small, P. M., and Barry, C. E. (2007). The W-Beijing lineage of *Mycobacterium tuberculosis* overproduces triglycerides and has the DosR dormancy regulon constitutively upregulated. *J. Bacteriol.* 189, 2583–2589.
- Rhoades, E. R., Archambault, A. S., Greendyke, R., Hsu, F.-F. F.-F., Streeter, C., and Byrd, T. F. (2009). *Mycobacterium abscessus* Glycopeptidolipids Mask Underlying Cell Wall Phosphatidyl-myo-Inositol Mannosides Blocking Induction of Human Macrophage TNF- by Preventing Interaction with TLR2. *J. Immunol.* 183, 1997–2007.
- Ribeiro, G. M., Matsumoto, C. K., Real, F., Teixeira, D., Duarte, R. S., Mortara, R. A., et al.

- (2017). Increased survival and proliferation of the epidemic strain *Mycobacterium abscessus* subsp. *massiliense* CRM0019 in alveolar epithelial cells. *BMC Microbiol.* 17, 195.
- Roach, T. I., Barton, C. H., Chatterjee, D., and Blackwell, J. M. (1993). Macrophage activation: lipoarabinomannan from avirulent and virulent strains of *Mycobacterium tuberculosis* differentially induces the early genes c-fos, KC, JE, and tumor necrosis factor- α . *J. Immunol.* 150, 1886–1896.
- Rodríguez-Güell, E., Agustí, G., Corominas, M., Cardona, P.-J., Casals, I., Parella, T., et al. (2006). The production of a new extracellular putative long-chain saturated polyester by smooth variants of *Mycobacterium vaccae* interferes with Th1-cytokine production. *Antonie Van Leeuwenhoek* 90, 93–108.
- Rogall, T., Wolters, J., Flohr, T., and Böttger, E. C. (1990). Towards a phylogeny and definition of species at the molecular level within the genus *Mycobacterium*. *Int. J. Syst. Bacteriol.* 40, 323–330.
- Rohde, K., Yates, R. M., Purdy, G. E., and Russell, D. G. (2007). *Mycobacterium tuberculosis* and the environment within the phagosome. *Immunol. Rev.* 219, 37–54.
- Rombouts, Y., Burguière, A., Maes, E., Coddeville, B., Ellass, E., Guérardel, Y., et al. (2009). *Mycobacterium marinum* lipooligosaccharides are unique caryophyllose-containing cell wall glycolipids that inhibit tumor necrosis factor- α secretion in macrophages. *J. Biol. Chem.* 284, 20975–20988.
- Roux, A.-L., Ray, A., Pawlik, A., Medjahed, H., Etienne, G., Rottman, M., et al. (2011). Overexpression of proinflammatory TLR-2-signalling lipoproteins in hypervirulent mycobacterial variants. *Cell. Microbiol.* 13, 692–704.
- Roux, A.-L., Viljoen, A., Bah, A., Simeone, R., Bernut, A., Laencina, L., et al. (2016). The distinct fate of smooth and rough *Mycobacterium abscessus* variants inside macrophages. *Open Biol.* 6, 160185.
- Roy, S., Sharma, S., Sharma, M., Aggarwal, R., Bose, M., and Roy, S. (2004). Induction of nitric oxide release from the human alveolar epithelial cell line A549: an in vitro correlate of innate immune response to *Mycobacterium tuberculosis*. *Immunology* 112, 471–480.

- Rüger, K., Hampel, A., Billig, S., Rücker, N., Suerbaum, S., and Bange, F. C. (2014). Characterization of rough and smooth morphotypes of *Mycobacterium abscessus* isolates from clinical specimens. *J. Clin. Microbiol.* 52, 244–250.
- Sánchez-Chardi, A., Olivares, F., Byrd, T. F., Julián, E., Brambilla, C., and Luquin, M. (2011). Demonstration of cord formation by rough *Mycobacterium abscessus* variants: Implications for the clinical microbiology laboratory. *J. Clin. Microbiol.* 49, 2293–2295.
- Scherman, M. S., Winans, K. A., Stern, R. J., Jones, V., Bertozzi, C. R., and McNeil, M. R. (2003). Drug targeting *Mycobacterium tuberculosis* cell wall synthesis: Development of a microtiter plate-based screen for UDP-galactopyranose mutase and identification of an inhibitor from a uridine-based library. *Antimicrob. Agents Chemother.* 47, 378–382.
- Schlesinger, L. S., Bellinger-kawahara, C. G., Horwitz, M. A., and Payne, R. (1990). Phagocytosis of *Mycobacterium tuberculosis* is mediated by human monocyte complement receptors and complement component C3. *J. Immunol.* 144, 2771–2780.
- Schwab, U., Rohde, K. H., Wang, Z., Chess, P. R., Notter, R. H., and Russell, D. G. (2009). Transcriptional responses of *Mycobacterium tuberculosis* to lung surfactant. *Microb. Pathog.* 46, 185–193.
- Secanella-Fandos, S., Luquin, M., Pérez-Trujillo, M., and Julián, E. (2011). Revisited mycolic acid pattern of *Mycobacterium confluentis* using thin-layer chromatography. *J. Chromatogr. B. Analyt. Technol. Biomed. Life Sci.* 879, 2821–6.
- Seeliger, J., and Moody, D. B. (2016). Monstrous Mycobacterial Lipids. *Cell Chem. Biol.* 1, 2015–2017.
- Seligman, A. M., Wasserkrug, H. L., and Hanker, J. S. (1966). A new staining method (OTO) for enhancing contrast of lipid-containing membranes and droplets in osmium tetroxide-fixed tissue with osmiophilic thiocarbohydrazide (TCH). *J. Cell Biol.* 30, 424–432.
- Sequeira, P. C., Senaratne, R. H., and Riley, L. W. (2014). Inhibition of toll-like receptor 2 (TLR-2)-mediated response in human alveolar epithelial cells by mycolic acids and *Mycobacterium tuberculosis* mce1 operon mutant. *Pathog. Dis.* 70, 132–140.

- Sibley, L. D., Hunter, S. W., Brennan, P. J., and Krahenbuhl, J. L. (1988). Mycobacterial lipoarabinomannan inhibits gamma interferon-mediated activation of macrophages. *Infect. Immun.* 56, 1232–1236.
- Sinsimer, D., Huet, G., Manca, C., Tsenova, L., Koo, M. S., Kurepina, N., et al. (2008). The phenolic glycolipid of *Mycobacterium tuberculosis* differentially modulates the early host cytokine response but does not in itself confer hypervirulence. *Infect. Immun.* 76, 3027–3036.
- Spahlinger, H., Macassey, L. L., Williams Saleeby, C., Khan, A., and Henderson, A. (1934). *Spahlinger contra tuberculosis 1908-1934.*, ed. Bale & Danielsson London.
- Stanford, J. L., Rook, G. a, Bahr, G. M., Dowlati, Y., Ganapati, R., Ghazi, S. K., et al. (1990). *Mycobacterium vaccae* in immunoprophylaxis and immunotherapy of leprosy and tuberculosis. *Vaccine* 8, 525–530.
- Stanford, J., Stanford, C., and Grange, J. (2004). Immunotherapy with *Mycobacterium vaccae* in the treatment of tuberculosis. *Front. Biosci.* 9, 1701–19.
- Stenger, S., and Modlin, R. L. (2002). Control of *Mycobacterium tuberculosis* through mammalian Toll-like receptors. *Curr. Opin. Immunol.* 14, 452–457.
- Stern, S. T., Adiseshaiah, P. P., and Crist, R. M. (2012). Autophagy and lysosomal dysfunction as emerging mechanisms of nanomaterial toxicity. *Part. Fibre Toxicol.* 9, 20.
- Stokes, R. W., Norris-Jones, R., Brooks, D. E., Beveridge, T. J., Doxsee, D., and Thorson, L. M. (2004). The glycan-rich outer layer of the cell wall of *Mycobacterium tuberculosis* acts as an antiphagocytic capsule limiting the association of the bacterium with macrophages. *Infect. Immun.* 72, 5676–5686.
- Tabouret, G., Astarie-Dequeker, C., Demangel, C., Malaga, W., Constant, P., Ray, A., et al. (2010). *Mycobacterium leprae* Phenolglycolipid-1 Expressed by Engineered *M. bovis* BCG modulates early interaction with human phagocytes. *PLoS Pathog.* 6.
- Torrelles, J. B., Azad, A. K., and Schlesinger, L. S. (2006). Fine discrimination in the recognition of individual species of phosphatidyl-myo-inositol mannosides from *Mycobacterium tuberculosis* by C-type lectin pattern recognition receptors. *J. Immunol.* 177, 1805–1816.

- Tsenova, L., Ellison, E., Harbacheuski, R., Moreira, A. L., Kurepina, N., Reed, M. B., et al. (2005). Virulence of selected *Mycobacterium tuberculosis* clinical isolates in the rabbit model of meningitis is dependent on phenolic glycolipid produced by the bacilli. *J. Infect. Dis.* 192, 98–106.
- Ufimtseva, E. (2015). Mycobacterium-Host Cell Relationships in Granulomatous Lesions in a Mouse Model of Latent Tuberculous Infection. *Biomed Res. Int.* 2015, 948131.
- Underhill, D. M., Ozinsky, A., Smith, K. D., and Aderem, A. (1999). Toll-like receptor-2 mediates mycobacteria-induced proinflammatory signaling in macrophages. *Proc. Natl. Acad. Sci. U. S. A.* 96, 14459–63.
- van der Werf, M. J., Ködmön, C., Katalinić-Janković, V., Kummik, T., Soini, H., Richter, E., et al. (2014). Inventory study of non-tuberculous mycobacteria in the European Union. *BMC Infect. Dis.* 14, 62.
- Vergne, I., Chua, J., Singh, S. B., and Deretic, V. (2004). Cell biology of *Mycobacterium tuberculosis* phagosome. *Annu. Rev. Cell Dev. Biol.* 20, 367–394.
- Watanabe, M., Ohta, A., Sasaki, S. I., and Minnikin, D. E. (1999). Structure of a new glycolipid from the *Mycobacterium avium*-*Mycobacterium intracellulare* complex. *J. Bacteriol.* 181, 2293–2297.
- Wayne, L. G., and Kubica, G. P. (1986). “The mycobacteria,” in *Bergey’s Man. Syst. Bacteriol.*, eds. H. JG, S. PH, M. NS, and S. ME (Williams & Wilkins, Baltimore MD), 1435–1457.
- Weiss, G., and Schaible, U. E. (2015). Macrophage defense mechanisms against intracellular bacteria. *Immunol. Rev.* 264, 182–203.
- WHO (2017). Global tuberculosis report 2017. World Health Organization.
- Wickremasinghe, M. I., Thomas, L. H., and Friedland, J. S. (1999). Pulmonary epithelial cells are a source of IL-8 in the response to *Mycobacterium tuberculosis*: essential role of IL-1 from infected monocytes in a NF-kappa B dependent network. *J. Immunol.* 163, 3936–3947.
- Yang, J., Hooper, W. C., Phillips, D. J., and Talkington, D. F. (2002). Regulation of proinflammatory cytokines in human lung epithelial cells infected with

- Mycoplasma pneumoniae*. *Infect Immun* 70, 3649–3655.
- Yang, J., Hooper, W. C., Phillips, D. J., Tondella, M. L., and Talkington, D. F. (2003). Induction of Proinflammatory Cytokines in Human Lung Epithelial Cells during *Chlamydia pneumoniae* Infection. *Infect. Immun.* 71, 614–620.
- Yang, X. yan, Chen, Q. fei, Cui, X. hua, Yu, Y., and Li, Y. ping (2010). *Mycobacterium vaccae* vaccine to prevent tuberculosis in high risk people: A meta-analysis. *J. Infect.* 60, 320–330.
- Yuan, Y., and Barry, C. E. (1996). A common mechanism for the biosynthesis of methoxy and cyclopropyl mycolic acids in *Mycobacterium tuberculosis*. *Proc. Natl. Acad. Sci. U. S. A.* 93, 12828–12833.
- Zambrano, M. M., and Kolter, R. (2005). Mycobacterial biofilms: A greasy way to hold it together. *Cell* 123, 762–764.
- Zhang, Y., Broser, M., Cohen, H., Bodkin, M., Law, K., Reibman, J., et al. (1995). Enhanced interleukin-8 release and gene expression in macrophages after exposure to *Mycobacterium tuberculosis* and its components. *J. Clin. Invest.* 95, 586–592.
- Zlotnik, A., and Yoshie, O. (2000). Chemokines: A New Classification Review System and Their Role in Immunity. *Immunity* 12, 121–127.
- Zuber, B., Chami, M., Houssin, C., Dubochet, J., Griffiths, G., and Daffé, M. (2008). Direct visualization of the outer membrane of mycobacteria and corynebacteria in their native state. *J. Bacteriol.* 190, 5672–5680.

8

Manuscripts of this thesis



Mycobacteria Clumping Increase Their Capacity to Damage Macrophages

Cecilia Brambilla^{1†}, Marta Llorens-Fons^{1†}, Esther Julián¹, Estela Noguera-Ortega¹, Cristina Tomàs-Martínez¹, Miriam Pérez-Trujillo², Thomas F. Byrd³, Fernando Alcaide⁴ and Marina Luquin^{1*}

¹ Departament de Genètica i de Microbiologia, Facultat de Biociències, Universitat Autònoma de Barcelona, Bellaterra, Spain, ² Servei de Resonància Magnètica Nuclear and Departament de Química, Universitat Autònoma de Barcelona, Bellaterra, Spain, ³ Division of Infection Diseases, Department of Medicine, The University of New Mexico School of Medicine, Albuquerque, NM, USA, ⁴ Servei de Microbiologia, Hospital Universitari de Bellvitge-Institut d'Investigació Biomèdica de Bellvitge, Universitat de Barcelona, Barcelona, Spain

OPEN ACCESS

Edited by:

Leland Shapiro,
University of Colorado Denver, USA

Reviewed by:

Sascha Brunke,
Hans Knöll Institute, Germany
Yutaka Handa,
National Center For Global Health
and Medicine, Japan

*Correspondence:

Marina Luquin
marina.luquin@uab.cat

[†] These authors have contributed
equally to this work.

Specialty section:

This article was submitted to
Infectious Diseases,
a section of the journal
Frontiers in Microbiology

Received: 28 July 2016

Accepted: 20 September 2016

Published: 04 October 2016

Citation:

Brambilla C, Llorens-Fons M,
Julián E, Noguera-Ortega E,
Tomàs-Martínez C, Pérez-Trujillo M,
Byrd TF, Alcaide F and Luquin M
(2016) Mycobacteria Clumping
Increase Their Capacity to Damage
Macrophages.
Front. Microbiol. 7:1562.
doi: 10.3389/fmicb.2016.01562

The rough morphotypes of non-tuberculous mycobacteria have been associated with the most severe illnesses in humans. This idea is consistent with the fact that *Mycobacterium tuberculosis* presents a stable rough morphotype. Unlike smooth morphotypes, the bacilli of rough morphotypes grow close together, leaving no spaces among them and forming large aggregates (clumps). Currently, the initial interaction of macrophages with clumps remains unclear. Thus, we infected J774 macrophages with bacterial suspensions of rough morphotypes of *M. abscessus* containing clumps and suspensions of smooth morphotypes, primarily containing isolated bacilli. Using confocal laser scanning microscopy and electron microscopy, we observed clumps of at least five rough-morphotype bacilli inside the phagocytic vesicles of macrophages at 3 h post-infection. These clumps grew within the phagocytic vesicles, killing 100% of the macrophages at 72 h post-infection, whereas the proliferation of macrophages infected with smooth morphotypes remained unaltered at 96 h post-infection. Thus, macrophages phagocytose large clumps, exceeding the bactericidal capacities of these cells. Furthermore, proinflammatory cytokines and granuloma-like structures were only produced by macrophages infected with rough morphotypes. Thus, the present study provides a foundation for further studies that consider mycobacterial clumps as virulence factors.

Keywords: *Mycobacterium abscessus*, virulence factors, infection of macrophages, clumps, cords, rough morphotypes, smooth morphotypes

INTRODUCTION

The genus *Mycobacterium* contains important human pathogens, such as *Mycobacterium tuberculosis*, *M. leprae*, and *M. ulcerans*. Furthermore, non-tuberculous mycobacterial species, as inhabitants of the environment, are important re-emerging opportunistic pathogens (Pimm et al., 2004; Falkinham, 2009, 2013; van der Werf et al., 2014). In solid media, mycobacterial strains

Abbreviations: CLSM: confocal laser scanning microscopy; CM: complete medium, Dulbecco's modified Eagle's medium with fetal bovine serum; DPPC: dipalmitoyl phosphatidylcholine; h. p. i.: hours post-infection; IL-6: interleukin 6; MOI: multiplicity of infection; PBS: phosphate saline buffer; R: rough; S: smooth; SEM: scanning electron microscopy; TEM: transmission electronic microscopy; TLR-2: Toll like receptor-2; TNF- α : tumor necrosis factor α ; ZN: Ziehl-Neelsen.

display different colony morphotypes. Rough colony morphotypes (R) are characterized by an irregular dry surface with many wrinkles and crests, whereas smooth colony morphotypes (S) show an even, bright and moist texture (Belisle and Brennan, 1989; Muñoz et al., 1998; Rüger et al., 2014). *M. tuberculosis* have a highly conserved R morphotype, whereas non-tuberculous mycobacterial species show both morphotypes, and spontaneous S to R and R to S morphology shifts have also been described (Byrd and Lyons, 1999; Howard et al., 2006; Agustí et al., 2008; Park et al., 2015). The S to R variation is accompanied by the loss of surface glycolipids, such as glycopeptidolipids (GPL) or lipooligosaccharides (LOS) (Belisle and Brennan, 1989; Muñoz et al., 1998; Pang et al., 2013). Genetic evidence supporting the relationship between colonial morphotypes and the loss of surface glycolipids has been reported (Deshayes et al., 2008; Pawlik et al., 2013; Boritsch et al., 2016). Another phenotypic difference between S and R morphotypes is that R morphotypes show increased cellular aggregation. The bacilli of R morphotypes remain attached during replication, forming compact colonies containing structures that resemble cords (Howard et al., 2006; Agustí et al., 2008). In liquid media, R morphotypes aggregate to form clumps. Large clumps acquire cord morphologies (Julián et al., 2010; Sánchez-Chardi et al., 2011; Brambilla et al., 2012). In previous studies, the R morphotypes of *M. avium*, *M. kansasii*, *M. marinum*, and *M. abscessus* are more virulent than the S morphotypes (Belisle and Brennan, 1989; Kansal et al., 1998; Catherinot et al., 2007). The species *M. canettii*, also referred to as “smooth tubercle bacilli,” is closely related to *M. tuberculosis* and exhibits an S morphotype. In contrast to *M. tuberculosis*, isolates of *M. canettii* are rare and restricted to some regions of Africa. A recent study reported the increased virulence of a spontaneous R morphotype of *M. canettii* versus the wild S morphotype (Boritsch et al., 2016).

The identification of factors that confer more virulence to R morphotypes would increase the current understanding of the mechanisms involved in the pathogenesis of tuberculosis and other mycobacterial diseases and contribute to the development of new drugs.

A majority of the studies performed to determine the mechanisms that confer more virulence to R morphotypes have primarily focused on *M. abscessus*, a re-emerging pathogenic species that causes serious chronic pulmonary infections in patients with underlying respiratory diseases, such as bronchiectasis or cystic fibrosis (Petrini, 2006; Medjahed and Singh, 2010; Lee et al., 2015). *M. abscessus* strains isolated from humans display colonies with S and R morphotypes, and several studies have demonstrated that R morphotypes are more virulent than S morphotypes (Byrd and Lyons, 1999; Sanguinetti et al., 2001; Howard et al., 2006; Catherinot et al., 2007, 2009; Rüger et al., 2014). In *M. abscessus*, the more virulent R morphotypes have been associated with hyper-proinflammatory responses to mycobacterial Toll like receptor-2 (TLR-2) ligands expressed on the cell surface (Gilleron et al., 2008; Rhoades et al., 2009; Roux et al., 2011).

In addition to the molecules expressed on the surface of R morphotypes, the formation of clumps (only present in R

morphotypes) could also play a role in the increased virulence of these morphotypes. Currently, there are no studies investigating the interactions of clumps with the host, as most infection studies are conducted using homogeneous bacterial suspensions containing isolated bacilli. To obtain non-aggregating cultures, mycobacteria are cultured in media containing detergents, such as Tween, or are subjected to physical disaggregation procedures to obtain a homogeneous suspension of isolated bacilli (Byrd and Lyons, 1999; Stokes et al., 2004; Howard et al., 2006; Catherinot et al., 2007; Bernut et al., 2014; Leisching et al., 2016). However, inside the host, mycobacteria exist in a detergent-free environment, and R mycobacteria replicates initially forming small clumps that eventually become large clumps with cording morphology. Clumps and cords are not laboratory artifacts, as the presence of the clumps and cords of *M. abscessus* and *M. marinum* have been reported in zebrafish (Clay et al., 2008; Bernut et al., 2014). Furthermore, the presence of *M. bovis* BCG cords in the cytoplasm of macrophages and the dendritic cells of mouse splenic granulomas (Ufimtseva, 2015) and clumps of *M. abscessus* in the sputum of patients with cystic fibrosis have been reported (Qvist et al., 2013). Thus, it is reasonable to assume that macrophages interact with clumps of R morphotypes and not with the isolated bacilli of R morphotypes inside the host. To verify this hypothesis, we infected macrophages with mycobacterial clumps.

Thus, the objective of the present study was to describe the initial interaction between the macrophages and bacterial clumps of *M. abscessus* R compared with that of the isolated bacilli of *M. abscessus* S. For infection studies, J774, a murine monocyte/macrophage cell line that enables the comparative study of virulence among mycobacterial strains in a homogeneous population, was used. (Ramakrishnan and Falkow, 1994; Gao et al., 2003; Indrigo et al., 2003; Tan et al., 2006; Julián et al., 2010).

The progression of infection inside macrophages was examined using confocal laser scanning microscopy (CLSM) and transmission electron microscopy (TEM). The different capacities of R and S morphotypes to kill macrophages and induce the formation of granulomas, and the secretion of IL-6 and TNF- α were determined (Welsh et al., 2008; Philips and Ernst, 2012). Previous studies have reported that pulmonary surfactant proteins A and D induce the agglutination of *M. tuberculosis* bacilli (Ferguson et al., 2006). In the present study, the interaction of clumps with dipalmitoyl phosphatidylcholine (DPPC), one of the most abundant lipids of pulmonary surfactant, was also investigated (Chimote and Banerjee, 2005).

MATERIALS AND METHODS

Bacterial Strains

The bacterial strains used in the present study were *M. abscessus* type strain DSMZ 44196^T, *M. abscessus* 390, *M. abscessus* BE37R, and *M. abscessus* BE48R (Table 1). The original *M. abscessus* type strain (DSMZ 44196^T) displayed S colonies on agar medium (called 44196S), but after a few passages on

TABLE 1 | Strains of *M. abscessus* used in the present study.

<i>M. abscessus</i> strains	Colonial morphology	Cord formation	Isolated
390S	Smooth	No	Natural mutant of 390R
390R	Rough	Yes	Isolated from an ileal granuloma in patient with Crohn's disease
DSMZ 44196 ^T S	Smooth	No	Type strain
DSMZ 44196 ^T R	Rough	Yes	Natural mutant of DSMZ 44196 ^T S
BE37R	Rough	Yes	Isolated from sputum in patient with severe pulmonary disease
BE48R	Rough	Yes	Isolated from sputum in patient with severe pulmonary disease

agar medium, natural R colony mutants appeared (44196R). *M. abscessus* 390 was isolated in pure culture from an ileal granuloma in a patient with Crohn's disease (Byrd and Lyons, 1999). *M. abscessus* 390 displayed R colonies on agar medium (390R), but after serial passages on agar medium, an S morphotype was isolated (390S) (Byrd and Lyons, 1999). *M. abscessus* BE37R and BE48R were isolated from pulmonary disease patients hospitalized at Bellvitge University Hospital in Barcelona, Spain. BE37R and BE48R were identified using polymerase chain reaction and reverse hybridization (GenoType Mycobacterium CM[®], Hain Lifescience, Germany) and the partial sequencing of 16S rRNA. All strains were grown on trypticase soy agar (TSA; Scharlau, Spain) medium for 2 weeks at 37°C.

Colony Morphology

To determine the ultrastructure of the colonies, the bacteria were grown on TSA for 2 weeks at 37°C. The colonies were processed for scanning electronic microscopy (SEM) as previously described (Julián et al., 2010). Briefly, the colonies were recovered from the agar plate and fixed in 2.5% (vol/vol) glutaraldehyde in 0.1 M phosphate buffer (pH 7.4) for 2 h at 4°C. Subsequently, the samples were washed four times for 10 min each in 0.1 M phosphate buffer, post-fixed in 1% (wt/vol) osmium tetroxide and 0.7% ferrocyanide in phosphate buffer, followed by washing with water, dehydration in an ascending ethanol series (50, 70, 80, 90, and 95% for 10 min each and twice with 100% ethanol), and critical-point drying with CO₂. The samples were coated with gold and observed using an SEM EVO (Zeiss, Germany) at 15 kV.

Aggregate Size Analysis of the Bacterial Suspensions

Colonies of *M. abscessus*, cultivated for 2 weeks, were scraped from TSA plates and vigorously shaken in a tub with glass beads (Schlesinger et al., 1990; Julián et al., 2010). The bacteria were subsequently resuspended in phosphate-buffered saline (PBS), and large aggregates were allowed to sit for 10 min. The supernatant was recovered and adjusted to the McFarland standard one suspension, followed by centrifugation at 1500 g for 10 min at 4°C. The supernatant was removed, and the pellet was resuspended in Dulbecco's modified Eagle's medium (Gibco, USA) supplemented with L-glutamine, high glucose, and 10% heat-inactivated fetal bovine serum (Hyclone, USA); this was considered complete medium (CM). To break up the aggregates, the suspension was sonicated in an ultrasonic cell water bath

three times for 30 s each (Stokes et al., 2004; Julián et al., 2010). In a series of preliminary experiments, cell viability of each mycobacterial strain was tested after sonication in order to verify the cell counts obtained in McFarland adjustments. In all experiments, representative bacterial suspensions were serially diluted in PBS, and colony-forming units (CFU) were counted after plating on TSA.

The bacterial suspension was labeled with Phenolic Auramine (Mycobacteria Fluorescent Stain – Fluka, USA), according to the manufacturer's instructions, and the images were generated using a TCS-SP5 CLSM (Leica, Germany) with a Plan Apo 63× (numerical aperture [NA], 1.4) oil objective, operating at a zoom of 1.8. This procedure facilitated the quantification of the bacteria number per ml in bacterial solution adjusted to the McFarland standard 1. To analyze the clump sizes, horizontal (x-z) optical sections of twenty fields for each sample were captured, and the fluorescence intensity and area were measured. To quantify the size ranges based on the number of bacilli in each clump, the area sizes were classified as described: areas ≤3 μm² were considered as 1–2 bacilli, areas between 3 and 6 μm² were considered as 3–4 bacilli, and areas >6 μm² were considered as five or more bacilli. The images were processed using ImageJ software (National Institutes of Health, USA).

Cell Culture

The murine macrophage cell line J774A.1 (DSMZ ACC 170) was maintained at 37°C in a 5% CO₂-humidified atmosphere in CM containing 100 U/ml penicillin G (Laboratorios Ern, Spain) and 100 μg/ml streptomycin (Laboratorios Rech-Jofre, Spain).

Phagocytosis Assay

For phagocytosis analyses, macrophage cells (5 × 10⁵/well) were cultured on plates (Mat Tek, USA) with CM for 24 h at 37°C in a humidified atmosphere with 5% CO₂. The macrophages were infected with R and S morphotypes at a MOI of 10:1 and 100:1, respectively. In a set of previous experiments, we observed a more inefficient phagocytosis of the S morphotype as has been previously observed by other authors (Etienne et al., 2002; Villeneuve et al., 2003; Kocíncová et al., 2009); thus, to obtain a similar average of macrophage infection for both morphotypes, a higher MOI was used in infection experiments with the S morphotype. These MOI levels yielded between 50 and 60% of macrophages infected at 3 h.p.i. In addition, three wells per dish were left uninfected as a negative control. After infection, the CM was removed,

and the macrophages were washed three times with fresh CM to extract extracellular bacteria, followed by fixation with 4% paraformaldehyde (Sigma–Aldrich, USA) in PBS for 10 min. Subsequently, the macrophages were washed with PBS and air dried for 30 min. For CLSM observation, the mycobacteria were stained with Phenolic Auramine (Mycobacteria Fluorescent Stain – Fluka, USA) according to the manufacturer's instructions. The macrophages were labeled with 1 μ l red fluorescent CellMask (Molecular Probes, USA)/ml of PBS for 10 min at room temperature and subsequently washed with PBS. The images were obtained using a TCS-SP5 CLSM (Leica, Germany) equipped with a Plan Apo 63 \times (numerical aperture [NA], 3.0) oil objective in horizontal (x–z) optical sections. The images were subsequently analyzed using Imaris v. 6.1.0. scientific software (Bitplane, Switzerland). Ten fields per sample (approximately two hundred macrophages) were considered. The assay was performed twice.

Transmission Electron Microscopy (TEM)

For TEM analysis, infected macrophages were fixed with a solution containing 2% (wt/vol) paraformaldehyde (Merck, Ireland) and 2.5% (vol/vol) glutaraldehyde (Merck, Ireland) in 0.1 M phosphate buffer (Sigma–Aldrich, USA) at pH 7.4 for 1 h. After fixation, the infected macrophages were recovered using a cell scraper and were processed following conventional procedures (Lee et al., 2011). The sections were observed using a Jeol 1400 transmission electron microscope (Jeol, Japan).

Macrophage Viability

Macrophages viability was measured by two different assays: trypan blue exclusion and CLSM assay. The macrophages were seeded onto 48-well tissue culture plates (Thermo Fisher Scientific, Denmark) at 6×10^4 cells per well in CM and were incubated at 37°C in a 5% CO₂-humidified atmosphere. After 24 h, the macrophages were infected as described above. At 3 h.p.i., the medium was removed, and the macrophages were washed three times with CM to remove extracellular bacteria and were then incubated with fresh CM at 37°C. At 24-h intervals, the infected macrophages were washed again three times to prevent bacterial overgrowth in the extracellular medium. At different time points after infection (3, 24, 48, 72, and 96 h), the supernatant was removed, and the macrophages were gently washed with PBS, trypsinized (trypsin-EDTA, PAA, Austria) for 10 min and subsequently stained with trypan blue (Gibco, USA). Viable macrophages were counted using a Neubauer chamber. Each assay was performed in triplicate, and the experiment was performed three times.

For the CLSM assay, 5×10^5 macrophages per well were plated in culture dishes (Mat Tech, USA) and infected as described above. At different time points after infection (3, 24, 48, 72, and 96 h), the macrophages were labeled with 0.5 μ l/ml of green fluorescent 4 mM Calcein acetoxymethyl and 0.2 μ l/ml of red fluorescent 2 mM Ethidium homodimer-1, LIVE/DEAD® Viability/Cytotoxicity Kit (Molecular Probes, USA) for 10 min at room temperature, and then washed with CM before being observed. Labeled macrophages were examined

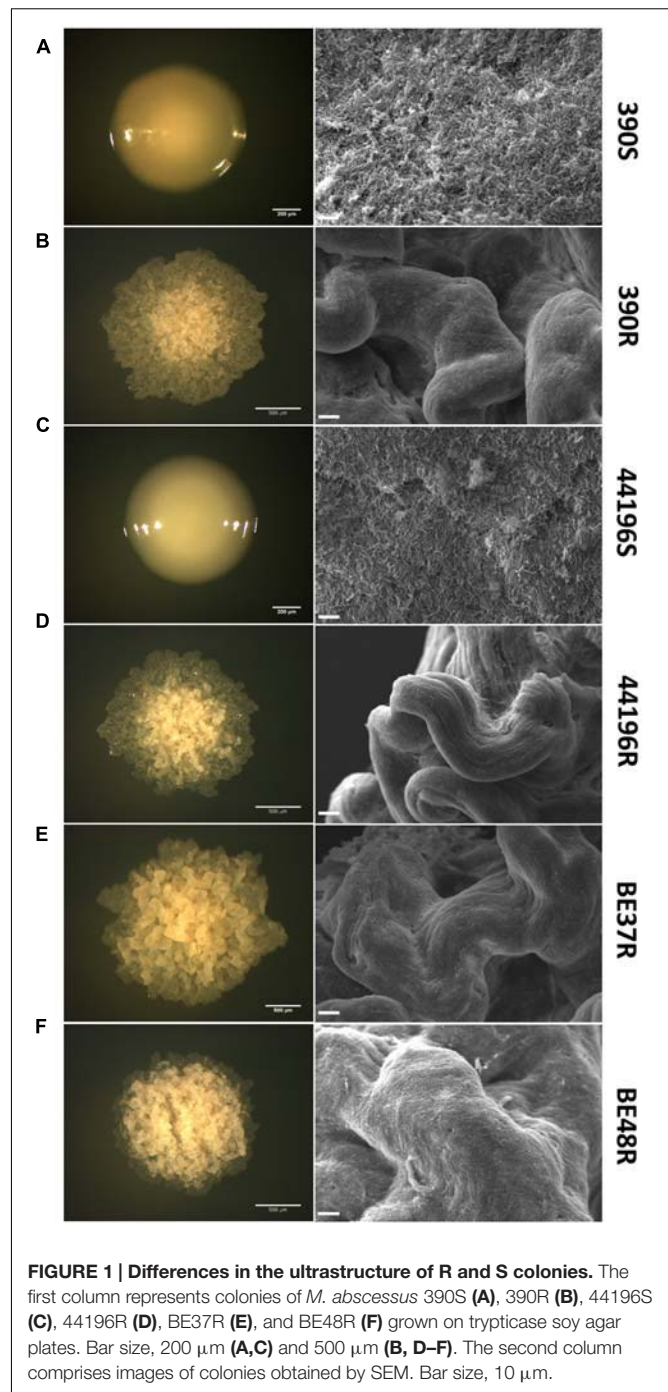


FIGURE 1 | Differences in the ultrastructure of R and S colonies. The first column represents colonies of *M. abscessus* 390S (A), 390R (B), 44196S (C), 44196R (D), BE37R (E), and BE48R (F) grown on trypticase soy agar plates. Bar size, 200 μ m (A,C) and 500 μ m (B, D–F). The second column comprises images of colonies obtained by SEM. Bar size, 10 μ m.

under a CLSM (FV1000-Olympus) using a Plan Apo 20 \times (numerical aperture [NA], 1.5). For the processing of the images ImageJ software (National Institutes of Health, USA) was used. Ten random fields were taken for each treatment and the mean of live cells per field was calculated.

Granuloma-Like Structure Analysis

The macrophages were seeded onto 8-well sterile glass chamber slides (Thermo Fisher Scientific, Denmark) and infected

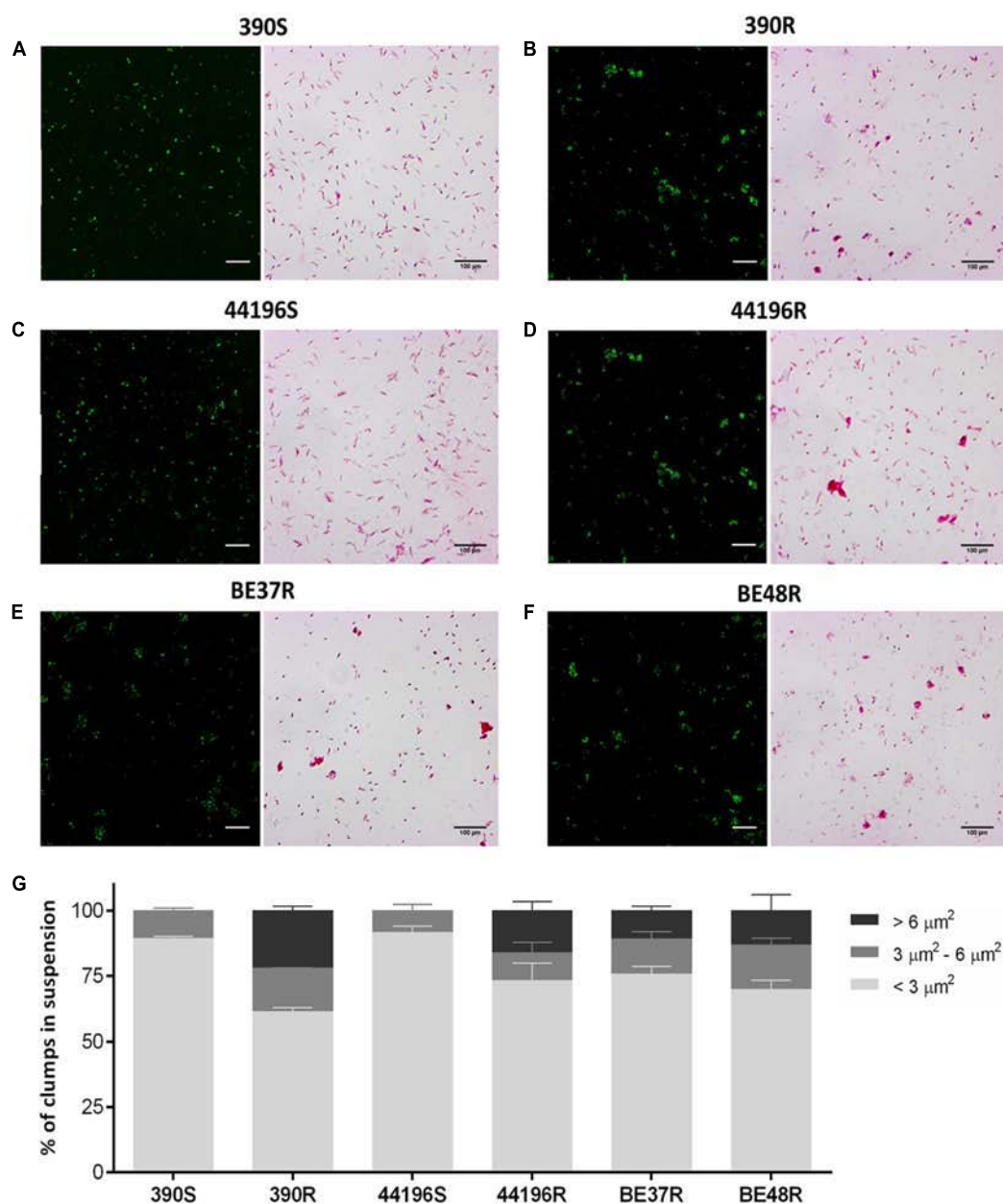


FIGURE 2 | Analysis of the aggregates in the bacterial suspensions. (A–F) Images of CLSM and Ziehl–Neelsen staining showing bacterial aggregates or isolated bacilli from bacterial suspension. Bar size, 100 µm in the Ziehl–Neelsen staining images. For CLSM, the bacteria were stained with phenolic auramine (green). Bar size, 15 µm. **(A)** 390S, **(B)** 390R, **(C)** 44196S, **(D)** 44196R, **(E)** BE37R, **(F)** BE48R. **(G)** Show the results of the analysis of the percentages of clumps of different sizes in the bacterial suspensions. The results represent the mean ± SD of triplicate preparations.

as described above. At different time points after infection (3, 24, and 48 h), the supernatants were removed, and the samples were heat-fixed and stained using the Ziehl-Neelsen (ZN) method. Observations and images were obtained using an optical microscope (Leica, Germany) equipped with a DM500 digital camera system. For SEM analysis, glass coverslips (Nahita, Spain) were inserted in the 24-well culture plates, and the macrophages (1.2×10^5 /well) were subsequently seeded and infected as described above. Coverslip –

adhered macrophages were processed for SEM at different time points after infection (3, 24, and 48 h) as described above.

Cytokine Analysis

For cytokine analysis macrophages were infected with the same procedure as for viability assay. Supernatants were collected at different time points, without previous washing steps, and were centrifuged to eliminate the bacteria and/or

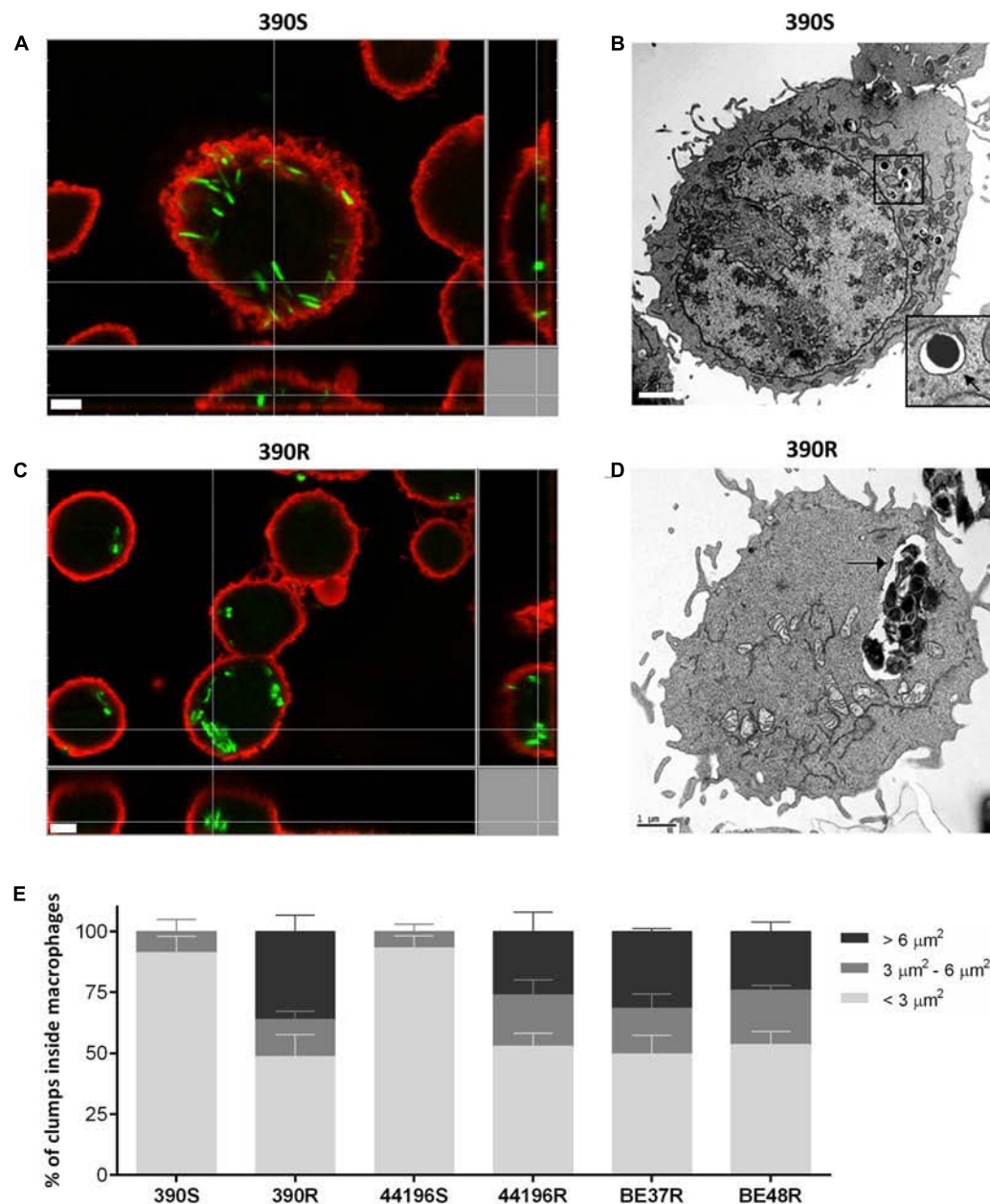


FIGURE 3 | Localization of intracellular bacteria using CLSM and transmission electron microscopy (TEM). (A,B) Images of macrophages infected with *M. abscessus* 390S. In (B), the membrane of phagocytic vesicle is indicated with a black arrow. Bar size, 2 μm . (C,D) Images of macrophages infected with 390R. (D) Intracellular clump of 390R inside a large phagocytic vesicle. The phagocytic vesicle membrane is indicated with a black arrow. Bar size, 1 μm . Bacteria in (A–C) were stained with phenolic auramine (green) and macrophage cell membranes stained with CellMask (red). Bar size, 5 μm . Similar images were obtained for the remaining strains. (E) Show the results of the analysis of the percentages of clumps of different sizes inside the macrophages. The results represent the mean \pm SD of triplicate preparations.

macrophages detached from the well, in order to avoid any interference in the ELISA assays. TNF- α (R&D Systems, USA) and IL-6 (BD Biosciences, Belgium) levels were measured at different time points after infection using commercially available enzyme-linked immunosorbent assays (ELISA) according to the manufacturer's instructions. All samples were analyzed in duplicate.

Assay of Bacterial Suspension Exposed to DPPC

A variation of the methods of Schwab et al. (Schwab et al., 2009) was used. Briefly, in a 24-well culture plate 100 μl of 13.5 mg/ml DPPC (Sigma–Aldrich, USA) in PBS was added to each well, and 100 μl of PBS per well was added to the controls. The plate

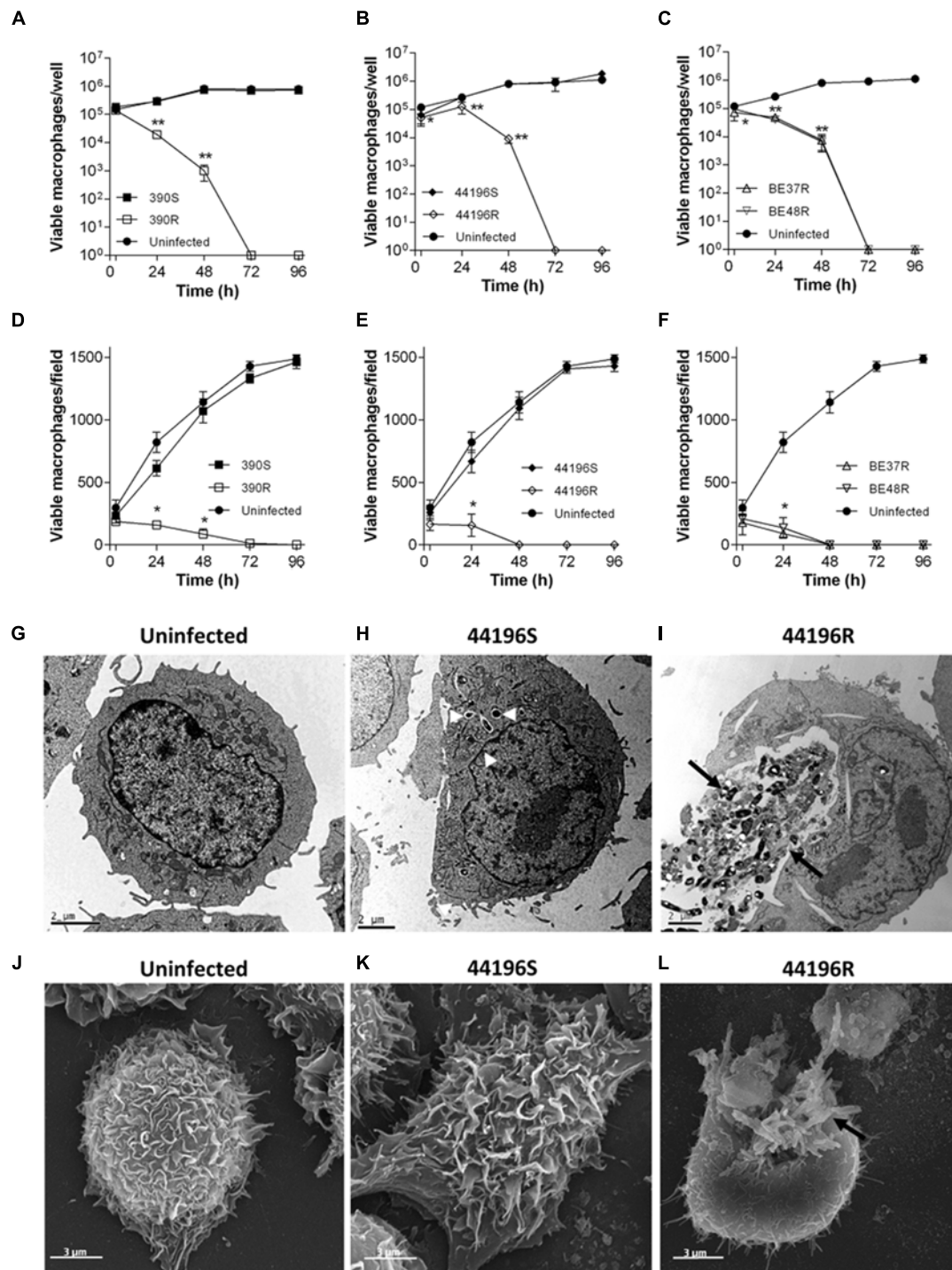


FIGURE 4 | Survival of macrophages, TEM and SEM images of uninfected and infected macrophages. (A–F) Viability of macrophages infected with *M. abscessus* strains, measured using a trypan blue exclusion assay (A–C) and a CLSM assay (D–F) at different time points after infection. The data are presented as the means \pm SD for triplicate wells of infected and uninfected macrophage cultures. The data are representative of one out of three independent experiments. * $P < 0.05$; ** $P < 0.001$, significant difference compared to uninfected macrophages (Student's *t*-test). **(G)** Representative TEM images of uninfected macrophages. **(H)** Macrophages infected with 44196S at 24 h.p.i. **(I)** Macrophages infected with 44196R at 24 h.p.i. Bar size, 2 μ m. **(J)** Representative SEM images of uninfected macrophages. **(K)** Macrophages infected with 44196S at 24 h.p.i. **(L)** Macrophages infected with 44196R at 24 h.p.i. Bar size, 3 μ m. Similar images were obtained for the other the strains. White arrows indicate isolated bacilli, and black arrows indicate bacterial clumps.

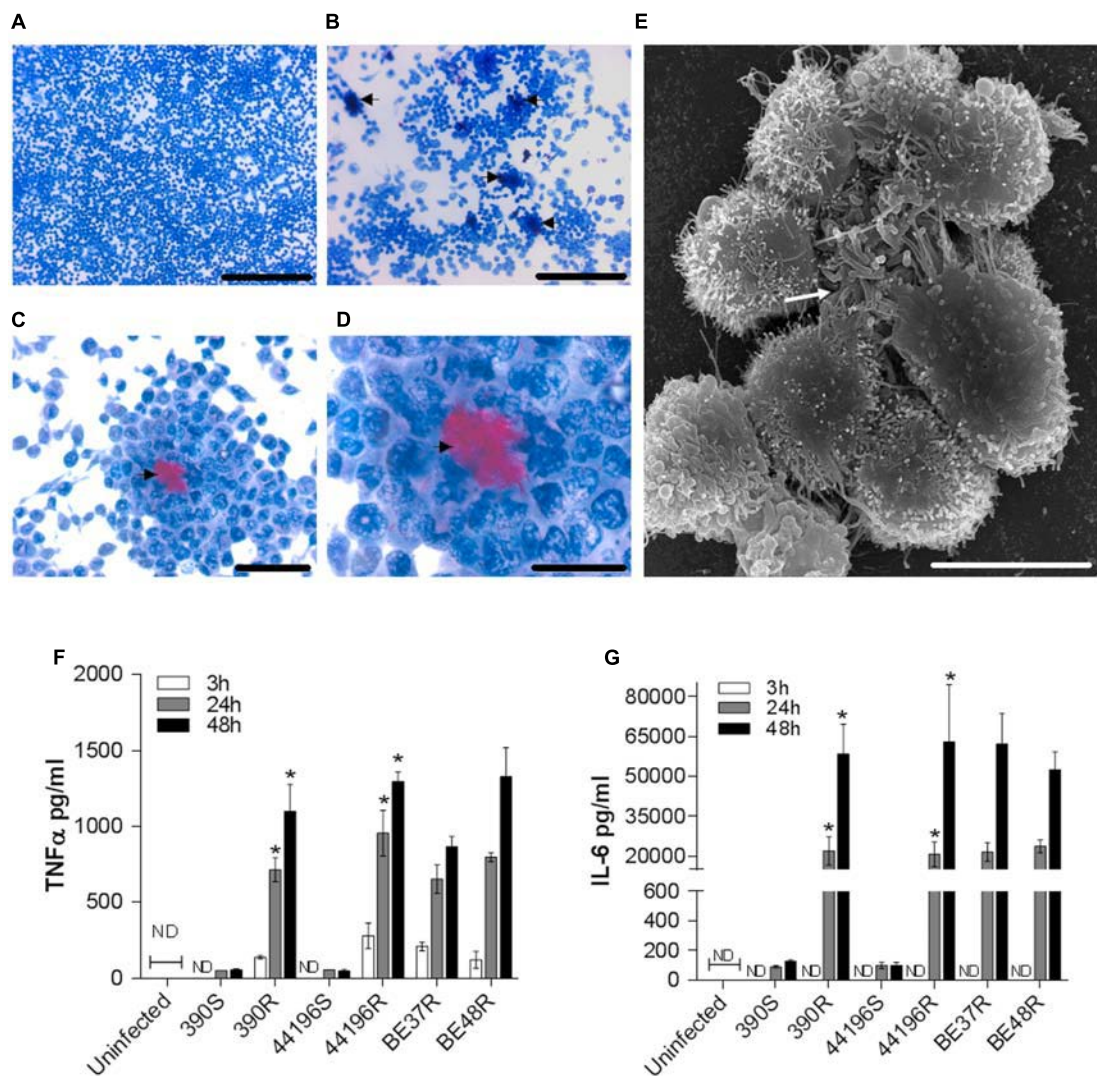


FIGURE 5 | Granuloma-like structures formed by macrophages infected with R morphotypes at 24 h.p.i. and secretion of cytokines by infected murine macrophages. (A–D) Representative light microscopy images of Ziehl-Neelsen-stained macrophages. **(A)** Macrophages infected with 390S. Bar size, 250 μ m. **(B–D)** Macrophages infected with 390R. The black arrow indicates clumps of bacilli stained in red. Bar sizes of 250 μ m in **(B)**, 50 μ m in **(C)** and 25 μ m in **(D)**. **(E)** Representative SEM image of a granuloma-like structure produced around a clump of 390R. Bar size, 10 μ m. White arrow indicates the bacterial clump. Similar images were obtained for the other strains. **(F–G)** The kinetics of TNF α **(F)** and IL-6 **(G)** production were analyzed using ELISA. The results represent the mean \pm SD of triplicate preparations. The data are representative of one out of three independent experiments. * $P < 0.001$, significant difference between cording and its respective non-cording morphotype (Student's t -test). ND, not detected.

was incubated at 37°C for 30 min, and subsequently 200 μ l of a bacterial suspension of *M. abscessus* 390R, prepared as previously described, was added to each well. After incubating the plate for 30 min at 37°C, the content of each well was mixed once with a micropipette and counted using CLSM as previously described.

Statistical Analysis

Comparisons between two parameters were evaluated by Student's t -test. Statistical analyses were performed using PAST3 software.

RESULTS

Only R Colonies Contained Attached Bacilli Forming a Cording Structure

It was easy to differentiate R and S colonies in agar media. The R colonies were characterized by an irregular dry surface with many wrinkles and crests (**Figures 1B,D–F**), whereas the S colonies (S) showed an even, bright and moist texture (**Figures 1A,C**). SEM was used to characterize the organization of the bacilli inside the colonies. SEM of

S colonies revealed masses of cells without orientation, and empty spaces were clearly visible among the single cells (Figures 1A,C). However, the bacilli in the R colonies were closely arranged end-to-end and side-to-side forming a cord (Figures 1B,D–F).

Macrophages Infected with R Morphotypes Phagocytosed Large Clumps of Bacilli

The clumps in bacterial suspensions used to infect macrophages were observed using ZN staining and quantified by CLSM (Figures 2A–F). After disaggregating the clumps of bacilli as described above, the suspensions of S morphotypes (390S and 44196S) contained $89.4\% \pm 0.8$ (mean \pm SD) and $91.7\% \pm 2.3$ isolated bacilli, respectively. Small aggregates of 3–4 bacilli represented $10.6\% \pm 0.9$ of the 390S suspensions and $8.3\% \pm 2.3$ of the 44196S suspensions (Figure 2G). The largest difference in the R morphotypes suspensions was the presence of aggregates of more than five bacilli that were not observed in the suspensions of smooth bacilli (Figure 2G).

The proportion of macrophages infected at 3 h.p.i. was similar for the two morphotypes (between 50 and 60%). Macrophages infected with smooth morphotypes contained mainly isolated bacilli at 3 h.p.i. (Figure 3A). TEM images clearly showed individual bacilli inside the phagocytic vesicles of macrophages infected with S morphotypes (Figure 3B). In contrast, between 24.1 and 36.1% of the bacilli observed at 3 h.p.i. inside macrophages infected with R morphotypes were organized in clumps of more than five bacilli (Figures 3C,E). TEM images revealed large clumps inside the phagocytic vesicles (Figure 3D).

Macrophages were Rapidly Damaged by Rough Morphotypes but were Unaffected by Smooth Morphotypes

Similar results were obtained using the two techniques to measure the macrophages viability. R morphotypes killed 100% of infected macrophages at 48–72 h.p.i.. Both techniques gave us complementary information: while trypan blue assay provides accurate quantification of viable cells being a more sensitive test, CLSM permits rapidly compare the variation of the number of viable cells between the different morphotypes infections. However, the growth of macrophages infected with S morphotypes was unaltered after 96 h.p.i., proliferating in a similar manner to uninfected macrophages (Figures 4A–F and Supplementary Figure 1). Consistent with the viability results, macrophages infected with S morphotypes showed similar appearance to uninfected macrophages by electron microscopy at 24 h.p.i. (Figures 4G,H,J,K). In contrast, damaged macrophages with extruding *M. abscessus* clumps were observed in the cultures infected with R morphotypes at 24 h.p.i. (Figures 4I,L).

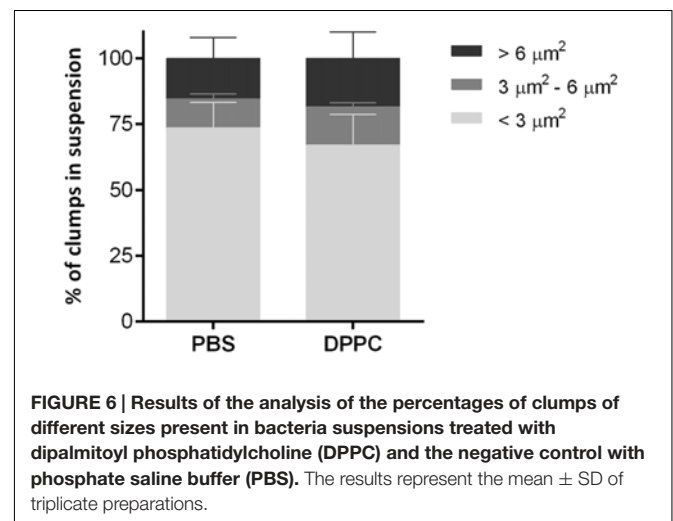
The Death of Macrophages was Preceded by the Formation of Granuloma-Like Structures and the Production of TNF- α and IL-6

Cultures stained with ZN at 24 h.p.i. showed no special organization of macrophages infected with smooth morphotypes (Figure 5A). In contrast, granuloma-like structures formed by a cluster of macrophages surrounding clumps of bacilli were observed in cultures infected with R morphotype (Figures 5B–D). SEM revealed the granuloma-like structures and the associated mycobacteria in greater detail (Figure 5E).

As granuloma formation and maintenance has been associated with the release of TNF- α and IL-6 in *M. tuberculosis*, we assessed the presence of these cytokines in the supernatants of infected macrophages. We observed that macrophages infected with R morphotypes released larger amounts of TNF- α and IL-6 at 24 and 48 h.p.i., whereas only trace amounts of these cytokines were detected in the culture supernatants of macrophages infected with S morphotypes (Figures 5F,G).

The Contact with the Major Component of Pulmonary Surfactant does not Affect the Clump Size

To determine whether DPPC, one of the most abundant lipids of pulmonary surfactant, could disaggregate mycobacterial clumps, a suspension of *M. abscessus* 390R was incubated with DPPC, and the formation of aggregates was comparatively quantified from the 390R suspension in PBS. No significant differences were observed between the two samples. The percentage of isolated bacilli was $67.1\% \pm 11.5$ (mean \pm SD) for the suspension treated with DPPC and $73.6\% \pm 9.6$ for the control with PBS. Clumps with 3–4 bacilli constituted $14.3\% \pm 1.5$ of the DPPC suspension and $11\% \pm 1.8$ of the PBS suspension, and large aggregates constituted $18.5\% \pm 10$ and $15.4\% \pm 7.8$, respectively, of the clumps observed (Figure 6). These results correspond to the mean \pm SD of the three independently performed experiments.



DISCUSSION

The results of the present study provide the first evidence that macrophages can phagocytose *M. abscessus* clumps, demonstrating that macrophages can interact with both clumps and isolated bacilli. No other studies have shown this capacity, as disaggregation techniques are typically used to obtain isolated R bacilli in the suspensions used to infect macrophages, or the information concerning the presence of clumps in these suspensions was omitted (Byrd and Lyons, 1999; Stokes et al., 2004; Howard et al., 2006; Catherinot et al., 2007; Bernut et al., 2014; Leisching et al., 2016). Using CLSM and TEM, we observed the presence of clumps of R morphotypes at an early stage of infection (3 h.p.i.), suggesting that the bacilli result from engulfment but not from replication inside the phagocytic vesicles. Thus, the engulfment of clumps of R morphotypes corresponds with the first R *M. abscessus*-macrophage interaction, as R bacilli form aggregates, and these aggregates have been observed *in vivo* (Clay et al., 2008; Qvist et al., 2013; Bernut et al., 2014; Ufimtseva, 2015). TEM revealed that as the clumps grow inside the phagocytic vesicles, these bacteria kill macrophages, which subsequently liberate large clumps of bacilli into the extracellular space. Previous studies have reported that these clumps grow in the extracellular space, producing large cords that cannot be phagocytosed (Bernut et al., 2014). The TEM images obtained in the present study are consistent with the 100% macrophage mortality observed for macrophages infected with R morphotypes 390R, 44196R, BE37R, and BE48R. In contrast, no effects in macrophages containing isolated S bacilli inside phagocytic vesicles were observed. In addition to the destruction of macrophages, the formation of granulomas and the release of significant amounts of proinflammatory cytokines were only observed in R morphotypes. These results are in agreement with the hypervirulence reported for 390R and 44196R in cellular cultures and animal models, in contrast with the inability of isogenic S variants (390S and 44196S) to produce illness (Byrd and Lyons, 1999; Howard et al., 2006; Catherinot et al., 2007; Bernut et al., 2014). These results are also consistent with the virulence of the respiratory isolates BE37R and BE48R. The factors that confer additional virulence to R morphotypes remain obscure, but it has been postulated that glycopeptidolipids mask immunostimulatory cell wall components, TLR-2 ligands such as phosphatidyl-myo-inositol mannosides, lipomannan and lipoarabinomannan, that enable S variants to colonize the respiratory tract of patients with cystic fibrosis or bronchiectasis (Qvist et al., 2013), prior to the switch to R morphotypes lacking glycopeptidolipids and expressing these TLR-2 ligands on the cell surface (Gillerson et al., 2008; Rhoades et al., 2009). Notably, a more recent study proposed that the lipoproteins on the cell surface of R morphotypes are responsible for TLR-2 activation and discarded the role of phosphatidyl-myo-inositol mannosides, lipomannan and lipoarabinomannan as TLR-2 activators because these factors were not detected on the cell surface of R morphotypes (Roux et al., 2011).

Thus, different groups are working on the surface exposed virulence factors that make more virulent the R morphotypes,

however, most of these virulence factors are unknown yet. But the fact that the macrophage may engulf groups over five bacilli or more in a single phagocytic vesicle means that macrophage has to deal with more of these virulence factors. Our main contribution, to the knowledge of virulence mechanisms, has been to show that the macrophage can engulf such large aggregates of bacteria and therefore should be face to a major amount of virulence factors whatever they are.

Consequently, it is reasonable to assume that the accumulation of these virulence factors could overwhelm the bactericidal capabilities of these cells. The present study is a preliminary study providing a foundation for further investigations of the role of clumps in the pathogenicity of mycobacterial R morphotypes. The compounds that agglutinate mycobacterial bacilli and facilitate clump formation remain unknown because, to date, these factors have been underestimated as a result of the generalized use of homogeneous bacterial suspensions in experimental procedures.

Future studies will involve the examination of these components to identify the clumping factors as important therapeutic targets.

AUTHOR CONTRIBUTIONS

Conceived and designed the experiments: CB, ML-F, EJ, and ML. Performed the experiments: CB, ML-F, EN-O, CT-M, and MP-T. Analyzed the data CB, ML-F, EN-O, EJ, MP-T, and ML. Contributed reagents/materials/analysis tools TB and FA. Contributed to the writing of the manuscript: CB, ML-F, EJ, MP-T, TB, FA, and ML.

FUNDING

This work was financially supported by grants from the Spanish Ministry of Science and Innovation (Instituto de Salud Carlos III-PII2/00025), the European Regional Development Fund (FEDER), and the Generalitat of Catalunya (2014SGR-132).

ACKNOWLEDGMENTS

We thank Dra. Mónica Roldán, Meritxell Vendrell Flotats and Martí de Cabo Jaume (Microscopy Service of Universitat Autònoma de Barcelona) for excellent technical assistance with CLSM and Alejandro Sánchez Chardi for excellent technical assistance with SEM and TEM.

SUPPLEMENTARY MATERIAL

The Supplementary Material for this article can be found online at: <http://journal.frontiersin.org/article/10.3389/fmicb.2016.01562>

REFERENCES

- Agustí, G., Astola, O., Rodríguez-Güell, E., Julián, E., and Luquin, M. (2008). Surface spreading motility shown by a group of phylogenetically related, rapidly growing pigmented mycobacteria suggests that motility is a common property of mycobacterial species but is restricted to smooth colonies. *J. Bacteriol.* 190, 6894–6902. doi: 10.1128/JB.00572-08
- Belisle, J. T., and Brennan, P. J. (1989). Chemical basis of rough and smooth variation in mycobacteria. *J. Bacteriol.* 171, 3465–3470.
- Bernut, A., Herrmann, J.-L., Kissa, K., Dubremetz, J.-F., Gaillard, J.-L., Lutfalla, G., et al. (2014). *Mycobacterium abscessus* cording prevents phagocytosis and promotes abscess formation. *Proc. Natl. Acad. Sci. U.S.A.* 111, E943–E952. doi: 10.1073/pnas.1321390111
- Boritsch, E. C., Frigui, W., Cascioferro, A., Malaga, W., Etienne, G., Laval, F., et al. (2016). pks5-recombination-mediated surface remodeling in *Mycobacterium tuberculosis* emergence. *Nat. Microbiol.* 1:15019. doi: 10.1038/nmicrobiol.2015.19
- Brambilla, C., Sánchez-Chardi, A., Pérez-Trujillo, M., Julián, E., and Luquin, M. (2012). Cyclopropanation of α -mycolic acids is not required for cording in *Mycobacterium brumae* and *Mycobacterium fallax*. *Microbiology* 158, 1615–1621. doi: 10.1099/mic.0.057919-0
- Byrd, T. F., and Lyons, C. R. (1999). Preliminary characterization of a *Mycobacterium abscessus* mutant in human and murine models of infection. *Infect. Immun.* 67, 4700–4707.
- Catherinot, E., Clarissou, J., Etienne, G., Ripoll, F., Emile, J. F., Daffé, M., et al. (2007). Hypervirulence of a rough variant of the *Mycobacterium abscessus* type strain. *Infect. Immun.* 75, 1055–1058. doi: 10.1128/IAI.00835-06
- Catherinot, E., Roux, A. L., Macheras, E., Hubert, D., Matmar, M., Dannhoffer, L., et al. (2009). Acute respiratory failure involving an R variant of *Mycobacterium abscessus*. *J. Clin. Microbiol.* 47, 271–274. doi: 10.1128/JCM.01478-08
- Chimote, G., and Banerjee, R. (2005). Lung surfactant dysfunction in tuberculosis: effect of mycobacterial tubercular lipids on dipalmitoylphosphatidylcholine surface activity. *Colloids Surf. B Biointerfaces* 45, 215–223. doi: 10.1016/j.colsurfb.2005.08.014
- Clay, H., Volkman, H. E., and Ramakrishnan, L. (2008). Tumor necrosis factor signaling mediates resistance to mycobacteria by inhibiting bacterial growth and macrophage death. *Immunity* 29, 283–294. doi: 10.1016/j.immuni.2008.06.011
- Deshayes, C., Kocincová, D., Etienne, G., Reyrat, J.-M., and Daffé, J.-M. (2008). “Glycopeptidolipids: a complex pathway for small pleiotropic molecules,” in *The Mycobacterial Cell Envelope*, eds M. Reyrat, M. Reyrat, and G. Avenir (Washington, DC: ASM Press), 345–365.
- Etienne, G., Villeneuve, C., Billiam-Jacobe, H., Astarie-Dequeker, C., Dupont, M.-A., and Daffé, M. (2002). The impact of the absence of glycopeptidolipids on the ultrastructure, cell surface and cell wall properties, and phagocytosis of *Mycobacterium smegmatis*. *Microbiology* 148, 3089–3100. doi: 10.1099/00221287-148-10-3089
- Falkinham, J. O. (2009). Surrounded by mycobacteria: nontuberculous mycobacteria in the human environment. *J. Appl. Microbiol.* 107, 356–367. doi: 10.1111/j.1365-2672.2009.04161.x
- Falkinham, J. O. (2013). Ecology of nontuberculous mycobacteria—where do human infections come from? *Semin. Respir. Crit. Care Med.* 34, 95–102. doi: 10.1055/s-0033-1333568
- Ferguson, J. S., Martin, J. L., Azad, A. K., McCarthy, T. R., Kang, P. B., Voelker, D. R., et al. (2006). Surfactant protein D increases fusion of *Mycobacterium tuberculosis*-containing phagosomes with lysosomes in human macrophages. *Infect. Immun.* 74, 7005–7009. doi: 10.1128/IAI.01402-06
- Gao, L.-Y., Laval, F., Lawson, E. H., Groger, R. K., Woodruff, A., Morisaki, J. H., et al. (2003). Requirement for kasB in *Mycobacterium mycolic acid* biosynthesis, cell wall impermeability and intracellular survival: implications for therapy. *Mol. Microbiol.* 49, 1547–1563. doi: 10.1046/j.1365-2958.2003.03667.x
- Gillerson, M., Jackson, M., Puzo, G., and Nigou, J. (2008). “6 Structure, biosynthesis, and activities of the phosphatidyl-myo-inositol-based lipoglycans,” in *The Mycobacterial Cell Envelope*, eds M. Daffé, J. M. Reyrat, and G. Avenir (Washington, DC: American Society of Microbiology), 75–105. doi: 10.1128/9781555815783.ch6
- Howard, S. T., Rhoades, E., Recht, J., Pang, X., Alsup, A., Kolter, R., et al. (2006). Spontaneous reversion of *Mycobacterium abscessus* from a smooth to a rough morphotype is associated with reduced expression of glycopeptidolipid and reacquisition of an invasive phenotype. *Microbiology* 152, 1581–1590. doi: 10.1099/mic.0.28625-0
- Indrigo, J., Hunter, R. L., and Actor, J. K. (2003). Cord factor trehalose 6,6'-dimycolate (TDM) mediates trafficking events during mycobacterial infection of murine macrophages. *Microbiology* 149, 2049–2059. doi: 10.1099/mic.0.26226-0
- Julián, E., Roldán, M., Sánchez-Chardi, A., Astola, O., Agustí, G., and Luquin, M. (2010). Microscopic cords, a virulence-related characteristic of *Mycobacterium tuberculosis*, are also present in nonpathogenic mycobacteria. *J. Bacteriol.* 192, 1751–1760. doi: 10.1128/JB.01485-09
- Kansal, R. G., Gomez-Flores, R., and Mehta, R. T. (1998). Change in colony morphology influences the virulence as well as the biochemical properties of the *Mycobacterium avium* complex. *Microb. Pathog.* 25, 203–214. doi: 10.1006/mpat.1998.0227
- Kocincová, D., Winter, N., Euphrasie, D., Daffé, M., Reyrat, J.-M., Etienne, G., et al. (2009). The cell surface-exposed glycopeptidolipids confer a selective advantage to the smooth variants of *Mycobacterium smegmatis* in vitro. *FEMS Microbiol. Lett.* 290, 39–44. doi: 10.1111/j.1574-6968.2008.01396.x
- Lee, J., Repasy, T., Papavinasundaram, K., Sassetti, C., and Kornfeld, H. (2011). *Mycobacterium tuberculosis* induces an atypical cell death mode to escape from infected macrophages. *PLoS ONE* 6:e18367. doi: 10.1371/journal.pone.0018367
- Lee, M., Sheng, W., Hung, C., Yu, C., Lee, L., and Hsueh, P. (2015). *Mycobacterium abscessus* complex infections in humans. *Emerg. Infect. Dis.* 21, 1638–1646. doi: 10.3201/2109.141634
- Leisching, G., Pietersen, R. D., Mpongosh, V., Van Heerden, C., Van Helden, P., Wiid, L., et al. (2016). The host response to a clinical MDR mycobacterial strain cultured in a detergent-free environment: a global transcriptomics approach. *PLoS ONE* 11:e0153079. doi: 10.1371/journal.pone.0153079
- Medjahed, H., and Singh, A. K. (2010). Genetic manipulation of *Mycobacterium abscessus*. *Curr. Protoc. Microbiol.* Chapter 10:Unit 10D.2. doi: 10.1002/9780471729259.mc10d02s18
- Muñoz, M., Raynaud, C., Lanéelle, M., Julián, E., López Marín, L. M., Silve, G., et al. (1998). Specific lipooligosaccharides of *Mycobacterium mucogenicum* sp. nov. (formerly *Mycobacterium chelonae*-like organisms): identification and chemical characterization. *Microbiology* 144, 137–148. doi: 10.1099/00221287-144-1-137
- Pang, L., Tian, X., Pan, W., and Xie, J. (2013). Structure and function of mycobacterium glycopeptidolipids from comparative genomics perspective. *J. Cell. Biochem.* 114, 1705–1713. doi: 10.1002/jcb.24515
- Park, I. K., Hsu, A. P., Tettelin, H., Shallom, S., Drake, S. K., Ding, L., et al. (2015). Clonal diversification, changes in lipid traits and colony morphology in *Mycobacterium abscessus* clinical isolates. *J. Clin. Microbiol.* 53, 3438–3447. doi: 10.1128/JCM.02015-15
- Pawlik, A., Garnier, G., Orgeur, M., Tong, P., Lohan, A., Le Chevalier, F., et al. (2013). Identification and characterization of the genetic changes responsible for the characteristic smooth-to-rough morphotype alterations of clinically persistent *Mycobacterium abscessus*. *Mol. Microbiol.* 90, 612–629. doi: 10.1111/mmi.12387
- Petrini, B. (2006). *Mycobacterium abscessus*: an emerging rapid-growing potential pathogen. *APMIS* 114, 319–328. doi: 10.1111/j.1600-0463.2006.apm_390.x
- Philips, J. A., and Ernst, J. D. (2012). Tuberculosis pathogenesis and immunity. *Annu. Rev. Pathol.* 7, 353–384. doi: 10.1146/annurev-pathol-011811-132458
- Primm, T. P., Lucero, C. A., and Falkinham, J. O. (2004). Health impacts of environmental mycobacteria. *Clin. Microbiol. Rev.* 17, 98–106. doi: 10.1128/CMR.17.1.98-106.2004
- Qvist, T., Eickhardt-Sørensen, S. R., Katzenstein, T. L., Pressler, T., Iversen, M., Andersen, C. B., et al. (2013). WS1.5 First evidence of *Mycobacterium abscessus* biofilm in the lungs of chronically infected CF patients. *J. Cyst. Fibros.* 12, S2. doi: 10.1016/S1569-1993(13)60006-5
- Ramakrishnan, L., and Falkow, S. (1994). *Mycobacterium marinum* persists in cultured mammalian cells in a temperature-restricted fashion. *Infect. Immun.* 62, 3222–3229.
- Rhoades, E. R., Archambault, A. S., Greendyke, R., Hsu, F.-F., Streeter, C., and Byrd, T. F. (2009). *Mycobacterium abscessus* glycopeptidolipids mask underlying cell wall phosphatidyl-myo-inositol mannoses blocking induction of human macrophage TNF- α by preventing interaction with TLR2. *J. Immunol.* 183, 1997–2007. doi: 10.4049/jimmunol.0802181

- Roux, A.-L., Ray, A., Pawlik, A., Medjahed, H., Etienne, G., Rottman, M., et al. (2011). Overexpression of proinflammatory TLR-2-signalling lipoproteins in hypervirulent mycobacterial variants. *Cell. Microbiol.* 13, 692–704. doi: 10.1111/j.1462-5822.2010.01565.x
- Rüger, K., Hampel, A., Billig, S., Rücker, N., Suerbaum, S., and Bange, F. C. (2014). Characterization of rough and smooth morphotypes of *Mycobacterium abscessus* isolates from clinical specimens. *J. Clin. Microbiol.* 52, 244–250. doi: 10.1128/JCM.01249-13
- Sánchez-Chardi, A., Olivares, F., Byrd, T. F., Julián, E., Brambilla, C., and Luquin, M. (2011). Demonstration of cord formation by rough *Mycobacterium abscessus* variants: implications for the clinical microbiology laboratory. *J. Clin. Microbiol.* 49, 2293–2295. doi: 10.1128/JCM.02322-10
- Sanguinetti, M., Ardito, F., Fiscarelli, E., La Sorda, M., D'Argenio, P., Ricciotti, G., et al. (2001). Fatal pulmonary infection due to multidrug-resistant *Mycobacterium abscessus* in a patient with cystic fibrosis. *J. Clin. Microbiol.* 39, 816–819. doi: 10.1128/JCM.39.2.816-819.2001
- Schlesinger, L. S., Bellinger-kawahara, C. G., Horwitz, M. A., and Payne, R. (1990). Phagocytosis of *Mycobacterium tuberculosis* is mediated by human monocyte complement receptors and complement component C3. *J. Immunol.* 144, 2771–2780.
- Schwab, U., Rohde, K. H., Wang, Z., Chess, P. R., Notter, R. H., and Russell, D. G. (2009). Transcriptional responses of *Mycobacterium tuberculosis* to lung surfactant. *Microb. Pathog.* 46, 185–193. doi: 10.1016/j.micpath.2008.12.006
- Stokes, R. W., Norris-Jones, R., Brooks, D. E., Beveridge, T. J., Doxsee, D., and Thorson, L. M. (2004). The glycan-rich outer layer of the cell wall of *Mycobacterium tuberculosis* acts as an antiphagocytic capsule limiting the association of the bacterium with macrophages. *Infect. Immun.* 72, 5676–5686. doi: 10.1128/IAI.72.10.5676-5686.2004
- Tan, T., Lee, W. L., Alexander, D. C., Grinstein, S., and Liu, J. (2006). The ESAT-6/CFP-10 secretion system of *Mycobacterium marinum* modulates phagosome maturation. *Cell. Microbiol.* 8, 1417–1429. doi: 10.1111/j.1462-5822.2006.00721.x
- Ufimtseva, E. (2015). *Mycobacterium*-host cell relationships in granulomatous lesions in a mouse model of latent tuberculous infection. *Biomed. Res. Int.* 2015, 948131. doi: 10.1155/2015/948131
- van der Werf, M. J., Ködmön, C., Katalinić-Janković, V., Kummik, T., Soini, H., Richter, E., et al. (2014). Inventory study of non-tuberculous mycobacteria in the European Union. *BMC Infect. Dis.* 14:62. doi: 10.1186/1471-2334-14-62
- Villeneuve, C., Etienne, G., Abadie, V., Montrozier, H., Bordier, C., Laval, F., et al. (2003). Surface-exposed glycopeptidolipids of *Mycobacterium smegmatis* specifically inhibit the phagocytosis of mycobacteria by human macrophages: identification of a novel family of glycopeptidolipids. *J. Biol. Chem.* 278, 51291–51300. doi: 10.1074/jbc.M306554200
- Welsh, K. J., Abbott, A. N., Hwang, S. A., Indrigo, J., Armitage, L. Y., Blackburn, M. R., et al. (2008). A role for tumour necrosis factor- α , complement C5 and interleukin-6 in the initiation and development of the mycobacterial cord factor trehalose 6,6'-dimycolate induced granulomatous response. *Microbiology* 154, 1813–1824. doi: 10.1099/mic.0.2008/016923-0

Conflict of Interest Statement: The authors declare that the research was conducted in the absence of any commercial or financial relationships that could be construed as a potential conflict of interest.

Copyright © 2016 Brambilla, Llorens-Fons, Julián, Noguera-Ortega, Tomás-Martínez, Pérez-Trujillo, Byrd, Alcaide and Luquin. This is an open-access article distributed under the terms of the Creative Commons Attribution License (CC BY). The use, distribution or reproduction in other forums is permitted, provided the original author(s) or licensor are credited and that the original publication in this journal is cited, in accordance with accepted academic practice. No use, distribution or reproduction is permitted which does not comply with these terms.

Supplementary Material

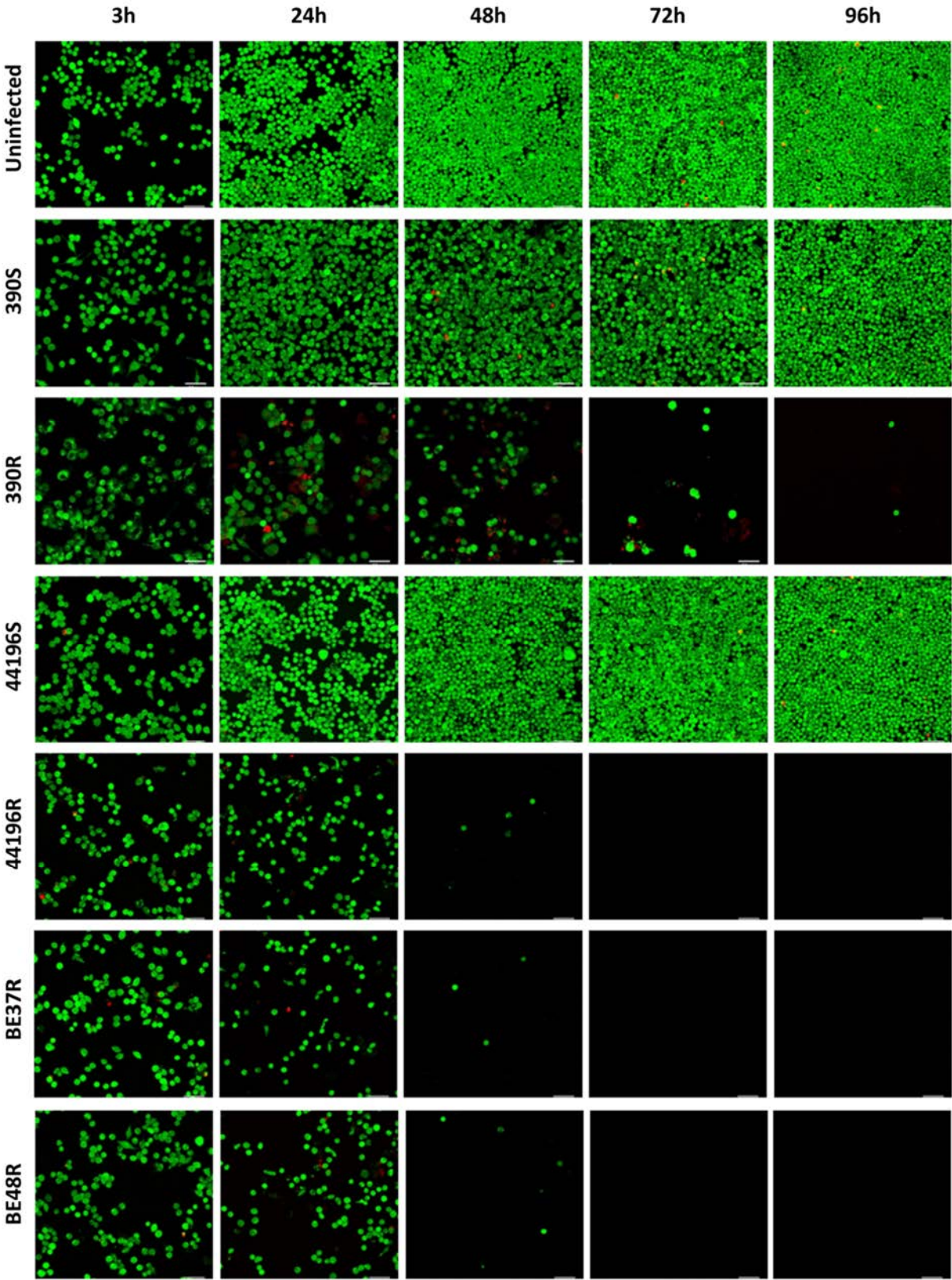
Mycobacteria clumping increase their capacity to damage macrophages

Cecilia Brambilla, Marta Llorens-Fons, Esther Julián, Estela Noguera-Ortega, Cristina Tomàs-Martínez, Miriam Pérez-Trujillo, Thomas F. Byrd, Fernando Alcaide, and Marina Luquin*

*** Correspondence:** Marina Luquin (mail to: marina.luquin@uab.cat)

1 Supplementary Figures and Tables

1.1 Supplementary Figures



Supplementary Fig. 1: Representative images of macrophages infected with R and S morphotypes of *M. abscessus*, and uninfected macrophages, at different time points after infection. Macrophages were labelled with green fluorescent Calcein acetoxymethyl (viable cells) and red fluorescent Ethidium homodimer-1(unviable cells). Bar size 50 μm .



Trehalose Polyphleates, External Cell Wall Lipids in *Mycobacterium abscessus*, Are Associated with the Formation of Clumps with Cording Morphology, Which Have Been Associated with Virulence

Marta Llorens-Fons¹, Míriam Pérez-Trujillo², Esther Julián¹, Cecilia Brambilla¹, Fernando Alcaide³, Thomas F. Byrd⁴ and Marina Luquin^{1*}

¹ Departament de Genètica i de Microbiologia, Facultat de Biociències, Universitat Autònoma de Barcelona, Barcelona, Spain, ² Servei de Resonància Magnètica Nuclear and Departament de Química, Universitat Autònoma de Barcelona, Barcelona, Spain, ³ Servei de Microbiologia, Hospital Universitari de Bellvitge-IDIBELL, Universitat de Barcelona, Barcelona, Spain, ⁴ The University of New Mexico School of Medicine, Albuquerque, NM, United States

OPEN ACCESS

Edited by:

Mattias Collin,
Lund University, Sweden

Reviewed by:

Anna Upton,
TB Alliance, United States
Chad W. Euler,
Hunter College (CUNY), United States

*Correspondence:

Marina Luquin
marina.luquin@uab.cat

Specialty section:

This article was submitted to
Infectious Diseases,
a section of the journal
Frontiers in Microbiology

Received: 25 May 2017

Accepted: 11 July 2017

Published: 25 July 2017

Citation:

Llorens-Fons M, Pérez-Trujillo M, Julián E, Brambilla C, Alcaide F, Byrd TF and Luquin M (2017) Trehalose Polyphleates, External Cell Wall Lipids in *Mycobacterium abscessus*, Are Associated with the Formation of Clumps with Cording Morphology, Which Have Been Associated with Virulence. *Front. Microbiol.* 8:1402. doi: 10.3389/fmicb.2017.01402

Mycobacterium abscessus is a reemerging pathogen that causes pulmonary diseases similar to tuberculosis, which is caused by *Mycobacterium tuberculosis*. When grown in agar medium, *M. abscessus* strains generate rough (R) or smooth colonies (S). R morphotypes are more virulent than S morphotypes. In searching for the virulence factors responsible for this difference, R morphotypes have been found to form large aggregates (clumps) that, after being phagocytosed, result in macrophage death. Furthermore, the aggregates released to the extracellular space by damaged macrophages grow, forming unphagocytosable structures that resemble cords. In contrast, bacilli of the S morphotype, which do not form aggregates, do not damage macrophages after phagocytosis and do not form cords. Cording has also been related to the virulence of *M. tuberculosis*. In this species, the presence of mycolic acids and surface-exposed cell wall lipids has been correlated with the formation of cords. The objective of this work was to study the roles of the surface-exposed cell wall lipids and mycolic acids in the formation of cords in *M. abscessus*. A comparative study of the pattern and structure of mycolic acids was performed on R (cording) and S (non-cording) morphotypes derived from the same parent strains, and no differences were observed between morphotypes. Furthermore, cords formed by R morphotypes were disrupted with petroleum ether (PE), and the extracted lipids were analyzed by thin layer chromatography, nuclear magnetic resonance spectroscopy and mass spectrometry. Substantial amounts of trehalose polyphleates (TPP) were recovered as major lipids from PE extracts, and images obtained by transmission electron microscopy suggested that these lipids are localized to the external surfaces of cords and R bacilli. The structure of *M. abscessus* TPP was revealed to be similar to those previously described in

Mycobacterium smegmatis. Although the exact role of TPP is unknown, our results demonstrated that TPP are not toxic by themselves and have a function in the formation of clumps and cords in *M. abscessus*, thus playing an important role in the pathogenesis of this species.

Keywords: *Mycobacterium abscessus*, trehalose polyphleates, CORDS, clumps, rough morphotypes, smooth morphotypes, virulence factors

INTRODUCTION

Nontuberculous mycobacteria are species of the *Mycobacterium* genus other than the *Mycobacterium tuberculosis* complex and *Mycobacterium leprae*. The overall prevalence of lung disease related to NTM is increasing worldwide and is caused by *Mycobacterium avium* complex, *Mycobacterium kansasii*, and increasingly, *Mycobacterium abscessus*, which is the species most commonly implicated in human pulmonary disease (McShane and Glassroth, 2015; Brown-Elliott and Philley, 2016; Koh et al., 2017). Similarly to *M. tuberculosis*, the agent of human tuberculosis, *M. abscessus* induces the production of granulomas and persists inside granulomas, developing caseous lesions in pulmonary tissue (Medjahed et al., 2010). *M. abscessus* pulmonary infections are of special importance in patients with underlying respiratory diseases such as bronchiectasis and cystic fibrosis (McShane and Glassroth, 2015; Brown-Elliott and Philley, 2016; Koh et al., 2017). In some of these patients, the therapeutic treatment is ineffective, and they experience chronic infections for long periods of time, frequently with a fatal outcome.

Mycobacterium abscessus strains isolated from humans form smooth (S) or rough (R) colonies when grown on agar medium. S colonies exhibit a bright and moist texture related to the presence of cell surface-exposed glycopeptidolipids (GPL), whereas R colonies are characterized by an irregular dry surface with many wrinkles and crests and are devoid of GPL (Howard et al., 2006; Nessar et al., 2011; Howard, 2013). Various studies have reported that R morphotypes produce the most severe illness in humans (Sanguinetti et al., 2001; Catherinot et al., 2007, 2009; Jönsson et al., 2007). In a recent and very interesting study, 50 serial isolates from nine patients with persistent *M. abscessus* infections have been analyzed on the basis of colony morphology (Park et al., 2015). The authors have found that R isolates predominate at later times during the course of the disease (median follow-up was 8 years). In six out of the nine patients, the colony morphology of the serial isolates was initially S before becoming predominantly R. Serial isolates from the other three patients

showed R colony morphology throughout the course of the disease.

The increasing clinical importance of *M. abscessus* has piqued the interest of several groups of researchers who have developed different animal models with which to study the pathogenesis of this species (for a recent review, see Bernut et al., 2017). In these studies, R morphotypes have been found to be hyperlethal for mice and zebra fish embryos, whereas S morphotypes are unable to produce infection (Byrd and Lyons, 1999; Howard et al., 2006; Bernut et al., 2014; Roux et al., 2016). The observations from human and animals indicate that the ability to switch between S and R morphotypes allows *M. abscessus* to transition between a colonizing phenotype and a more virulent, invasive form.

It is therefore of great importance to determine what factors allow the morphotype R to be much more virulent than the S morphotype.

Both morphotypes are able to grow inside macrophages but exhibit distinct behaviors. As it is possible to see in the study performed by Brambilla et al. (2016), phagosomes of macrophages infected with R morphotype contain more than one bacillus at 3 h post-infection (h.p.i), and of those, up to 30% of phagosomes contain clumps of more than five bacilli. In contrast, phagosomes of macrophages infected with the S morphotype contain mainly isolated bacilli (Byrd and Lyons, 1999; Brambilla et al., 2016; Roux et al., 2016). This distinct fate has been related to the highly aggregative nature of R morphotype bacilli, which grow close together, leave no spaces among them and form large aggregates (clumps) (Sánchez-Chardi et al., 2011; Brambilla et al., 2016). At 48–72 h.p.i, macrophages infected with the R morphotype are destroyed, thus releasing large clumps of bacilli outside the cells; however, macrophages infected with the S morphotype are unaffected. Using zebra fish embryos it is possible to visualize as extracellular clumps, which grow extensively forming cords (cording), that were unphagocytatable for macrophages and neutrophils promoting rapid larval death (Bernut et al., 2016). In this model, the S morphotype is unable to produce infection. In addition, an R mutant defective in cording exhibits impaired replication in zebra fish (Halloum et al., 2016). These results relate clumps of cording morphology to virulence in *M. abscessus*, and, interestingly, cording has also been related to virulence in *M. tuberculosis*, a species with a very stable R morphotype (Middlebrook et al., 1947).

Cords are snake-like structures that are formed through end-to-end and side-to-side aggregation of bacilli, in which the orientation of the long axis of each cell is parallel to the long axis of the cord (Julián et al., 2010). Microscopic cords were described for the first time by Robert Koch in *M. tuberculosis*

Abbreviations: BSA, bovine serum albumin; CLSM, confocal laser scanning microscope; CM, complete medium; DMEM, Dulbecco's Modified Eagle's Medium; DMSO, dimethyl sulfoxide; FA, formaldehyde; GA, glutaraldehyde; MS, mass spectrometry; MTT, 3-(4,5-dimethylthiazol-2-yl)-2,5-diphenyltetrazolium bromide; NMR, nuclear magnetic resonance; NTM, nontuberculous mycobacteria; OsO₄, osmium tetroxide; PBS, phosphate-buffered saline; PE, petroleum ether; RPMI, Roswell Park Memorial Institute medium; SEM, scanning electron microscope; TAG, triacylglycerides; TDM, trehalose dimycolate; TEM, transmission electron microscope; TLC, thin layer chromatography; TPP, trehalose polyphleates.

(Koch, 1882). Various studies performed with natural and constructed mutants of *M. tuberculosis* have confirmed the correlation between cording and virulence in this species (for a review, see Glickman, 2008). Some of *M. tuberculosis* constructed mutants defective in cording exhibit altered structures of their mycolic acids (Glickman et al., 2000). Other *M. tuberculosis* non-cording mutants are defective in the production of some extractable glycolipids, but preserve mycolic acid structures and profiles (Glickman, 2008). In *M. abscessus*, cording was described for the first time in the 390R strain as well as the lack of cording of the related 390 S morphotype (Howard et al., 2006). An R mutant of *M. abscessus* defective in cording shows an altered ratio of α -mycolic acid to α' -mycolic acid but no differences in their structures (Halloum et al., 2016). Thus, to date there is not a unique candidate for cording. The cell wall of mycobacteria is very rich in complex lipids that interact with one another and with polysaccharides and proteins, thereby forming a definite and stable wall architecture (Daffé et al., 2014; Jankute et al., 2015), so it is logical to assume that the elimination or modification of one of these lipids may disrupt the original configuration by eliminating the organization in cords even if these lipids are not directly responsible for cording.

Another approach to shed new light on the cell wall components responsible for cording, following the pioneering studies performed by Bloch, is to disrupt cords with organic solvents and analyze the lipids present in the organic extracts (Bloch, 1950).

The objective of this work was to identify the compounds responsible for cording in *M. abscessus* by breaking the cords with PE and identifying the lipids present in the PE extracts. Furthermore, because mycolic acids are a candidate responsible for cording, we studied the composition and structure of mycolic acids of R (cording) and S (non-cording) morphotypes that were derived from the same parent strain. The localization of candidate lipids on the surfaces of cords and bacilli was accomplished by TEM.

MATERIALS AND METHODS

Mycobacterial Strains and Growth Conditions

The bacterial strains used in this study were *M. abscessus* 390, *M. abscessus* type strain DSMZ 44196^T, and a clinical isolate of *M. abscessus* BE48. S and R morphotypes of *M. abscessus* 390 and DSMZ 44196^T were obtained in previous studies (Byrd and Lyons, 1999; Brambilla et al., 2016). For the clinical isolate *M. abscessus* BE48, the strain was initially R, but we obtained the S morphotype after several passages on agar medium. All strains were grown in Middlebrook 7H9 broth (Difco, United States) for pellicle formation and in Middlebrook 7H9 agar (Difco, United States) for colony morphology observation and mycolic acid extraction. One liter bottles with 100 ml of Middlebrook 7H9 broth were inoculated with 1 ml of bacterial suspension, adjusted to No. 1 of the McFarland standards of turbidity. Pellicles of *M. abscessus* grew

at the air-medium interface of Middlebrook 7H9 broth at 37°C.

Mycolic Acid Extraction and Purification

For extraction and methylation of mycolic acids, bacteria scraped from Middlebrook 7H9 agar plates were subjected to an acid methanolysis procedure (Minnikin et al., 1980). Briefly, 50 mg of scraped bacteria were treated with 2 ml of methanol, toluene and sulfuric acid (30:15:1; v:v:v) and heated at 80°C overnight, and the samples were then extracted twice with *n*-hexane. The *n*-hexane extracts that contained the methyl mycolates were evaporated to dryness at 40°C under nitrogen stream. The mycolates were concentrated by precipitation in cold methanol (4°C, overnight) and analyzed by conventional TLC on silica gel-coated plates (G-60, Merck, Germany). The 10 μ l of each sample was loaded to the TLC and plates were developed with *n*-hexane/diethyl ether (85:15; v:v, three runs). The mycolates were observed as dark spots after the plates were sprayed with phosphomolybdic acid (VWR, United States; 10% in ethanol) and charred at 120°C. Purification of mycolates was performed by using preparative TLC plates with a concentration zone (G-60, Merck, Germany) that were developed as described above. Mycolates were visualized with iodine vapors, scraped from TLC plates and recovered with diethyl ether. The purification steps were monitored by TLC as described above.

Analysis of Mycolic Acids by Nuclear Magnetic Resonance Spectroscopy

Purified dried mycolates were dissolved in 600 μ l of CDCl₃ (99.80% D, Cortecnet, France) and transferred to 5-mm-diameter NMR tubes. NMR experiments were recorded on a Bruker Avance II 600 (Bruker Biospin, United States) equipped with a 5 mm TBI probe with Z-gradients that operated at a ¹H NMR frequency of 600.13 MHz and at 298.0 K. 1D ¹H NMR spectra were acquired using a standard 90° pulse sequence with an acquisition time of 1.71 s and a relaxation delay of 3 s. Data sets were collected as 32k data points with a spectral width of 9590 Hz and as the sum of 128 transients. The resulting free induction decays were Fourier transformed, manually phased, and baseline corrected. All spectra were calibrated using the residual solvent signal (CHCl₃) at a chemical shift (δ) of 7.27 ppm. The relative molar ratios of characteristic molecular moieties were determined by the integration of representative resonances.

Scanning Electron Microscopy

The spreading pellicles that formed on the surface of the liquid medium were collected with a 0.2 μ m nuclepore membrane (Whatman, United Kingdom) and processed for analysis by scanning electron microscopy (SEM) as previously described (Brambilla et al., 2016). Briefly, pellicles were fixed in 2.5% (vol/vol) glutaraldehyde in 0.1 M phosphate buffer (pH 7.4) for 2 h at 4°C and then washed four times for 10 min each in 0.1 M phosphate buffer. Then, the samples were post-fixed in 1% (wt/vol) OsO₄ and 0.7% ferrocyanide in phosphate buffer and

washed with water. This process was followed by dehydrating the samples in an ascending ethanol series (50, 70, 80, 90, and 95% for 10 min each and twice with 100% ethanol) and subsequently critical-point drying the samples with CO₂. Finally, the samples were coated with gold and observed using an SEM EVO (Zeiss, Germany) at 15 kV.

Observation of Cords and Clumps after Application of PE to *M. abscessus* Pellicles

After 2 weeks of growing in Middlebrook 7H9 broth, *M. abscessus* formed a consistent pellicle at the air-medium interface. A superficial lipid extract of these pellicles was performed by using a modification of Bloch's protocol (Bloch, 1950). Briefly, pellicles of *M. abscessus* were filtered. Then, avoiding the complete drying of the pellicles, we placed 1.5 g of each sample in a beaker with 40 ml of PE (40–60°C b.p.) and agitated them for 5 min. After that, the PE extracts were filtered and evaporated. Then, one part of the cellular residue formed by the treated bacteria was recovered in a tube with glass beads, which was shaken for 10 min. Then, 2 ml of PBS was added, the tube was shaken for 10 s, and three drops of the suspension were placed in a slide and left to dry. As a control, bacteria were treated with the same protocol but without the PE extraction step. All the samples were stained using Ziehl-Neelsen stain. Another part of the cellular residue was plated in agar plates to test the viability of the treated bacteria by CFUs count and to observe the colonial morphology. After growing, these treated bacteria were inoculated in Middlebrook 7H9 broth and the biopellicles formed were extracted with PE as described above.

Analysis of the Lipidic Components of the PE Extract

A series of TLCs were performed to study the lipidic profile of the PE extracts, using 10 µl of all samples for each TLC. For unidimensional TLCs, the mobile phases that were used were PE 60–80°C/diethyl ether (90:10, v/v), chloroform/methanol (85:15, v/v), and chloroform/methanol/water (60:35:8, v/v/v; and 90:10:1, v/v/v). For bidimensional TLCs, the mobile phase used were first direction PE 60–80°C/ethyl acetate (98:2, v/v, thrice), second direction PE 60–80°C/acetone (98:2, v/v, once); first direction PE 60–80°C/acetone (98:2, v/v, thrice), second direction toluene/acetone (95:5, v/v, once); first direction chloroform/methanol (96:4, v/v, once), second direction toluene/acetone (80:20, v/v, once); and first direction chloroform/methanol/water (100:14:0.8, v/v/v, once), second direction chloroform/acetone/methanol/water (50:60:2.5:3, v/v/v/v, once). Compounds in the TLC plates were revealed by using anthrone (Merck, Germany; 1% in sulfuric acid) or phosphomolybdic acid (VWR, United States; 10% in ethanol) and then heating the plate at 120°C or by using molybdenum blue (Sigma, United States) without heat.

Purification and Structural Characterization of Compounds X, Y, Z and Triacylglycerides by NMR and Mass Spectrometry

Compounds X, Y, Z and TAGs were purified by column chromatography. Approximately 50 mg of PE extract obtained as described above was added to a Silica Gel 60 (Merck, Germany) column. A series of solvent mixtures of PE 60–80°C with increasing concentrations of diethyl ether was used for the elution of the PE-extracted components.

Purified compounds were dissolved in 600 µL of CDCl₃ (99.80% D, Cortecnet, France) and analyzed by NMR spectroscopy. The equipment described operating at ¹H and ¹³C NMR frequencies of 600.13 and 150.90 MHz, respectively, and at 298.0 K, was used. 1D ¹H spectra of the three compounds were acquired and processed using the same parameters previously described. 2D ¹H,¹H-COSY; ¹H,¹³C-HSQC; ¹H,¹³C-HMBC; and ¹H-DOSY experiments were performed using standard Bruker pulse sequences and acquired under routine conditions. Chemical shifts were referenced to the residual solvent signals (δ_H, 7.26 and δ_C, 77.0 ppm). Proton signal multiplicity is indicated in the text by d (doublet), t (triplet), dd (double doublet) and m (multiplet). In the case of compounds Y and Z, standard 1D ³¹P spectra were also recorded.

For MS, purified compounds X, Y, and Z were dissolved in 50 µl of chloroform/methanol (2:1, v/v). This suspension was mixed with a matrix made of 10 mg/ml 1,8,9-anthracenetriol (dithranol) at a 1:1 ratio, and 1 µl of the mix was deposited on a ground steel plate. The sample was analyzed using a negative polarity reflectron and an acceleration voltage of 25 kV in a MALDI-TOF UltrafleXtreme (Bruker Daltonics, United States). The calibration was performed using external calibrators (Bruker Daltonics, United States).

Study of the *M. abscessus* Cell Wall by TEM

Mycobacterium abscessus pellicles were collected in sterilized filters, passed to a tube and processed for TEM observation. Two processes were used to observe the samples: the conventional preparation, as described by Bleck et al. (2010); and the OTO method, as described by Seligman et al. (1966). Briefly, samples for the conventional preparation were fixed in 4% FA and 5% GA in 0.1 M HEPES (4-(2-hydroxyethyl)piperazine-1-ethanesulfonic acid) buffer (pH 7.4). Post-fixation was performed with 2% OsO₄ in PBS for 1 h at room temperature. Then, the samples were dehydrated in an ascending ethanol series and post-stained with saturated uranyl acetate at the 90% ethanol step for 30 min at 37°C. Bacteria were finally embedded in epoxy resin, and ultrathin sections were made (Bleck et al., 2010). For the OTO method, ultrathin sections that were previously fixed with OsO₄ but were not post-stained with uranyl acetate were exposed to a 1% hot aqueous solution of TCH (thiocarbohydrazide) for 1 h at 50°C, and this was followed by four to eight washes with hot water. Then, the sections were again exposed to OsO₄ (Seligman

et al., 1966; Hall et al., 2012). This method results in further deposition of osmium on the samples and increases lipid contrast (Belazi et al., 2009). All samples were observed using a JEOL 1400 (Japan) TEM equipped with a Gatan ES1000W Erlangshen CCD (United States) camera.

Coating of Beads and the Study of Bead Organization after Coating

Amine-modified yellow-green latex beads (Sigma, United States) with an average diameter of 1 μm were used and coated with TPP A by using variations of the protocols described by Kang and Schlesinger (1998) and Vergne et al. (2004). Briefly, 5 μl of bead suspension at an initial concentration of 4.6×10^{10} beads/ml were transferred to a tube and these beads washed twice with 0.05 M carbonate-bicarbonate buffer (pH 9.6) and coated with purified TPP obtained from the R morphotype of the *M. abscessus* 390 strain and maintained in DMSO (Merck, Germany). Beads were incubated in 8% DMSO in PBS with 0.8 mg/ml of TPP for 2 h at 37°C with agitation. Control uncoated beads were treated with 8% DMSO in PBS without TPP. After the 2 h incubation, the beads were washed twice with PBS and blocked with 5% BSA (Roche, Germany) in PBS for 1 h at 37°C with agitation to prevent non-specific binding. After that, beads were washed once with 0.5% BSA in PBS.

The successful coating with TPP was demonstrated by staining the beads with Nile Red (Sigma-Aldrich, United States). Briefly, 1 μl of 0.5 mg/ml Nile Red in ethanol was added to 50 μl of beads, which were incubated for 10 min at 37°C. Then, the beads were washed three times with PBS (Christensen et al., 1999), and 10 μl of the bead suspension was spread on a slide by using a coverslip. Nile Red-stained TPP-coated beads were observed with a CLSM using a TCS-SP5 CLSM (Leica, Germany) with a PlanApo 63 (numerical aperture [NA] 1.4) oil objective.

To determine the organization of TPP-coated and uncoated beads, images of the bead suspension were obtained using a CLSM and analyzed with ImageJ software (National Institutes of Health, United States). The analysis described three types of aggregates, depending on their area: fewer than 3 μm^2 , between 3 and 6 μm^2 , and more than 6 μm^2 (Brambilla et al., 2016). The area covered by each type of aggregate was added, and the statistical analysis was performed to determine the percentages of area that were covered by each type of aggregate. All experiments were conducted three times.

Study of Macrophage Viability When in Contact with Beads

J774 murine macrophage cell line was used for the experiments and maintained at 37°C in a humidified atmosphere of 5% CO₂ in Dulbecco's modified Eagle's medium with L-glutamine and high glucose (DMEM) (Gibco, Austria). This media was supplemented with 10% heat-inactivated fetal bovine serum (FBS) (HyClone, United Kingdom), 100 U/ml penicillin G (LERN, Spain), and 100 $\mu\text{g}/\text{ml}$ streptomycin (Reig Jofre, Spain), which was considered to be CM.

J774 macrophages cells were seeded into 96-well tissue culture plates (Thermo Fisher Scientific, Denmark) at a density of 1.5×10^4 cells per well in CM and incubated for 24 h. Then, TPP-coated and uncoated beads were added on the macrophage cultures at an optimized ratio of 30 beads per macrophage (Brambilla, 2015). The medium was removed 3 h later, and the cultures were washed three times with PBS and then incubated with CM. At different time points (24, 48, and 72 h), culture supernatants were recovered, and the MTT assay was performed with the cells as described previously (Noguera-Ortega et al., 2016). Viability was calculated using the control wells that contained untreated cells as a reference representing 100% growth.

As a positive control for virulence, J774 macrophages were infected with *M. abscessus* 390R strain as previously described (Brambilla et al., 2016). To prove if PE-treatment had any effect in the virulence of the bacteria, J774 macrophages were also infected with *M. abscessus* 390R PE-treated.

Analysis of the Cytokine Production by Macrophages Treated with Beads

Supernatants of macrophages treated with beads were recovered at different time points, in the manner explained above, and centrifuged to eliminate macrophages that had detached from the well; the concentrations of TNF- α (R&D Systems, United States) and IL-6 (BD Biosciences, United States) were determined, following the manufacturer instructions.

Study of the Phagolysosome Fusion in J774 Macrophages

J774 macrophages were seeded onto CLSM culture dishes (Mat Tech, United States) at a concentration of 2.5×10^5 cells per dish. Those macrophages were cultured in DMEM with LysoTracker Red DND-99 (Life Technologies, United States) at a concentration of 1:10000. The 24 h after the seeding, cells were placed in contact with beads in order to compare the phagolysosome fusion between macrophages with uncoated beads versus macrophages with TPP-coated beads. After 24 h, dishes were observed using a TCS-SP5 CLSM (Leica, Germany) with a PlanApo 63 (NA, 1.4) oil objective, operating at a zoom of 2.5. One hundred macrophages were counted for each sample, and colocalization between LysoTracker and the green fluorescence produced by the beads was calculated using Pearson's correlation coefficient.

Statistical Analysis

Analysis of the percentage of aggregates and comparison of the macrophage viability with TPP-coated and uncoated beads were made using multiple *t*-tests. Statistical significance was determined using the Holm-Sidak method, an extension of the Holm-Bonferroni method, in Prism 6 (Version 6.01, GraphPad Software, United States). Differences were considered to be significant at $p < 0.05$.

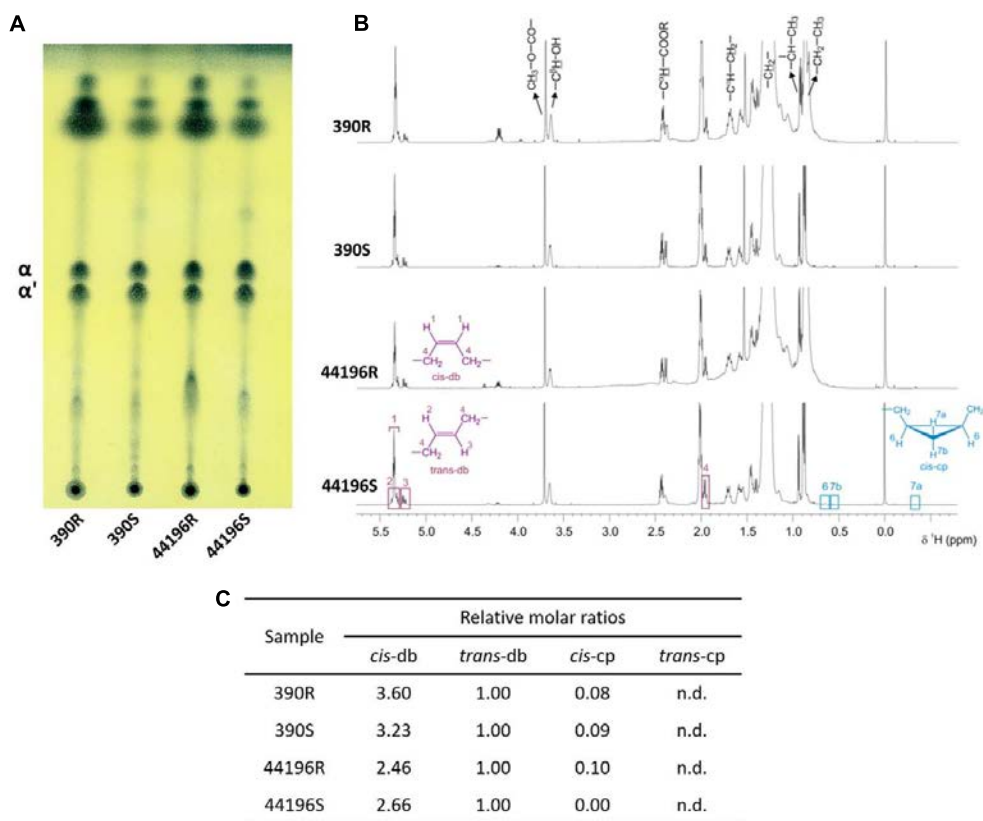


FIGURE 1 | Structure of mycolic acids. **(A)** TLC analysis of mycolates from *M. abscessus* strains. TLC was developed with *n*-hexane-diethyl ether at 85:15 (three runs). α (α -mycolates) α' (α' -mycolates). **(B)** ^1H NMR spectra of purified mycolates from *M. abscessus* strains. Spectra acquired at a temperature of 298.0 K and in a magnetic field of 600.13 MHz. **(C)** Relative molar ratios of molecular moieties *cis*-db, *trans*-db, *cis*-cp, and *trans*-cp of mycolates from *M. abscessus*; db (double bonds), cp (cyclopropane ring), n.d. (not detected).

RESULTS

Both Morphotypes Had the Same Proportion of Mycolic Acids with no Differences in Structure

When the mycolic acid profiles of S and R morphotypes of *M. abscessus* 390 and 44196 were determined by TLC, no differences were detected in the ratios of α -mycolic and α' -mycolic acids. In both strains, the two morphotypes produced similar amounts and ratios of the mycolic acids (Figure 1A). As shown in Figure 1B, the NMR analysis indicated that both strains had a very similar spectrum for purified mycolic acid methyl esters. In a comparison of the relative molar ratios, samples from the R and S morphotypes showed the same average of *cis* and *trans* double bonds, and cyclopropane rings were detected only in trace amounts (Figure 1C).

R Morphotypes Produced Rough Pellicles in Which Bacilli Organized into Cords

All R morphotypes (390R, 44196R, and BE48R), when grown on liquid media, produced thick and wrinkled pellicles with

structures that resembled macroscopic cords. When observed with SEM, pellicles from the R morphotype showed an organization of their bacilli that was typical of that in cord-forming mycobacteria (Figure 2A). In contrast, all S morphotypes (390S, 44196S, and BE48S) produced a thin pellicle with a flat surface. No organization of the bacilli in clumps or cords was observed when the ultrastructure of these pellicles was observed by SEM (Figure 2A).

Cord Disorganization Was Observed after Treatment of Pellicles of R Morphotypes with PE

Pellicles of R morphotypes that were untreated or treated with PE were observed by using optical microscopy after they were stained with the Ziehl-Neelsen method. Bacteria in the untreated samples were aggregated, forming clumps and cords, and only a few bacteria were solitary (Figure 2B). However, disintegration of clumps and cords was observed in samples treated with PE. In these samples, higher amounts of free bacteria in all the fields monitored from each preparation were clearly observed. Although in some points there were still some aggregates, the disorganization of the clumps and cords was evident (Figure 2B).

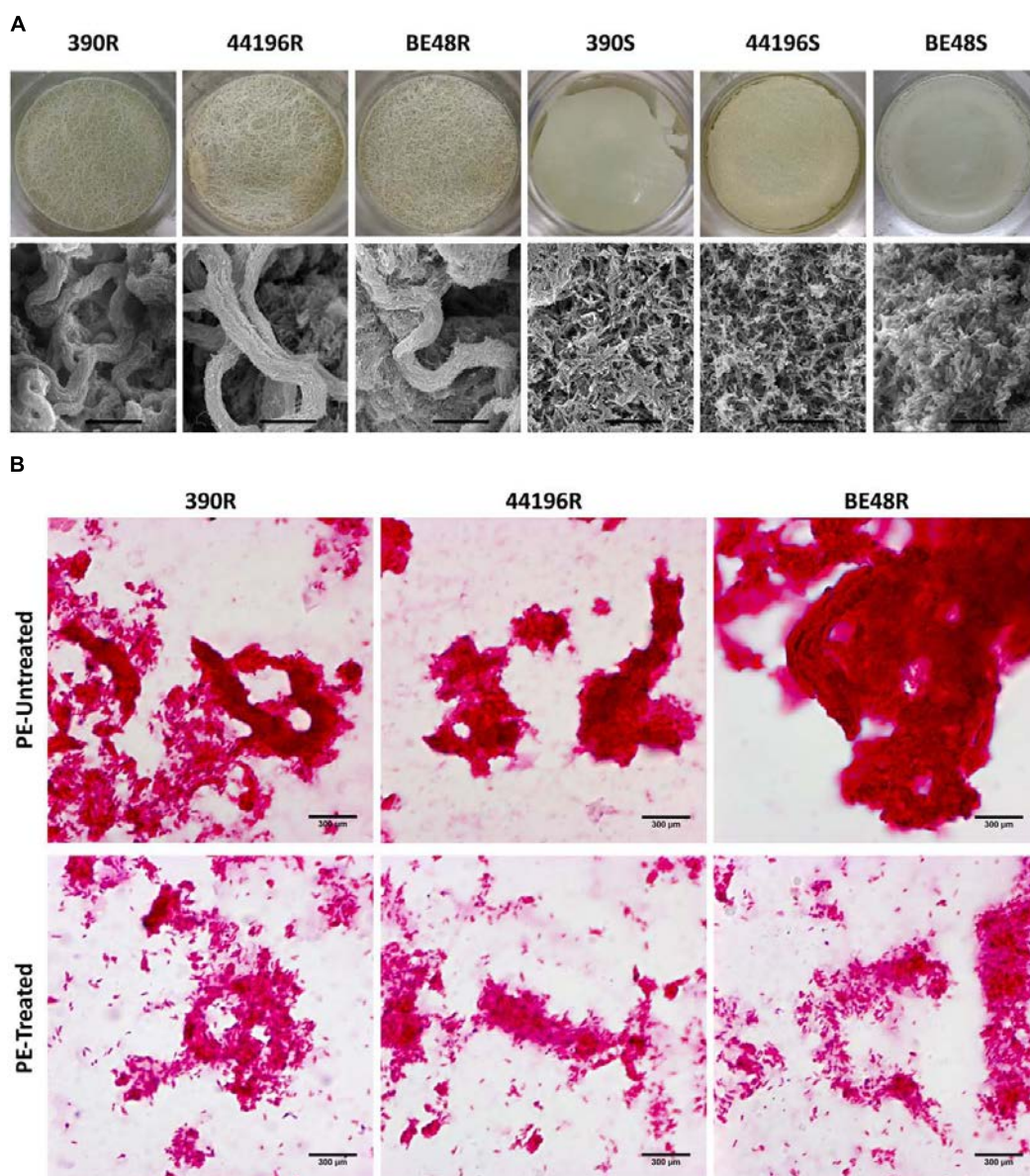


FIGURE 2 | Pellicles and microscopic cords of untreated bacteria, and cord disorganization in PE-treated bacteria. **(A)** Images of the pellicles formed by all morphotypes of *M. abscessus* in 1 L bottles with 100 ml of medium, and their ultrastructure, as determined by SEM. Bar size 15 μm . **(B)** Observation by optical microscopy of untreated and treated with PE for 5 min samples, both stained using the Ziehl-Neelsen method. Bar size 300 μm .

Regarding viability, no effect of the PE treatment was observed in the CFU count. The viability of the bacteria was not affected for the extraction, and the same occurred with the colonial morphology.

TPP Were Detected in the PE Extract from the R Morphotypes

Organic material was detected only when PE extracts from R morphotypes were developed in unidimensional TLC eluted with PE 60–80°C/diethyl ether (90:10, v/v) and bidimensional TLC eluted with PE 60–80°C/ethyl acetate (98:2, v/v, thrice,

first direction) and PE 60–80°C/acetone (98:2, v/v, once, second direction). When PE extracts were monitored with other TLC developing systems, no organic material was observed. In samples from R morphotypes, two relevant compounds (X and Y) were observed when unidimensional TLC plates were revealed with phosphomolybdic acid (Figure 3A). After PE extracts were fractionated on a silica gel column, a third compound that was retained at the point of sample application in TLC was purified (compound Z) (Supplementary Figure S1). Only trace amounts of compound X were detected in samples from 390S and BE48S strains (Figure 3A), and none of the compounds were detected in the 44196S extract. Trace amounts of TAG were detected in

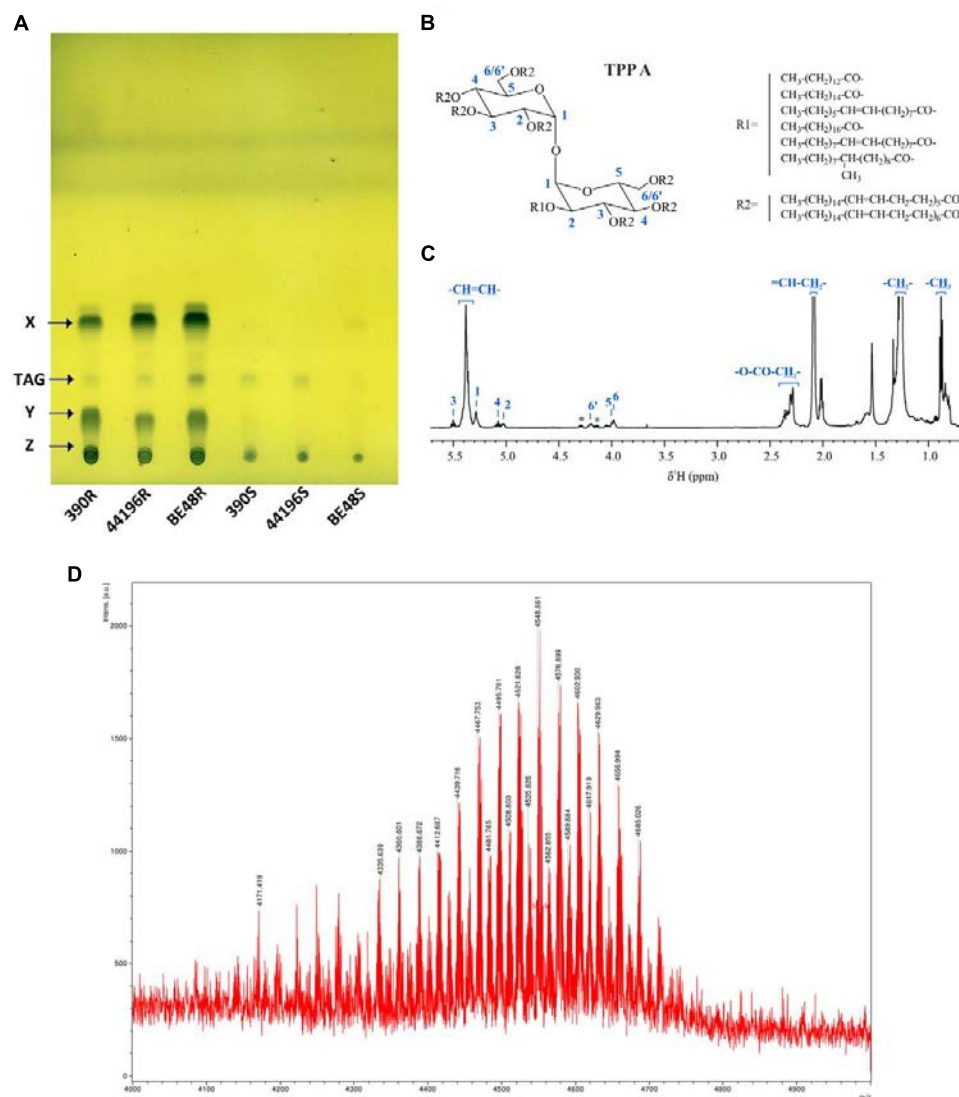


FIGURE 3 | Detection and characterization of compound X. **(A)** TLC of all PE extracts. The solvent system used was PE 60–80°C/diethyl ether (90:10, v/v), and the plates were revealed with 10% phosphomolybdic acid. X (Compound X), TAG (Triacylglycerides), Y (Compound Y), Z (Compound Z). **(B)** Chemical structure of Compound X purified from *M. abscessus* 390R. Length and structure of R1 and R2 were obtained from Burbaud et al. (2016). **(C)** ^1H NMR spectra of compound X in CDCl_3 with peaks corresponding to the TPP A assignment (asterisks denote signals of TAG impurities). **(D)** MALDI-TOF mass spectrum of compound X (region between m/z 4000 and 5000 is magnified).

all the morphotypes. TAG of the 390R strain were purified and identified by NMR (Supplementary Figure S2). No other lipidic compounds were detected in these PE extracts. When extraction with PE was extended from 5 to 15 min, compound X spots showed more intensity in S morphotype samples, thus suggesting that S morphotypes can synthesize this compound but that it is not exposed on the surface (Supplementary Figure S3). No differences in the lipidic profile were observed in the PE extracts from bacteria cultured after being extracted.

Purified compound X was identified by NMR spectroscopy and MS as TPP type A (Figure 3B). The identification was made on the basis of comparison with previous data (Burbaud et al., 2016). Figure 3C shows the ^1H NMR spectrum

of TPP A. The characteristic ^1H and ^{13}C resonances of TPP A glucosyl units were clearly observed. A doublet at 5.28 ppm corresponding to anomeric proton H1, the characteristic triplet at 5.50 ppm corresponding to H3 and peaks at 5.07 (t), 5.03 (dd), 4.20 (m), 3.98 (m) and 3.97 (m) ppm corresponding to H4, H2, H6, H6', and H5, respectively, were identified. ^1H , ^1H -COSY correlations, as well as carbon resonances of glucosyl units, obtained from ^1H , ^{13}C -HSQC and ^1H , ^{13}C -HMBC spectra, were in accordance with the TPP A structure and with previously described values. The intense signals corresponding to the polyunsaturated fatty acyl substituents are indicated in the figure. The MALDI-TOF MS analysis further confirmed the identity of the molecule (Figure 3D) (Burbaud et al., 2016). Residual TAG

was detected by both NMR and MS (indicated with asterisks in the ^1H spectrum on **Figure 3D**) (More detail in Supplementary Figure S4).

Compounds Y and Z were isolated and analyzed separately by NMR spectroscopy and MS. The concerted analysis of the NMR spectra allowed for their ^1H and ^{13}C NMR characterization (Supplementary Figures S5, S6). Both compounds were identified as TPP molecules. The ^1H spectra and 2D correlations showed the same signals as TPP A plus some new peaks. In both cases, the presence of a characteristic multiunsaturated system (broad peak at δ_{H} 5.4 ppm correlated via HSQC to a peak at δ_{C} 127–130 ppm), as well as methylene (δ_{H} 1.2–1.3 ppm) and methyl groups (δ_{H} 0.9 ppm) characteristic of alkyl chains were observed. The same ^1H and ^{13}C NMR signals corresponding to the TPP A trehalose unit were exhibited in spectra of Y and Z, thus suggesting that they have a common glucosyl residue. In the case of compound Y, H3 (3.54 ppm) and H4 (3.82 ppm) of the second glucosyl residue were strongly shielded compared with those of TPP A (5.50 and 5.07 ppm, respectively), which suggests that position 3 and/or 4 are not acylated. Similarly, H4 (3.82 ppm), H6 (3.58 ppm) and H6' (3.53 ppm) of the second glucosyl residue of Z were strongly shielded compared with analogous protons of TPP A (5.07, 4.20, and 3.98 ppm, respectively), which suggests that position 4 and/or 6 are not acylated. These results were supported by MS analyses (Supplementary Figure S7). Compounds Y and Z yielded analogous MALDI-TOF MS spectra, which indicates that they are structural isomers. Their mass also suggested the lack of one R2 substituent compared with TPP A (an envelope of peaks between m/z 4093 and 3849 for Y and Z, in contrast with m/z 4596 and 4297 for TPP A).

R Morphotypes Had an Electrodense Material in the Outer Layer of the Cell Wall

When bacilli of the R and S morphotypes of *M. abscessus* were visualized by TEM, some electrodense layers and some electrotransparent layers were detected on their cell wall. It was of special interest that electrodense material irregularly accumulated in the outer layer of the bacilli from the R morphotype (**Figure 4A**), whereas this material did not accumulate in the S morphotype cell wall (**Figure 4A**). When a minor magnification of the TEM images was analyzed, the cord organization in the R morphotype and the accumulation of this electrodense material outside the cord were observed (**Figure 4B**).

The OTO stain provides a major contrast of the lipidic components because it augments the OsO_4 deposit on these lipids. An important accumulation of OsO_4 was observed outside the bacilli in R morphotypes from the samples treated with this stain, and no accumulation was observed in S morphotypes (**Figure 4C**).

TPP-Coated Beads Formed Aggregates

The coating of beads by TPP A was confirmed by CLSM, because Nile Red stained the lipids coating the beads (**Figures 5A,B**), and these beads appeared to be surrounded by red fluorescence.

When observed by CLSM, the TPP A-coated beads presented more aggregation than uncoated beads. Statistical analysis showed significant differences between the areas of the aggregates of the two samples, thus indicating that TPP A-coated beads produced larger aggregates than uncoated beads (**Figure 5C**). The percentage of aggregates that were larger than $6 \mu\text{m}^2$ was $20.4\% \pm 5.7$ (mean \pm SD) for the uncoated beads and $38.9\% \pm 6.2$ ($p < 0.05$) for the TPP A-coated beads. The difference in area between aggregates of uncoated beads that were smaller than $3 \mu\text{m}^2$ ($57.0\% \pm 2.3$ of the area covered) and aggregates of TPP A-coated beads of the same size ($38.8\% \pm 7.5$ of the area covered) was also significant (**Figure 5C**). These results are obtained from beads coated with TPP A. However, beads were coated also with a mix of the three compounds described by NMR (TPP A, Y, and Z), all TPP molecules, and no differences were observed between the results obtained with the beads coated with TPP A and those obtained with the beads coated with the mix of TPP molecules (TPP A, Y, and Z compounds) (data not shown).

TPP-Coated Beads Had no Effect on the Viability of Macrophages

As observed with CLSM, macrophages did not distinguish between uncoated and TPP A-coated beads in phagocytosis (**Figure 5D**). Both types of beads were found inside the cells and in a similar ratio. J774 macrophages with phagocytized uncoated beads represented a percentage of $32.39\% \pm 5.08$ from the total of counted macrophages, and macrophages with phagocytized TPP A-coated beads represented the $37.69\% \pm 9.73$. Moreover, macrophage viability was not altered after the interaction with TPP A-coated beads. No significant differences were observed in the viability of macrophages in contact with uncoated beads or TPP A-coated beads (**Figure 5E**). When cytokine production was analyzed, no production of $\text{TNF-}\alpha$ and IL-6 was detected in macrophages treated either with uncoated or TPP A-coated beads (data not shown). Also related with the possible effect of TPP A on the viability of macrophages, no differences were observed when analyzing the colocalization of the beads inside the macrophages with acidic vesicles. Pearson's correlation coefficient was of 0.40 ± 0.16 for uncoated beads and of 0.54 ± 0.15 for TPP A-coated beads (the results represent the mean \pm SD of triplicate preparations) (**Figure 5F**). Similar results were obtained when macrophages were in contact with beads coated with the mix of TPP molecules (TPP A, Y, and Z compounds), that is no effect on the viability of the macrophages was observed (**Figure 5E**) and no production of $\text{TNF-}\alpha$ and IL-6 was detected (data not shown). Bacteria from R morphotype had the expected action in front of macrophages, as it has been already published (Brambilla et al., 2016). 390R strain killed all macrophages within 72 h. No difference between these results and the results obtained from bacteria PE-treated were observed (**Figure 5E**).

DISCUSSION

Cords are the first virulence factor described in *M. tuberculosis*. They were first observed by Robert Koch in 1882, and their significance increased in 1947 when studies by Middlebrook

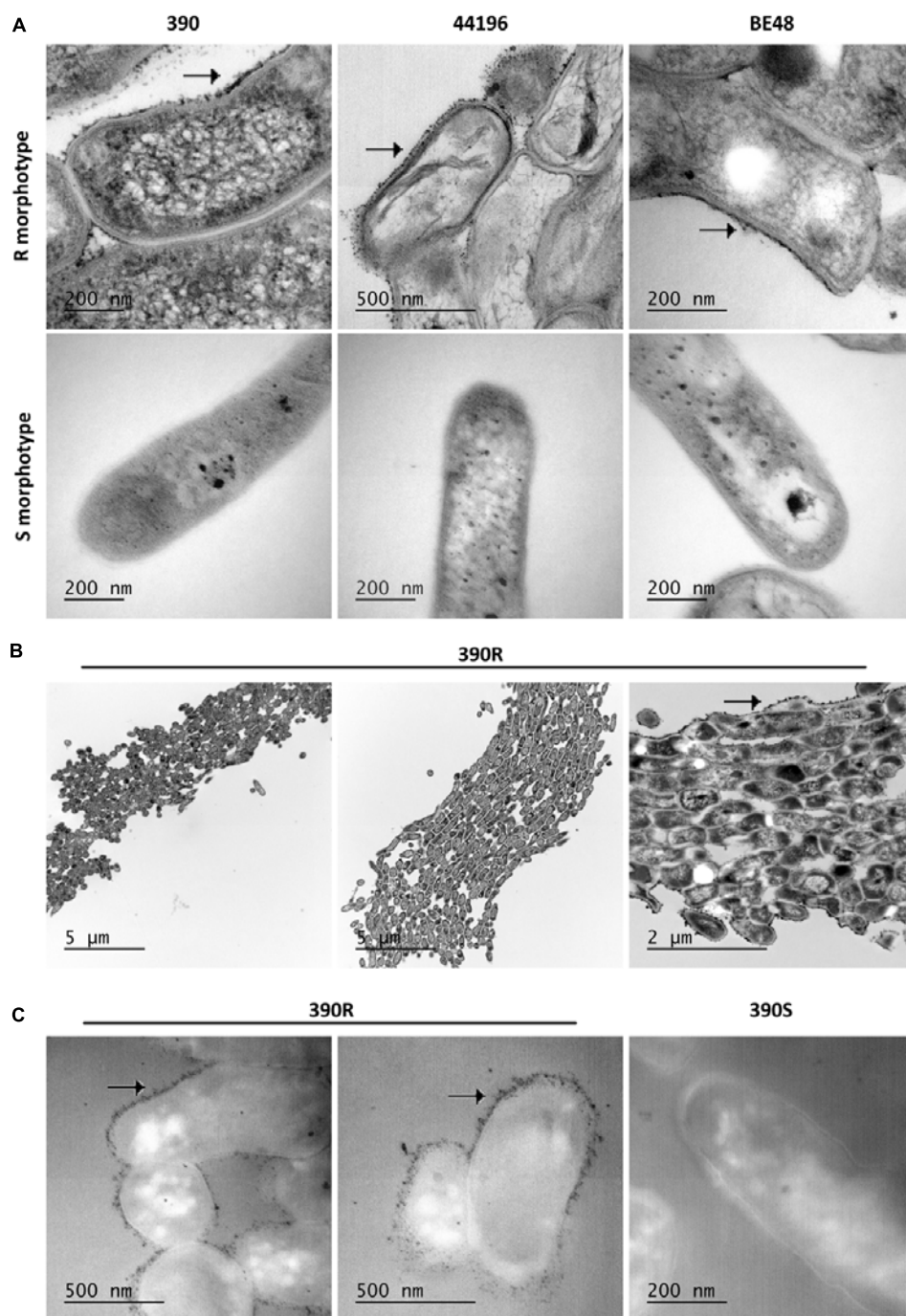


FIGURE 4 | An electron-dense material is observed on the cell wall of R morphotypes. **(A)** Images obtained by TEM of *M. abscessus* bacilli. Arrows indicate the accumulation of electron-dense material on the wall of the R morphotype. **(B)** Example of cord formation in *M. abscessus* 390R. Arrows indicate the accumulation of electron-dense material outside the cord. **(C)** Images of OTO staining, showing an important deposit of OsO₄ in the R morphotype and no deposits in the S morphotype. Images from *M. abscessus* 390R. Similar images were obtained from the other strains.

linked this phenotypic characteristic to the virulence of *M. tuberculosis* complex microorganisms (Middlebrook et al., 1947). In 1950, Hubert Bloch disrupted the cords in few minutes by using paraffin oil, PE, pure hexane and heptane but not with aqueous solutions. From these results, Bloch hypothesized that

the substance responsible for the formation of cords might be a lipid and could be isolated from the extracts that were obtained with the abovementioned organic solvents (Bloch, 1950). Because cording was related to virulence, Bloch's next objective was to identify a toxic substance in these extracts. Thus, from PE

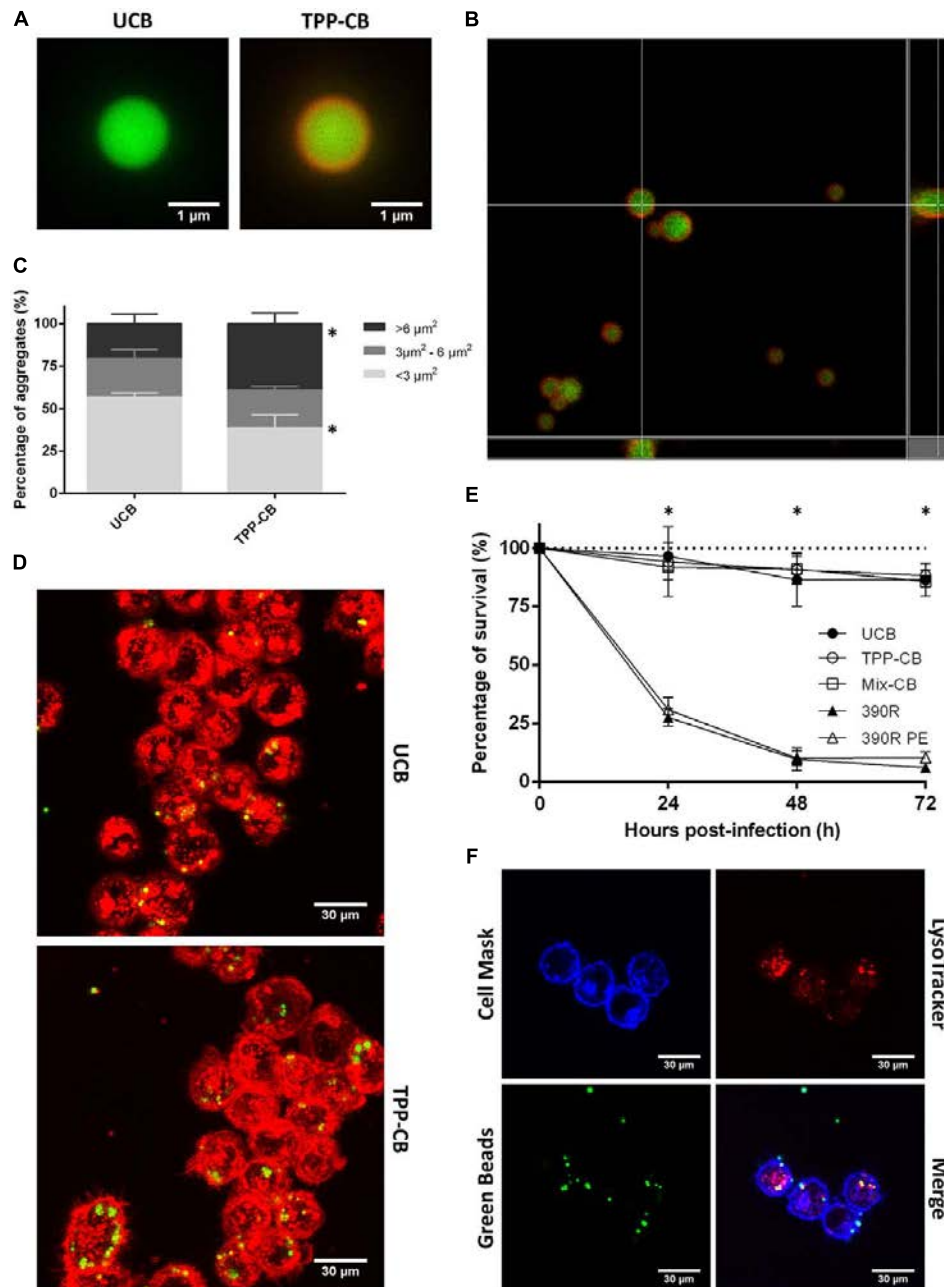


FIGURE 5 | Beads are covered by TPP, and they do not have a toxic effect when in contact with macrophages. **(A,B)** Beads are in green and TPP-coating is observed as the red covering, owing to staining with Nile Red. Bar size in **(A)** 1 μm . **(C)** Results of the study of bead aggregation. * $p < 0.05$ in multiple t -test. The results represent the mean \pm SD of triplicate preparations. **(D)** Example of the images obtained by CLSM that were used to study the aggregation of the beads; macrophages phagocytose both types of beads. Bar size 30 μm . **(E)** Viability of macrophages treated with uncoated beads; TPP A-coated beads; beads coated with TPP A, compound Y and Z; 390R *M. abscessus* strain and 390R *M. abscessus* PE treated. Significant differences were detected only between macrophages treated with beads and macrophages infected with bacteria (* $p < 0.05$). The data are representative of one out of three independent experiments. **(F)** Images of colocalization of beads and acidic vesicles. Macrophages in blue stained with Cell Mask Deep Red, beads in green and acidic vesicles in red with LysoTracker Red. Bar size 30 μm . UCB (Uncoated beads), TPP-CB (TPP A-coated beads), Mix-CB (beads coated with TPP A, compound Y and Z), 390R (*M. abscessus* 390R strain), 390R PE (*M. abscessus* 390R treated with PE).

extracts, he purified a toxic compound that he named “cord factor” (Bloch et al., 1953). This toxic compound was found in very small proportions, representing approximately 1% of the

total PE extract (Bloch et al., 1953). In collaboration with Noll, Bloch identified the toxic compound as trehalose-6,6'-dimycolate (TDM) (Noll et al., 1956). Hence, TDM was associated with

the term “cord factor,” an error that has persisted and causes many mycobacteriologists to associate the formation of cords with the TDM compound. As Bloch himself explained, TDM was termed “cord factor” because it was obtained from “cord-forming” strains of mycobacteria and not because it was the compound responsible for the formation of such cords (Bloch et al., 1953). Agreeing with Bloch’s result that TDM represents only the 1% of the surface-extracted lipids, other authors have reported that TDM is not on the surface of *M. tuberculosis* or on the surface of *M. abscessus* (Ortalo-Magné et al., 1996; Burbaud et al., 2016). In accordance with these previous studies, we did not find TDM in PE extracts.

Genetic validation of the link between cording and virulence in *M. tuberculosis* and *M. abscessus* has been obtained through natural and constructed mutants, most of which exhibit alterations in the synthesis or structure of the lipids of the cell wall; thus, they are consistent with the Bloch studies attributing the formation of cords to a lipid substance (Glickman, 2008). Studies performed with genetically defined mutants of *M. tuberculosis* have suggested that cording may be related to the structure of mycolic acids (Glickman et al., 2000). That investigation has attributed the need for a proximal cyclopropane in α -mycolic acids for cording in *M. tuberculosis*. Thus, we found it interesting to investigate the presence of cyclopropane rings in α - and α' -mycolic acids of the non-cording (390S, 44196S) and cording morphotypes (390R, 44196R). Both acids from all sources possessed approximately the same amounts of *cis*-double bonds, and cyclopropane rings were nearly absent. Recently, a cord-deficient *M. abscessus* mutant has been generated, and no differences have been found in the cyclopropanation of mycolic acids between the mutant and the parent strains (Halloum et al., 2016). These results indicate that in *M. abscessus*, the formation of cords is not related to the presence of cyclopropane rings in α and α' -mycolic acids. However, the abovementioned cord-deficient *M. abscessus* mutant exhibits an alteration in its ratio of mycolic acids. The authors have reported that the α -mycolic acid is the major mycolic acid in the parental cording R strain, whereas in the non-cording mutant, the major mycolic acid is the α' -mycolic acid (Halloum et al., 2016). Our results showed no differences in the ratio of mycolic acids in cording and non-cording morphotypes, thus indicating that both morphotypes have a similar amount of α - and α' -mycolic acids. The difference between the results obtained by Halloum et al. (2016) and our results is that they used a mutant deficient in a gene related to mycolic acid biosynthesis, and we used natural morphotypes, that do not seem to have the biosynthesis of mycolic acids affected as measured by TLC and NMR analysis in our assays. Thus, we did not find a correlation between mycolic acids and cording, in accordance with later models of the mycobacterial cell wall that have proposed that these lipids are deeply embedded in the cell wall (Daffé et al., 2014; Jankute et al., 2015). Mycolic acids are major components of the cell envelope of mycobacteria and play a crucial role in its architecture, so we hypothesized that mutants with alterations in mycolic acids might have a modification in their cell wall that causes a change in the cording morphotype, even though mycolic acids do not have a direct role in cord formation.

In the present work, only one major compound, identified as TPP A, was extracted from the surface of R morphotypes but not from the surface of S morphotypes of *M. abscessus* strains. TPP were first characterized in *Mycobacterium phlei* as a trehalose that was acylated with long polyunsaturated fatty acids (called phleic acids because they were also first described in *M. phlei*) (Asselineau et al., 1969, 1972; Asselineau and Montrozier, 1976). Recently, TPP have been detected in *M. smegmatis*, *M. abscessus*, *M. avium*, and other NTM, and those from *M. smegmatis* have been structurally characterized (Burbaud et al., 2016). In this work, we structurally characterized TPP A from the *M. abscessus* 390R strain. We found a major TPP A that was similar to TPP A in *M. smegmatis* and two other minor TPP species (Burbaud et al., 2016).

OsO₄, a commonly used stain for lipids in electron microscopy, makes the lipids appear as an electron-dense zone (Daffé et al., 1989; Bleck et al., 2010). In the images obtained by TEM, a very electron-dense material was observed in the outermost layer of the R bacilli and cords. The OTO method particularly enhances the contrast of the lipid components of the cell that were stained by OsO₄, and with this method, we corroborated the presence of lipids in the external surface of R but not S bacilli (Seligman et al., 1966; Daffé et al., 1989). The obvious candidates for such reactions are TPP, because they were the major lipids extracted from the mycobacterial surface with PE. Consequently, TEM images reinforced the hypothesis that TPP are exposed on the surface of R morphotypes of *M. abscessus* but not on the surface of S morphotypes. Considering this difference, we used beads that were similar in size to bacteria and coated them with TPP A and found that the TPP A-coated beads aggregated more than uncoated beads. When the beads had this compound on their surface, as occurred in R morphotypes of *M. abscessus*, they tended to produce more clumps. TPP are one of the largest known lipids in mycobacteria (Seeliger and Moody, 2016), and their role in the mycobacterial envelope is unknown, but biochemical analyses and microscopy results obtained in this work suggest that TPP may be necessary for the formation of clumps and cords. The very hydrophobic nature of clumps and cords is in accord with the surface exposure of these giant lipids.

We found that TPP are not toxic, by themselves, to the macrophages, do not cause the release of proinflammatory cytokines and do not prevent the phagolysosome fusion. This result is consistent with those of Bloch, who had found that only 1% of the PE extract of cording *M. tuberculosis* is toxic (Bloch et al., 1953). What, then, could be the role of TPP in the increased virulence of *M. abscessus* cording strains? It is reasonable to assume that macrophages that engulf a clump of five or more bacilli in a single phagocytic vesicle should encounter more virulence factors (Brambilla et al., 2016). At present, the majority of these factors are unknown, although the more virulence of R morphotypes has been associated with hyper-proinflammatory responses produced by mycobacterial Toll like receptors ligands as phosphatidyl-myo-inositol mannosides, lipomannan, lipoarabinomannan and lipoproteins (Gilleron et al., 2008; Rhoades et al., 2009; Roux et al., 2011). Therefore, TPP make bacilli aggregate, forming clumps that, when phagocytosed, overwhelm the bactericidal capabilities

of macrophages. The release of large clumps by damaged macrophages is followed by the formation of cords, a process that protects mycobacteria from phagocytosis (Bernut et al., 2014). Making the cord formation an important determinant of virulence.

In summary, the novel findings reported in this work are: (i) the description for the first time of the fine structure of mycolic acids of cording and non-cording morphotypes derived from the same parent strain of *M. abscessus*; (ii) the confirmation that in natural mutants of *M. abscessus* no differences exist in mycolic acid composition between cording and non-cording morphotypes; (iii) the structural characterization of TPP in *M. abscessus* strains; (iv) the location of lipidic compounds on the surface of cording R morphotypes of *M. abscessus* but not in the surface of non-cording S morphotypes; (v) the determination of the aggregative capacity of TPP; and (vi) the determination of the no toxicity of TPP for macrophages. All these findings allow us to propose TPP as candidate molecules responsible for the formation of clumps and cords in R *M. abscessus* strains.

Because the *papA3*, *pks*, *fadD23*, and *mmpL10* genes have recently been found to be involved in the biosynthesis and transport of TPP (Burbaud et al., 2016), it will be possible to confirm the role of TPP in cording-defective mutants. With regard to *M. tuberculosis*, no TPP have been described in this species, but other acylated trehaloses that are closely related in structure to TPP (sulfolipids, diacyltrehaloses, and polyacyltrehaloses) are present in the cell walls of this species and related with hydrophobicity and pathogenicity (Daffé et al., 2014; Jankute et al., 2015, 2017). Future studies are necessary to clarify the role of these acylated trehaloses in the cording of *M. tuberculosis*.

AUTHOR CONTRIBUTIONS

Conceived and designed the experiments: ML-F, EJ, and ML. Performed the experiments: ML-F, MP-T, and CB.

REFERENCES

- Asselineau, C. P., Mohtrozier, H., and Promé, J. (1969). Présence d'acides polyinsaturés dans une bactérie. *Eur. J. Biochem.* 10, 580–584. doi: 10.1111/j.1432-1033.1969.tb00728.x
- Asselineau, C. P., and Montrozier, H. L. (1976). Étude du processus de biosynthèse des acides phléiques, acides polyinsaturés synthétisés par *Mycobacterium phlei*. *Eur. J. Biochem.* 63, 509–518. doi: 10.1111/j.1432-1033.1976.tb10254.x
- Asselineau, C. P., Montrozier, H. L., Promé, J., Savagnac, A. M., and Welby, M. (1972). Étude d'un glycolipide polyinsaturé synthétisé par *Mycobacterium phlei*. *Eur. J. Biochem.* 28, 102–109. doi: 10.1111/j.1432-1033.1972.tb01889.x
- Belazi, D., Solé-Domènech, S., Johansson, B., Schalling, M., and Sjövall, P. (2009). Chemical analysis of osmium tetroxide staining in adipose tissue using imaging ToF-SIMS. *Histochem. Cell Biol.* 132, 105–115. doi: 10.1007/s00418-009-0587-z
- Bernut, A., Herrmann, J.-L., Kissa, K., Dubremetz, J.-F., Gaillard, J.-L., Lutfalla, G., et al. (2014). *Mycobacterium abscessus* cording prevents phagocytosis and promotes abscess formation. *Proc. Natl. Acad. Sci. U.S.A.* 111, E943–52. doi: 10.1073/pnas.1321390111
- Bernut, A., Herrmann, J.-L., Ordway, D., and Kremer, L. (2017). The diverse cellular and animal models to decipher the physiopathological traits of *Mycobacterium abscessus* infection. *Front. Cell. Infect. Microbiol.* 7:100. doi: 10.3389/fcimb.2017.00100

Analyzed the data ML-F, MP-T, EJ, and ML. Contributed reagents/materials/analysis tools TB and FA. Contributed to the writing of the manuscript: ML-F, MP-T, EJ, CB, TB, FA, and ML.

FUNDING

This work was funded by the Spanish Ministry of Science and Innovation (Instituto de Salud Carlos III-PI12/00025), the Spanish Ministry of Economics and Competitiveness (SAF2015-63867-R), the European Regional Development Fund (FEDER), and the Generalitat of Catalunya (2014SGR-132). ML-F was recipient of a fellowship from the Universitat Autònoma de Barcelona.

ACKNOWLEDGMENTS

We would like to thank Martí de Cabo Jaume (Microscopy Service of Universitat Autònoma de Barcelona) for excellent technical assistance with CLSM; Josep M. Rebled (CCiT-UB) for excellent advice regarding the SEM; and Rosa M. Rabanal (Unitat de Patologia Murina i Comparada, Departament de Medicina i Cirurgia Animals, Universitat Autònoma de Barcelona) and Eduard Torrents (Institute for Bioengineering of Catalonia) for excellent assistance with their equipment. MALDI-TOF analyses were carried out in the LP-CSIC/UAB, a member of ProteoRed network.

SUPPLEMENTARY MATERIAL

The Supplementary Material for this article can be found online at: <http://journal.frontiersin.org/article/10.3389/fmicb.2017.01402/full#supplementary-material>

- Bernut, A., Viljoen, A., Dupont, C., Sapriel, G., Blaise, M., Bouchier, C., et al. (2016). Insights into the smooth-to-rough transitioning in *Mycobacterium boletii* unravels a functional Tyr residue conserved in all mycobacterial MmpL family members. *Mol. Microbiol.* 99, 866–883. doi: 10.1111/mmi.13283
- Bleck, C. K. E., Merz, A., Gutierrez, M. G., Walther, P., Dubochet, J., Zuber, B., et al. (2010). Comparison of different methods for thin section em analysis of *Mycobacterium smegmatis*. *J. Microsc.* 237, 23–38. doi: 10.1111/j.1365-2818.2009.03299.x
- Bloch, H. (1950). Studies on the virulence of tubercle bacilli; isolation and biological properties of a constituent of virulent organisms. *J. Exp. Med.* 91, 197–218. doi: 10.1084/jem.91.2.197
- Bloch, H., Sorkin, E., and Erlenmyer, H. (1953). A toxic lipid component of the tubercle bacillus (cord factor). I. Isolation from petroleum ether extracts of young bacterial cultures. *Am. Rev. Tuberc.* 67, 629–643.
- Brambilla, C., Llorens-Fons, M., Julián, E., Noguera-Ortega, E., Tomàs-Martínez, C., Pérez-Trujillo, M., et al. (2016). Mycobacteria clumping increase their capacity to damage macrophages. *Front. Microbiol.* 7:1562. doi: 10.3389/fmicb.2016.01562
- Brambilla, C. (2015). *Estudio de la Formación de Cuerdas Microscópicas en el Género Mycobacterium y su Implicación en la Virulencia de Mycobacterium abscessus*. Barcelona: Universitat Autònoma de Barcelona.

- Brown-Elliott, B. A., and Philley, J. V. (2016). Rapidly growing mycobacteria. *Microbiol. Spectr.* 5, doi: 10.1128/microbiolspec.TNM17-0027-2016
- Burbaud, S., Laval, F., Lemassu, A., Daffé, M., Guilhot, C., and Chalut, C. (2016). Trehalose polyphleates are produced by a glycolipid biosynthetic pathway conserved across phylogenetically distant mycobacteria. *Cell Chem. Biol.* 23, 278–289. doi: 10.1016/j.chembiol.2015.11.013
- Byrd, T. F., and Lyons, C. R. (1999). Preliminary characterization of a *Mycobacterium abscessus* mutant in human and murine models of infection. *Infect. Immun.* 67, 4700–4707.
- Catherinot, E., Clarissou, J., Etienne, G., Ripoll, F., Emile, J. F., Daffé, M., et al. (2007). Hypervirulence of a rough variant of the *Mycobacterium abscessus* type strain. *Infect. Immun.* 75, 1055–1058. doi: 10.1128/IAI.00835-06
- Catherinot, E., Roux, A. L., Macheras, E., Hubert, D., Matmar, M., Dannhoffer, L., et al. (2009). Acute respiratory failure involving an R variant of *Mycobacterium abscessus*. *J. Clin. Microbiol.* 47, 271–274. doi: 10.1128/JCM.01478-08
- Christensen, H., Garton, N. J., Horobin, R. W., Minnikin, D. E., and Barer, M. R. (1999). Lipid domains of mycobacteria studied with fluorescent molecular probes. *Mol. Microbiol.* 31, 1561–1572. doi: 10.1046/j.1365-2958.1999.01304.x
- Daffé, M., Crick, D. C., and Jackson, M. (2014). Genetics of capsular polysaccharides and cell envelope (Glyco)lipids. *Microbiol. Spectr.* 2:14. doi: 10.1128/microbiolspec.MGM2-0021-2013.f1
- Daffé, M., Dupon, M., and Gas, N. (1989). The cell envelope of *Mycobacterium smegmatis*: cytochemistry and architectural implications. *FEMS Microbiol. Lett.* 52, 89–93.
- Gillerson, M., Jackson, M., Nigou, J., and Puzo, G. (2008). *The Mycobacterial Cell Envelope*, eds G. Avenir, M. Daffé, and J.-M. Reyat American (Washington, DC: American Society of Microbiology). doi: 10.1128/9781555815783
- Glickman, M. S. (2008). "Cording, cord factors, and trehalose dimycolate," in *The Mycobacterial Cell Envelope*, eds M. Daffé and J.-M. Reyat (Washington, DC: ASM Press), 63–73. doi: 10.1128/9781555815783
- Glickman, M. S., Cox, J. S., and Jacobs, W. R. (2000). A novel mycolic acid cyclopropane synthetase is required for cording, persistence, and virulence of *Mycobacterium tuberculosis*. *Mol. Cell* 5, 717–727. doi: 10.1016/S1097-2765(00)80250-6
- Hall, D. H., Hartwig, E., and Nguyen, K. C. Q. (2012). Modern electron microscopy methods for *C. elegans*. *Methods Cell Biol.* 107, 93–149. doi: 10.1016/B978-0-12-394620-1.00004-7
- Halloum, I., Carrère-Kremer, S., Blaise, M., Viljoen, A., Bernut, A., Le Moigne, V., et al. (2016). Deletion of a dehydratase important for intracellular growth and cording renders rough *Mycobacterium abscessus* avirulent. *Proc. Natl. Acad. Sci.* 113, E4228–E4237. doi: 10.1073/pnas.1605477113
- Howard, S. T. (2013). Recent progress towards understanding genetic variation in the *Mycobacterium abscessus* complex. *Tuberculosis* 93(Suppl.), S15–20. doi: 10.1016/S1472-9792(13)70005-2
- Howard, S. T., Rhoades, E., Recht, J., Pang, X., Alsop, A., Kolter, R., et al. (2006). Spontaneous reversion of *Mycobacterium abscessus* from a smooth to a rough morphotype is associated with reduced expression of glycopeptidolipid and reacquisition of an invasive phenotype. *Microbiology* 152, 1581–1590. doi: 10.1099/mic.0.28625-0
- Jankute, M., Cox, J. A. G., Harrison, J., and Besra, G. S. (2015). Assembly of the mycobacterial cell wall. *Annu. Rev. Microbiol.* 69, 405–423. doi: 10.1146/annurev-micro-091014-104121
- Jankute, M., Nataraj, V., Lee, O. Y.-C., Wu, H. H. T., Ridell, M., Garton, N. J., et al. (2017). The role of hydrophobicity in tuberculosis evolution and pathogenicity. *Sci. Rep.* 5, 1–25. doi: 10.1038/s41598-017-015010
- Jönsson, B. E., Gilljam, M., Lindblad, A., Ridell, M., Wold, A. E., and Welinder-Ölsson, C. (2007). Molecular epidemiology of *Mycobacterium abscessus*, with focus on cystic fibrosis. *J. Clin. Microbiol.* 45, 1497–1504. doi: 10.1128/JCM.02592-06
- Julián, E., Roldán, M., Sánchez-Chardi, A., Astola, O., Agustí, G., and Luquin, M. (2010). Microscopic cords, a virulence-related characteristic of *Mycobacterium tuberculosis*, are also present in nonpathogenic mycobacteria. *J. Bacteriol.* 192, 1751–1760. doi: 10.1128/JB.01485-09
- Kang, B. K., and Schlesinger, L. S. (1998). Characterization of mannose receptor-dependent phagocytosis mediated by *Mycobacterium tuberculosis* lipaarabinomannan. *Infect. Immun.* 66, 2769–2777.
- Koch, R. (1882). Classics in infectious diseases. The etiology of tuberculosis: Robert Koch. Berlin, Germany 1882. *Rev. Infect. Dis.* 4, 1270–1274. doi: 10.1093/clinids/4.6.1270
- Koh, W.-J., Jeong, B.-H., Kim, S.-Y., Jeon, K., Park, K. U., Jhun, B. W., et al. (2017). Mycobacterial characteristics and treatment outcomes in *Mycobacterium abscessus* Lung disease. *Clin. Infect. Dis.* 64, 309–316. doi: 10.1093/cid/ciw724
- McShane, P. J., and Glassroth, J. (2015). Pulmonary disease due to nontuberculous mycobacteria current state and new insights. *Chest* 148, 1517–1527. doi: 10.1378/chest.15-0458
- Medjahed, H., Gaillard, J. L., and Reyrat, J. M. (2010). *Mycobacterium abscessus*: a new player in the mycobacterial field. *Trends Microbiol.* 18, 117–123. doi: 10.1016/j.tim.2009.12.007
- Middlebrook, G., Dubos, R. J., and Pierce, C. (1947). Virulence and morphological characteristics of mammalian tubercle bacilli. *J. Exp. Med.* 86, 175–184. doi: 10.1084/jem.86.2.175
- Minnikin, D. E., Hutchinson, I. G., Caldicott, A. B., and Goodfellow, M. (1980). Thin-layer chromatography of methanolsates of mycolic acid-containing bacteria. *J. Chromatogr.* 188, 221–233. doi: 10.1016/S0021-9673(00)88433-2
- Nessar, R., Reyrat, J.-M., Davidson, L. B., and Byrd, T. F. (2011). Deletion of the *mmpL4b* gene in the *Mycobacterium abscessus* glycopeptidolipid biosynthetic pathway results in loss of surface colonization capability, but enhanced ability to replicate in human macrophages and stimulate their innate immune response. *Microbiology* 157, 1187–1195. doi: 10.1099/mic.0.046557-0
- Noguera-Ortega, E., Secanella-Fandos, S., Eraña, H., Gasió, J., Rabanal, R. M., Luquin, M., et al. (2016). Nonpathogenic *Mycobacterium brumae* inhibits bladder cancer growth in vitro, ex vivo, and in vivo. *Eur. Urol. Focus* 2, 67–76. doi: 10.1016/j.euf.2015.03.003
- Noll, H., Bloch, H., Asselineau, J., and Lederer, E. (1956). The chemical structure of the cord factor of *Mycobacterium tuberculosis*. *Biochim. Biophys. Acta* 20, 299–309. doi: 10.1016/0006-3002(56)90289-X
- Ortalo-Magné, A., Lemassu, A., Lanéelle, M. A., Bardou, F., Silve, G., Gounon, P., et al. (1996). Identification of the surface-exposed lipids on the cell envelopes of *Mycobacterium tuberculosis* and other mycobacterial species. *J. Bacteriol.* 178, 456–461. doi: 10.1128/jb.178.2.456-461.1996
- Park, I. K., Hsu, A. P., Tettelin, H. H., Shallom, S. J., Drake, S. K., Ding, L., et al. (2015). Clonal diversification, changes in lipid traits and colony morphology in *Mycobacterium abscessus* clinical isolates. *J. Clin. Microbiol.* 53, 3438–3447. doi: 10.1128/JCM.02015-15
- Rhoades, E. R., Archambault, A. S., Greendyke, R., Hsu, F.-F., Streeter, C., and Byrd, T. F. (2009). *Mycobacterium abscessus* glycopeptidolipids mask underlying cell wall phosphatidyl-myo-inositol mannosides blocking induction of human macrophage TNF-alpha by preventing interaction with TLR2. *J. Immunol.* 183, 1997–2007. doi: 10.4049/jimmunol.0802181
- Roux, A.-L., Ray, A., Pawlik, A., Medjahed, H., Etienne, G., Rottman, M., et al. (2011). Overexpression of proinflammatory TLR-2-signalling lipoproteins in hypervirulent mycobacterial variants. *Cell. Microbiol.* 13, 692–704. doi: 10.1111/j.1462-5822.2010.01565.x
- Roux, A.-L., Viljoen, A., Bah, A., Simeone, R., Bernut, A., Laencina, L., et al. (2016). The distinct fate of smooth and rough *Mycobacterium abscessus* variants inside macrophages. *Open Biol.* 6:160185. doi: 10.1098/rsob.160185
- Sánchez-Chardi, A., Olivares, F., Byrd, T. F., Julián, E., Brambilla, C., and Luquin, M. (2011). Demonstration of cord formation by rough *Mycobacterium abscessus* variants: implications for the clinical microbiology laboratory. *J. Clin. Microbiol.* 49, 2293–2295. doi: 10.1128/JCM.02322-10
- Sanguinetti, M., Ardito, F., Fiscarelli, E., La Sorda, M., D'Argenio, P., Ricciotti, G., et al. (2001). Fatal pulmonary infection due to multidrug-resistant *Mycobacterium abscessus* in a patient with cystic fibrosis. *J. Clin. Microbiol.* 39, 816–819. doi: 10.1128/JCM.39.2.816-819.2001
- Seeliger, J., and Moody, D. B. (2016). Monstrous mycobacterial lipids. *Cell Chem. Biol.* 1, 2015–2017. doi: 10.1016/j.chembiol.2016.02.004
- Seligman, A. M., Wasserkug, H. L., and Hanker, J. S. (1966). A new staining method (OTO) for enhancing contrast of lipid-containing membranes and droplets in osmium tetroxide-fixed tissue with osmophilic thiocarbohydrazide(TCH). *J. Cell Biol.* 30, 424–432. doi: 10.1083/jcb.30.2.424

Vergne, I., Chua, J., Singh, S. B., and Deretic, V. (2004). Cell biology of *Mycobacterium tuberculosis* phagosome. *Annu. Rev. Cell Dev. Biol.* 20, 367–394. doi: 10.1146/annurev.cellbio.20.010403.114015

Conflict of Interest Statement: The authors declare that the research was conducted in the absence of any commercial or financial relationships that could be construed as a potential conflict of interest.

Copyright © 2017 Llorens-Fons, Pérez-Trujillo, Julián, Brambilla, Alcaide, Byrd and Luquin. This is an open-access article distributed under the terms of the Creative Commons Attribution License (CC BY). The use, distribution or reproduction in other forums is permitted, provided the original author(s) or licensor are credited and that the original publication in this journal is cited, in accordance with accepted academic practice. No use, distribution or reproduction is permitted which does not comply with these terms.

Supplementary Material

Trehalose polyphleates, external cell wall lipids in *Mycobacterium abscessus*, are associated with the formation of clumps with cording morphology, which have been associated with virulence

Marta Llorens-Fons, Míriam Pérez-Trujillo, Esther Julián, Cecilia Brambilla, Fernando Alcaide, Thomas F. Byrd, Marina Luquin*

***Corresponding author:** Marina Luquin (mailto:marina.luquin@uab.cat)

1 Supplementary Figures and Tables

1.1 Supplementary Figures

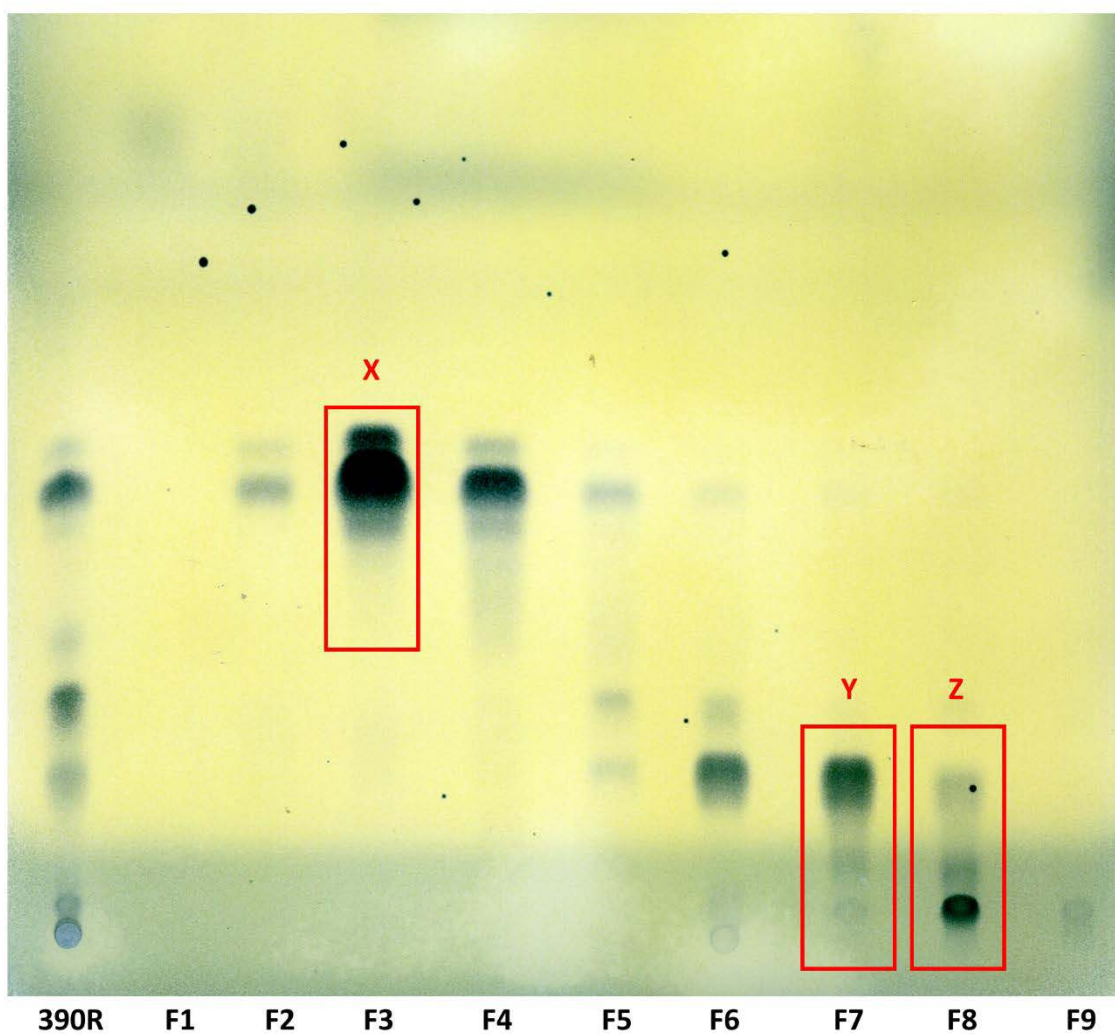


Figure S1. TLC of all the fractions (F1-F9) obtained when performing a column chromatography to the PE extract from 390R *M. abscessus*. The solvent system used was PE 60-80°C/diethyl ether (90:10, v/v), and the plate was stained with 10% phosphomolybdic acid. Fractions 3, 7 and 8, corresponding to compound X, compound Y and compound Z, were analyzed by NMR and MS.

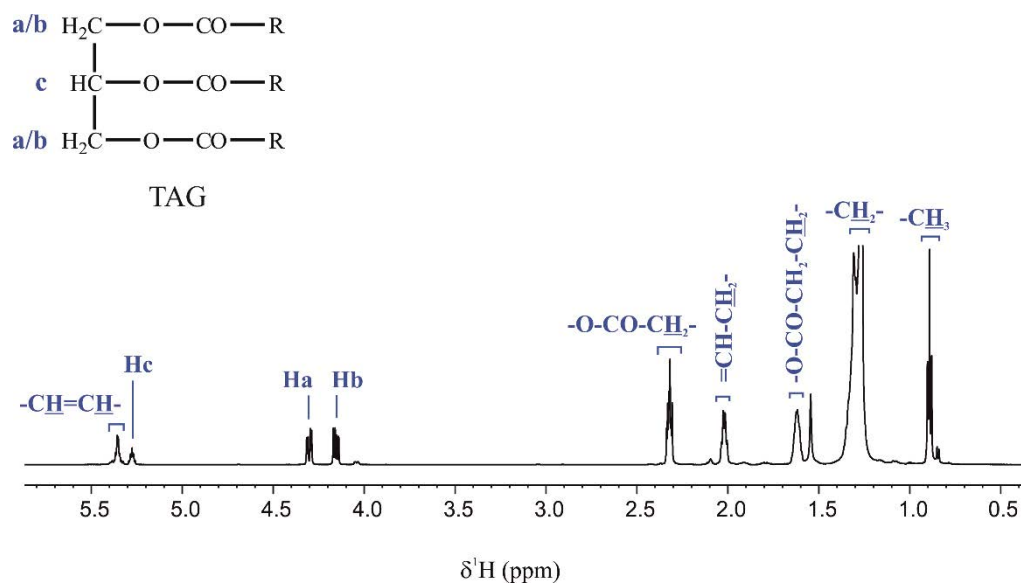


Figure S2. ¹H NMR spectrum of TAG from PE extract of 390R *M. abscessus* strain in CDCl₃, at a magnetic field of 600.13 MHz and 298.0 K of temperature.

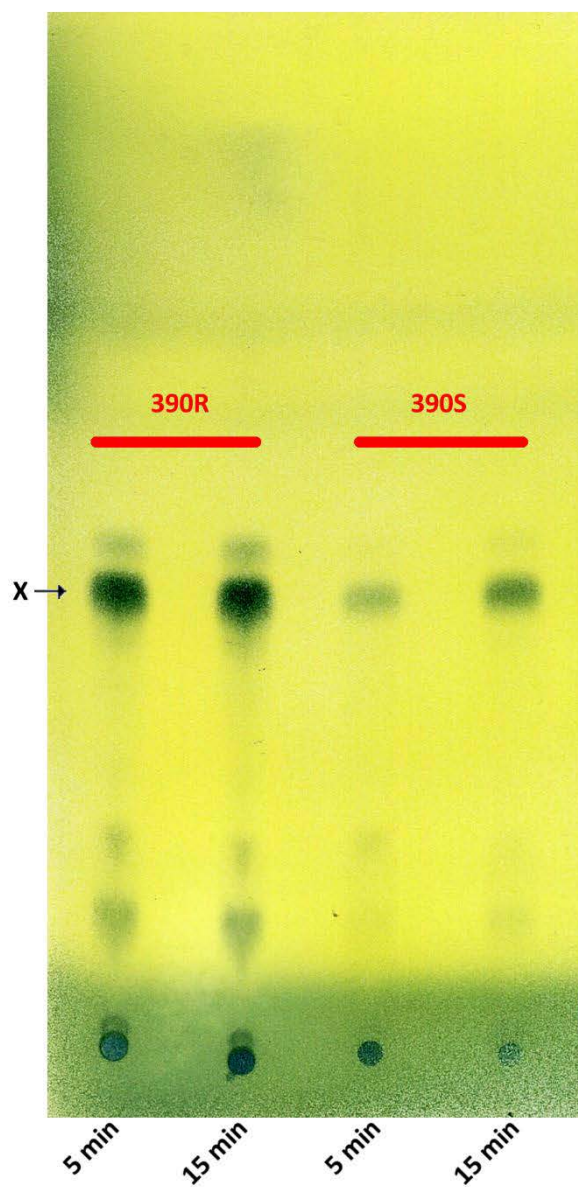


Figure S3. TLC of the PE extracts obtained from 390R and 390S after 5 minutes and after 15 minutes of extraction. The solvent system used was PE 60-80°C/diethyl ether (90:10, v/v), and the plate was revealed with 10% phosphomolybdic acid. X indicate compound X or TPP-A.

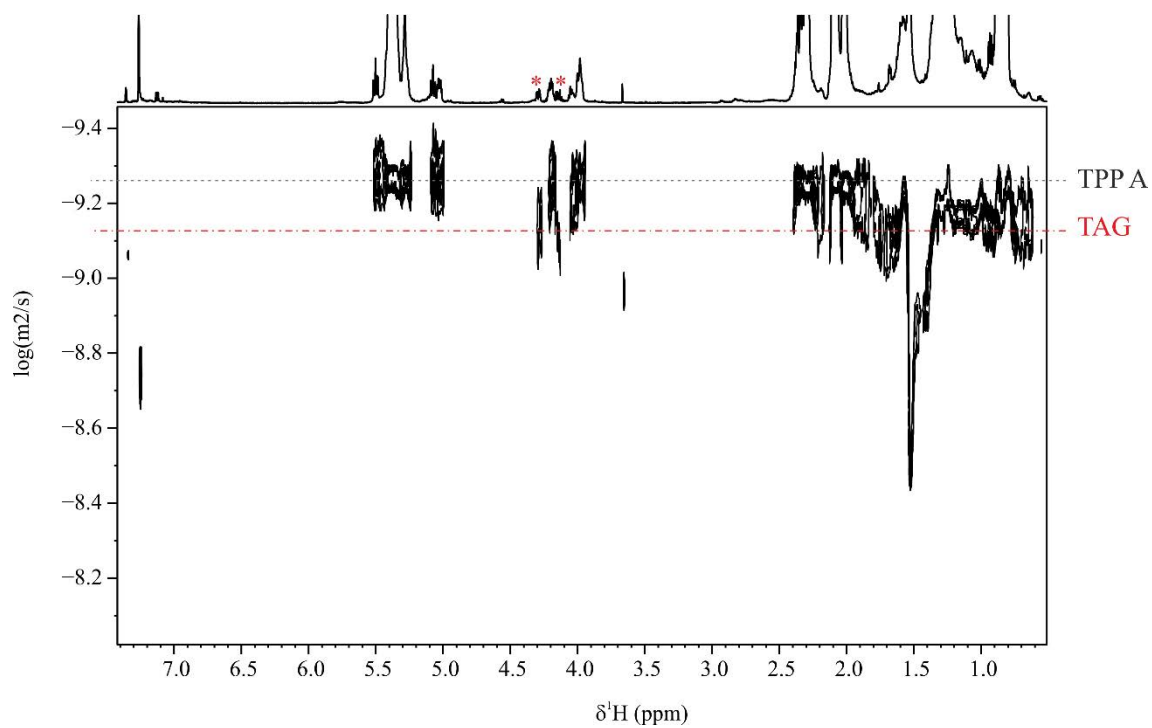


Figure S4. 2D DOSY spectrum of TPP-A from PE extract of 390R *M. abscessus* strain in CDCl_3 at a magnetic field of 600.13 MHz and 298.0 K of temperature; asterisks denote signals of TAG.

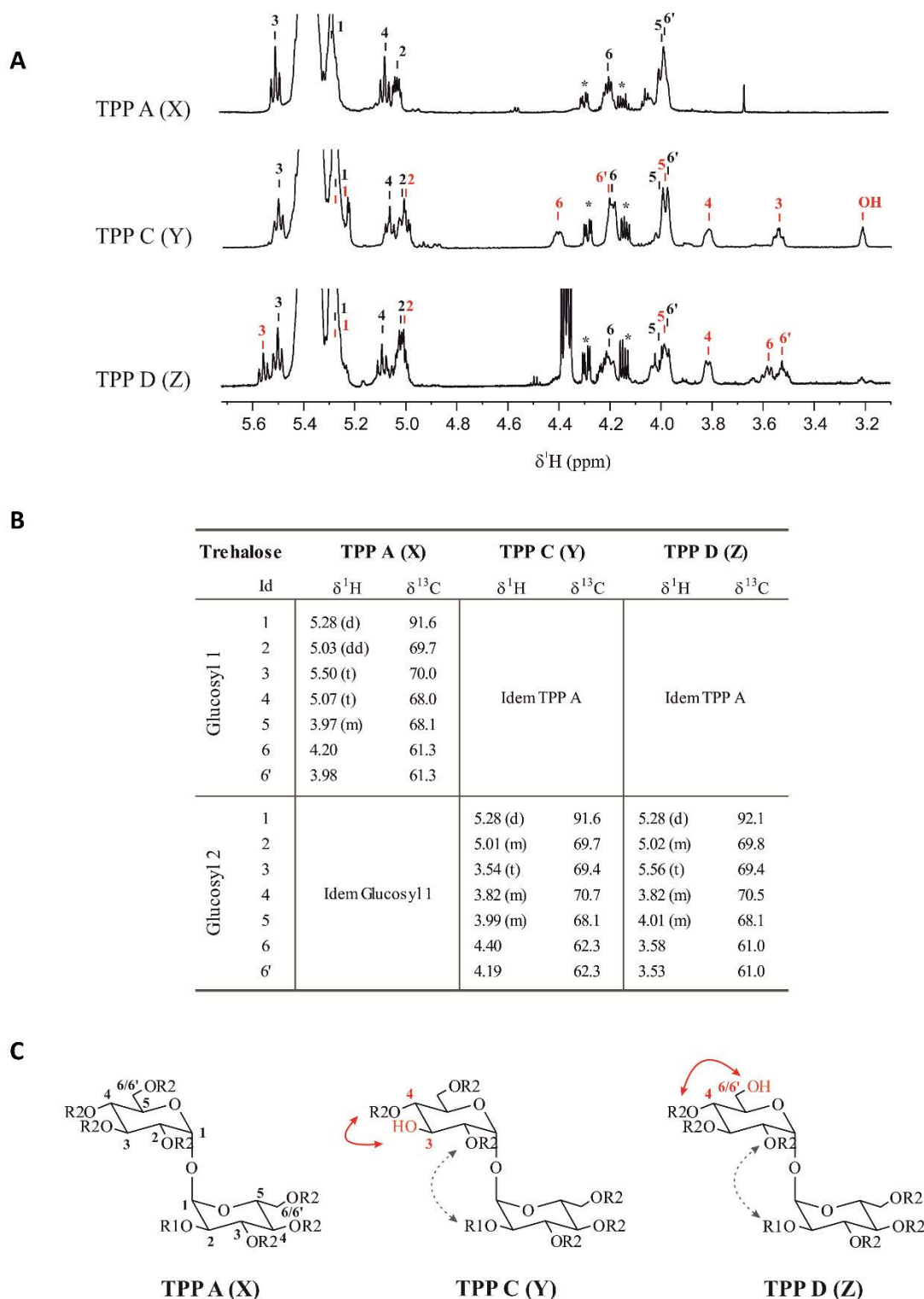


Figure S5. (A) ^1H NMR spectra in CDCl_3 (enlargement of the region between 5.7 and 3.4 ppm); asterisks denote signals of TAG; (B) ^1H and ^{13}C NMR characterization of the trehalose units and (C) suggested structures for TPP A (compound X), TPP C (compound Y) and TPP D (compound Z).

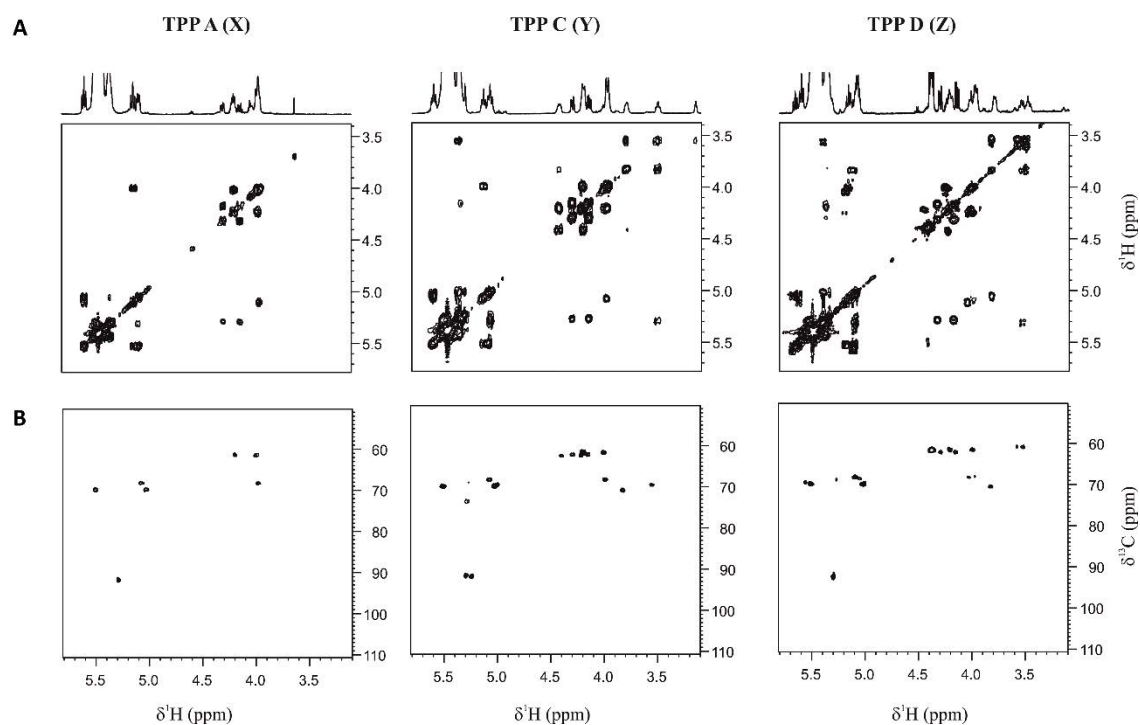


Figure S6. (A) 2D ${}^1\text{H}, {}^1\text{H}$ -COSY and (B) ${}^1\text{H}, {}^{13}\text{C}$ -HSQC of TPP A (compound X), TPP C (compound Y) and TPP D (compound Z) in CDCl_3

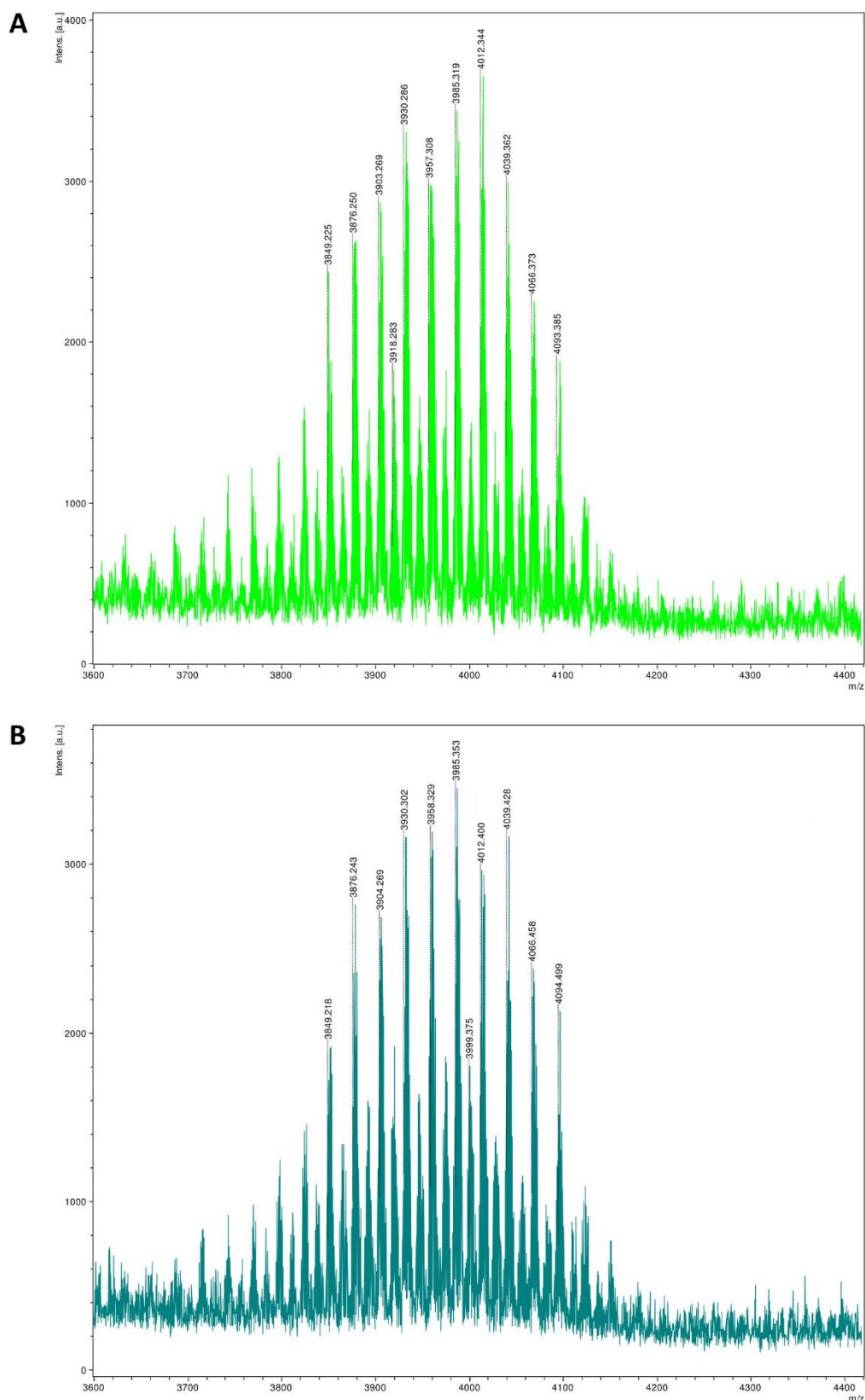
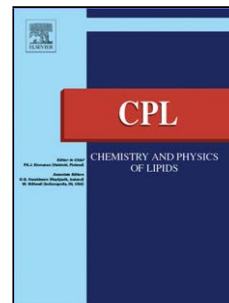


Figure S7. MALDI-TOF MS spectra of **(A)** TPP C (compound Y) and **(B)** TPP D (compound Z) (region between m/z 3600 and 4400 was magnified).

Accepted Manuscript

Title: Molecule confirmation and structure characterization of pentatriacontatrienyl mycolate in *Mycobacterium smegmatis*

Authors: Marta Llorens-Fons, Esther Julián, Marina Luquin, Míriam Pérez-Trujillo



PII: S0009-3084(17)30297-9
DOI: <https://doi.org/10.1016/j.chemphyslip.2017.12.006>
Reference: CPL 4625

To appear in: *Chemistry and Physics of Lipids*

Received date: 6-11-2017
Revised date: 15-12-2017
Accepted date: 26-12-2017

Please cite this article as: Llorens-Fons, Marta, Julián, Esther, Luquin, Marina, Pérez-Trujillo, Míriam, Molecule confirmation and structure characterization of pentatriacontatrienyl mycolate in *Mycobacterium smegmatis*. *Chemistry and Physics of Lipids* <https://doi.org/10.1016/j.chemphyslip.2017.12.006>

This is a PDF file of an unedited manuscript that has been accepted for publication. As a service to our customers we are providing this early version of the manuscript. The manuscript will undergo copyediting, typesetting, and review of the resulting proof before it is published in its final form. Please note that during the production process errors may be discovered which could affect the content, and all legal disclaimers that apply to the journal pertain.

Molecule confirmation and structure characterization of pentatriacontatrienyl mycolate in *Mycobacterium smegmatis*

Marta Llorens-Fons¹, Esther Julián¹, Marina Luquin^{1*}, Míriam Pérez-Trujillo^{2*}

¹ Departament de Genètica i de Microbiologia, Facultat de Biociències, Universitat Autònoma de Barcelona, E-08193, Bellaterra, Barcelona, Spain.

² Servei de Ressonància Magnètica Nuclear i Departament de Química, Facultat de Ciències i Biociències, Universitat Autònoma de Barcelona, E-08193, Bellaterra, Barcelona, Spain.

*Corresponding coauthor: Míriam Pérez-Trujillo (E-mail: miriam.perez@uab.cat)

*Corresponding coauthor: Marina Luquin (E-mail: marina.luquin@uab.cat)

HIGHLIGHTS

- Mycolate ester wax found in *Mycobacterium smegmatis* was accurately characterized
- Mycolate ester wax structure corresponds to pentatriacontatrienyl mycolate, PTTM 1
- The characterization was based on 1D and 2D NMR analysis
- These results allow the future quick identification by a 1D ¹H NMR experiment

ABSTRACT

Mycobacterium smegmatis is often used to study the different components of mycobacterial cell wall. Mycolic acids are important components of mycobacterial cell wall that have been associated with virulence. Recently, a novel lipid containing mycolic acids has been described in *M. smegmatis*. However, some uncertainties regarding the structure of this molecule named mycolate ester wax have been reported. The objective of this work was to perform an in depth structural study of this molecule for its precise characterization. Using ¹H and ¹³C NMR spectroscopy, the molecular structure of mycolate ester wax found in *M. smegmatis* has been elucidated. The

characterization was complemented with MS analyses. This molecule is formed by a carbon chain with three methyl substituted olefinic units and a mycolate structure with *trans* double bonds and *cis* cyclopropane rings. The present molecular study will facilitate the detection and identification of pentatriacontatrienyl mycolate in future studies by the performance of a simple 1D ^1H NMR experiment.

KEYWORDS

Mycobacterium smegmatis, Pentatriacontatrienyl Mycolate, Mycolic Acids, Mycolate Ester Wax, NMR, MS

ABBREVIATIONS

MS: Mass spectrometry

MALDI: Matrix-assisted laser desorption/ionization

NMR: Nuclear magnetic resonance

PE: Petroleum ether

PTTM: Pentatriacontatrienyl Mycolate

TLC: Thin layer chromatography

1. INTRODUCTION

Mycobacteria are important pathogens for humans. *Mycobacterium tuberculosis* infects one-third of the world population, and 1.8 million of deaths have been reported in 2016 due to tuberculosis disease (World Health Organization, 2016). In addition to the species that are part of the *Mycobacterium tuberculosis* complex, the genus *Mycobacterium* contains more than 170 species that inhabit the environment. Some of them are opportunistic pathogens causing lung diseases and extrapulmonary infections (Falkinham III, 2009; Fedrizzi et al., 2017).

Bacilli of some mycobacterial species, when grow in liquid culture display a strong propensity to attach to each other forming pellicles at the air-liquid interface with a variety of microscopic as well as macroscopic multicellular structures (Julián et al., 2010). Formation of very wrinkled pellicles at the air-liquid surface has been related with a major hydrophobicity and virulence in *M. tuberculosis* strains (Jankute et al., 2017). Some studies revealed that the extracellular matrix of pellicles formed by *M. tuberculosis* and *Mycobacterium smegmatis* are rich in free mycolic acids and mycolic acid-containing lipids (Ojha et al., 2008, 2010; Pacheco et al., 2013). Mycolic acids are

major components of the cell envelope of mycobacteria and play a crucial role in its architecture. These molecules are formed by a very long β -hydroxyl fatty acid chain with an α -alkyl side chain (Marrakchi et al., 2014). They are covalently linked to the arabinogalactan-peptidoglycan inner layer of mycobacterial cell wall and are also found in the most external surface of mycobacteria cells forming part of non-covalently associated lipids (Daffé, M., Reyrat, 2008; Jankute et al., 2015). Many studies on mycobacterial lipids have been done in *M. smegmatis*. This species serves as tractable model system for experiments that can be conducted rapidly and safely outside the biosafety level 3 suite, in contrast to work done using with *M. tuberculosis*. As an example of lipid studies, a novel mycolic acid-containing lipid named mycolate ester wax and associated to the formation of wrinkled pellicles in *M. smegmatis* has been recently described (Pacheco et al., 2013).

Some uncertainties regarding the structure of mycolate ester wax found in *M. smegmatis* have been reported. Initially, this lipid was characterized by Chen et al. (Chen et al., 2006) as mycoloyl diacylglycerol, based on mass spectrometric (MS) analyses. Later, Pacheco et al. (Pacheco et al., 2013) described the same molecule as a pentatriacontatrienyl mycolate, also based on MS. In both studies the identification was based on the same analytical technique and both agreed that it was a mycolate derivative, corresponding to *M. smegmatis* mycolic acids. However, they came to different conclusions about the nature of such derivative, a diacylglyceryl or a pentatriacontatrienyl. In the present work, an in-depth structural study of mycolate ester wax found in *M. smegmatis*, based on nuclear magnetic resonance (NMR) spectroscopy and MS analyses, to confirm and characterize accurately the structure of the mycolate ester wax is carried out.

2. MATERIALS AND METHODS

2. 1. Sample preparation

M. smegmatis ATCC 35797 was grown in Middlebrook 7H9 broth (Difco, USA) at 37°C. After two weeks of growth, pellicles formed in the interface air-medium were filtered and superficially extracted as previously described (Llorens-Fons et al., 2017). Briefly, the filtered pellicles were extracted with petroleum ether (PE) (40-60°C b.p.) for 5 minutes, and the extract was dried at 40°C under nitrogen stream. The extract was analyzed by thin layer chromatography (TLC) on silica gel-coated plates (G-60, Merck, Germany), using PE (60-80°C b.p.)/diethyl ether (90:10, v/v) as mobile phase.

Compounds in the TLC plates were revealed using phosphomolybdic acid (VWR, USA; 10% in ethanol) and then heating the plate at 120°C.

The spot A detected by TLC was purified from the PE extract by column chromatography. Briefly, 50 mg of the PE extract was added to a Silica Gel 60 (Merck, Germany) column and a series of solvent mixtures of PE (60-80°C b.p.) with increasing concentrations of diethyl ether was used for its elution. The dried fraction containing spot A was used for MS and NMR analyses.

2. 2. MS analysis

This analysis was performed using ESI/MS, MALDI/MS and MALDI-LIFT/MS. For ESI+, purified spot A (ca. 1 mg of dried material) was dissolved in 500 µl of CHCl₃/IPA (3:1, v/v) and manually injected to a micrOTOF-Q II (Bruker Daltonics, USA). For MALDI, spot A was dissolved in 50 µl of CHCl₃/CH₃OH (2:1, v/v) and mixed with a matrix of 10 mg/ml 1,8,9-anthracenetriol (ditranol) at a 1:1 ratio. 1 µl of the sample mixed with the matrix was deposited on a ground steel plate. To acquire the MS spectrum the sample was analyzed using a negative polarity reflectron and an acceleration voltage of 25 kV in a MALDI-TOF UltrafleXtreme (Bruker Daltonics, USA). To obtain the fragmentation spectrum of some specific signals a LIFT method was used. The calibration was performed using external calibrators (Bruker Daltonics, USA).

2. 3. NMR analysis

For the NMR analysis purified spot A (ca. 3 mg of dried material) was dissolved in 600 µL of CDCl₃ (99.80 % D, Cortecnet, Voisins-le-Bretonneux, France) and transferred to 5-mm diameter NMR tubes. A Bruker Avance II 600 NMR spectrometer (Bruker Biospin, Rheinstetten, Germany) equipped with a 5 mm TBI probe with Z-gradients, operating at a ¹H NMR frequency of 600.13 and at 298.0 K of temperature, was used for the NMR experiments. 1D ¹H NMR spectra were acquired using a standard 90° pulse sequence, with an acquisition time of 1.71 s and a relaxation delay of 2 s. The data were collected into 32 K computer data points, with a spectral width of 9590 Hz and as the sum of 128 transients. The resulting free inductions decays (FIDs) were Fourier transformed, manually phased, and baseline corrected. 2D ¹H,¹H-COSY (Correlation Spectroscopy); ¹H,¹H-TOCSY (Total Spectroscopy); ¹H,¹³C-HSQC (Heteronuclear Single Quantum Coherence) and ¹H,¹³C-HMBC (Heteronuclear Multiple Bond

Correlation) experiments were performed using standard Bruker pulse sequences and acquired under routine conditions. All the spectra were calibrated using the residual solvent signal (CHCl_3 , δ_{H} , 7.26 and δ_{C} , 77.0 ppm). Chemical shift data are expressed in ppm and coupling constant (J) values in Hz. Multiplicity of peaks is abbreviated as d (doublet), t (triplet) and ddd (double doublet of doublets). Integration was performed with MestreNova 8 (Mestrelab Research S.L.) and its global spectral deconvolution (GSD) application.

3. RESULTS AND DISCUSSION

3. 1. Detection of spot A and confirmation of the structure by MS

Spot A was visualized by using TLC in the PE extract from *M. smegmatis*. This compound was less polar than triacylglycerides, which were observed below (Figure 1a). After column chromatography, purified spot A was recovered in the fraction eluted with 94:6 PE 60-80°C (b.p.)/diethyl ether. An small amount of purified spot A was analyzed by ESI-MS and MALDI-TOF to confirm that the extracted compound corresponded to the same molecule analyzed and described in previous works (Chen et al., 2006; Pacheco et al., 2013).

The ESI-MS spectrum was similar to the one presented by Pacheco et al. (Pacheco et al., 2013) with coincident peaks as at m/z 1589 and m/z 1631 (Figure 1b). The positive MALDI spectrum was consistent with the results of the ESI-MS and reproduced the results obtained by Chen et al. (Chen et al., 2006). The three peaks separated by an increment of 14 amu corresponding to m/z 1616, m/z 1630 and m/z 1644 were observed also in the spectrum presented by Chen et al. (Figure 1c)

Finally, a positive MALDI-LIFT spectrum of the parent $[\text{M}+\text{H}]^+$ at m/z 1630 yielded a fragment of m/z 1145 (most intense peak of the spectrum), which typically corresponds to mycolic acids type I (α -mycolic acids) of *M. smegmatis* with a chain length of C76 (total carbon number of the free acid) (Laval et al., 2001). (Figure 1d). Assuming a similar fragmentation behavior for peaks at m/z 1616 and m/z 1644 (Figure 1c), the three peaks (m/z 1616, 1630 and 1644) would correspond to derivatives of a series of α -mycolic acids with chain lengths C75, C76 and C77, respectively. The difference between the parent peak at m/z 1630 and the fragment at m/z 1145, which corresponds to 485 uma, gives information about the molecular weight of the ambiguously described part of the molecule, i.e. the nature of the derivative. This difference is in agreement

with the chemical structure obtained from the NMR study (described in the next section), the pentatriacontatrienyl mycolate (PTTM) (35:3) **1** (Figure 2).

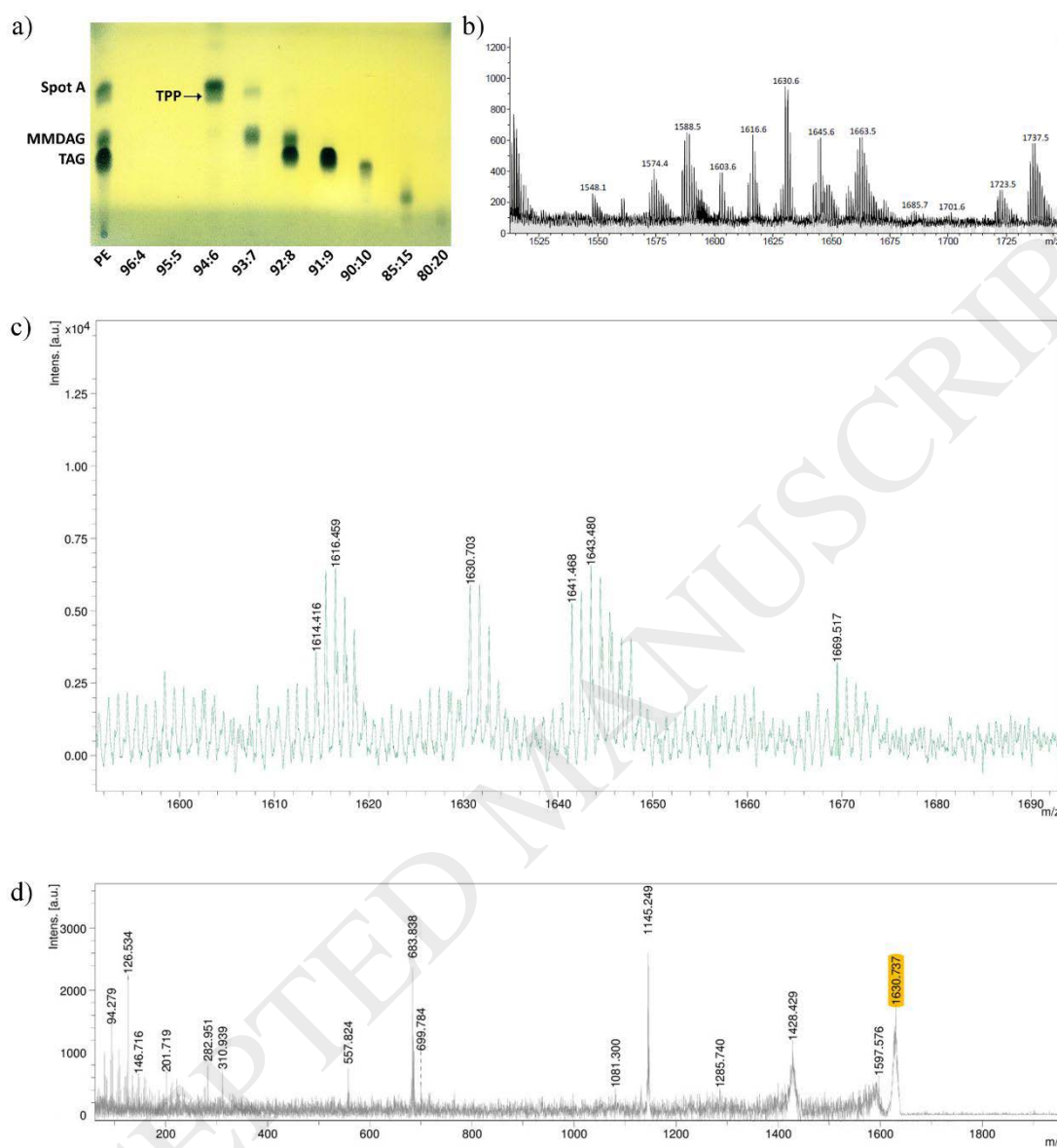


Figure 1. TLC and MS spectra of Spot A. a) TLC of the different fractions obtained by column chromatography from PE extract of *M. smegmatis*. Spot A indicates the spot of mycolate ester wax, MMDAG indicate the monomermicolyl diacylglycerols and TAG the triacylglycerols. Trace amounts of trehalose polyphleates (TPP) are indicated with an arrow. The first line of the TLC represents PE extract before fractionated using the chromatography column, and the other lines represent the eluted fractions from the column chromatography with the indicated proportions of PE 60-80°C (b.p.)/diethyl ether. b) ESI+ MS, amplifying the region between 1500 m/z and 1750 m/z; c) positive MALDI mass spectrum, amplifying the region between 1600 m/z and 1700 m/z and d)

positive MALDI-LIFT spectrum of the parent $[M+H]^+$ at 1630 m/z of the extract corresponding to spot A.

3. 2. Molecular structure characterization by NMR spectroscopy

Purified spot A was dissolved in $CDCl_3$ and analyzed by NMR spectroscopy. The NMR analysis, together with the MS information, confirmed the structure of the molecule as pentatriacontatrienyl mycolate (PTTM) (35:3) **1**, shown in Figure 2; where the PTTM **1** is formed by three methyl substituted olefinic units (A, B and C) in the carbon chain and the mycoloyl part contains *trans* double bonds (*trans*-db) and *cis* cyclopropane (*cis*-cp) in its structure.

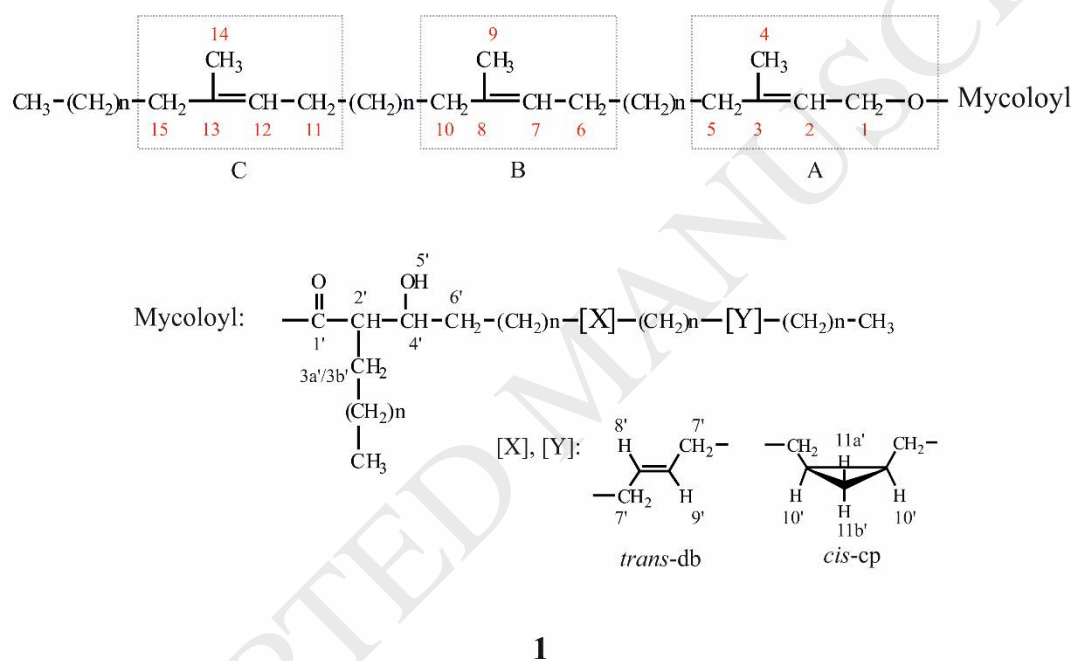


Figure 2. Structure of the PTTM (35:3) **1**.

The complete 1H and ^{13}C NMR characterization of the molecule was achieved by the performance of a battery of 1D and 2D NMR experiments (1D 1H , 1D 1H selective TOCSY, 1H - 1H COSY, 1H - 1H TOCSY and 1H - 1H NOESY, 1H - ^{13}C HSQC and 1H - ^{13}C HMBC) and the coordinated analysis of the resulting spectra (Breitmaier, 2002; Secanella-Fandos et al., 2011; Williams et al., 2016). The detailed NMR study was performed with a Bruker Avance 600 spectrometer working at 298.0 K.

The ^1H NMR spectrum of the sample is represented in Figure 3, with the resonances of the PTTM **1** assigned. Peaks corresponding to protons of the pentatriacontatrienyl structure and the mycoloyl unit are indicated in red and black numbers, respectively.

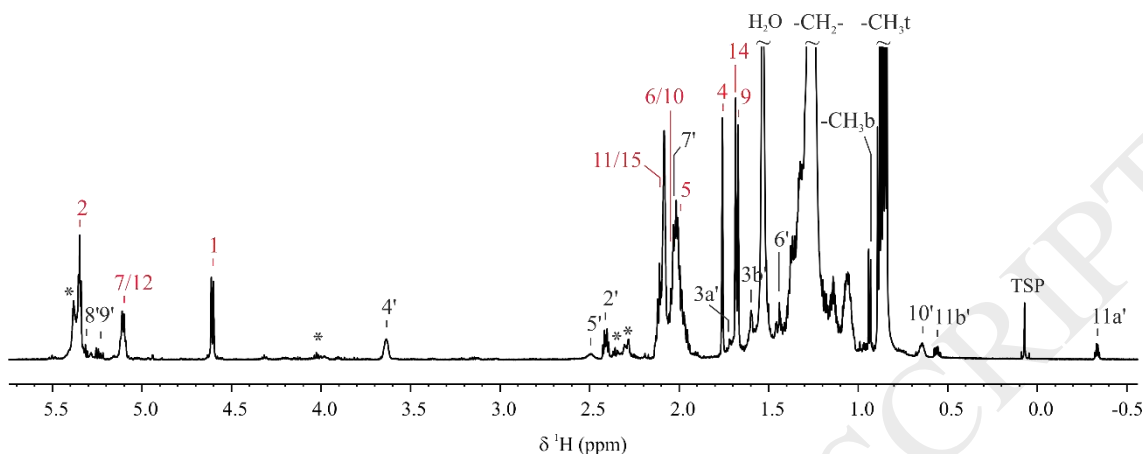


Figure 3. ^1H -NMR spectrum of purified spot A, with signals of PTTM **1** assigned. Asterisks indicate residual amount of trehalose polyphleates type A. Spectrum acquired at 298.0 K and at a magnetic field of 600 MHz.

Regarding the pentatriacontatrienyl structure, in red in Figure 3, there was a characteristic sharp doublet at 4.61 ppm with a coupling constant, J , of 7.2 Hz corresponding to H1, which correlated to C1 peak at 60.8 ppm via HSQC. As well, the same H1 signal correlated to olefinic H2 (triplet at 5.35 ppm) via COSY, with methyl protons H4 (sharp intense singlet at 1.76 ppm) via TOCSY and with olefinic quaternary carbon C3 (142.5 ppm) via HMBC. H2 and H4 signals correlated to the peak of methylene protons adjacent to the double bond, H5 (2.01 ppm), via TOCSY. Signals of carbons directly bonded to spin system A protons (Figure 2) were assigned via HSQC. By an analogous reasoning, proton and carbon chemical shifts of spin systems B and C of the pentatriacontatrienyl moiety were identified. Olefinic protons H7 signal resonated at 5.14 ppm as a triplet (with a J of 5.9 Hz), being partially overlapped with analogous H12 (5.13 ppm) triplet of spin system C. H7 correlated via COSY to H6 (2.04 ppm) and via TOCSY to methyl protons H9 (an intense singlet at 1.69 ppm) and to methylene protons H10 (2.03 ppm). Similarly to spin systems A and B, spin system C was assigned presenting as characteristic resonances H12 (triplet at 5.13 partially overlapped with H7 triplet) and methyl protons H14 (intense singlet at 1.67 ppm). C6 to C15 resonances were identified via HSQC and HMBC. To elucidate the position of spin

systems B and C in the molecular structure, NOE signals between proton resonances of different spin systems were searched in the 2D NOESY correlation without success. The order suggested in Table 1 was based on the slight difference between chemical shifts of protons H7 and H12, but it would be possible that the assignment of spin system B corresponded to C and *vice versa*. This fact, however, does not affect the molecular structure, just the assignment of the peaks.

Signals corresponding to the mycoloyl unit were indicated in black in Figure 3. At 2.41 ppm α -carboxylic proton H2' (directly bonded to C2' at 50.9 ppm via HSQC) correlated via COSY to β -carboxylic protons H3a' and H3b' (1.71 and 1.59 ppm) (bonded to C3' at 29.7 ppm) and to β -carboxylic proton H4' at 3.64 ppm (bonded to C4' at 72.2 ppm). The broad signal at 2.49 ppm corresponded to the hydroxylic proton, H5'. The spectrum showed typical signals corresponding to olefinic protons of *trans* double bonds, multiplets at 5.34 and 5.24 ppm (H8' and H9', respectively). Also, the protons adjacent to the double bond, H7', were identified at 2.02 ppm via COSY and TOCSY correlations. Typical signals corresponding to *cis*-cyclopropane rings were observed at 0.65 (H10', broad), 0.56 (H11b' ddd, 8.2, 8.2, 4.2 Hz) and -0.34 ppm (H11a', ddd, 4.2, 5.3, 5.3 Hz). Regarding the whole molecule, methylene chains resonated about 1.28-1.23 ppm (broad intense signal), branched methyl groups, CH₃b, at 0.94 ppm (d, 6.7 Hz) and terminal methyl groups, CH₃t, resonated between 0.89 and 0.84 ppm (t, 6.8 Hz) (Yuan and Barry, 1996; Watanabe et al., 1999).

Finally, HMBC correlations between H1 and H2' with same carboxylic carbon C1' at 175.5 ppm, confirmed that both structures, pentatriacontatrienyl and mycoloyl, belonged to the same molecule. In addition peak integrations were in accordance with the described structure. The full ¹H and ¹³C characterization of compound **1** was collected in Table 1 and 2D correlations were gathered in the Supporting Information (Figure S1 to Figure S4).

Table 1. ¹H and ¹³C NMR chemical shifts and H-H *J* couplings of PTTM **1**.

Id	¹ H		¹³ C	
	δ (¹ H) [ppm]	(mult., * <i>J</i> _{H,H}) [Hz]	δ (¹³ C) [ppm]	
1	4.606	(d, <i>J</i> _{1,2} =7.2)	60.82	A
2	5.353	(t, <i>J</i> _{2,1} =7.2)	118.95	
3	-		142.54	

Pentatriacontatrienyl

4	1.759	(s)	23.29	B
5	2.011	(m, ov)	32.02	
6	2.043	(m, ov)	32.20	
7	5.138	(t, $J_{7,6}=5.9$)	124.37	
8	-		135.83	
9	1.686	(s)	23.32	
10	2.034	(m, ov)	32.20	
11	2.089	(m, ov)	32.34	C
12	5.128	(t, $J_{12,11}=5.9$)	124.21	
13	-		135.83	
14	1.671	(s)	23.32	
15	2.101	(m, ov)	32.34	
1'	-		175.49	Mycology
2'	2.410	(m)	50.89	
3a'	1.711	(m, ov)	29.68	
3b'	1.593	(m, ov)	29.68	
4'	3.636	(m, br)	72.21	
5'	2.495	(m, br)	-	
6'	1.441	(m)	35.88	
7'	2.016	(m, ov)	n.d. **	
8'	5.339	(dd, ov.)	n.d.	
9'	5.236	(dd, $J_{9,8}=15.3$ $J_{9,7}=7.6$)	n.d.	
10'	0.644	(m, br)	n.d.	
11a'	-0.334	(ddd, $J_{11a',10'}=5.3$ $J_{11a',10}=5.3$ $J_{11a',11b}=4.2$)	n.d.	
11b'	0.559	(ddd, $J_{11b',10}=8.2$ $J_{11b',10'}=8.2$ $J_{11b',11a}=4.2$)	n.d.	
-	[1.285- 1.232]		[30.65- 28.91]	
CH2-				
-				
CH3b	0.94	(d, $J=6.7$)	20.76	
-	[0.894- 0.841]		[14.17 - 22.51]	
CH3t				

* s (Singlet), d (doublet), t(triplet), ddd (doublet of doublets of doublets), m (multiplet), br (broad), ov (overlapped). ** n.d. (not detected, not enough signal).

A residual amount of trehalose polyphleates type A (Burbaud et al., 2016; Seeliger and Moody, 2016; Llorens-Fons et al., 2017) in spot A that we were unable to separate by column chromatography (Figure 1a), was observed by both NMR (indicated with asterisks in Figure 3) and MS spectra (data not shown).

3. 3. Rapid detection and identification of PTTM 1 and differentiation from other mycolate derivatives by 1D ^1H NMR

The accurate identification of mycolate ester wax found in *M. smegmatis* as pentatriacontatrienyl mycolate (PTTM) **1** (Figure 2) and its complete ^1H and ^{13}C NMR structural elucidation (Table 1), allows from now on the quick direct detection and identification of this mycolate derivative and its differentiation from others by the performance of a simple 1D ^1H NMR experiment. The characteristic doublet at 4.61 ppm (corresponding to H1 of the trienyl chain), the three intense singlets at 1.76, 1.69 and 1.67 ppm (corresponding to the alkene methyl substituents of the trienyl chain) and the intense peaks related to the unsaturation of the trienyl chain, makes simple the identification and differentiation of **1** from other mycolate derivatives, such as methyl mycolates. This is exemplified in Figure 4. Finally, ^1H qNMR (quantitative NMR) spectroscopy could be applied, as well, for the rapid quantification of PTTM **1** (Pauli et al., 2012).

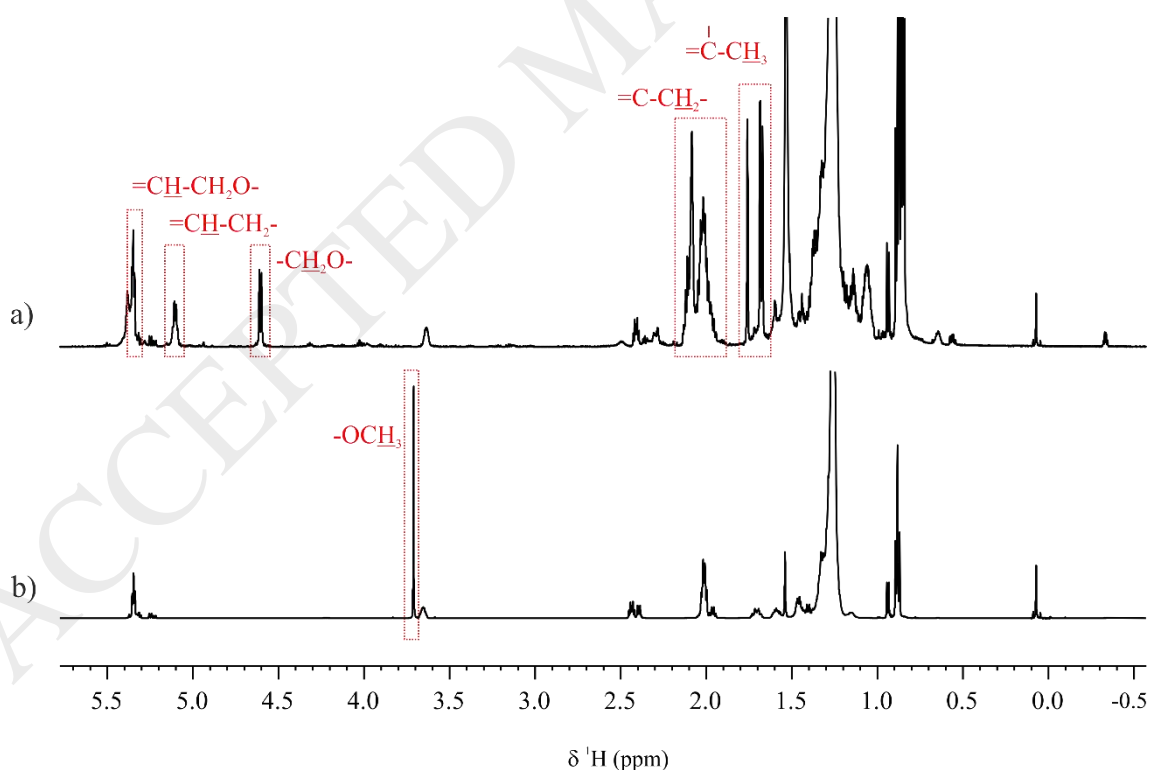


Figure 4. ^1H -NMR spectrum of a) PTTM **1** from *M. smegmatis* and b) α -methyl mycolate from *M. abscessus* (Llorens-Fons et al., 2017). Spectra acquired in CDCl_3 , at 298.0 K and at a magnetic field of 600 MHz.

4. CONCLUSIONS

In the present work, the lipid mycolic ester wax found in *M. smegmatis* was unequivocally characterized as PTTM **1** (Figure 2), with three methyl substituted olefinic units in the carbon chain of the pentatriacontatrienyl, and *trans* double bonds and *cis* cyclopropane in the mycolate structure. The characterization was based on the analyses of a set of 1D and 2D NMR experiments, and the compound mass was confirmed by MS. The present characterization of PTTM **1** allows from now on, the quick direct detection and identification of PTTM **1** by the performance of a simple 1D ^1H NMR spectrum.

ACKNOWLEDGEMENTS

Authors thank the Servei de Ressonància Magnètica Nuclear (SeRMN) of the Universitat Autònoma de Barcelona for allocating instrument time to this project and the Proteomics facility of the UAB (SePBioEs) where the mass spectrometry analyses were carried out.

FUNDINGS

This work was funded by the Spanish Ministry of Science and Innovation (Instituto de Salud Carlos III-PI12/00025), the European Regional Development Fund (FEDER), and the Generalitat of Catalunya (2014SGR-132). Marta Llorens-Fons was recipient of a fellowship from the Universitat Autònoma de Barcelona.

REFERENCES

- Breitmaier, E. (2002). *Structure elucidation by NMR in organic chemistry : a practical guide*. 3rd ed. , ed. E. Breitmaier Wiley.
- Burbaud, S., Laval, F., Lemassu, A., Daffé, M., Guilhot, C., and Chalut, C. (2016). Trehalose Polyphleates Are Produced by a Glycolipid Biosynthetic Pathway Conserved across Phylogenetically Distant Mycobacteria. *Cell Chem. Biol.* 23, 278–289. doi:10.1016/j.chembiol.2015.11.013.
- Chen, J. M., German, G. J., Alexander, D. C., Ren, H., Tan, T., and Liu, J. (2006). Roles of Lsr2 in colony morphology and biofilm formation of *Mycobacterium*

- smegmatis*. *J. Bacteriol.* 188, 633–641. doi:10.1128/JB.188.2.633-641.2006.
- Daffé, M., Reyrat, J. M. (2008). *The Mycobacterial Cell Envelope*. 1st ed. , ed. J.-M. R. Daffé, M. ASM Press.
- Falkinham III, J. O. (2009). Surrounded by mycobacteria: Nontuberculous mycobacteria in the human environment. *J. Appl. Microbiol.* 107, 356–367. doi:10.1111/j.1365-2672.2009.04161.x.
- Fedrizzi, T., Meehan, C. J., Grottola, A., Giacobazzi, E., Fregni Serpini, G., Tagliazucchi, S., et al. (2017). Genomic characterization of Nontuberculous Mycobacteria. *Sci. Rep.* 7, 45258. doi:10.1038/srep45258.
- Jankute, M., Cox, J. A. G. G., Harrison, J., and Besra, G. S. (2015). Assembly of the Mycobacterial Cell Wall. *Annu. Rev. Microbiol.* 69, 405–423. doi:10.1146/annurev-micro-091014-104121.
- Jankute, M., Nataraj, V., Lee, O. Y.-C., Wu, H. H. T., Ridell, M., Garton, N. J., et al. (2017). The role of hydrophobicity in tuberculosis evolution and pathogenicity. *Sci. Rep.* 5, 1–10. doi:10.1038/s41598-017-01501-0.
- Julián, E., Roldán, M., Sánchez-Chardi, A., Astola, O., Agustí, G., and Luquin, M. (2010). Microscopic cords, a virulence-related characteristic of *Mycobacterium tuberculosis*, are also present in nonpathogenic mycobacteria. *J. Bacteriol.* 192, 1751–60. doi:10.1128/JB.01485-09.
- Laval, F., Lanéelle, M. A., Déon, C., Monsarrat, B., and Daffé, M. (2001). Accurate Molecular Mass Determination of Mycolic Acids by MALDI - TOF Mass Spectrometry. *Anal. Chem.* 73, 4537–4544.
- Llorens-Fons, M., Pérez-Trujillo, M., Julián, E., Brambilla, C., Alcaide, F., Byrd, T. F., et al. (2017). Trehalose Polyphosphates , External Cell Wall Lipids in *Mycobacterium abscessus*, Are Associated with the Formation of Clumps with Cording Morphology , Which Have Been Associated with Virulence. *Front. Microbiol.* 8, 1–15. doi:10.3389/fmicb.2017.01402.
- Marrakchi, H., Lanéelle, M.-A., Daffé, M., and Daffé, M. (2014). Mycolic Acids : Structures, Biosynthesis, and Beyond. *Chem. Biol.* 21, 34–52. doi:10.1016/j.chembiol.2013.11.011.
- Ojha, A. K., Baughn, A. D., Sambandan, D., Hsu, T., Trivelli, X., Guerardel, Y., et al. (2008). Growth of *Mycobacterium tuberculosis* biofilms containing free mycolic acids and harbouring drug-tolerant bacteria. *Mol. Microbiol.* 69, 164–174. doi:10.1111/j.1365-2958.2008.06274.x.

- Ojha, A. K., Trivelli, X., Guerardel, Y., Kremer, L., and Hatfull, G. F. (2010). Enzymatic Hydrolysis of Trehalose Dimycolate Releases Free Mycolic Acids during Mycobacterial Growth in Biofilms. *J. Biol. Chem.* 285, 17380–17389. doi:10.1074/jbc.M110.112813.
- Pacheco, S. A., Hsu, F. F., Powers, K. M., and Purdy, G. E. (2013). MmpL11 protein transports mycolic acid-containing lipids to the mycobacterial cell wall and contributes to biofilm formation in *Mycobacterium smegmatis*. *J. Biol. Chem.* 288, 24213–24222. doi:10.1074/jbc.M113.473371.
- Pauli, G., Jaki, B., Gödecke, T., and Lankin, D. (2012). Quantitative ¹H NMR: development and potential of a method for natural products analysis - An Update. *J. Nat. Prod.* 75, 834–851. doi:10.1021/np200993k.
- Secanella-Fandos, S., Luquin, M., Pérez-Trujillo, M., and Julián, E. (2011). Revisited mycolic acid pattern of *Mycobacterium confluentis* using thin-layer chromatography. *J. Chromatogr. B. Analyt. Technol. Biomed. Life Sci.* 879, 2821–6. doi:10.1016/j.jchromb.2011.08.001.
- Seeliger, J., and Moody, D. B. (2016). Monstrous Mycobacterial Lipids. *Cell Chem. Biol.* 1, 2015–2017. doi:10.1016/j.chembiol.2016.02.004.
- Watanabe, M., Ohta, A., Sasaki, S. I., and Minnikin, D. E. (1999). Structure of a new glycolipid from the *Mycobacterium avium*-*Mycobacterium intracellulare* complex. *J. Bacteriol.* 181, 2293–2297.
- Williams, A., Martin, G., and Rovnyak, D. (2016). *Modern NMR Approaches to the Structure Elucidation of Natural Products: Volume 2: Data Acquisition and Applications to Compound Classes*. 1st ed. , eds. A. Williams, G. Martin, and D. Rovnyak Cambridge: Royal Society of Chemistry doi:10.1039/9781849734684.
- World Health Organization (2016). Global tuberculosis report 2016. Available at: http://www.who.int/tb/publications/global_report/gtbr2016_executive_summary.pdf [Accessed December 4, 2017].
- Yuan, Y., and Barry, C. E. (1996). A common mechanism for the biosynthesis of methoxy and cyclopropyl mycolic acids in *Mycobacterium tuberculosis*. *Proc. Natl. Acad. Sci. U. S. A.* 93, 12828–12833. Available at: <http://www.pnas.org/content/93/23/12828.full>.

Supporting Information

Molecule confirmation and structure characterization of pentatriacontatrienyl mycolate in *Mycobacterium smegmatis*

Marta Llorens-Fons¹, Esther Julián¹, Marina Luquin^{1*}, Míriam Pérez-Trujillo^{2*}

¹ Departament de Genètica i de Microbiologia, Facultat de Biociències, Universitat Autònoma de Barcelona, E-08193, Bellaterra, Barcelona, Spain.

² Servei de Ressonància Magnètica Nuclear i Departament de Química, Facultat de Ciències i Biociències, Universitat Autònoma de Barcelona, E-08193, Bellaterra, Barcelona, Spain.

*Corresponding coauthor: Míriam Pérez-Trujillo (E-mail: miriam.perez@uab.cat)

*Corresponding coauthor: Marina Luquin (E-mail: marina.luquin@uab.cat)

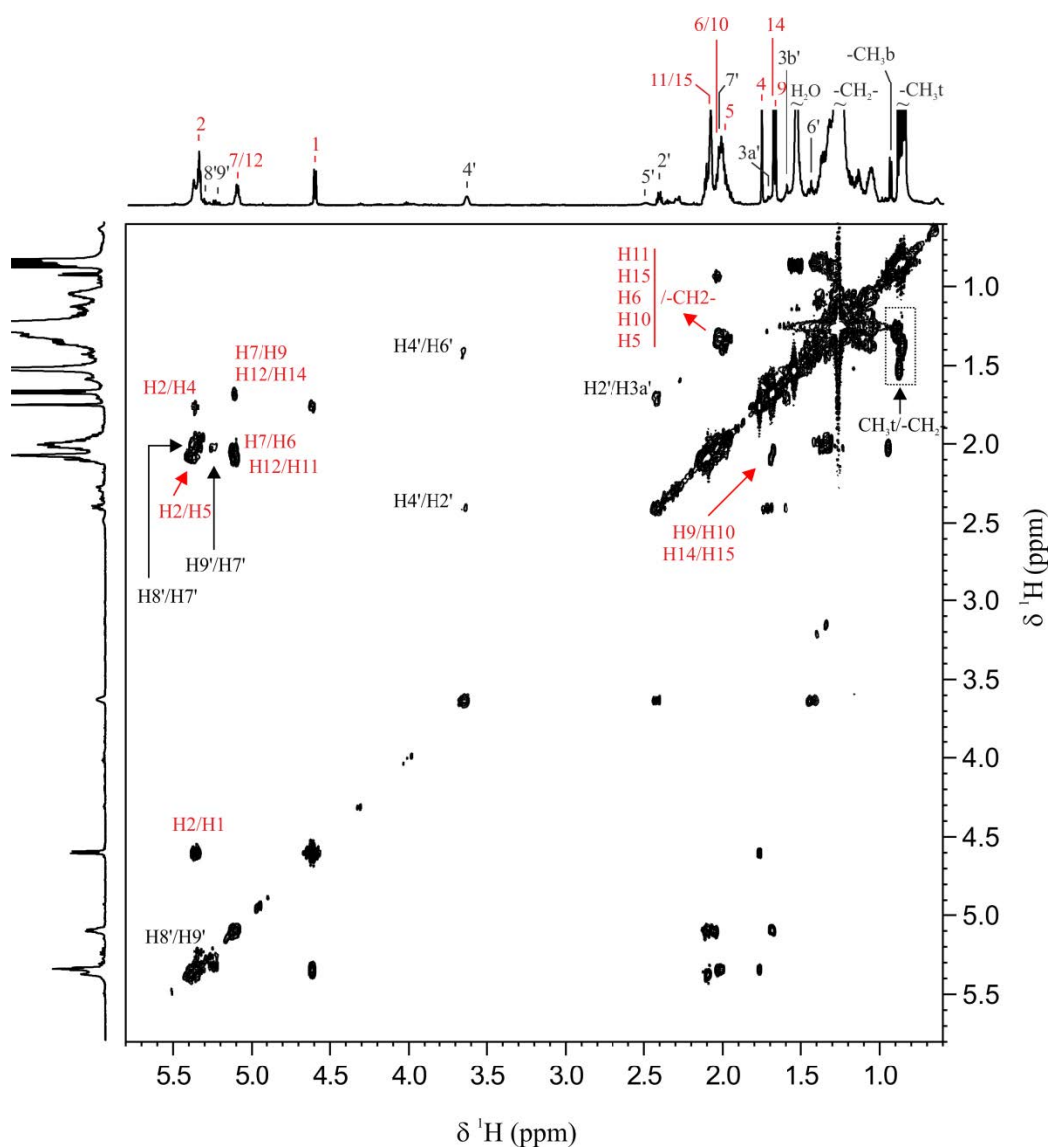


Figure S1. ^1H - ^1H COSY of the sample corresponding to purified spot A (PTTM **1**).

Spectra recorded at a magnetic field of 600.13 MHz and at 298.0 K of temperature.

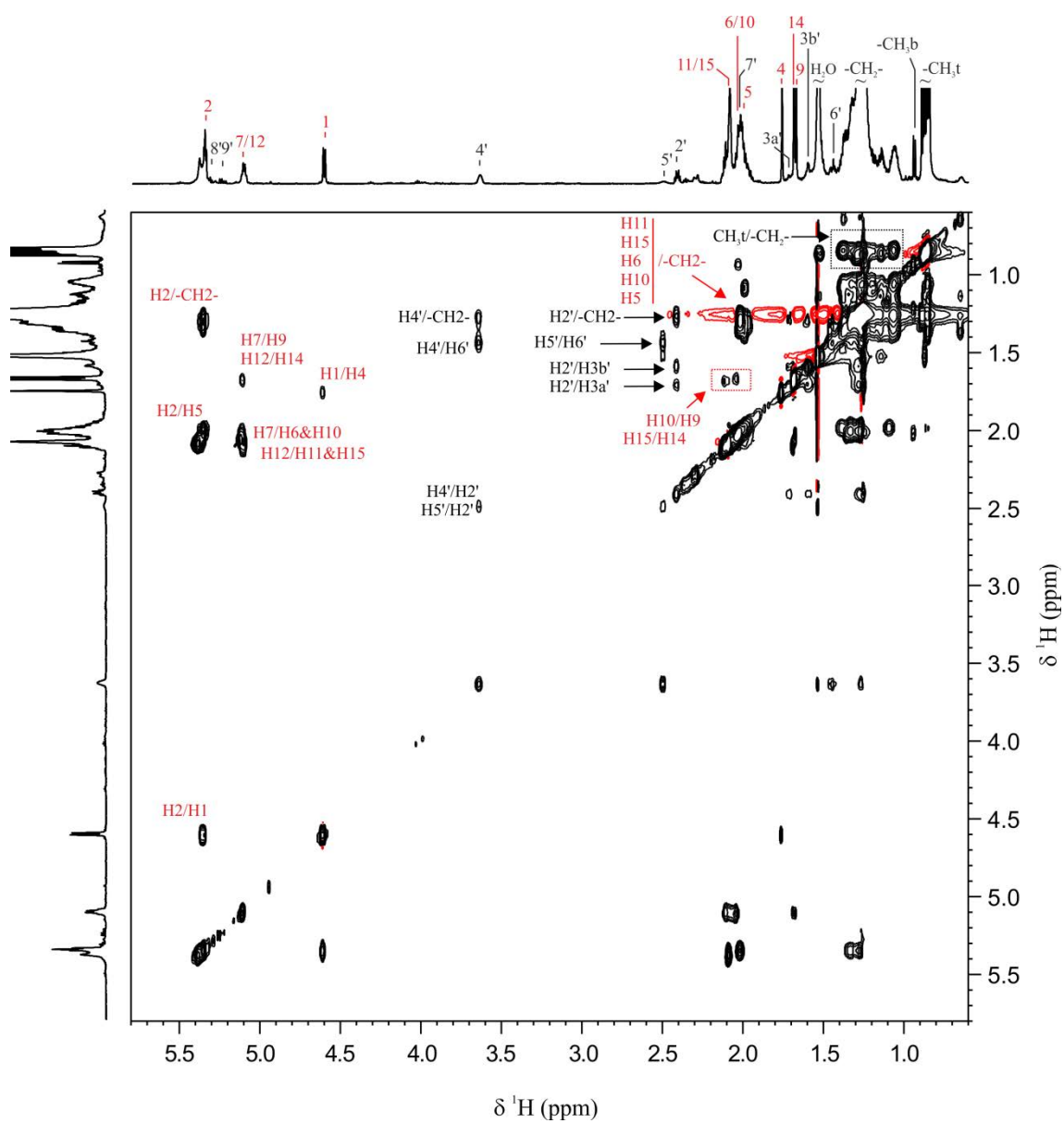


Figure S2. ^1H - ^1H TOCSY of the sample corresponding to purified spot A (PTTM **1**). Spectra recorded at a magnetic field of 600.13 MHz and at 298.0 K of temperature.

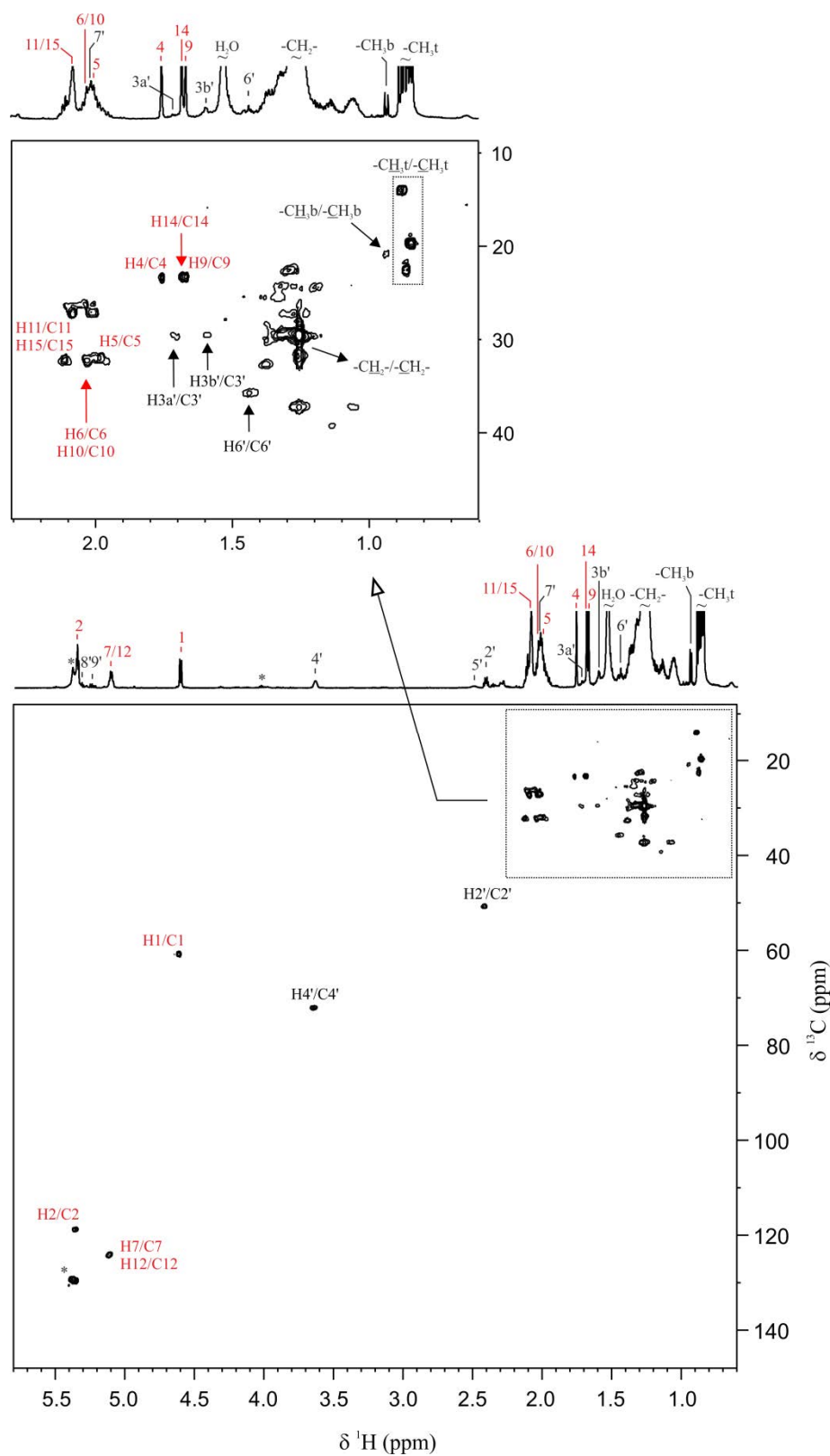


Figure S3. ^1H - ^{13}C HSQC of the sample corresponding to purified spot A (PTTM 1) with an extension of the aliphatic region. Spectra recorded at a magnetic field of 600.13 MHz and at 298.0 K of temperature.

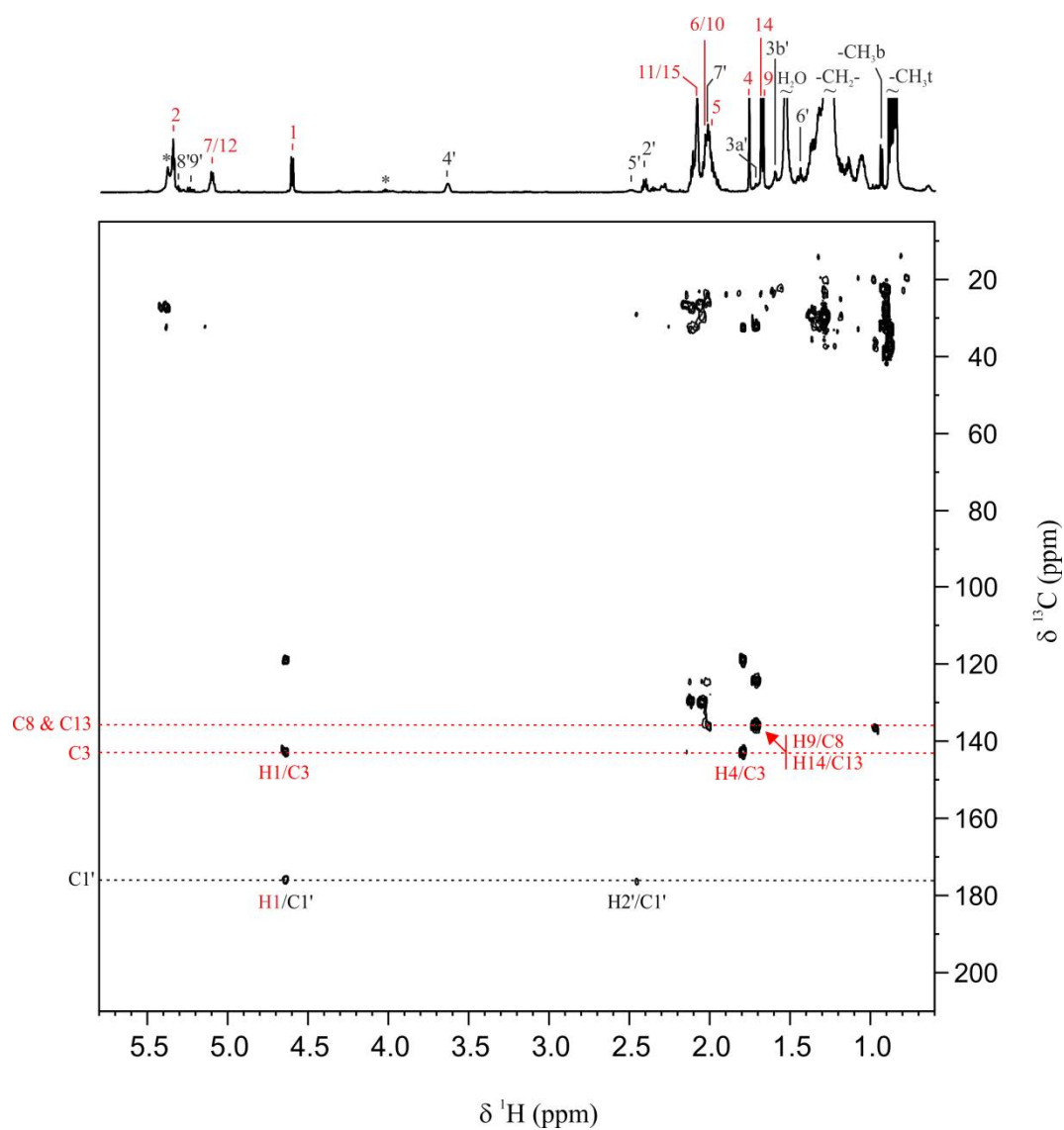


Figure S4. ^1H - ^{13}C HMBC of the sample corresponding to purified spot A (PTTM **1**).

Spectra recorded at a magnetic field of 600.13 MHz and at 298.0 K of temperature.